Bone Reconstruction of Goat Femur Segmental Defects using Tissue-Engineered Bioceramic Scaffolds with Osteogenically Induced Mesenchymal Stem Cells and Platelet-rich Plasma

A THESIS SUBMITTED

BY

MANITHA B. NAIR

IN PARTIAL FULFILLMENT OF THE REQUIREMENTS

FOR THE DEGREE OF

DOCTOR OF PHILOSOPHY

SREE CHITRA TIRUNAL INSTITUTE FOR
MEDICAL SCIENCES AND TECHNOLOGY
THIRUVANANTHAPURAM – 695 012

AUGUST 2009

DECLARATION

I, Manitha B. Nair, hereby declare that I had personally carried out the work depicted in the thesis entitled "**Bone Reconstruction of Goat Femur Segmental Defects using Tissue-Engineered Bioceramic Scaffolds with Osteogenically Induced Mesenchymal Stem Cells and Platelet-rich Plasma**" under the direct supervision of Dr. Annie John, Scientist-E, Division of Implant Biology, Biomedical Technology Wing, Sree Chitra Tirunal Institute for Medical Sciences and Technology, Thiruvananthapuram, Kerala, India. External help sought are acknowledged.

Manitha B. Nair

Dr. Annie John,
Scientist E

Transmission Electron Microscopy Laboratory,
Division of Implant Biology,
Biomedical Technology Wing,
Sree Chitra Tirunal Institute for Medical Sciences and Technology,
Thiruvananthapuram – 695012

CERTIFICATE

This is to certify that Ms. Manitha B. Nair, Division of Implant Biology of this Institute, has fulfilled the requirements of the regulations relating to the nature and prescribed period of research for the Ph. D degree of the Sree Chitra Tirunal Institute for Medical Sciences and Technology, Thiruvananthapuram. The work entitled "**Bone Reconstruction of Goat Femur Segmental Defects using Tissue-Engineered Bioceramic Scaffolds with Osteogenically Induced Mesenchymal Stem Cells and Platelet-rich Plasma**" was carried out under my direct supervision.

Dr. Annie John

THE THESIS

ENTITLED

Bone Reconstruction of Goat Femur Segmental Defects using Tissue-Engineered Bioceramic Scaffolds with Osteogenically Induced Mesenchymal Stem Cells and Platelet-rich Plasma

SUBMITTED

BY

Ms. MANITHA B. NAIR

FOR

DOCTOR OF PHILOSOPHY

SREE CHITRA TIRUNAL INSTITUTE FOR

MEDICAL SCIENCES AND TECHNOLOGY

THIRUVANANTHAPURAM – 695 012

EVALUATED AND APPROVED BY

Dr. ANNIE JOHN
Scientist E
(Supervisor)

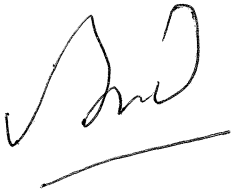

Dr. K. P. ARAVINDAN
Prof. & HOD Pathology
Medical College, Calicut

Even though I walk through the darkest valley, I will fear no evil,

For you are with me, your road and your staff, they comfort me.....

CONTENTS

Acknowledgements

This is perhaps the easiest and hardest chapter that I have to write. It will be simple to name all the people that helped to get this done, but it will be tough to thank them enough.

I have no words to express my personal gratitude to my supervisor, Dr. Annie John who first brought me into the world of tissue engineering. Her approach enabled me to develop independent thinking and an ability to stand up for what I believe is right. She was always accessible and willing to help her students with her advice and suggestions.

I thank the Council of Scientific and Industrial Research, India for the fellowship provided during the doctoral programme. I am grateful to the Department of Biotechnology for providing "The International Travel grant" to present research paper in TERMIS-NA 2007 conference.

I thank my Doctoral Advisory Committee members, Dr. Mira Mohanty, Dr. T. V. Kumary, Dr. H. K. Varma and Dr. Samson Neissiah for their valuable time and encouragements in my work. The valuable suggestions of Dr. H. K. Varma in the area of material science improved the quality of this study.

The Director, SCTIMST and The Head, BMT Wing is greatly acknowledged for the facilities provided throughout the doctoral programme. I am very much indebted to The Registrar and The Deputy Registrar for all the academic assistance in this venture.

I am obliged to Mr. Suresh Babu S. for his help regarding material synthesis and characterization.. I am grateful to all members of Bioceramics lab, especially Mr. Vijayan, Dr. Manoj Komath, and Mr. Sreekanth for all the support during my work.

It is difficult to overstate my pleasure to Dr. K. V. Menon, Dr. Sanjay, Dr. Abijith, Dr. Umashankar P. R, Dr. Sachin J Shenoy and Dr. Harikrishnan.V.S for planning and conducting my experimental studies in vivo. It was with the proposal of Dr. K. V. Menon that I chose to study in the area of segmental bone defects.

Dr. Lissy K. Krishnan, because of madam's forethought only, I have entered into the world of cell culture and have done fibrin glue studies. All staff of Thrombosis Research Unit, especially, Priyanka and Juliet were with me for completing my platelet studies. Dr. Krishnaprasad, Mrs. Sreerekha and Mrs. Anumol were friendly and helped me to do flow cytometric analysis.

Dr. Michael Gelinsky, Dr. Anne Bernhardt Dr. Anja, Dr. Ulla are thanked for numerous stimulating discussions, help with experimental setup and general advice for my experiments with human stem cells. In particular, I would like to acknowledge the help of Dr. Anne for her assistance with all types of technical problems - at all time in Max Bergmann Centre for Biomaterials, Dresden, Germany.

Dr. T. V. Anilkumar, whose training and friendly discussions, gave me awareness about confocal microscopy. I am very much indebted to Dr. Kalliyana Krishnan V for taking interest in micro-CT studies and providing valuable suggestions about Raman spectroscopy. I greatly acknowledge Mr. Sreekumar R for scanning electron microscopy studies. I thank Dr. Roy Joseph for mechanical testing studies and Mr. Ramesh Babu. V for proving all the helps for dissecting PMMA embedded tissue samples.

Special thanks are due to Dr. A. C. Fernandez for his mental support whenever I found difficult in my personal life. Dr. P. V. Mohanan and his staff are greatly acknowledged for small animal studies.

All staff and students of Histopathology and Tissue culture Laboratory were friendly to me. Dr. Sabareeswaran and Mrs. Sulekha Baby were there to teach me histopathological doubts. Mrs. Vshavasudev, Dr. P. R. Anilkumar and Mr. Tilak are thanked for all the help during my work.

I gratefully and wholeheartedly acknowledge the friendly support and patience from my lab mates, Mrs. Susan, Mr. Francis, Mrs. Devi, Mrs Beena, Mr. Vipin and Mr. Sandeep.

Dr. Divya, Ms. Madhumati, Dr. Asha, Ms. Asharani, Mrs. Josna, Mrs. Neena, Ms. Bindu, Mr. Rammohan, Mr. Joseph, Mr. Sajeesh and Mr. Renjith, you all were there whenever there was a need. Special thanks to Ms. Ragaseema, Mrs. Viji, Mr. Sudhaker and Mr. Unnikrishnan for their prayers, constant encouragement and caring when it was most required.

My father, Chechi and my Adith without mentioning about them, how I will finish this chapter?

According to the Jewish proverb, 'The last, Ah!, the last is the most precious' in love and respect of my mother's mental support to this work. I can only echo Rabbi Akiva's words to his disciples: My knowledge and what I learn is all due to her.

Oh God, nothing that I have or could have done in my life is worthy of the eternal love and mercy that you showered on me. I dedicate this thesis to Thee, Oh Lord.

Manitha B. Nair

LIST OF FIGURES

LIST OF TABLES

ABBREVIATIONS

ALP	Alkaline Phosphatase
bFGF	Basic fibroblast growth factor
BMD	Bone mineral density
BMP	Bone morphogenetic protein
BMSCs / OS-	Bone marrow-derived mesenchymal stem cells
BSA	Bovine serum albumin
BSP	Bone silao protein
cLSM	Confocal laser scanning microscope
CPCSEA	Committee for the purpose of Control and Supervision of Experiments on animals
DMEM	Dulbecco's modified Eagle's medium
ECM	Extracellular matrix
EDS	Energy dispersive x-ray spectroscopy
EGF	Epidermal growth factor
ELISA	Enzyme-linked immunosorbent assay
ESEM	Environmental scanning electron microscope
FBS	Fetal bovine serum
FCS	Fetal calf serum
FG	Fibrin glue
FGF	Fibroblast growth factor
FTIR	Fourier Transform Infrared spectroscopy
gBMSCs	Goat bone marrow-derived mesenchymal stem cells
gOS+ cells	Goat osteogenic induced mesenchymal stem cells
HA	Hydroxyapatite
hBMSCs	Human bone marrow-derived mesenchymal stem cells
HCA	Hydroxycarbonate apatite
HOS	Human osteoblast
hOS+ cells	Human osteogenic induced mesenchymal stem cells
IAEC	Institutional Animal Ethics Committee

ICP	Inductively Coupled Plasma spectroscopy
IGF	Insulin-like growth factor
LDH	Lactate dehydrogenase
MEM	Minimal Essential Medium
MSCs	Mesenchymal stem cells
OS+ cells	Osteogenic induced mesenchymal stem cells
PBS	Phosphate buffered saline
PCNA	Proliferating cell nuclear antigen
PDGF	Platelet-derived growth factor
PE	Phycoerythrin
PF-4	Plasma factor 4
PLGA	Poly (lactic-co-glycolic acid)
PMMA	Polymethylmethacrylate
PRP	Platelet-rich plasma
rBMSCs	Rat bone marrow-derived mesenchymal stem cells
rOS+ cells	Rat osteogenic induced mesenchymal stem cells
SEM	Scanning electron microscope
TCP	Tricalcium phosphate
TCPS	Tissue culture polystyrene
TEOS	Tetraethyl orthosilicate
TGF- β	Transforming growth factor β
TPOS	Tetraethyl propylsilicate
TRAP	Tartrate Resistant Acid Phosphatase
VEGF	Vascular endothelial growth factor
XRD	X-ray diffraction technique
3D	Three dimensional

NOTATIONS

α	Alpha
β	Beta
µ	Micro
±	Plus or minus
%	Percentage
℃	Degree Celsius
Ct	Threshold cycle
c	concentration
h	hour
min	Minute
M	Molar
mM	millimolar
nM	Nanomolar
ml	Millilitre
µl	Microlitre
g	Gram
mg	Milligram
µg	Microgram
ng	Nanogram
cm	Centimeter
mm	Millimeter
µm	Micrometer
wt	Weight
MPa	Megapascal
kDa	Kilodaltons
IU	International Units

SYNOPSIS

The reconstruction of segmental bone defects resulting from trauma or pathologic situations like osteosarcoma, osteomyletis or osteoporosis represents the common and significant clinical problems today, which require bone-graft procedures to achieve union. Such situations may lead to complications such as shortening of the structures, nerve and vascular lesions, cutaneous loss, delayed edema and amputation of the involved member. The current treatment methods for segmental defects include autograft or allograft or distraction osteogenesis, but all of them are subject to limitations such as donor site morbidity, limited supply of material, risk of infection, immune rejection, pin tract infection, long term hospitalization etc.

The restoration of the structural and functional integrity of the damaged bone requires (a) the 3D extracellular matrix for the attachment of cells into the osseous defect (b) pluripotent mesenchymal stem cells capable of differentiating into osteoblast cells (c) growth factors that can direct cells to migrate into the osseous defect, to proliferate and differentiate into osteoblast cells and (d) formation of a vascular network throughout the newly formed bone. It is here that the concept of tissue engineering gains relevance which utilize an appropriate bioresorbable and biocompatible 3D biomaterial (scaffold) with cells and / or growth factors for the stimulation of new bone formation in a defect site. The triad of tissue engineering - scaffold, cells and growth factors - can be used alone or in different combinations with the prospect of mimicking an autograft having the properties of biocompatibility, osteoconductivity and osteoinductivity. If the scaffolds alone are implanted into the defect, the repair is strongly dependent on the recruitment and proliferation of host cells. Conversely, in cell-mediated tissue engineering, the cells can be isolated from the patients and cultured on the scaffold *ex vivo* prior to implantation so that a 'living tissue substitute' may be transplanted to the defect site.

The challenge encountered in tissue engineering paradigm is that the physico-chemical nature of the biomaterial surface and the biological behaviour of the cell should coordinate in a sequestered pattern to form a functional tissue. Thus the selection of a biomaterial is an important aspect where the properties such as pore size, pore interconnections, surface topography, chemical composition becomes very

crucial. The biomaterials are ideally supposed to resorb at a rate comparable to that of the ingrowth of newly formed bony trabeculae. Furthermore, the vascularisation potential of the biomaterial is also of great concern because it has an effect on cell survival and subsequently bone formation.

Hard skeletal tissue is a complex composite consisting of cells embedded within a mineralized organic matrix with a structural similarity to hydroxyapatite (HA). On account of this similarity, synthetic bioactive ceramic like HA has been extensively used as a skeletal replacement material with no systemic toxicity or immunological reactions. However, HA degrades very slowly in course of time and therefore may remain as a permanent implant in the body which results in long-term failure. Despite calcium and phosphorous, substitutions of various other elements occur at trace level in bone mineral which play an important role in the biological activity of bone. Among these elements, the significant role of silicon (Si) in the growth and development of bone and cartilage has been reported. In addition, the incorporation of Si into the composition of bioactive ceramics becomes of great interest because of their ability to nucleate the precipitation and formation of a calcium phosphate layer on the implant surface leading to enhanced bone formation and thereby bone bonding. In addition, these materials can undergo resorption in par with bone formation.

In order to promote bone formation, supplement of the cells and the growth factors having osteoinductive capability is critical. Bone marrow has been shown to contain a population of cells called mesenchymal stem cells (BMSCs) that possess self renewal ability and osteogenic differentiation in an osteoconductive environment. These cells can be administered to the defect site by soaking the scaffold in fresh bone marrow, but practicality of obtaining enough bone marrow with the requisite number of BMSCs is limited. Therefore techniques capable of isolating and culture expanding BMSCs on scaffolds would be of great benefit for enhancing bone regeneration, particularly in large defects. Similar to osteogenic cells, the osteoinductive stimuli may also be induced by supplying growth factors. An easy and more physiological way of application of growth factors to defect site is via the use of platelet-rich plasma (PRP), a thrombocyte concentrate made of autologous blood. Platelets are a rich source of many growth factors such as platelet-derived growth factor, transforming growth factor beta, fibroblast growth factor, vascular endothelial

growth factor, and insulin-like growth factor.

Research Proposal

Herein a tissue-engineering approach has been proposed, i.e. the combination of BMSCs and PRP with a novel 3D bioactive ceramic (silica-based HA) as bone substitute for the repair of segmental defects in goat model. Silica-based HA included in this study was Triphasic ceramic coated hydroxyapatite (HASi) whose efficacy was compared with that of Hydroxyapatite (HA). The objectives were achieved in three phases.

1. **Physicochemical characterization of bioactive ceramics**
2. **Evaluation of tissue-engineered constructs *in vitro* - Platelet-rich plasma / fibrin glue coated and uncoated bioactive ceramics in conjunction with BMSCs**
3. **Evaluation of tissue-engineered bioactive ceramics *in vivo* - Extraskeletal and orthotopic implantation**

This dissertation is divided into six chapters: Introduction, Materials and methods, Results and discussion (Three sections) followed by Summary and Conclusion.

Chapter 1 – Introduction

This chapter begins with the problems associated with segmental defects that occur due to trauma, osteoporosis or osteosarcoma and the limitations of current bone reconstruction techniques. In order to develop an ideal bone graft, one has to understand the basics of bone structure and bone healing process which was reviewed. Bone tissue engineering, an innovative approach in Regenerative Medicine today requires suitable scaffolds in combination with living osteoprogenitor cells or growth factors for the regeneration of bone is discussed. The major challenges and the main criteria that a scaffold should meet in bone tissue engineering are highlighted. The roles of bioactive ceramics like HA, tricalcium phosphate (TCP) and silica-based biomaterials as scaffolds for the repair of segmental bone defects over the past decades have been reviewed. And above all, the relevance of mesenchymal stem cells and platelet-rich plasma for cell and growth factor mediated tissue engineering was also discussed.

Chapter 2 – Materials and methods

1. Physicochemical characterization of bioactive ceramics:

Bioactive ceramics like HA and HASi was gifted from Bioceramics Laboratory, SCTIMST. HA was synthesized by wet precipitation method involving calcium nitrate and ammonium dihydrogen phosphate and sintered at 1200℃. For synthesizing HASi, sintered HA was dipped in silica sol prepared by the hydrolysis of tetraethyl orthosilicate (TEOS) in an ethanol– water system followed by a second sintering at 1200℃. The microstructure, elemental distribution, phase composition, crystallinity, functional group, porosity and pore size of these materials were characterized by environmental scanning electron microscopy (ESEM), Elemental dispersive analysis by X-ray (EDS), X-ray diffraction technique (XRD), Fourier transform infrared spectroscopy (FTIR), and mercury porosimetry. The *in vitro* degradation of HA and HASi were studied as per ISO standard 10993-13. For this, the materials were immersed in phosphate buffered saline (PBS) and the changes with respect to phase composition and functional groups of these materials were monitored for a period of 2 months. In addition, the cytotoxicity and cytocompatibility of HA and HASi was determined with L929 mouse fibroblast cell line and Human osteoblast (HOS) cell line respectively.

2. Evaluation of tissue-engineered constructs *in vitro*:

BMSCs were isolated and induced to differentiate into osteogenic lineage (OS+ cells) by providing osteogenic supplements. The proliferation and differentiation potential of gBMSCs in several passages were studied by trypan blue staining and alkaline phosphatase (ALP) activity respectively. BMSCs and OS+ cells (goat and human origin) were then cultured on HA and HASi separately for a period of 28 days. In the second set of experiments, these materials were coated with PRP and fibrin glue (FG – osteoinductive protein) and cultured with OS+ cells (goat origin). The coating of PRP and FG on HA and HASi were confirmed through various assays (platelet count and lactate dehydrogenase assay (LDH) for platelet adhesion; P-selectin and plasma factor 4 release for platelet activation and ESEM-EDS & Raman spectroscopy for FG adhesion). These tissue-engineered constructs (uncoated and PRP / FG coated HA and HASi with cells) were then evaluated in terms of cell adhesion and morphology (SEM); cell viability, (acridine orange and ethidium bromide staining by confocal laser scanning microscopy (cLSM) and flow cytometry

as well as by LDH assay); cell migration (Stevenal's blue and van Gieson's picrofuschin staining by Light microscopy) cell proliferation (proliferating cell nuclear antigen (PCNA) staining by flow cytometry and DNA content by picogreen assay); cell cycle analysis (propidium iodide staining by flow cytometry); and osteogenic differentiation by determining ALP activity and expression (biochemical estimation, cLSM for ALP activity and Real-time PCR for ALP expression), ostepontin expression (cLSM, flow cytometry and Real-time PCR), osteocalcin (ELISA technique and Real-time PCR).

3. Evaluation of tissue-engineered constructs *in vivo* - Extraskeletal and orthotopic site:

Extraskeletal site (muscle) in rat model: The vascularisation and osteoinductive potential of bare HA and HASi (without cells) in comparison with tissue-engineered HA and HASi (cultured with OS+ cells of rat origin for 7 days) at the extraskeletal site of rat model was evaluated at 2 and 4 weeks. Hematoxylin and eosin staining was done for studying vascularisation. Stevenal's blue and van Gieson's picrofuschin staining for neo-osteogenesis, ELF-97 staining for ALP activity and micro-computed tomography (micro-CT) for mineralization was done for determining osteoinduction.

Orthotopic site (femur) in goat model): The progress of bone regeneration in par with material degradation was studied in a 2 cm segmental defect created in the femur of the goat model. Three groups were included for the implantation in the study (a) bare HASi (without cells or PRP) (b) HASi cultured with OS+ cells of goat origin for 7 days (c) HASi cultured with OS+ cells of goat origin for 7 days + PRP liquid delivered at the defect site at the time of surgery. The performances among the three groups were compared for 2 and 4 months. Bare HASi groups were additionally determined for 6 and 12 months. The retrieved tissues were analyzed through radiography, histology (Stevenal's blue and van Gieson's picrofuschin staining), histomorphometry, EDS, micro-CT, computed tomography. The biochemical analysis of ALP and tartrate resistant acid phosphatase (TRAP) in the serum of the goat model was done. The material remained at the defect site was also characterized through XRD and FTIR.

Results and Discussion

Chapter 3: Physicochemical characterization of bioactive ceramics

The coating of silica over HA was firstly confirmed in HASi. ESEM-EDS depicted that the core of HASi was polycrystalline with elements like Ca and P while the coated layer contained Si in addition to Ca and P and was porous and less crystalline due to Si rich liquid phase formation. XRD revealed that HA has only hydroxyapatite phase. However for HASi, the core phase was hydroxyapatite together with the peaks for hydroxyapatite, tricalcium phosphate, and calcium silicate in the outer coated layer. The FTIR spectra obtained for HA showed the characteristic triplet peak for phosphate at 961cm^{-1}, 1054cm^{-1} and 1088cm^{-1} and hydroxyl groups at 3570 cm^{-1}, while in HASi the peak at 1088 cm^{-1} was absent and the intensity of hydroxyl peak (3570 cm^{-1}) was weak. This may be due to the substitution of silicate group for phosphate group. Mercury intrusion technique and SEM depicted the interconnected porous nature of HA and HASi with pore size of about 50 – 500 µm. The degradation studies showed that tricalcium phosphate and calcium silicate present in the outer coating layer of HASi disappeared after immersing in PBS for 2 months however there was no change for HA. This indicated the solution-mediated degradation of HASi. Cytotoxicity studies with L929 fibroblast cells confirmed the non-cytotoxicity of HA and HASi after direct contact with cells (ISO 10993-5). HOS cells adhered and spread on HA and HASi, with better preference on HASi.

Chapter 4: Evaluation of tissue-engineered constructs *in vitro* - Platelet-rich plasma / fibrin glue coated and uncoated bioactive ceramics in conjunction with BMSCs

The mesenchymal origin of BMSCs was characterized using markers like CD 44 and vimentin staining. These cells were able to differentiate into osteogenic lineage *in vitro* as defined by the production of collagen-rich matrix, and non-collagenous proteins like ALP and the formation of mineralized matrix. BMSCs in passage 2 to 5 possessed similar expansion and differentiation potential and was selected for further tissue engineering studies. BMSCs and OS+ cells (goat and human origin) showed adhesion, spreading, viability and proliferation on HA and HASi, with significantly improved performance by OS+ cells on HASi. The cells were able to migrate towards the internal voids of HASi, while on HA, most of the cells were restricted on the periphery of the material. In addition, HASi augmented osteoblast

commitment and represented "mature osteoblast cells or osteocytes" better than HA, as revealed by the differentiation studies. This is because the surface chemistry of silica-based materials is amenable to extracellular matrix proteins that facilitate cell adhesion and other cellular activities. Since OS+ cells showed improved response than BMSCs, further studies were carried out only with OS+ cells. The performance of goat and human cells were comparable in almost all *in vitro* studies, giving a hope for extrapolating the results of bone regeneration studies in goat model for human in future.

The coating of HA and HASi with PRP and FG enhanced the cellular behaviour than uncoated biomaterials, depicting that the temporary extracellular matrix provided by FG and growth factors released by activated PRP is a favorite peptide habitat for the cells. The cells were most compatible with FG coated matrices, still PRP was selected as signaling agent for *in vivo* studies because it is cheap and easy to prepare. Another interesting finding was that the viability and proliferation of cells on uncoated HASi was significantly higher than PRP and FG coated HA after second week, signifying that the stimulus issued by the silica content of HASi has reached a stage above the level of stimulus given by PRP and FG in HA.

Chapter 5: Evaluation of tissue-engineered bioactive ceramics *in vivo* - Extraskeletal and orthotopic implantation

Heterotopic implantation studies showed that the vascularisation was low at the defect site implanted with HA, both in bare and tissue-engineered group. However HASi and tissue-engineered HASi groups showed a notable increase in the number of endothelial cells together with thin walled blood capillaries and blood vessels, attributing the role of silica in improving vascularisation. Similarly, bare and tissue-engineered HA did not reveal any active site of osteoid deposition in extraskeletal site. Nevertheless, immature woven bone with osteoblast-like cells was seen around and within the pores of tissue-engineered HASi group. This was further confirmed through ALP activity and mineralization studies. The time required for osteogenic cells to fabricate bone is dependent on the local microenvironment (chemistry) provided by scaffold and the interactions with the host. Thus silica in HASi has proved to be a positive factor for the improved vascularisation at the recipient site which is a dire necessity for bone formation and bone turnover. Since HASi proved to be a better substrate than HA, the regeneration of bone in segmental defect was

studied with HASi only.

Orthotopic implantation studies showed that bone had regenerated to bridge the segmental defect (2 cm) and good integration of the material with the host bone on either side at an early period of 6 weeks. The new bone formation advanced and was similar at the peripheral region of the defect in all the three groups, indicating the osteoconductive and osteointegrative nature of HASi. A notable difference between the three groups was there in the mid region of the defect. Osteoblast-like cells at 2 months, immature woven bone at 4 months, mature lamellar bone at 6 months and complete bone remodeling at 12 months was observed in bare HASi groups in the mid region of the defect. Astonishingly, in tissue-engineered HASi groups, improved and faster osteogenesis was observed where immature woven bone at 2 months and mature lamellar bone was formed at 4 months. Additionally, the interconnected porous structure and the presence of silica directed a progressive degradation (mainly osteoclast-mediated) of HASi scaffolds. The process was enhanced in tissue-engineered group highlighting the dependence of material upon the cell and extracellular matrix deposition for attracting osteoclast cells. The possible mechanism was hypothesized based on the significant expression of extracellular matrix proteins like osteopontin on HASi, which promote the adhesion of osteoclast to the scaffold surface. There were no significant difference between PRP delivered and non-delivered tissue-engineered groups, with slightly better performance in the PRP delivered groups.

Chapter 6 - Summary and conclusion of the results

HASi, a new silica-based bioactive ceramic was synthesized to project as a bone substitute for the repair of segmental defect. In HASi, the silicon ions were incorporated as an outer coating layer on HA in order to achieve the dual properties of HA and silica in one product. *In vitro* studies showed that the highly interconnected porous structure and chemical composition of HASi was more favourable for the cellular activities than HA. HASi was also capable of enhancing neo-vascularisation than HA, giving a hope for the problem of the diffusion of oxygen and nutrients for maintaining cell survival in large sized bone defects. Orthotopic experiments revealed that HASi is osteoconductive, osteointegrative and degradative in nature without fibrous tissue formation and inflammation. The vascularisation, osteoconductive and osteoinductive property of HASi was significantly enhanced and

faster in tissue-engineered groups where the cells on scaffolds may have secreted inductive factors that enhance the osteogenic process. This gives a hope for geriatric patients and also patients with debilitating patients where the native stem cell number is low to bring about effective regeneration and repair. Thus the study suggested the possibility of using tissue-engineered HASi in clinical situations of segmental defects like osteosarcoma or osteomyelitis or in trauma which still remains a formidable clinical challenge in clinical Orthopaedic reconstructive surgery.

CHAPTER 1

INTRODUCTION

1.1 Summary

The repair of large segmental defects in diaphyseal bone is a significant problem confronted by orthopaedic surgeons today. Such bone loss results from high energy trauma, osteomyelitis, congenital pseudoarthrosis or extensive excision of malignant conditions. Osteotomy followed by bone distraction (the Ilizarov technique) or autografts or allografts are the most currently used therapeutic approaches for the repair of segmental defects. The Ilizarov technique relies on the regeneration potential of bone, while the success is counter balanced by long recovery time, pin tract infection and high inconvenience for the patient (Ilizarov GA *et al.,* 1969; Green SA *et al.,* 1992). Autogenous bone graft procedures are considered 'the gold standard' and are having the success rate of 80% to 90%. However, harvesting autograft requires an additional surgery at the donor site that can result in many problems like inflammation and chronic pain. In addition, after grafting, complications such as infections and non-unions frequently occur especially in larger shaft reconstructions (Seiler JG *et al.,* 2000; Hill NM *et al.,* 1999). Allograft bone taken from donors or cadavers carries the risk of blood-borne diseases and can be used only in countries where fresh-frozen grafts are correctly stored and donor-receiver matched (Gitelis S *et al.,* 2002). Therefore, intensive research efforts are still underway to seek more alternative graft materials for improving the healing of segmental bone defects.

In bone healing, healthy progenitor cells recruited to an injured site deposit extracellular matrix (ECM) and create the necessary bridge in the gap for promoting the regeneration of damaged bone. A promising approach developed based on this natural phenomenon is "Tissue Engineering," which combines engineering principles with life sciences and exploits the body's inherent repair mechanism to facilitate the

regeneration of tissues. Tissue engineering consist of three basic components (a) bioresorbable and biocompatible 3D biomaterial (scaffold) to serve as the matrix (b) osteogenic cells (c) growth factors, which can be used independently or in combination.

The scaffolds for osteogenesis should mimic bone morphology, structure and function to optimize the integration into surrounding tissue. Appropriate porosity and pore size are necessary for the scaffolds to maximize space for cell attachment, growth and ECM production. The interconnected porous architecture is another important criterion that allows even supply of nutrients and oxygen within 3D tissue-engineered constructs. Hulber *et al.,* (1972) demonstrated that porous discs of a near inert ceramic exhibited thinner fibrous encapsulation with faster healing in surrounding muscle and connective tissue when compared to dense discs of the same composition implanted in the same site. This resulted from mechanical interlock, which reduced motion between host tissue and implant, eliciting more passive response from the host. Furthermore, the scaffold should be degradable and the degradation rate must be tuned appropriately with the growth rate of neo-tissue, in such a way that by the time the injury site is totally regenerated the scaffold is totally degraded (Salgado AJ *et al.,* 2004).

The selection of the biomaterial component of tissue engineering is crucial. A wide variety of biomaterials including metals, polymers and ceramics have been investigated during the past 30 years, but no single material posses all the properties required for an ideal bone graft. Among these biomaterials, there has been a sustained interest in bioactive ceramics like hydroxyapatite (HA, Ca_{10} $(PO_4)_6(OH)_2$) because of its similarity in chemical composition to natural bone and are biocompatible, osteoconductive and osteointegrative (Hench LL *et al .,* 1993). But the use of HA is limited for the repair of segmental defects because of its poor degradation rate and the lack of osteoinductivity. Hence the interest has developed in the substitution of controlled levels of different elements into HA lattice to enhance biocompatibility and degradation rate.

In recent years, some silicon containing bioactive materials have shown promise in the development of bone implants such as bioactive glass and silicon-doped calcium phosphate materials. When exposed to body fluids, these materials undergo

corrosion with a leaching of alkali ions resulting in the formation of a silica gel and a calcium phosphate layer on their surface. Successively, the calcium phosphate layer will recrystallise into hydroxycarbonate apatite (HCA) layer *in vitro* and *in vivo*. HCA layer of silica-based biomaterials are more similar in terms of crystallinity to the apatite of bone tissue and consequently a greater bone bonding has been reported for these materials than for HA (Porter AE *et al.,* 2004a; Porter AE *et al.,* 2004b). In addition, localization of the element silicon in the active areas of young bone and its importance in bone metabolism has been reported (Carlisle EM 1980). Silicon has the capacity to stimulate osteoblast proliferation and differentiation and to activate bone-related gene expression (Reffitt DM *et al.,* 2003). Therefore bioactive materials that combine the properties of HA and silicon may open up possibilities to generate novel bone substitutes for the repair of segmental defects.

The second main component of tissue engineering is the "cells", which are cultured on the biomaterial *ex vivo* and thus allowing the development of living 3D tissue with ECM for implantation. This approach necessitates large quantities of cells, but the requirement is difficult to satisfy with differentiated osteoblasts because of their limited doublings in culture. A solution for insufficient cell supplies is to engineer bone defect with stem cells. A characteristic feature of stem cells is to self-renew in an undifferentiated state for prolonged period while retaining the ability to differentiate into one lineage (unipotent), into multiple cell types (multipotent) or into cells derived from all three embryonic germ layers (pluripotent). Embryonic stem cells have many advantages, however, problems with teratoma formation and immune rejection must be overcome before these cells will be practical for therapeutic use (Winkler J *et al.,* 2005). Adult stem cells are more beneficial whose properties include immuno-compatibility of autologous cells, ease of inducing differentiation to a specific lineage and availability (Barrilleaux B *et al.,* 2006). Therefore wide spread attention have focused on the isolation and expansion of a population of adult stem cells located in the bone marrow called mesenchymal stem cells (MSCs) for the regeneration of large bone defects. Bone marrow-derived mesenchymal stem cells (BMSCs) have the ability to differentiate to osteoblasts and promote bone-specific protein synthesis and mineralization in an osteoinductive environment (Haynesworth *et al.,* 1992; Krebsbach *et al.,* 1999). Since bone marrow contains stem cells that posses osteogenic potential, some experimental therapies

based on the implantation of fresh autologous marrow for skeletal repair had developed (Connolly *et al.,* 1991; Hernigou *et al.,* 2006). Nevertheless, the practicality of obtaining enough bone marrow with the requisite number of osteoprogenitor cells is limited, particularly as a consequence of aging or disease (Egrise *et al.,* 1992; D'Ippolito *et al.,* 1999). Thus the current approach is to combine culture-expanded BMSCs with an appropriate scaffold to stimulate bone regeneration and restore functional bone tissue.

The development of osteoblasts from BMSCs is characterized by a sequence of events involving cell proliferation, expression of bone-related proteins (cell differentiation) and synthesis of collagenous ECM. The characterization of these events would provide knowledge about the factors that govern the process of bone formation. The biomaterial should be able to promote each of the discrete stages in osteoblast differentiation pathway. Thus the performance of tissue-engineered constructs must be investigated initially in an *in vitro* cell culture system followed by successful testing in laboratory animals (Oliva A *et al.,* 1998).

The third component of tissue engineering is "growth factors", which can be either combined with biomaterials or delivered directly to the defect site (Tementoff JS *et al.,* 2000). Growth factors influence chemotaxis, differentiation, proliferation and synthetic activity of bone cells, thereby regulating physiological remodeling and fracture healing. Numerous growth factors such as bone morphogenetic proteins (BMP), platelet-derived growth factor (PDGF), transforming growth factor β (TGF-β) and insulin-like growth factor (IGF) have a stimulating effect on bone healing (Vehof *et al.,* 2002; Jansen *et al.,* 2005). But, these growth factors are very expensive (Calabresi *et al.,* 1998). Alternatively, platelet-rich plasma (PRP), a volume of autogenous plasma that has platelet concentration above baseline, is a proven source of these growth factors (Fréchette *et al.,* 2005; van den Dolder *et al.,* 2006). Similar to PRP, fibrin glue (FG), a biopolymer matrix, also contains smaller amounts of many growth factors like TGF-β1, basic fibroblast growth factor (bFGF), epidermal growth factor (EGF), vascular endothelial growth factor (VEGF) and other biomolecules like fibronectin (Ho W *et al.,* 2006). The osteoinductive property of FG has already been reported (Abiraman S *et al.,* 2002). FG has been used to enhance osteogenesis in human maxillary and mandibular bone (Marrini E *et al.,* 1994).

1.2 Review of Literature

1.2.1 Bone biology

Bone is a complex, highly organized and specialized connective tissue remarkable for its hardness, resilience, characteristic growth mechanism and regenerative capacity. It is important to understand the complex anatomy in detail in order to comprehend the cascade of bone healing in defects and to construct the appropriate bone substitute.

1.2.1.1 Structure of bone

Bone tissue in the adult skeleton is arranged in two architectural forms: Trabecular or cancellous or spongy bone (around 20% of the total skeleton) and cortical or compact bone (around 80% of the total skeleton). The proportions of these two architectural forms differ at various locations in the skeleton (Buckwalter JA *et al.,* 1996). Cortical bone is almost solid, being only 10% porous and can be divided into different subgroups: long bones (femur and tibia), short bones (wrist and ankle) and flat bones (skull vault and irregular bones). Trabecular bone presents higher porosity (50 - 90%), making its modulus and ultimate compressive strength around 20 times inferior than that of cortical bone. It is commonly found in the metaphysis of long bones and in the vertebral bodies. An outer bone sheath called the periosteum covers both cortical and cancellous bone, which is continuous except near the joints and is composed of two layers. The outer layer is fibrous while the inner layer is more vascularised and contains cells that are capable of becoming osteoblasts (Sikavitsas VI *et al.,* 2001).

Cortical bone, responsible for the mechanical and protective function, consists mainly of a number of cylindrical units termed Haversian systems or osteons. Each osteon consists of a central Haversian canal, which contains neurovascular bundle surrounded by 4 -20 concentric lamellae of collagen fibers. Between these lamellae are a number of small spaces termed lacunae where osteocytes are housed and interconnected through long cytoplasmic processes arranged in canaliculi. Cancellous bone has sponge-like morphology with a honeycomb of branching bars, plates and rods of various sizes called trabeculae, accountable for the metabolic function of bone (Sikavitsas VI *et al.,* 2001).

Although bone tissue is populated by a variety of cells, its functional integrity is maintained by three different cell types: osteoblasts, osteocytes and osteoclasts. Osteoblasts are mature and metabolically active bone forming cells whose process can be subdivided into three stages: a) proliferation b) synthesis of collagenous and non-collagenous proteins constituting the osteoid matrix and its maturation and c) mineralization. Osteocytes are mature osteoblasts trapped within the bone matrix which are involved in the control of extracellular concentration of calcium and phosphorous as well as adaptive remodeling behaviour via cell-to-cell interactions in response to local environment. Osteoclasts are multinucleated bone resorbing cells that release hydrolytic enzymes and resorb the organic and inorganic matrices of bone (Buckwalter JA *et al.,* 1996).

1.2.1.2 Biochemistry of bone

Bone is a dense multi-phase material or composite made up of cells embedded in a matrix composed of an organic component (osteoid) (30 - 35% of dry weight) and an inorganic calcium phosphate component (HA) (65 - 70% of dry weight) (Camerson DA 1972). The organic matrix consist of approximately 90% type I collagen and 10% different non-collagenous proteins such as osteocalcin, matrix Gla protein, bone silao protein (BSP), osteopontin and alkaline phosphatase (ALP). Each of non-collagenous proteins is synthesized at each stage of osteoblast differentiation. In general ALP, BSP and Collagen I are early markers of osteoblast differentiation while osteopontin and osteocalcin appear late, parallel with mineralization (Robey PG 1996; Butler WT 2000).

The inorganic matter of bone consists of submicroscopic deposits of a form of calcium phosphate having a similar (not identical) chemical formula of $(Ca_{10}\ [PO_4]_6\ [OH]_2$ and a Ca: P ratio of 1.8 to 3.2 (Fountos G *et al.,* 1997, Tzaphlidou M *et al.,* 2003). The collagenous and non-collagenous proteins in bone matrix are responsible for promoting the initial nucleation and deposition of bone apatite and regulating the orientation, size and growth rate of crystals. After nucleation, amorphous calcium phosphate may be the first precipitate, which is then converted to octacalcium phosphate and finally to HA that give rigidity and strength to the bone (Eanes E 1992).

1.2.1.3 Bone healing process

The molecular and cellular patterns of bone repair after injury are similar to bone formation in an embryo, suggesting analogous mechanisms for the bone formation in adult and embryonic skeletons (Hing KA 2004). The healing of defect can occur in two ways: (a) Direct or primary healing (b) Indirect or secondary healing.

In direct healing, the bone on one side of cortex unites with the bone on other side of cortex to re-establish the mechanical continuity and occur without callus formation. This process occurs by rigid internal fixation and the stability of fracture reduction is ensured by a substantial decrease in interfragmentary strain (Webb JCJ *et al.,* 2000).

Indirect healing occurs with a callus precursor stage and involves three distinct but overlapping stages like (a) the early inflammatory stage (b) the repair stage and (c) the late remodeling stage (Greenbaum MA *et al.,* 1993). In the inflammation stage, haematoma and hemorrhage formation together with the recruitment of inflammatory cells occur at the defect site, which peaks 24 h following the injury and is completed by the first week. The platelets are activated and release growth factors that recruit MSCs and guide their proliferation and differentiation at the defect site. Clinically inflammatory stage is associated with pain, swelling and heat. In the repair stage, stem cells that are stimulated begin to produce new blood vessels, fibroblasts and form granulation tissue (osseous or cartilaginous tissue) in the space between the fracture fragments and later undergo mineralization. This stage lasts for about two weeks and clinically corresponds to the time when clinical union is established. The local environment determines the route of differentiation undertaken by an osteogenic cell to form osseous tissue either through intramembranous ossification (mesenchymal stem cells to osteoblast cells to bone) or through endochondral ossification (mesenchymal stem cells to chondroblasts to bone). High vascularity i.e. the availability of nutrients and oxygen in the surrounding environment is necessary for the nourishment of osteoblast cells while chondroblasts require little or no oxygen for metabolism. Thus based on internal vascular network, the development of bone occurs. In the remodeling stage, the woven bone is transformed into lamellar bone and the process is completed by the return of original shape, structure and mechanical strength of the normal bone. Remodeling of bone occurs slowly over months to years and is facilitated by mechanical stress placed on the bone.

1.2.2 Segmental bone defect- A clinical problem

Bone has the remarkable capacity to heal without scar formation, but this regenerative process fails in patients with large bone lesions or impaired wound healing, requiring clinical intervention. Segmental bone defects are a serious problem where the entire segment of cortical bone is resected and there are often complications such as shortening of the structures, nerve and vascular lesions, cutaneous loss, delayed edema, which can lead to the amputation of the involved member (DeCoster TA *et al.,* 2004). Because of the absence of vascularisation and functional stimulation in these areas and the frequent presence of local infection, the treatment of these lesions is generally complex and has negative long-term impact on patient lives. Segmental bone defect can result from (a) acute trauma (b) chronic infection requiring bone resection (c) chronic non unions due to osteoporosis / osteomyletis / osteogenesis imperfecta / osteosarcoma.

The most common clinical situation of segmental bone defect is the open fracture of long bone due to acute trauma (Bonnevialle P *et al.,* 2003; Giannoudis PV *et al.,* 2003). Open fracture always has some degree of comminution and it is recommended to remove bone fragments that are contaminated and devoid of soft-tissue attachment. Inadequate resection of bone increases the risk of chronic infection because this contaminated devitalized tissue is an excellent medium for infection and the injured blood supply limits the body's local resistance to infection. Some fractures that initially do not have segmental bone loss become complicated by chronic infections and resection of bone are necessary to control the infection.

Chronic non unions can happen due to pathological conditions like osteomyletis or osteoporosis or osteogenesis imperfecta. Osteomyletis is an inflammation or swelling of bone tissue that usually occur as a result of bacterial bloodstream infection, that spreads to the bone (Kocaoglu M *et al.,* 2006). It can also occur from a nearby infection due to traumatic injury or frequent medication injections or surgical procedure. Osteoporosis is a condition characterized by the loss of normal density of bone resulting in fragile bone. This disease represents one of the most common bone disorders currently afflicting human populations and can occur due to hormonal disorders or as a result of medications, specifically glucocorticoids (Mauney JR *et al.,* 2005; Cole ZA *et al.,* 2008). Osteogenesis imperfecta is a

heterogeneous group of genetic disorders characterized by excessive bone fragility and accompanied by skeletal deformities such as osteoporosis. The prevalence of osteogenesis imperfecta within the population is reported at approximately 1 in 15,000 - 20,000 cases per year with incidences occurring within all racial and ethnic groups. The inability of osteoblasts to generate sufficient quantities of structurally normal osseous matrix has been implicated as one of the major causes of skeletal deficiencies observed in these patients (Mauney JR *et al.,* 2005). Osteosarcoma is a type of bone cancer that develops in bone. The exact cause is not known, but it is believed to be due to DNA mutations - either inherited or acquired after birth (Chang DW *et al.,* 2005). These pathologic conditions are very much problematic in aged patients where there is drastic reduction in the number and activity of osteoprogenitor cells (Evans CE *et al.,* 1990) and a decrease in signaling molecules such as estrogen, IGF-I, and TGF-β (Nicolas V *et al.,* 1994) to regenerate bone.

1.2.3 Current treatments for segmental defect

1.2.3.1 Autogenous graft

Autologous bone graft that is bone taken from one part of the patient's own body, has been the gold standard of bone replacement for many years because it provides osteogenic cells as well as essential osteoinductive and osteoconductive elements for healing (Duffy GP *et al.,* 2000; Morsi E 2002). Vascularised bone grafts can be harvested from iliac crest or fibula and have a success rate of 80% to 90% with no risks of immune rejection or disease transfer. As autograft resorbs, re-vascularization attracts mesenchymal-type cells into the area where they differentiate into osteogenic or chondrogenic lineage.

However, the problems with autograft may at times outweigh the benefits. The supply is always limited to fit in the size of defect occur in the long bones of lower limb, e.g. femur and tibia (Abdollahi K *et al.,* 1999). Another major drawback is that the harvesting of autograft requires an additional surgery and this adds a degree of morbidity and may involve massive blood loss, sepsis and pain and an increased risk for the patient (Prolo DJ *et al.,* 1985). With the autograft procedure, the operation time is also prolonged considerably with increased costs. Fracture through the graft has been reported in 25% cases and is most common when the graft begins to resorb without subsequent bone formation or when the graft does not hypertrophy

that may necessitate reparative surgery with additional morbidity (Minami *et al.,* 1993). In one retrospective study (1950 – 1969), it was estimated that with 118 autograft taken from the iliac crest, 6% had minor complaints such as harvest site pain, hypersensitivity and buttocks anesthesia (Cockin J 1971). Younger *et al.*, 1989 examined the medical records of 239 patients and found an overall major complication rate of 8.6% and a minor complication rate of an additional 20.6%. Vail *et al.,* (1996) reported 19% incidence of donor site morbidity in their series of 247 vascularised fibula grafts which includes objective - more weakness, subjective - discomfort in the ankle and other sites in the leg and sensory abnormalities.

1.2.3.2 Allograft

Allograft bone involves harvesting and processing bone from a cadaver and transplanting to a patient. It has been used extensively in the reconstruction of bone defects after tumour excision and is available in abundant supply. But the rate of incorporation of allograft is lower than with autograft (D'Agostino P *et al.,* 2007).

Allograft demonstrates a lower osteogenic capacity and therefore new bone formation may occur at a slower rate. It introduces the possibility of pathogen transfer from donor to host and although infrequent, infections ascribed to donor-host transmission following allografting procedures do occur. Some (Boyce T *et al.,* 1999) have estimated that the risk of human immunodeficiency virus transmission with allograft bone is 1 in 1.6 million populations. Hepatitis B and hepatitis C transmission have also been reported with allograft tissue (Tomford WW 1995; Centers for Disease Control and Prevention 2001, 2002).

1.2.3.3 Distraction osteogenesis

The technique introduced by Russian orthopedic surgeon Gavril Ilizarov is a widely used method of treatment for segmental bone defects (Huang SC 1997; Cattaneo R *et al.,* 1992). In this technique, a corticotomy (cutting of cortical bone into two, leaving intact the medullary vessels and periosteum) is followed by gradual movement of two cut ends of the bone during the distraction phase allowing new bone to form in the gap. The limb is stabilized with a circular external fixator. The common distraction rate for lower limbs is 1 mm per day and if the rate is rapid, the bone pieces will be joined with fibrous tissue rather than osseous tissue.

Besides the positive impact, there is a high chance of traction injury to nerves and other soft tissues. The pin track can become infected and a major neurovascular bundle may be punctured during pin placement. The docking site may need additional bone grafting for bony union This technique requires specialized training and equipment, long treatment durations and it is associated with frequent complications (Green SA *et al.,* 1992; Tomić S *et al.,* 2007).

1.2.4 Necessity for an ideal bone graft

Due to several problems associated with correct therapies and to improve countless lives of patients, demand for an ideal bone graft for the repair of segmental defects has necessitated. The best bone substitutes are naturally those with biomechanical and biological properties most closely resembling those of normal bone.

An ideal bone graft should be (a) Biocompatible (b) osteoconductive (c) osteointegrative (d) osteoinductive (e) osteogenic (Damien CJ *et al.,* 1991). Biocompatible materials do not irritate the surrounding structures, do not provoke an abnormal inflammatory response, do not elicite allergic reactions and do not cause cancer. Osteoconductive materials allow the ingrowth of blood vessels and osteoprogenitor cells from the recipient bed into the implant and this property is found in cancellous autografts and allografts, demineralized bone matrix, HA, collagen and calcium phosphate materials. Osteoinductive materials recruit MSCs located near the graft or from revascularization and induce the differentiation of stem cells into osteoblasts. The process is typically associated with the presence of bone growth factors or cells within the graft material. Osteogenesis is the ability to produce new bone that depends on the presence of live bone cells (osteoprogenitior cells or inducible osteogenic precursor cells) in the graft, which participate in the early stages of healing process and unite the graft material with host bone. This property is found only in fresh autogenous bone and in bone marrow cells.

1.2.5 Bone Tissue Engineering

An important approach to develop an ideal bone graft is to allow natural tissues to regenerate at defect site by providing a structural support for the proliferation and differentiation of cells. Such a regeneration induction can be achieved by a new emerging field of medical science called “Tissue Engineering.” It is defined as “an

interdisciplinary field of research that applies the principles of engineering and life sciences towards the development of biological substitutes that restore, maintain or improve tissue function" (Langer R et al., 1993). It utilizes a 3D porous biomaterial with cells and growth factors to fill the tissue void, to provide structural support and to form tissue with in the body upon transplantation. Thus the triad of tissue engineering consists of (a) 3D biomaterial (scaffold) (b) cells and (c) growth factor, each of these can be used independently or in combination. Among them, the scaffold is main component in determining the ultimate achievement of tissue-engineered graft.

1.2.5.1 Triad of Bone Tissue Engineering

Bone has a 3D configuration that demands a 3D biomaterial that mimics bone morphology, structure and function in order to optimize the integration into surrounding tissue (Temenoff JS *et al.,* 2000; Salgado AJ *et al.,* 2004). The biomaterial should fulfill some essential requirements in order to be recognized as an "ideal material". It should well integrate in the host tissue without eliciting an immune response (biocompatible). It should have interconnected porosity to direct the cells to grow into desired physical form and to support vascularisation of the ingrown tissue. Pore size is a very important issue because if the pores are too small, pore occlusion by the cells will happen that will prevent cellular penetration and neovascularization of the inner area of the scaffold. The optimal pore size ranges between 200 - 400 µm since an average size of human osteon is approximately 223 µm (Holmes RE 1979). Surface properties, both chemical and topographical, are related with the protein adsorption capability of the biomaterial and thus can control and affect cellular adhesion and proliferation (Zhu X *et al.,* 2004). Another important property of concern is degradation, where the degradation rate of biomaterial must be tuned appropriately with the growth rate of neo-tissue (Hutmacher DW 2000). The degradable products from the biomaterial and its effect on body should also be considered for the success of the scaffold. In addition, the scaffold must be sterilizable to prevent infection and the method of sterilization must not interfere with the bioactivity of the material or significantly alter its chemical composition, since this could modify the material's biocompatibility or degradation products.

The second important module of tissue engineering is the cells. Bone contains a variety of cell types: vascular cells, marrow cells, pre-osteoblasts, osteoblasts,

osteocytes, chondroblasts and osteoclasts, all executing distinct cellular functions to allow the bone to work as a highly dynamic organ (Wiesmann HP *et al.,* 2004). All these cells are necessary to build up a 'real' bone, but the application of living osteogenic cells is considered to be sufficient for engineering bone *in vitro*. An ideal cell source should be easily expandable to higher passages, non-immunogeneic and have a protein expression pattern similar to the tissue to be regenerated. Thus better cell source is 'osteoblasts' taken from patient's own body (Salgado AJ *et al.,* 2004; Wiesmann HP *et al.,* 2004). Another alternative is 'adult stem cells', which are undifferentiated cells with a high proliferation capability, being capable of self-renewal, multilineage differentiation and above all, regeneration of tissues.

The third approach in tissue engineering is the use of growth factors together with scaffolds so that it can initiate intracellular signaling that will lead to different events such as cell adhesion, proliferation, migration and differentiation. The most common growth factors that are realistically proposed for bone tissue engineering applications include BMPs, TGF- β, FGF, IGF I and II and PDGF (Salgado AJ *et al.,* 2004). In 1965, Urist discovered that demineralized bone matrix could induce bone formation when placed ectopically in subcutaneous tissue and the capability was attributed to BMPS, which is expressed during the early phases of fracture healing (Urist MR 2002). TGF- β recruit MSCs to the healing site, stimulates osteoblast-like cells to proliferate, promotes collagen production and increases callus formation on the fracture healing site (Zimmermann G *et al.,* 2003). IGF I and II have similar effects on bone metabolism and upon injury they stimulate type I collagen synthesis and increase matrix apposition rates. They also maintain collagen integrity in the bone microenvironment by decreasing collagen synthesis or by increasing the expression of interstitial collagenase by osteoblasts (Jadlowiec JA *et al.,* 2003). FGF is involved in the regulation of the delicate balance between bone forming cells and bone resorbing cells and the development of new blood vessels (Hurley MM *et al.,* 2002). It has also a role on the stimulation of an osteogenic phenotype through the activation of Cbaf-1/Runx 2 nuclear transcription factor. PDGF produced by osteoblasts, platelets and monocytes is believed to have a role in the migration of MSCs to the wound healing site (Khan S *et al.,* 2000).

1.2.5.2 Scaffolds for Bone Tissue Engineering

The scaffolds for bone tissue engineering include metals, polymers and ceramics. Each of these materials has its own advantages and disadvantages.

1.2.5.2.1 Metals

Metals provide strength and toughness that are required in load-bearing parts of the body and these include engineering alloys such as cobalt-chromiun alloys, stainless steel and titanium alloys. Porous-coated vitallium intramedullary rods exosteally bridged 1 cm segmental defects in rabbit tibias (Collier JP *et al.,* 1976). The bioactive titanium cage enhanced the bone repairing process and achieved the torsional stiffness and lamellar bone by 8 weeks in a 1 cm segmental defect in rabbit femur (Shunsuke F *et al.,* 2003). The patients who sustained open Gustilo-Anderson Type IIIB tibia fractures resulted in segmental bone loss was reconstructed successfully with a cylindrical titanium mesh cage packed with a composite of cancellous allograft and demineralized bone matrix putty (Attias N *et al.,* 2006). The cylindrical titanium mesh cage packed and surrounded with a standard volume of morselized canine cancellous allograft and canine demineralized bone matrix facilitated healing of a canine femur diaphyseal segmental defects (3 cm).

Neverthless, the risks of infection and difficulty with the removal of metallic cages are concerns. These implants corrode in an *in vivo* environment, which cause harmful effect on the surrounding tissues and organs (Høl PJ *et al.,* 2008; Singh R 2007). Another crisis is stress shielding, which occur due to higher modulus of elasticity of the metals that prevents the bone from being properly loaded and lead to bone resorption (Hassan MH 2004; Simon JA 1997; Pietrzak WS 1996). Thus the use of metallic implants is of considerable concern for the repair of segmental defects.

1.2.5.2.2 Polymers

The medical use of synthetic polymers has a long history, but there are very few polymers as potential matrices of bone analogues. It include natural polymers (fibrin, collagen, gelatin, hyaluronan) and synthetic polymers (poly (lactic acid) (PLA), poly (glycolic acid) (PGA), poly (lactic-co-glycolic acid) (PLGA). PLGA capsules implanted in a 0.5 cm segmental femoral defect in rats did not show bridging of the defect at 8 weeks after implantation (Isobe M *et al.,* 1999). Four centimeter long diaphyseal

segmental defects in the tibiae of Swiss mountain sheep covered with resorbable membranes from poly (LDL-lactide) did not show bone healing (Gugala Z *et al.,* 1999). Tubular microporous membranes prepared from poly (L/D-lactide) formed fibrous tissue layer at host bone-implant interface while poly(L/DL-lactide) exhibited osteointegration with bone in diaphyseal segmental defects (1 cm) in the radii of mature rabbits (Gogolewski S *et al.,* 2000). When PLGA with similar porosity to human trabecular bone was evaluated for the repair of femoral segmental defect in New Zealand white rabbits, the bone formation index was low (Fialkov JA *et al.,* 2003). PLGA coated gelatin sponge failed to show radiographic union in a 1.5 cm unilateral segmental bone defect created in the ulnar diaphysis of a Japanese white rabbit (Kokubo S *et al.,* 2003). Thus most of the polymers failed to integrate with bone, leading to fibrous tissue formation and inflammation.

1.2.5.2.3 Bioactive ceramics

The third group of scaffolds, bioactive ceramics is the most preferred biomaterial after autograft because of its characteristics to form biologically active HCA layer on the surface of the material upon implantation, providing interfacial bond. Bioactive ceramics include calcium phosphate ceramics like HA and Tricalcium phosphate (TCP) and also Bioglass and A-W glass-ceramics (Wang M 2003).

1.2.6 Calcium phosphate ceramics as scaffolds for Bone Tissue Engineering

Using a synthetic compound that is similar in composition to bone apatite is perceived to be more advantageous for replacing hard tissue. On account of this, synthetic stoichiometric HA has been extensively utilized as a skeletal replacement material (Hench LL *et al.,* 1993). HA is having a definite composition, Ca_{10} $(PO_4)_6(OH)_2$ and has as a theoretical composition of 39.68 wt% Ca, 18.45 wt% P, Ca / P wt ratio of 2.151 and Ca / P molar ratio of 1.667. It possess a hexagonal Bravais lattice and a P63 / m space group with cell dimensions of a = 9.1404 and c = 6.8747 Å. HA possess excellent biocompatibility and osteoconductivity which has been related to their propensity to nucleate HCA crystals. When placed in bone tissue, a gradual change on the ceramic surface occurs that leads to the dissolution of calcium and phosphate ions from HA. This process may either occur through surrounding environment (extracellular fluid) or mediate by osteoclasts. Dissolution

generates increased concentration of calcium and inorganic phosphate in the space between the existing bone and the implant. The precipitation of HA into this space results in a carbonate-containing, calcium deficient hydroxyapatite (HCA) layer at the surface and promotes bonding of the implant with the bone without an intervening fibrous layer (Daculsi G *et al.,* 1990; Tachibana Y *et al.,* 2003).

Another attractive member of the calcium phosphate family is TCP (Ca_3 $(PO_4)_2$), which plays an important role as a bioresorbable bioceramic. Similar to HA, TCP also form HCA layer and has been used for bone repair in the form of blocks or granules (El-Ghannam A 2005).

1.2.6.1 Tissue Engineering approaches with calcium phosphate ceramics

There are three tissue engineering approaches for the healing of bone: (a) Tissue in growth - The biomaterial simply acts as a matrix to encourage the migration and proliferation of cell types from the host tissue to form a new tissue. Thus, healing is dependent upon the contribution from native cells (b) Cell transplantation - The cells are isolated from the patient, expanded *in vitro,* seeded on the biomaterial and transplanted into the defect site and (c) Delivery of bioactive molecules - the growth factors are delivered to the defect site either directly or after encapsulated in the biomaterial (Temenoff JS *et al.,* 2000). Three approaches of tissue engineering with calcium phosphate ceramics for the repair of segmental defects are discussed below.

1.2.6.1.1 Tissue ingrowth

When coralline HA and sintered TCP were evaluated to quantitate the bone ingrowth and biodegradability in the diaphysis of rabbit tibias (0.3 cm in diameter by 0.8 cm in length), bone regeneration was noticed in two scaffolds, but HA did not show appreciable degradation until 24 weeks (Shimazaki K *et al.,* 1985). One study was designed to determine which of the several bone grafting materials would be the most appropriate substitute for autogenous grafts in the treatment of long bone segmental defects. The segmental defect (1 cm in rabbit ulna) was repaired with autogenous iliac crest bone, autogenous cortical bone (ulna), HA, HA-demineralized bone matrix composite graft, freeze-dried bone (allograft) and demineralized bone matrix. The results showed that the demineralized bone matrix and HA-

demineralized bone matrix composite graft is comparable in performance with autograft in mechanical strength and rate of union. On the contrary, freeze-dried bone and HA did not appear to be a suitable material for grafting segmental bone defects (Hopp SG *et al.,* 1989). Another study reported that between 1981 and 1986, HA was used in 45 patients, combined with autologous cancellous bone graft in 38 cases and used alone in seven cases to fill bone defects after removal of bone cysts and in trauma, for long fusions in patients with scoliosis, for non-union in lumbosacral area, for anterior vertebral fusions, in limb sparing operations for malignant bone tumours and in revised operations after failed joint endoprostheses. About 36 patients were reviewed up to sixty months after operation and the results were encouraging with no difference in progress compared with patients in whom simple autologous bone grafts had been used (Heise U *et al.,* 1990). The cylinders of HA, bioactive glass and TCP showed bone-implant union when implanted in tibial segmental defects in sheep at 4 months (Gao TJ *et al.,* 1995). When biocoral and TCP cylinders were implanted in osteotomized sheep tibial defects (1.6 cm in length), better osteointegration and biomechanical performance was observed in biocoral cylinders and seemed to be superior to TCP after 16 weeks (Gao TJ *et al.,* 1997). Porous ceramic cylinders consisting of HA (65%) and β-TCP (35%) showed a radiographic union at the interface between host bone and implants when implanted in the femora (2.1 cm) of adult female dogs. A small amount of trabecular bone formed at the cut ends of the cortex of host bone, but the mid region of defect was filled with fibrous tissue (Bruder SP *et al.,* 1998b). Extensive integration of HA with host bone was detected when implanted in tibial diaphyseal defect (3.5 cm) of adult sheep (Marcacci M *et al.,* 1999). When porous interconnected HA and HA / TCP (60 / 40) ceramics were used in segmental bone defects in rabbits, the densities at the bone-ceramic interface decreased gradually with time indicating its limited application in the treatment of segmental bone defects (Balçik C *et al.,* 2007).

1.2.6.1.2 Cell Transplantation

Eventhough osteoblasts are the preferred cell source, there are very few reports showing the application of calcium phosphate ceramics in combination with osteoblasts for segmental defects. This is because of the limited doubling potential of osteoblasts *in vitro* so that it may be insufficient to rebuild damaged bone tissue in a reasonable time (Salgado AJ *et al.,* 2004). In addition, in certain bone related

diseases osteoblasts may not be appropriate for transplantation because their protein expression profile is below the expected values (Heath CA 2000).

Therefore, the first cell-based attempt for bone tissue engineering was focused on fresh autologous or syngenic bone marrow, a source of osteogenic cells. The addition of autologous bone marrow to HA ceramics did improve healing of a segmental defect (3 cm) in the midshaft of sheep tibia (Wippermann B *et al.,* 1999). The combination of resorbable calcium phosphate ceramics with autologous bone marrow does not provide an alternative for autologous bone grafting in a 3 cm tibial segmental defect (Blokhuis TJ *et al.,* 2000). When a 3 cm segmental defect in the tibia of sheep model was repaired with autologous bone marrow and HA, bony bridging in the defect was enhanced than with HA alone group (den Boer FC *et al.,* 2003). In most of the studies, the addition of bone marrow did not improve bone healing because osteoprogenitors represent only 0.001% of the nucleated cells in adult marrow and it is impractical to obtain sufficient amounts of bone marrow to heal large defects.

The current state of art within bone tissue engineering consists of the combination of culture-expanded MSCs with 3D porous biomaterials. In 1997, Kadyiala *et al.,* showed that MSCs in combination with porous ceramic scaffolds could repair segmental defects (0.8 cm) in the femora of rats in 8 weeks. Human MSCs loaded ceramics were significantly stronger and regenerated bone in segmental defect in the femur of adult athymic rats at 12 weeks (Bruder SP *et al.,* 1998c). Autologous MSCs cultured onto porous ceramic cylinders consisting of HA (65%) and β-TCP (35%) regenerated lamellar bone throughout the defect (2.1 cm) in canine model at 16 weeks (Bruder SP *et al.,* 1998b). The use of autologous BMSCs in conjunction with HA resulted in faster bone repair compared to HA alone when implanted in tibia of sheep model (Kon E *et al.,* 2000). The bone defect (2.1 cm) in the femoral diaphysis of adult dogs was repaired with allogeneic MSCs loaded onto a hollow ceramic cylinder consisting of HA-TCP. Histologically by eight weeks, a callus spanned the length of the defect and at sixteen weeks, new bone had formed throughout the implant (Arinzeh TL *et al.,* 2003). Engineering bones with porous TCP and autologous MSCs in sheep metatarsus were capable of repairing segmental defect (2.5 cm) almost completely at 24 weeks in creep substitution way without progression through a cartilaginous intermediate (Li Z *et al.,* 2005). Highly porous HA

scaffolds loaded with *in vitro* expanded BMSCs depicted new bone from week 8 and was arrested at week 24 (Komlev VS *et al.,* 2006) in immunodeficient mice. Autogenous BMSCs with β-TCP ensured bone formation and vascularisation throughout the defects (3 cm) in the mandibles of the dog (He Y *et al.,* 2007).

1.2.6.1.3 Delivery of bioactive molecules

When bFGF gene modified MSCs seeded on porous β-TCP ceramics and grafted into 1.5 cm segmental bone defect in the radius of New Zealand white rabbits, bone healing was accelerated through capillary regeneration (Guo X *et al.,* 2006). The release of BMP-2 from the encapsulated PLGA / HA composite scaffolds increased the bioactivity of the material leading to improved new bone formation in segmental defects *in vivo* (Fu YC *et al.,* 2008).

1.2.7 Challenges in Bone Tissue Engineering

The main problem encountered in bone tissue engineering is the design of an ideal biomaterial. The degradation nature of biomaterial is an important issue where the degradation rate of material should be in par with the rate of tissue regeneration. If the material degrades faster, it will not support tissue mechanically. Whereas, if the degradation rate of biomaterial is poor, the full repair or function or remodeling of bone could be limited because of long term foreign sequestration in the body. HA is resistant to resorption *in vivo*, which occurs at a rate of 1 - 2% per year (Constantino *et al.,* 1994). On the other hand, TCP was found to resorb within days to weeks *in vitro* and *in vivo* and the bone volume produced will always be less than the volume of TCP resorbed (Holinger JO *et al.,*1996). The biodegradation of TCP and HA relies on solution and osteoclast-mediated mechanisms, both of which are related to implant surface area and surface chemistry (Hing KA 2006). This signifies the importance of the selection of the material with appropriate chemical composition and porosity for the intended application.

Another relevant limitation of many tissue-engineering attempts is the insufficient oxygenation and nutrition of cells and ultimately mass infection in the central portion of the 3D biomaterial after transplantation. *In vivo*, the distance between cells and blood capillaries, which provide nutrients and oxygen and at the same time account for waste elimination, ranges from 20 – 200 µm. *In vitro*, sufficient nutrition and

oxygenation of cells by diffusion is limited to a distance of 100 – 200 µm (Volkmer E *et al.,* 2008). Small pore size of the scaffolds may in fact become a limiting factor for the size of blood vessels and thus restrict blood flow beyond a limit. Thus in large-sized tissue-engineered constructs, a gradient in tissue quality emerge including inhomogeneous cellular proliferation and differentiation from outer areas of the scaffold towards the centre of the constructs (Mastrogiacomo M *et al.,* 2006b; Scaglione S *et al.,* 2008). Therefore the internal architecture of 3D biomaterial is a major aspect that influences vascularisation, which is a dire necessity for the survival of transplanted cells in tissue-engineered constructs.

1.3 Development of hypothesis

The mainstay of this study was to propose a novel 3D bioactive ceramic for the repair of segmental defects. Since synthetic HA is associated with problems like degradation, the modification of the chemical composition of HA was done by incorporating silica with the proposition of improving the properties like osteoconduction, osteointegration and degradation. The material was designed with interconnected open porosity to avoid major limits to vascularisation and neo-bone matrix deposition. This architecture and chemical composition may offer to the cells an osteoconductive surface to adhere, proliferate, differentiate and deposit mineralized matrix and thus allowing in principle an exponential bone ingrowth. The engineering of this biomaterial with MSCs may generate osteoinductive signals at the site of bony repair, equivalent to a true autologous bone-graft. In addition, the delivery of growth factors at the injury site may improve the proliferation and differentiation of indigenous MSCs and direct vascular ingrowth for enhanced bone healing. Thus our focus was on assuring the cytocompatibility and functionality of MSCs on the material *in vitro* followed by its ability to support vascularisation, osteoconduction, osteoinduction and osteointegration *in vivo.* The influence of growth factors on the proliferation and functionality of cells was also studied *in vitro* and *in vivo*.

1.3.1 Scaffold of choice

1.3.1.1 Role of silica in bone physiology

Bone mineral is calcium phosphate based with various substitutions, in particular carbonate ions that are found up to 8 wt% as well as elements such as Na, Mg, K, Sr, Zn, Ba, Cu, Al, Fe, F, Cl and Si that occur at trace levels (< 1 wt%) (Elliot J 1994). These substitutions in the apatite structure play important role in the biological activity and in particular silicon (Si) has found to be essential for normal bone growth and development (Carlisle EM 1972). Si is present at a level of 100 ppm in bone and ligaments and 200 – 600 ppm in cartilage and other connective tissues (Schwarz K 1973). The presence of Si in ECM components implies its role as a biological cross-linking agent that contributes to the architecture and resilience of connective tissues (Schwarz K 1973). Carlisle has demonstrated significant dependence of healthy skeletal development on Si (Carlisle EM 1970; Carlisle EM 1980). In one study, rats raised with Si supplemented diet showed 33.8% increase in growth rate compared to Si deficient animals (Schwarz K *et al.,* 1972). Si was implicated in early biomineralisation process when electron microprobe examination of bones showed Si localized at active calcification sites in the bones of young mice and rats (Carlisle EM 1970). Aqueous Si in the form of orthosilicic acid ($Si(OH)_4$) was able to induce the precipitation of HA from electrolyte solutions even in the presence of proteins that normally inhibits its precipitation (Damen JJ *et al.,* 1992; Tanizawa Y *et al.,* 1995). A recent comparison of dietary Si intake with bone mineral density (BMD) in humans found that BMD was positively and significantly linked to dietary Si intake in men and premenopausal women (Jugdaohsingh R *et al.,* 2004). Studies using dietary supplementation of Si with ovarectomised mice indicate Si has roles in the remodeling process in bone (Nielsen F *et al.,* 2004). Aqueous Si has been shown to enhance osteoblast proliferation, differentiation and collagen production and to have dose dependent effect on osteoclast cells under *in vitro* conditions (Pietak AM *et al.,* 2007).

1.3.1.2 Silica-based biomaterials

Given the significant roles of Si in the enhancement of bone growth, it is not surprising that bioceramics that incorporate Si into their composition demonstrate higher bioactivity. These include materials with high Si levels such as Bioglass and

apatite-wollastonite as well as calcium phosphate based materials with trace levels of Si doping such as Si-HA and Si-TCP. On immersion in body fluids, these materials facilitate three general processes at the interface on the implant side: leaching, dissolution and precipitation. Leaching is characterized by a rapid exchange of sodium or potassium with H^+ and H_3O^+ ions in extracellular fluid, where the process is controlled by diffusion. Network dissolution occurs concurrently by breaking of Si-O-Si-O-Si bonds through the action of hydroxyl (OH) ions and form silicic acid [Si $(OH)_4$]. The hydrated silica (SiOH) undergoes rearrangements by polycondensation of neighboring silanols, resulting in a silica-rich gel layer. In the precipitation reaction, calcium and phosphate ions released from the material together with those from extracellular fluid form an amorphous calcium-phosphate-rich layer on the surface. It later crystallizes to form HCA structure by incorporating carbonate ions (OH^-, CO_3^{2-} or F^-) from the solution. Rapid growth of HCA agglomerates incorporates collagen fibrils that promote bonding with bone (Hench LL *et al.,* 1993; Nordström EG *et al.,* 2001).

Bioglass are melt-derived glasses having the base components of SiO_2, Na_2O, CaO and P_2O_5 in specific proportions. The first and most well studied composition termed Bioglass® 45S5 contains 45% SiO_2, 24.5% Na_2O, 24.4% CaO and 6% P_2O_5, all in weight percent, was introduced by Hench in 1970s (Hench LL *et al.,* 1993). A study comparing *in vivo* bone ingrowth and *in vitro* apatite formation on Na_2O-CaO-SiO_2 glasses illustrated that the depth of bone ingrowth among glass particles increased in proportion to their apatite forming ability *in vitro*. Furthermore, silicate ion substitution stimulated osteoblast-like cell activity *in vitro* when compared to stoichiometric HA (Fujibayashi S *et al.,* 2003). However, Bioglass is not suitable for major load-bearing applications due to its bending strength which is in the range of 40 - 60 MPa. Another drawback is mechanical weakness and low fracture toughness due to an amorphous two-dimensional network (Wang M 2003). Additionally, the presence of Na_2O in Bioglass can cause rapid change in interfacial pH in biological fluids. Very few reports have showed the use of bioactive glass for the repair of segmental defects. The bone formation was observed in a segmental defect created on the radius of adult Black Bengal goats, 3 months post-implantation (Nandi SK *et al.,* 2008). Nova Bone - a synthetic bioactive glass particulate consisting of 45% silicon dioxide, 45% sodium oxide, 5% calcium and 5% phosphate regenerated bone in frontal bone

defect (1 cm x 2 cm) that occurred in a patient due to trauma (Copcu E *et al.,* 2007).

The second group of silicate glasses includes glass ceramics, which is prepared by melting and controlled crystallization method by Kokubo in 1982 (Hench LL *et al.,* 1993). This glass ceramic was named apatite / wollastonite (A-W) after the names of crystalline phases. It is commercially called Cerabone® A-W, which comprises of apatite, wollastonite and residual glassy phase in 38, 34 and 28 wt% respectively. The composition of glassy phase estimated to be MgO 16.6, CaO 24.2 and SiO_2 59.2 wt% (Hench LL *et al.,* 1993). The bioactivity of glass ceramics is much higher than that of sintered HA (Wang M 2003). They are being used as space fillers in the iliac crest, as vertebral and as posterior lumbar fusion body cages. The applications of glass ceramics are limited for the repair of segmental defects because they are not as strong as biostable ceramics. One study has showed the use of glass-ceramic in a segmental defect (1.6 cm) in the tibia of the rabbit where a calcium-phosphorus layer without interposition of soft tissue was observed at the interface (Kitsugi T *et al.,* 1989).

The third group is Si-substituted calcium phosphate ceramics. Two main examples are Si-HA and Si-α-TCP. The single-phase Si-HA materials are manufactured commercially by Apatech Ltd. under the trade name ActifuseTM and multiphase Si-α-TCP by Millennium Biologix Corporation under the trade name SkeliteTM (Pietak AM *et al.,* 2007). The synthesis of Si-HA and Si-α-TCP has focused on wet chemical methods where Si is introduced as a chemical carrier from tetraethyl or propyl ortho-silicate (TEOS or TPOS). The phase composition of the materials are highly dependent on Ca / (P+Si) and Ca / P ratio of the system, the level of Si addition, the method of introducing Si to CaP and sintering conditions, most notably the sintering temperature. Silica substituted materials increased the bioactivity even in the presence of inhibitors to calcium phosphate precipitation (Damen JJ *et al.,* 1992). The time required for forming the spontaneous precipitation of HCA layer decreased with increasing silicate ion substitution in simulated body fluids (Porter AE *et al.,* 2004a; Porter AE *et al.,* 2004b). An *in vivo* study comparing the biological activity of Si-HA and HA granules reported a 14.5% increase in bone ingrowth in Si-HA versus HA controls (Patel N *et al.,* 2002). In addition to enhanced bioactivity, silica based ceramics degrade faster than HA. A preferential release of silicate ions from Si-HA was demonstrated since the incorporation of silicate ions into HA lattice would distort

and destabilize the structure, therefore making silicate ions to dissolve energetically favorable from HA (Pietak AM *et al.,* 2007). In addition, Si-TCP and Si-HA materials supported the development of osteoclasts from mononuclear precursors and thereby lead to the resorption of the material by these cells (Botelho CM *et al.,* 2006). Even if ActifuseTM and SkeliteTM have many positive qualities, they are usually prepared as granule formats, which is not intended to use for bone defects in load bearing areas (Pietak AM *et al.,* 2007). Nevertheless, one study has showed that Si-TCP promoted the repair of a segmental defect in sheep model (4.5 cm) and after 2 years, the material was completely resorbed with the regeneration of highly mineralized lamellar bone (Mastrogiacomo M *et al.,* 2006a).

1.3.2 Cell of choice

1.3.2.1 Mesenchymal stem cells

In bone tissue engineering, there has been special interest in stem cells located in the bone marrow known as mesenchymal stem cells. The idea that bone marrow contained some kind of osteogenic precursor cells started in 1963, when Petrakova showed that by implanting pieces of bone marrow under the renal capsule, it was possible to obtain an osseous tissue. Almost 20 years later, Caplan gave these cells the name they have today, mesenchymal stem cells (Caplan AI 1991). MSCs have been isolated from various tissues, including bone marrow, fat, umbilical cord blood, and even peripheral blood and among them bone marrow is the most preferred source. These cells can be cultured and expanded *in vitro* and can differentiate into bone, cartilage, fat, muscle, skin, tendon and other tissues of mesenchymal origin, through what is called "The Mesengenic Process" (Caplan AI 2005). The multipotency of MSCs has been further exemplified by the observation that after the transplantation of these cells into a host animal, an ectopic ossicle consisting of osteoblastic, adipogenic and chondrogenic tissue phenotypes has been developed (Mauney JR *et al.,* 2005).

The deployment of MSCs have been reported for many bone regeneration studies. Previous works have demonstrated that MSCs alone can be used in the repair of bone (Pelled G *et al.,* 2002; Mauney JR *et al.,* 2005). But if a defect is filled with MSCs alone, it require a great many of MSCs and it is difficult to keep MSCs in the defect region, which will ultimately lead to the formation of connective tissue than

true bone (Turgeman G *et al.,* 2001). For this, MSCs have been combined *ex vivo* with 3D porous ceramics which has been demonstrated to enhance their osteogenic capacity by accelerating bone formation and osseointegration (Bruder SP *et al.,* 1998a; Warren SM *et al.,* 2004).

Although the implantation of MSC-seeded biomaterials has shown to significantly increase skeletal repair, additional *in vitro* culture methods have been developed that promote osteogenic differentiation of MSCs *in vitro* in lieu of *in vivo* incorporation. For example, precultivation of MSCs on HA constructs in the presence of osteogenic supplements including dexamethasone, ascorbic acid and β-glycerophosphate prior to implantation not only fostered an increased rate of *in vivo* osteogenesis but also the level of osteogenic markers, which was comparable to those seen in autologous cancellous bone. Those cell-loaded ceramics succeeded in creating bone formation in rats (Bruder SP *et al.,* 1998c), dogs (Arinzeh TL *et al.,* 2003) and sheep (Kon E et *al.,* 2000). β-TCP loaded with osteogenically induced autologous BMSCs have repaired goat tibial defects (2.6 cm) completely and attained mineral density similar to normal bone at 32 weeks post-implantation when compared to material alone (Liu G *et al.,* 2008).

1.3.3 Signaling molecules of choice

1.3.3.1 Platelet-rich plasma

It is expected that the biological effect of multiple growth factors on the enhancement of tissue regeneration and repair is greater than that of a single growth factor. However, the cost of almost all genetically engineered growth factors is prohibitively high and dilemma exists about their safety in human administration (Calabresi PA *et al.,* 1998). Alternately PRP, which is a rich source of platelets, is a proven source of many growth factors like PDGF, TGF-β, VEGF and IGF-I (Anitua E *et al.,* 2007). The local delivery of a wide range of growth factors and proteins in PRP serve as osteoinductive matrix for bone formation (Anitua E *et al.,* 2006). Segmental bone defects (1 cm) created in the mid-upper part of bilateral radius of New Zealand white rabbits were entirely healed after 12 weeks when filled with artificial bone and PRP (Zhang CQ *et al.,* 2004). Demineralized bone and cancellous chip grafts clotted with PRP showed more mature bone when implanted in a 2.1 cm long osteoperiosteal femoral defect in canine model (Brodke D *et al.,* 2006). The bilateral implantation of

polycaprolactone-TCP composite with PRP into 0.8 cm rat femoral defects accelerated early vascular ingrowth and improved longer-term functional integration when compared to a group without PRP after 3 weeks (Rai B *et al.,* 2007).

The therapeutic osteogenic effect of local platelet administration depends on the amount of delivered growth factors. The growth factors are released from platelets when they are activated with triggering agents like bovine thrombin or calcium chloride. However the use of bovine thrombin has been reported to be associated with the development of antibodies to factor V and XI, which can result in the risk of life threatening coagulopathies (Landesberg R *et al.,* 1998). Consequently, the effect of PRP on the healing of segmental bone defects without using any triggering agents remains a challenging question.

1.3.3.2 Fibrin glue

Fibrin glue is a biopolymer matrix commonly used for surgical homeostasis and tissue sealing and is known to be critical in the normal wound healing process (Jackson MR 2001; Albala DM 2003). Commercially, fibrin is manufactured for clinical use as a two-component system consisting of thrombin and fibrinogen cryoprecipitated from blood plasma, which also contains smaller amounts of many growth factors like TGF-β, bFGF, EGF and VEGF (Ho W *et al.,* 2006). *In vitro* studies indicate that FG can support the growth, migration and differentiation of several cell types: MSCs (Bensaïd W *et al.,* 2003), endothelial cells (Sporn LA *et al.,* 1995) and fibroblast cells (Meana A *et al.,* 1998). The ease of cell and growth factor delivery with FG has heightened its potential in bone repair applications. When fibrin was used as an injectable delivery vehicle, heterotopic bone formation was observed with a fibrin-cell-periosteal ECM system on the dorsum of athymic mice (Isogai N *et al.,* 2000). Different biomaterials such as coral, bone-derived materials, bioactive glass ceramics and synthetic calcium phosphate have been mixed with FG, resulting in a significant positive effect on osteointegration and bone colonization (Le Guéhennec L *et al.,* 2004). The osteoinductive potential of fibrin has been implicated based on a study with FG and calcium phosphate calcium silicate system, where new bone formation was observed at an extraskeletal site (muscle) in mice at day 15 (Abiraman *et al.,* 2002). Similar results were obtained by Yamada *et al.*, (2003) with the association of β-TCP-FG-MSC at 8 weeks in heterotopic sites in rats.

1.3.4 Animal models

Appropriate animal models are required to assess the clinical outcome of bone tissue engineering. In general, the best model system is the one which most closely mimics the clinical situation for which this technology is being developed (Einhorn TA 1999). Most bone related research conducted to date has been in rats (Bruder SP *et al.,* 1998c), rabbits (Hagino T *et al.,* 1999), dogs (Bruder SP *et al.,* 1998b) or goats (Zhu *et al.,* 2006). Several factors that affect the choice of an animal model include the biology and anatomy of the animal model; the age of the animal and the spontaneous healing potential of the investigated animal (Holy CE *et al.,* 2000). Larger animals like goat or sheep show bone growth and remodeling similar to that observed in humans and are preferable for such studies. Smaller animals such as mice or rats rarely exhibit lamellar cortical bone remodeling and are adequate for studying initial bone formation. Age of the animal is another factor that determines the success of tissue engineering strategy because bone growth and remodeling diminish as age increases (Quarto R *et al.,* 1995). Size of the defect is another important issue since it is related to the healing properties of the implants. In segmental defect, the entire segment of cortical bone is resected and the bone at either end of the defect is immobilized using a fixation nail or plate to avoid the movement from either bone end. If the fixation is improper, the movement of bone pieces may occur, which result in non-union regardless of the dimensions of the size of the defect (Hollinger JO *et al.,* 1990).

Ectopic or extraskeletal implantation refers to the implantation of the material in a different tissue other than skeletal site. It helps to observe whether the scaffold has osteoinductive property in sites devoid of osteoprogenitor cells and adequate porosity for tissue and blood vessel-in-growth. Muscle and subcutaneous tissues are the most common implantation sites for osteoinductive bioassays. Rats and mice are the most preferred animal for this purpose. Goshima *et al.,* (1991) were the first to demonstrate new bone deposition in porous bioceramic scaffolds seeded with cells when implanted subcutaneously into immuno compromised mice.

Osteoproductive properties in general and osteoconduction in particular, are evaluated in orthotopic sites. Goats are suitable models for large animal studies because they allow implantation of large fixation devices and their bone metabolism

is similar to that of humans (Simmons DJ 1976). The healing of segmental defect (2.5 cm) created in the goat's femur has recently been characterized using corals as scaffold of choice (Zhu *et al.,* 2006).

1.4 Objectives

The focus of this study was to propose a novel biomaterial having the dual benefits of HA and Si for the repair of segmental defect in goat model. The material comprised of a porous HA dipped in silica sol to get a coating layer of silica over HA and named as Triphasic ceramic coated hydroxypatite (HASi). The physicochemical characterization of HASi was initially done in comparison with HA. Tissue-engineered constructs were fabricated *in vitro* using uncoated / PRP / FG coated HA and HASi (separately) in combination with BMSCs / osteogenic induced BMSCs (OS+ cells) to elucidate the influence of each of these components on cellular behaviour. The vascularisation and osteoinductive property of tissue-engineered HA and HASi in comparison with bare HA and HASi (without cells) was determined by placing these materials at an extraskeletal site of rat model. Finally the ability of bare and tissue-engineered HASi to regenerate bone in par with material degradation was studied by creating a segmental defect (2 cm) in the femur of the goat model.

To achieve this goal, the study objectives were divided into three phases -

Phase I: Physicochemical characterization of bioactive ceramics, which includes:

- Synthesis and characterization of HASi in comparison with HA
- Degradation studies of HASi in comparison with HA
- Cytotoxicity and cytocompatibility studies of HASi and HA

Phase II: Evaluation of tissue-engineered constructs *in vitro* - Platelet-rich plasma / fibrin glue coated and uncoated bioactive ceramics in conjunction with BMSCs, which includes:

- The isolation, characterization and osteogenic differentiation of goat BMSCs
- The proliferation and differentiation potential of goat BMSCs in several passages

- The fabrication of tissue-engineered construct using HA and HASi in combination with BMSCs and OS+ cells separately (goat and human cells) and the evaluation of cellular responses in terms of viability, proliferation, morphology and osteogenic differentiation for a culture period of 28 days.
- The coating of PRP and FG on HA and HASi separately and the evaluation of the behaviour of goat OS+ cells on coated materials in comparison with uncoated HA and HASi for a culture period of 28 days.

Phase III: Evaluation of tissue-engineered bioactive ceramics *in vivo* - Extraskeletal and orthotopic implantation, which includes:

a) Extraskeletal (muscle) implantation studies in rat model

- The fabrication of tissue-engineered constructs in *vitro* using HA and HASi in combination with rat OS+ cells and the evaluation of cellular responses in terms of viability and osteogenic differentiation for a culture period of 7 days.
- The evaluation of vascularisation potential of bare (without cells) and tissue-engineered (with cells) HA and HASi.
- The evaluation of osteoinductive potential of bare (without cells) and tissue-engineered (with cells) HA and HASi.

b) Orthotopic (femur) implantation studies in goat model

- The fabrication of tissue-engineered constructs *in vitro* using HA and HASi in combination with goat OS+ cells for a culture period of 7 days.
- The validation of the ability of tissue-engineered HASi (with cells and PRP) in comparison with bare HASi (without cells and PRP) to regenerate bone and to undergo degradation in a segmental defect (2 cm) created in the femur of goat model.

Methods adopted for achieving the objectives are described in chapter 2 and the results are illustrated and discussed in chapters 3, 4 and 5. The results are summarized with conclusions in chapter 6.

CHAPTER 2

MATERIALS AND METHODS

2.1 Materials

Hydroxyapatite (HA) and Triphasic ceramic coated hydroxyapatite (HASi), synthesized as part of ongoing developmental programme of Bioceramics Laboratory, SCTIMST, Trivandrum, India, were gifted for this study.

2.1.1 Material Synthesis

2.1.1.1 Synthesis of HA

Hydroxyapatite powder was synthesized by wet precipitation method involving calcium nitrate and ammonium dihydrogen phosphate in the stoichiometric proportion at a pH of 11 and a temperature of 80°C. The precipitated HA powder was freeze dried and washed with distilled water to get rid of surface impurities such as nitrate and ammonium ions. HA powder having particle size less than 125 microns was mixed with aqueous solution of poly vinyl alcohol and gluteraldehyde solution and stirred for 30 min. To the resulting frothy slurry, benzoyl peroxide dispersed in benzene and N, N- dimethyl aniline were added and stirred for thorough mixing. The resulting frothy and viscous slurry was poured into plastic moulds and allowed to dry at room temperature. After drying, the blocks were biscuit fired at 300°C for 1h to remove the binder and then sintered at temperature between 1100℃ and 1300℃ for 1h to get porous HA.

2.1.1.2 Synthesis of HASi

Hydroxyapatite powder was synthesized by wet precipitation method involving calcium nitrate and ammonium dihydrogen phosphate in the stoichiometric proportion at a pH of 11 and a temperature of 80°C. The precipitated HA powder was freeze dried and washed with distilled water to get rid of surface impurities such as

nitrate and ammonium ions. HA powder having particle size less than 125 microns was mixed with aqueous solution of poly vinyl alcohol and gluteraldehyde solution and stirred for 30 min. To the resulting frothy slurry, benzoyl peroxide dispersed in benzene and N, N- dimethyl aniline were added and stirred for thorough mixing. The resulting frothy and viscous slurry was poured into plastic moulds and allowed to dry at room temperature. After drying, the blocks were biscuit fired at 300°C for 1 h to remove the binder and sintered at temperature between 1100°C and 1300°C for 1 h to get porous HA. These blocks were then dipped in silica sol prepared by the hydrolysis of TEOS in ethanol-water system for 1 min (sol gel method) and sintered at 1200°C for 2 h to get a coating of silica over HA. In order to determine the mass percentage of silica coated on HASi, the material was treated with HCl that dissolve Ca and P totally. The mass of HASi before and after treating with HCl was measured and found to be approximately 15 – 17 % silica.

2.1.2 Material sterilization

HA and HASi were polished in the form of discs in specific dimensions required for each experiment. The discs were washed with distilled water and subjected to ultrasonic cleaning (Cole parmer) (5 times, 10 min each) for the complete removal of fine powders adhered over the surface. The materials were then sterilized by steam sterilization method (121°C temperature and 15 psi pressure for 15 min) prior to *in vitro* and *in vivo* experiments.

2.1.3 Physicochemical characterization of Materials

2.1.3.1 Microstructure of HASi

HASi disc was fractured and the outer and inner areas were examined under environmental scanning electron microscope (ESEM) (FEI Quanta 200) at higher magnification in order to distinguish the microstructure in these areas.

2.1.3.2 Elemental analysis

HASi disc was fractured; outer and inner areas were examined under ESEM (FET Quanta 200) and the elements present in these areas (Ca, P and Si) were differentiated with energy dispersive x-ray spectroscopy (EDS) (OXFORD X-ray microanalysis software). The Ca / P ratio in HA and HASi was calculated to verify the phase or elemental purity during the preparation of materials.

2.1.3.3 Phase analysis

The phase analysis and crystallinity checkup of HA and HASi were done by x-ray diffraction technique (XRD). The materials were scanned between 20° and 40° 2 θ at a rate of 2° per minute under a step size of 0.02° using Cu-Kα1 radiation at a voltage of 40 kV and a current strength of 30 mA (Siemens D-5005). For this experiment, HASi was specifically prepared in dense form (without porosity), in order to differentiate the phases present in the outer and inner areas. Thus the surface of HASi disc was scanned firstly. The outer layer was then removed by grinding and thereafter the core of HASi was analyzed.

2.1.3.4 Functional groups studies

Fourier Transform Infrared Spectroscopy (FTIR) analysis was conducted on Thermo Nicolet 5700 spectrometer and the spectra were collected in diffuse reflectance (DRIFT) mode to determine the functional groups. HA and HASi were powered and mixed with optical grade KBr powder. The spectra were recorded at a resolution of 4 cm^{-1} and scanned between 400 to 4000 cm^{-1} with an average scan of 200. Pure KBr was used as the background.

2.1.3.5 Porosity studies

2.1.3.5.1 Scanning electron microscopy

HA and HASi discs were gold coated in an ion sputter (Hitachi E101) and examined for the microstructure, including porosity and morphology by scanning electron microscope (SEM) (Hitachi S2400).

2.1.3.5.2 Mercury Intrusion Technique

The porosity of HA and HASi was once again confirmed with mercury intrusion technique (Quantachrome, Pore Master®33). A few discs of known weight were loaded in the penetrometer cell of the equipment, evacuated and the mercury was filled under pressure. The volume of the mercury intruded was measured as a function of pressure. The total porosity and the percentage of open porosity were evaluated from the total volume of Hg intruded. The bulk density of the samples were also calculated from the differences in weight between empty cell filled with Hg and cell with sample filled with Hg.

2.1.3.6 Mechanical property

HA and HASi (n=10) were polished in the form of cylinders (2 cm height and 1 cm diameter) as per ASTM D 882-97 procedure. The compressive strength was analyzed using Universal Testing Machine (Instron Corporation Series IX Automated Materials Testing System) at a crosshead speed of 1 mm / min and full scale load range of 5 kN. Mean and standard deviation of stress at maximum was measured and expressed in megapascal (MPa).

2.1.4 *In vitro* degradation studies

HA and HASi were characterized for *in vitro* degradation as per ISO standard 10993-13. Accelerated degradation test (incubation temperature at 60℃) and real-time degradation test (incubation temperature at 37℃) were separately conducted. For this experiment, HA and HASi (n = 4) were polished in the form of blocks (1 cm x 1 cm); immersed in 10 ml phosphate buffered saline (PBS) and incubated at 37℃ and 60℃ for 60 days separately. The materials were then examined for phase composition and functional groups by XRD and FTIR respectively.

2.1.4.1 X-Ray Diffraction technique

HA and HASi blocks immersed in PBS were washed with deionised water (5 times), dried at 100℃ for 2 h and scanned for XRD as explained in section (2.1.3.3). The spectra of these materials were compared with raw HA and HASi (materials before immersed in PBS).

2.1.4.2 Fourier Transform Infrared Spectroscopy

HA and HASi blocks immersed in PBS were washed with deionised water (5 times), dried at 100℃ for 2 h, powdered and scanned for FT IR as explained in section (2.1.3.4). The spectra of these materials were compared with raw HA and HASi (materials before immersed in PBS).

2.1.5 Cytotoxicity and cytocompatibility studies with cell lines

The cytotoxicity and cytocompatibility studies of HA and HASi was done using L929 mouse fibroblast cell line and human osteoblast (HOS) cell line, provided by National Centre for Cell Sciences (NCCS), Pune, India. For this experiments, HA and HASi were polished in the size of 4 mm diameter and 2 mm thickness.

2.1.5.1 Cytotoxicity studies (Direct contact method)

In vitro cytotoxicity test was done as per ISO standard 10993-5 using L929 mouse fibroblast cell line after direct contact with HA and HASi. The cells were seeded (1 x 10^3 cells / well) in 24 well tissue culture polystyrene (TCPS) plates (Nunc) enriched with minimal essential medium (MEM) with 10% fetal bovine serum (FBS), 100 units / ml of penicillin and 100 µg / ml streptomycin (Sigma chemicals) and incubated at 37°C in humid atmosphere and 5% CO_2. When the cells attained confluency, sterilized HA and HASi disc were placed in direct contact with cells and incubated for 48 h under the same condition. Negative (ultra high molecular weight poly ethylene) and positive (copper) controls were used. After 48 h, the cells were observed under phase contrast microscope (DMIS, Leica) for any change in morphology or any other cytopathic effects when compared to negative and positive controls.

2.1.5.2 Cytocompatibility studies

HOS cells (1 x 10^3 cells / material) were seeded on the surface of HA and HASi blocks and maintained in MEM with 10% FBS, 100units / ml of penicillin and 100 µg / ml streptomycin and incubated at 37°C in humid atmosphere and 5% CO_2 for 48 h. The cell-cultured materials were fixed in 1% gluteraldehyde in Sorensen phosphate buffer (pH 7.4); rinsed with PBS; dehydrated in a graded ethanol series (30% ethanol for 10 min - 2 changes, 50% ethanol for 10 min - 2 changes, 70% ethanol for 10 min - 2 changes, 90% ethanol for 15 min - 2 changes and 100% ethanol for 15 min - 2 changes); critically point dried (Hitachi HCP-2), gold sputtered in vacuum (Hitachi E101) and examined by means of secondary imaging under 15 kV SEM (Hitachi S 2400).

2.2 Fabrication and evaluation of tissue-engineered constructs *in vitro*

The experiment was completed as two parts. In the first set of experiments, tissue-engineered constructs were fabricated by culturing BMSCs and OS+ cells on HA and HASi (goat and human cells separately). In the second set of experiments, HA and HASi were coated with PRP and FG separately and cultured with goat BMSCs. For these experiments, the materials were polished in the form of discs having 5 mm diameter and 5 mm thickness.

2.2.1 Culturing of goat bone marrow-derived mesenchymal stem cells

MSCs were isolated from the bone marrow of goat model. The mesenchymal origin of these cells was determined through markers like vimentin, CD34, CD44 and also through their ability to differentiate into osteoblasts. The proliferation and differentiation potential of BMSCs in different passages were also studied.

2.2.1.1 Isolation

As per the guidelines of the Institutional Animal Ethics Committee (IAEC) and Committee for the Purpose of Control and Supervision of Experiments on Animals (CPCSEA), goat bone marrow aspiration was conducted. BMSCs were isolated from the metaphyseal end of the humerus of adult goat weighing around 23 - 25 kg. With the animal under anesthesia, bone marrow biopsy of approximately 10 ml was aspirated using a bone marrow needle rinsed with 5000 IU / mL heparin and collected in a tube containing cell culture medium (α-MEM with 10% FBS, 200 units / ml of penicillin and 200 µg / ml of streptomycin) (Gibco, India). Clumps of cells were gently broken using 18 guage needle and centrifuged at 500g for 10 min. The pellet of cells were incubated in 5 ml α-MEM with 10% FBS, 100 units / ml of penicillin and 100 µg / ml of streptomycin at 37°C in humid atmosphere and 5% CO_2 in 25 cm^2 TCPS flask (Nunc, India). The medium was changed after 3 days to remove non-adherent cells and subsequently renewed twice a week. After 10 days in primary culture, the adherent goat BMSCs (gBMSCs) were released with 0.25% trypsin-EDTA (Gibco, India) for 5 min and centrifuged at 300g for 10 min. The cells were subcultured and passaged for the experiments.

2.2.1.2 Characterization of gBMSCs

2.2.1.2.1 Actin and nuclear staining

gBMSCs (1 x 10^4 cells in passage 2) after culturing for 48 h on glass cover slips (Blue star India) were washed with PBS and fixed with 3.7% paraformaldehyde in Sorensen phosphate buffer. The fixed cells after washing with PBS were permeabilised using 0.1% Triton X-100 for 5 min (Sigma Chemicals) in PBS. After washing three times with PBS, the cells were stained with rhodamine-phalloidin (1: 1000 in PBS) (Sigma chemicals) for 30 min and Hoechst 33258 for 1 h (1: 500 in PBS) (Sigma chemicals) in dark at room temperature for determining actin filament

(red) and nucleus (blue) respectively. The cells were then washed thoroughly with PBS and viewed under fluorescent microscope (Nikon Eclipse E600).

2.2.1.2.2 Vimentin staining

gBMSCs (1 x 10^4 cells in passage 2) after culturing for 7 days on glass cover slips (Blue star, India) were washed with PBS; fixed with 3.7% paraformaldehyde in Sorensen phosphate buffer; washed with PBS and blocked with 3% hydrogen peroxide (DakoCytomation LSAB ® + Kit, Peroxidase, USA) for 5 min to prevent non-specific binding. The primary antibody (mouse monoclonal anti-vimentin (Clone V9, Dako, Denmark) at a dilution of 1: 100 in 3% bovine serum albumin (BSA) was added overnight followed by incubation with peroxidase conjugated secondary antibody (DakoCytomation LSAB ® + Kit, Peroxidase, USA) for 30 min. It was then stained with DAB (3,3'-diaminobenzidine) chromogen solution for 5 min and counter stained with hematoxylin for 30 sec with washing in ammonium water. The cells were viewed (DAB -vimentin positive region (brown) and hematoxylin - nucleus (blue) under Light microscope (Nikon Eclipse E600).

2.2.1.2.3 Flow cytometric analysis of CD34 and CD44

gBMSCs (1 x 10^5 cells in passage 2) were cultured on 6 well TCPS plate (Nunc) for 48 h; washed with PBS; trypsinized with 0.25% trypsin-EDTA for 5 min and centrifuged at 300g for 10 min. The pellet was fixed with 3.7% paraformaldehyde in Sorensen phosphate buffer for 20 min, washed with PBS and centrifugation at 300g for 10 min at 4℃. The pellet was blocked with 3% B SA (50µl) in PBS for 30 min followed by washing with PBS and centrifugation. The pellet was then incubated with FITC labeled CD34 (1: 50 in 3% BSA) and phycoerythrin (PE) labeled CD44 (1: 50 in 3% BSA) (BD Biosciences, USA) for 1 h and the intensity of fluorescence was recorded under flow cytometry (BD Biosciences, FACS Aria). gBMSCs without staining, but trypsinized, fixed and washed under the same conditions were used as the control.

2.2.1.3 Osteogenic differentiation of gBMSCs

gBMSCs (1 x 10^4 cells in passage 2) were cultured in α-MEM with 10% FBS for 24 h in order to facilitate the cell adhesion and spreading. After 24 h, the cells were induced to differentiate into osteogenic lineage (gOS+ cells) by maintaining in

osteogenic medium (α-MEM with 15% FBS, 10 mM β-glycerophosphate, 10^{-8} M dexamethasone, 0.05 mg / ml L-ascorbic acid (Sigma chemicals), 100 units / ml of penicillin and 100 µg / ml of streptomycin). The osteogenic differentiation was confirmed through ALP activity, collagen, calcium and phosphorous staining.

2.2.1.3.1 Alkaline Phosphatase activity

The ALP activity of cells after 48 h (24 h in osteogenic medium) was determined with ELF-97 endogenous phosphatase detection kit (Invitrogen). After fixing in 3.7% paraformaldehyde in Sorensen phosphate buffer for 20 min, the cells were washed with PBS; permeabilised with 0.2% Triton X-100 in PBS for 5 min and blocked with 3% BSA in PBS for 30 min. The cytoskeletal actin filaments were stained with FITC-phalloidin (1: 100 in PBS) (Sigma chemicals) for 30 min. The cells were then stained with ELF-97 phosphatase substrate (component A was diluted 20 fold with component B (buffer) in detection kit) for 5 min and visualized through Hoechst filter of fluorescent microscope (Leica DM 6000).

2.2.1.3.2 Collagen staining

gOS+ cells after 28 days were fixed in 3.7% paraformaldehyde in Sorensen phosphate buffer for 20 min. After washing with PBS, the cells were incubated in Bouin's solution at 56℃ for 5 min; cooled in tap water at 18 - 20℃ and stained with Wright's hematoxylin for 5 min. It was then washed with schott's tap water and stained with trichrome stain for collagen (Sigma chemicals) for 5 min. The cells were again washed with distilled water; incubated with 0.5% glacial acetic acid for 1 min followed by washing with PBS, clearing in xylene, mounting in DPX and viewing under Light microscope (Nikon Eclipse E600).

2.2.1.3.3 Calcium staining

gOS+ cells after 28 days were fixed in 3.7% paraformaldehyde in Sorensen phosphate buffer; washed with PBS and stained with 1% alizarin red in α-MEM (Sigma chemicals) and xylenol orange (75 µg / mL α-MEM) (Sigma chemicals) separately for determining calcium. It was then viewed under Light microscope and fluorescence microscope (Nikon Eclipse E600) for assessing alizarin red and xylenol orange staining respectively.

2.2.1.3.4 Phosphorous staining

gOS+ cells after 28 days were fixed in 3.7% paraformaldehyde in Sorensen phosphate buffer; washed with distilled water; stained with 5% silver nitrate (Merck, India) in distilled water and exposed to ultraviolet light for 5 min. The cells were then thoroughly washed with distilled water, air dried and viewed under Light microscope (Nikon Eclipse E600).

2.2.1.4 Proliferation potential of gBMSCs

The effect of passage number on the proliferation potential of gBMSCs was determined in this study. gBMSCs of passage number 1 to 10 were seeded (1 $x10^4$ cells) separately in 25 cm^2 TCPS flasks (n=3) and maintained for 4 days. The cells were trypsinized with 0.25% trypsin-EDTA for 5 min and centrifuged at 300g for 10 min. The pellet was suspended in 1 ml medium; stained with trypan blue (Sigma chemicals) (10 µL cell suspension and 90 µL trypan blue) for assessing viability and manually counted using hemocytometer. The number of cells within the central counting area of hemocytometer was multiplied with 10^5 to obtain the actual number of cells in the suspension.

2.2.1.5 Differentiation potential of gBMSCs

The effect of passage number on the differentiation potential of gBMSCs (osteogenic differentiation) was evaluated through ALP activity, based on the hydrolysis of p-nitrophenyl phosphate (Sigma chemicals) to p-nitrophenol. For this, gBMSCs of passage number 1 to 6 were seeded ($1x10^5$ cells) separately on 6 well TCPS plates (n=3) and maintained in osteogenic medium for 7 days. The cells were washed with PBS twice and kept in -80℃ until analysis. Frozen cell samples were thawed for 20 min on ice and lysed with 300 µl 1% Triton X-100 for 50 min with sonication for 10 min. The cell lysate (25 µl) was added to 125 µl of ALP reaction buffer (Sigma chemicals) and the mixture was incubated at 37℃ fo r 30 min. 1 M NaOH was added to stop the enzymatic reaction. After centrifugation at 16,000 g for 10 min, 170 µl of supernatant was transferred to a microtiter plate and the absorbance was read at 405 nm (Erba Chem -7). A calibration line was constructed from different concentrations of p-nitrophenol. The ALP activity measured from each samples was related to the cell number in order to calculate the specific ALP activity.

The cell number was calculated by Picogreen® dsDNA Quantitation reagent (Molecular probes). The cell lysate (10 µl) prepared above was mixed with picogreen in Tris-EDTA buffer (190 µl) for 5 min and the intensity of fluorescence was measured with a multifunction microplate reader (Infinite F200, Tecan) at an excitation and emission wavelength of 485 / 535 nm. Relative fluorescence units were correlated with cell number using a calibration line constructed with increasing concentration of cells`.

2.2.2 Culturing of gBMSCs and osteogenic induced gBMSCs on bioactive ceramics

gBMSCs of passage number 2 to 5 was used for culturing on HA and HASi. gBMSCs were trypsinized with 0.25% trypsin-EDTA for 5 min and centrifuged at 300g for 10 min. The pellet was suspended in "X" mL medium and the cell number was counted manually using hemocytometer. 1×10^5 cells / material were seeded on each material, which was calculated according to the formula:

1×10^5 cells / Y mL = Number of cells observed in hemocytometer /

Volume of medium (X) used for suspending cells (mL)

By seeding "Y" mL of cells on the materials, the concentration of 1×10^5 cells will be obtained.

HA and HASi was conditioned by incubating in α-MEM with 10% FBS for 24 h at 37°C. gBMSCs were then seeded on all sides of conditioned HA and HASi placed in 48 well TCPS plates under static condition. After being incubated at 37°C for 30 min to allow cell attachment, the cells were maintained in α-MEM with 10% FBS. To induce the differentiation of gBMSCs into osteogenic lineage (gOS+ cells), osteogenic medium (section 2.21.3) was provided after 24 h. The medium change was done twice weekly.

2.2.3 Evaluation of gBMSCs and osteogenic induced gBMSCs on bioactive ceramics

2.2.3.1 Adhesion of gBMSCs

The adhesion of gBMSCs on HA and HASi at 1 h and 24 h was depicted through SEM. The cell-cultured materials were processed for SEM (section 2.1.5.2).

2.2.3.2 Viability of gBMSCs and osteogenic induced gBMSCs

2.2.3.2.1 Acridine orange and ethidium bromide staining- Confocal microscopy

The viability of gBMSCs at 48h was determined qualitatively by confocal laser scanning microscope (cLSM). For this, the cell-cultured materials were stained with 100 µl of acridine orange (10 µg / ml PBS) (Sigma chemicals) and ethidium bromide (15 µg / ml PBS) (Sigma chemicals) for 10 min. It was then washed with PBS and imaged using cLSM (Carl Zeiss LSM 510 Meta) at an excitation and emission wavelength of 480 / 526 and 518 / 605 for acridine orange and ethidium bromide respectively. The excitation of acridine orange and ethidium bromide was carried out with Argon / 2 laser. Green coloured cells were marked as live and red coloured cells as dead.

2.2.3.2.2 Acridine orange and ethidium bromide staining - Flow cytometry

gBMSCs grown on HA and HASi were washed with PBS; trypsinized with 0.25% trypsin-EDTA for 5 min and centrifuged at 300g for 10 min. The pellet was incubated with a combination of acridine orange and ethidium bromide as described in section 2.2.3.2.1. It was then washed with PBS and centrifugation at 300g for 10 min. The cell pellet was suspended in 300 µl PBS and the fluorescence was recorded by flow cytometer (BD Biosciences, FACS Aria). The cells without staining, but processed under the same conditions were taken as the control.

2.2.3.2.3 Lactate dehydrogenase assay

The cell viability was determined quantitatively through the total activity of lactate dehydrogenase (LDH) in the cell lysate using LDH reaction buffer (Cytotox96 kit, Promega, USA) It is measured in an enzymatic reaction that occurs in two steps (1) NAD+ is reduced to NADH / H+ by the LDH catalysed conversion of lactate to pyruvate (2) The catalyst (diaphorase) transfers H / H+ of NADH / H+ to tetrazolium salt INT which is reduced to formazan. This leads to colour change from pale yellow to red.

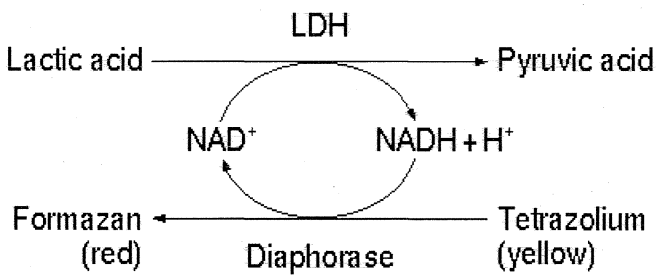

The viability of gBMSCs and gOS+ cells on day 7, 14, 21 and 28 days of cultivation were measured. For this, the cell-cultured materials (n=3) were washed with PBS twice and kept in -80°C until analysis. Frozen cell samples were thawed for 20 min on ice and lysed with 1% Triton X-100 (300 µl) for 50 min with sonication for 10 min. An aliquot of cell lysate (50 µl) was mixed with LDH substrate (50 µl) at room temperature and the enzymatic reaction was stopped after 30 min with 0.1 M acetic acid (50 µl). The absorbance was read at 492 nm (Erba Chem -7). The absorbance (OD values) was correlated with cell viability using a calibration line constructed with increasing concentrations of cells.

2.2.3.3 Proliferation of gBMSCs and osteogenic induced gBMSCs

2.2.3.3.1 Proliferating cell nuclear antigen staining

The proliferation of gBMSCs after 48 h was determined using proliferating cell nuclear antigen (PCNA) by flow cytometry. gBMSCs grown on HA and HASi were washed with PBS; trypsinized with 0.25% trypsin-EDTA for 5 min and centrifuged at 300g for 10 min. The cell pellet was incubated with PCNA (Santa Cruz Biotechnology) at a concentration of 0.1 µg / ml α-MEM for 30 min. It was then washed with PBS and centrifugation at 300g for 10 min. The cell pellet was suspended in 300 µl PBS and the histogram was recorded using flow cytometer (BD Biosciences, FACS Aria). The cells without staining, but processed under the same condition was taken as the control.

2.2.3.3.2 Picogreen assay

The proliferation of gBMSCs and gOS+ cells on day 7, 14, 21 and 28 was determined using Picogreen® dsDNA Quantitation reagent (Molecular probes). For this, the cell-cultured materials (n=3) were washed with PBS twice and kept in -80°C

until analysis. Frozen cell samples were thawed for 20 min on ice and lysed with 1% Triton X-100 (300 µl) for 50 min with sonication for 10 min. The lysate (10 µl) was mixed with picogreen in Tris-EDTA buffer (190 µl) for 5 min and the intensity of fluorescence was measured with a multifunction microplate reader (Infinite F200, Tecan) at an excitation and emission wavelength of 485 / 535 nm. Relative fluorescence units were correlated with cell number using a calibration line constructed with increasing concentration of cells.

2.2.3.4 Morphology of osteogenic induced gBMSCs

The morphology of gOS+ cells cultured on HA and HASi on day 14 and day 28 was determined through SEM. The cell-cultured materials were processed for evaluation as described in section 2.1.5.2.

2.2.3.5 In depth migration of osteogenic induced gBMSCs

2.2.3.5.1 Stevenal's blue and van Gieson's picrofuchsin staining

The migration of gOS+ cells towards the internal voids of HA and HASi was evaluated by Light microscopy after 14 and 28 days. The cell-cultured materials were fixed in 3.7% paraformaldehyde in Sorensen phosphate buffer; washed with PBS; dehydrated in ascending grade of isopropyl alcohol in distilled water series (70% isopropyl alcohol for 4 days; 80% isopropyl alcohol for 4 days; 96% isopropyl alcohol for 4 days; 100% isopropyl alcohol for 2 days; isopropyl alcohol: acetone (1: 1 v/v) for 1 day; 100% isopropyl alcohol for 1 day); infiltered in polymethylmethacrylate (PMMA - Merck, India) for 6 days (2 changes) and finally embedded in PMMA with 1% benzoyl peroxide (accelerator). The plastic sections of about 100 µm were sliced using high speed precision saw (Isomet ^{TM} 2000 Precision Saw, Buehler) and polished to get a thickness of 70 - 90 µm. The sections were then stained with Stevenal's blue at 60ºC for 15 min and counter stained with van Gieson's picrofuchsin for 5 min at room temperature and viewed under Light microscope (Nikon Eclipse E600).

2.2.3.5.2 Acridine orange and ethidium bromide staining

The viability of gOS+ cells migrated towards the internal voids of HA and HASi was determined by acridine orange and ethidium bromide staining by cLSM as described in section 2.2.3.2.1. The materials were scanned in z-axis up to 170 µm with a

scaling of 10 µm between each slice.

2.2.3.6 Differentiation of gBMSCs into osteogenic lineage

2.2.3.6.1 Specific Alkaline Phosphatase activity – Biochemical estimation

The specific ALP activity of gBMSCs and gOS+ cells grown on HA and HASi (n=3) was determined quantitatively after 7, 14, 21 and 28 days of cultivation, based on the hydrolysis of p-nitrophenyl phosphate (Sigma chemicals) to p-nitrophenol, as discussed in section 2.2.1.5.

2.2.3.6.2 Alkaline Phosphatase activity - ELF-97 staining

The ALP activity of gOS+ cells cultured on HA and HASi on day 10 was evaluated by staining with ELF-97 endogenous phosphatase detection kit (Invitrogen). For this, the samples after fixing in 3.7% paraformaldehyde in Sorensen phosphate buffer for 20 min were permeabilised with 0.2% Triton X-100 in PBS for 5 min. It was then blocked with 3% BSA in PBS for 30 min, stained with ELF-97 phosphatase substrate (component A was diluted 20 fold with component B (buffer) in detection kit) for 5 min and finally visualized through Hoechst long pass filter of cLSM (Carl Zeiss LSM 510Meta). The excitation source used for ELF-97 was blue diode at 405 nm.

2.2.3.6.3 Osteopontin expression - Flow cytometry

The expression of ostepontin on gOS+ cells cultured on HA and HASi was analyzed on day 7 and 21. gBMSCs cultured on 6 well TCPS plates were taken as the control. The cells on the materials and TCPS plates were washed with PBS; trypsinized with 0.25% trypsin-EDTA for 5 min and centrifuged at 300g for 10 min. The cell pellet was fixed with 3.7% paraformaldehyde in Sorensen phosphate buffer for 1h; washed with PBS followed by centrifugation at 500g for 10 min at 4℃. The pellet was then permeabilised with 0.2% Triton X-100 for 5 min followed by blocking with 3% BSA for 30 min. After washing with PBS and centrifugation at 500g for 10 min at 4℃, the pellet was incubated with 50 µL primary antibody (0.2 µg / µL 3% BSA) (K-20, Santa Cruz Biotechnology) for 1 h followed by FITC conjugated rabbit anti-goat secondary antibody (Abcam antibodies) (1: 100 in 3% BSA) for 1 h in dark. The signals were then recorded by flow cytometer (BD Biosciences, FACS Aria).

2.2.3.6.4 Osteopontin expression – Confocal microscopy

The expression of ostepontin on gOS+ cells cultured on HA and HASi (day 21) was confirmed through cLSM. The cell-cultured constructs after fixing with 3.7% paraformaldehyde in Sorensen phosphate buffer were washed with PBS; permeabilised with 0.2% Triton X-100 in PBS for 5 min at room temperature and blocked with 3% BSA for 30 min. After washing with PBS, the cells were incubated with 50 µL primary antibody (0.2µg / µL 3% BSA) for 1 h (K-20, Santa Cruz Biotechnology) followed by FTIC conjugated rabbit anti-goat secondary antibody (1: 100 in 3% BSA) and rhodamine B conjugated phalloidin (1: 100) (Sigma chemicals) for 1h (for actin staining). It was then washed with PBS thrice and visualized through cLSM (Carl Zeiss LSM 510 Meta).The excitation of FITC (480 / 525) was carried out with Argon / 2 laser and that of rhodamine B (540 / 625) with HeNe 543 laser.

2.2.3.6.5 Osteocalcin measurement

The concentration of osteocalcin in the medium in which gOS+ cells were grown on HA and HASi was determined through ELISA technique (BioSource hOST-EASIA Kit) as per manufacturer's instructions. gBMSCs cultured on 6 well TCPS plates were taken as the control. For this, the cell cultured medium (n=3) was collected on day 7, 14, 21 and 28 and kept at 4℃ until analysis . 25 µl of medium was pipetted out into microtitre plate coated with anti-osteocalcin antibody (monoclonal antibody 1) followed by 100 µl of anti-osteocalcin labelled with horseradish peroxidase (monoclonal antibody 2) and incubated for 2 h at room temperature on a horizontal shaker set at 700 rpm. After washing 3 times with wash solution, 100 µl of chromogen solution was added to each well and incubated for 30 min at room temperature with shaking at 700 rpm. 200 µl of stopping solution was pipetted out into each well and the absorbance was read at 405 nm against a reference filter of 630 nm (Erba Chem -7). The concentration of osteocalcin was measured from the OD value using a calibration curve plotted from the control (provided by the manufacturer).

2.2.4 Culturing of human bone marrow-derived mesenchymal stem cells

MSCs were isolated from the bone marrow aspirates of a healthy human donor (age 31 – kindly provided by Sabine Boxberger, University Hospital Carl Gustav Carus Dresden). Expansion of human BMSCs (hBMSCs) was performed in Dulbecco's

modified Eagle's medium (DMEM) with low glucose containing 10% fetal calf serum (FCS), 10 U / ml penicillin and 100 µg / ml streptomycin (Biochrom, Berlin, Germany) at 37℃ in a humidified, 7% CO_2 / 93% air incubator.

2.2.5 Culturing of hBMSCs and osteogenic induced hBMSCs on bioactive ceramics

hBMSCs of passage number 3 to 5 were used for culturing on HA and HASi. For this, hBMSCs were trypsinized with 0.25% trypsin-EDTA for 5 min, centrifuged at 1500 rpm for 5 min and the pellet was suspended in the respective medium mentioned above (section 2.2.4). 1×10^5 cells / material were calculated as described in the section 2.2.2 and seeded on all sides of conditioned HA and HASi (materials incubated in the medium for 24 h prior to cell seeding) placed in 48 well TCPS plates under static condition (Nunc). After being incubated at 37℃ for 30 min to allow initial cell attachment, the cells were cultivated in DMEM containing 2% FCS, 10 U / ml penicillin and 100 µg / ml streptomycin. To induce the differentiation of hBMSCs into osteogenic lineage (hOS+ cells), 10^{-7} M dexamethasone (Sigma-Aldrich, Taufkirchen, Germany), 3.5 mM β-glycerophosphate (Sigma), 50 µM L-ascorbic acid-2-phosphate (Sigma) and 2% FCS was added to DMEM. The medium change was done twice weekly.

2.2.6 Evaluation of hBMSCs and osteogenic induced hBMSCs on bioactive ceramics

2.2.6.1 Adhesion of hBMSCs

The adhesion of hBMSCs on HA and HASi was determined by SEM at 1 h, 4 h and 24 h. The cell-cultured materials were fixed with 2% gluteraldehyde in PBS for 30 min. Dehydration was performed with graded ethanol series (10% ethanol for 10 min; 30% ethanol for 10 min; 50% ethanol for 10 min; 70% ethanol for 10 min; 80% ethanol for 10 min; 96% ethanol for 10 min and absolute ethanol for 10 min) before critical-point drying using CPD 030 apparatus (BAL-TEC, Liechtenstein). The materials were mounted on stubs, gold coated using a Sputter Coater SCD 050 (BAL-TEC) and analyzed by SEM (IDSM 982 Gemini, Zeiss, Jena, Germany and Philips XL 30/ESEM operating in SEM mode).

2.2.6.2 Viability of hBMSCs and osteogenic induced hBMSCs

2.2.6.2.1 Calcein AM and 2 mM ethidium homodimer-1 staining

The viability of hBMSCs on HA and HASi was evaluated using LIVE/DEAD® viability / cytotoxicity kit (Molecular Probes, Eugene, USA). After 24 h of cell seeding, the samples were incubated with DMEM containing 4 mM calcein AM and 2 mM ethidium homodimer-1 for 30 min; washed with PBS thrice and imaged. The non-fluorescent calcein AM permeates the intact membrane of living cells and is converted into fluorescent calcein. Calcein was excited with Ar^+ laser at 495 nm and ethidium homodimer-1 with 528 nm HeNe laser using cLSM (Carl Zeiss 510 Meta, Jena, Germany).

2.2.6.2.2 Lactate dehydrogenase assay

The viability of hBMSCs and hOS+ cells on HA and HASi (n=3) after 1, 7, 14 and 21 days of cultivation was determined through the total activity of LDH in the cell lysate using LDH reaction buffer (Cytotox96 kit, Promega, USA) as described in section 2.2.3.2.3. The absorbance was then recorded with a multifunction micro plate reader (Spectra fluor plus, Tecan, Crailsheim, Germany).

2.2.6.3 Proliferation of hBMSCs and osteogenic induced hBMSCs

The proliferation of hBMSCs and hOS+ cells on HA and HASi (n=3) after 1, 7, 14 and 21 days of cultivation was evaluated using Picogreen® dsDNA Quantitation reagent (Molecular probes) as described in section 2.2.3.3.2 and the fluorescence was measured with a multifunction microplate reader (Spectra fluor plus, Tecan). Relative fluorescence units were correlated with cell number using a calibration line constructed with increasing concentrations of cells.

2.2.6.4 Morphology of osteogenic induced hBMSCs

The morphology of hOS+ cells cultured on HASi on day 14 and day 28 was determined through SEM. The cell-cultured materials were processed for evaluation as described in section 2.2.6.1.

2.2.6.5 Differentiation of hBMSCs into osteogenic lineage

2.2.6.5.1 Specific Alkaline Phosphatase activity - Biochemical estimation

The specific ALP activity of hBMSCs and hOS+ cells on HA and HASi (n=3) was determined after 1, 7, 14 and 21 days of cultivation, based on the hydrolysis of p-nitrophenyl phosphate to p-nitrophenol, as discussed in section 2.2.1.5.

2.2.6.5.2 Alkaline Phosphatase activity - ELF-97 staining

The ALP activity of hBMSCs and hOS+ cells cultured on HA and HASi on day 10 was determined qualitatively using ELF-97 endogenous phosphatase detection kit (Invitrogen). The cell-cultured materials were stained with TRITC-phalloidin (1: 100 in PBS) (Sigma chemicals) for 1 h and with ELF-97 phosphate substrate as described in section 2.2.3.6.2 and viewed under cLSM (cLSM 510 Meta - Zeiss, Jena, Germany). TRITC-phalloidin (for cytoskeletal actin filaments) was excited with HeNe 543 laser (550 / 570) and ELF-97 with blue diode at 405 nm

2.2.6.5.3 Real-time PCR

The gene expression of ALP and BSP II on hBMSCs and hOS+ cells grown on HA and HASi (n=3) was evaluated by real-time PCR using TaqMan probes which were labeled with FAM (6-carboxyfluorescein) at the 5'-end and TAMRA (N,N,N',N'-tetramethyl-6-carboxyrhodamine) at the 3'-end. At predetermined time points (1, 7 and 14 days) after culture, the cell-cultured materials were washed twice with PBS, and the total RNA was isolated using RNeasy Mini Kit (Qiagen, Hilden, Germany) following the procedure described by the manufacturer. Briefly, the cells were lysed by incubating with 350 µl RLT-buffer with β-Mercaptoethanol for 3 min followed by 250 µl of 100% ethanol. The RNA was cleaned up and concentrated using RNeasy MinElute Spin Column with centrifugation at 8000g for 15s. The DNA was then digested with 10 µl DNase I stock solution for 15 min followed by washing with buffers RW1 and RPE (kit component) and 80% ethanol and centrifugation at 8000g. 30 µl of RNase free water was pipetted out for cDNA synthesis.

cDNA was transcribed using 200 U of Superscript II Reverse Transcriptase (Invitrogen, Carlsbad, CA), 0.5 mM dNTPs (Invitrogen), 12.5 ng / µl random hexamers (MWG Biotech, Ebersberg, Germany) and 40 U of RNase inhibitor RNase OUT (Invitrogen). TaqMan PCRs were carried out in an ABI PRISM 7700 (Applied

Biosystems, Foster City, CA). The accumulation of PCR products was quantified using the comparative CT method in which the accumulated PCR products of each of the genes examined was normalized to the housekeeping gene GAPDH in the corresponding samples. The primers (MWG Biotech) for each gene are summarized in Table 1.

Gene	accession number	forward and reverse primer (5´-3´)	TaqMan probe (5´-3´) [1]
GAPDH	AF261085 [2]	GAAGGTGAAGGTCGGAGTC GAAGATGGTGATGGGATTTC	CAAGCTTCCCGTTCTC AGCC
ALP	ENST00000344573[3]	CCGTGGCAACTCTATCTTTGGCA GGCCCATTGCCATACAG	CCATGCTGAGTGACAC AGACAAGAAGCC
BSPII	ENST00000226284[3]	AAGCATGCCTACTTTTATCCTCA TTCATTCGATTCTTCATTGTTTTC TCC	TTTCCAGTTCAGGGCA GTAGTGACTCATCC

Table 2.1. Primer sequence and probes designed for real-time PCR analysis of the expression of osteoblast specific genes of human cells. [1] Probes were labeled with FAM (6-carboxyfluorescin) at the 5´end and TAMRA (N,N,N´,N´-teratmethyl-6-carboxyrhodamine) at the 3´end.[2] Entrez accession number, [3] Ensembl accession number

2.2.7 Platelet-rich plasma / Fibrin glue coated HA and HASi

2.2.7.1 Platelet-rich plasma (goat and human origin)

PRP was separated from the blood of goat and human and coated on HA and HASi. The adhesion of platelets on the materials and the activation of platelets when exposed to the materials were evaluated.

2.2.7.1.1 Preparation of platelet-rich plasma

Adult goats were used for the study as per the guidelines of IAEC and CPCSEA. About 12 ml of blood was obtained from the jugular vein of adult goats weighing around 23 - 25 kg and collected into tubes containing heparin (5 IU / mL of blood) as an anticoagulant. Similarly human blood was also collected from three normal adult individuals (Age 26 - 28). The platelets present in the whole blood were counted automatically using a hematology analyzer (Sysmex K-4500). Goat and human blood was centrifuged at 2500 rpm (1216g) for 5 min and the yellow plasma containing

PRP fraction (approximately 5 ml) was separated. The platelets present in PRP were then counted using a hematology analyzer (Sysmex K-4500).

2.2.7.1.2 Coating of platelet-rich plasma on bioactive ceramics

The coating of PRP (goat and human separately) on HA and HASi (n=3) was performed by immersing these materials in PRP solution (300 µl) in 48 well plate (Nunc) followed by agitation at 37℃ for 1 h.

2.2.7.1.3 Adhesion of platelets on bioactive ceramics

2.2.7.1.3.1 Percentage reduction

The platelets (goat and human) present in PRP before and after agitation with materials were counted automatically using a hematology analyzer (Sysmex K-4500). The platelets adhered to the materials were calculated from the reduction in the number of platelets in PRP after agitation with the materials (percentage reduction).

2.2.7.1.3.2 Lactate dehydrogenase assay

The adhesion of platelets (goat and human) on the materials was confirmed based on the kinetic determination of LDH activity. For this, the materials immersed in PRP solution for 1 h were washed two times with PBS and lysed with 1% Triton X-100 (300 µl) for 2 h in ice. The lysate (20 µl) was mixed with 500 µl of LDH substrate (Randox) at room temperature and the absorbance was read at 340 nm (Erba spectrophotometer). The absorbance (OD values) was correlated with the concentration of platelets using a calibration line constructed with increasing concentrations of platelets.

2.2.7.1.4 Activation of platelets exposed to bioactive ceramics

This part of experiment was done only with human platelets because of the limitation in the availability of anti-goat antibodies of P-selectin and plasma factor 4 (PF4).

2.2.7.1.4.1 P-selectin expression

PRP solution exposed to HA, HASi and 4 well TCPS plate (control) (Nunc) for 1 min and 60 min was collected and fixed with 3.4% paraformaldehyde in PBS for 20 min followed by centrifugation at 3000 rpm for 5 min. The pellet after diluting with ACD-

PBS was stained with R-phycoerythrin labelled P-selectin (Beckmancoulter) for 1 h at room temperature in dark and analysed by flow cytometer (BD Biosciences, FACS Aria).

2.2.7.1.4.2 Plasma factor 4 release

The release of PF4 from platelets was determined as per manufacture's instructions (Hyphen Biomed). Human PRP (200 µl) exposed to HA, HASi and 4 well TCPS plate (control) (Nunc) for 1 min and 60 min was added to micro ELISA plate coated with anti-PF4 antibody and incubated for 1 h at room temperature. After washing with wash buffer, 200 µl of conjugate (anti PF4 polyclonal antibody coupled with peroxidase) was added; incubated for 1 h; washed; followed by the addition of substrate chromogen (Tetramethylbenzidine / H_2O_2) for 5 min. The absorbance was read at 450 nm (Erba Chem -7). The absorbance (OD values) was correlated with concentration using a calibration line constructed with control provided by the manufacturers.

2.2.7.2 Fibrin glue (human origin)

Fibrin glue components (Fibrinogen and Thrombin in calcium chloride) were gifted by Thrombosis Research Unit, SCTIMST, India.

2.2.7.2.1 Coating of fibrin glue on bioactive ceramics

The sterilised HA and HASi was placed in 48 well plate and mixed with 2.5 mg fibrinogen for 20 min followed by polymerisation with 50 U / mL of thrombin in calcium chloride. All samples were incubated at 37°C for half an hour, frozen at -80℃ for 24h and freeze dried in a lyophilizer. The coating of FG on the materials was then confirmed.

2.2.7.2.1.1 Scanning electron microscopy

FG coating on HA and HASi was evaluated by ESEM (ESEM- FEI Quanta 200). The elements present in the coated materials (Ca, P, Si and C) were determined by EDS (OXFORD X-ray microanalysis software).

2.2.7.2.1.2 Raman spectroscopy

The coating of FG on HA and HASi was again confirmed through Raman

spectroscopy by comparing with uncoated materials. (BRUKER RFS 100/S, Germany). The samples were focused with a Ramanscope (BRUKER, Germany) having standard Geranium detector under 40x objective lens. Raman spectra were then recorded at a resolution of 4 cm^{-1} and scanned between 1000 to 2000 cm^{-1} for uncoated HA / FG coated HA and 500 to 3500 cm^{-1} for uncoated HASi / FG coated HASi. The average scan of 50 was taken with Raman laser power 430 mW.

2.2.8 Culturing of osteogenic induced gBMSCs on platelet-rich plasma / fibrin glue coated bioactive ceramics

The experiments were divided into three sets. In the first set of experiments, prior to cell seeding, HA and HASi were conditioned by incubating in α-MEM with 10% FBS at 37°C for 24 h. In the second and third set of experiments, HA and HASi were coated with PRP solution (goat origin) and FG (human origin) separately as described above. Thus total six groups of materials were included in the study (1) uncoated HA (HA) (2) uncoated HASi (HASi) (3) PRP coated HA (PHA) (4) PRP coated HASi (PHASi) (5) Fibrin glue coated HA (FHA) (6) Fibrin glue coated HASi (FHASi).

gBMSCs were seeded on all sides of the materials (1 x 10^5 cells / material) under static condition. After being incubated at 37°C for 30 min to allow cell attachment, α-MEM with 10% FBS was added for 24 h. After 24 h, the cells were induced to differentiate into osteogenic lineage by providing osteogenic medium (section 2.2.1.3). The osteogenic medium change was done twice weekly.

2.2.9 Evaluation of osteogenic induced gBMSCs on platelet-rich plasma / fibrin glue coated bioactive ceramics

2.2.9.1 Viability of osteogenic induced gBMSCs

2.2.9.1.1 Acridine orange and ethidium bromide staining

The viability of gOS+ cells on the materials on day 28 was determined qualitatively by cLSM as described in section 2.2.3.2.1. The excitation of acridine orange and ethidium bromide was carried out with Argon / 2 laser.

2.2.9.1.2 Lactate Dehydrogenase assay

The viability of gOS+ cells after 7, 14, 21 and 28 days of cultivation was determined quantitatively through the total activity of LDH in the cell lysate using LDH reaction buffer (Cytotox96 kit, Promega, USA) as described in section 2.2.3.2.3.

2.2.9.2 Proliferation of osteogenic induced gBMSCs

The proliferation of gOS+ cells after 7, 14, 21 and 28 days of cultivation was evaluated using Picogreen® dsDNA Quantitation reagent (Molecular probes) as described in section 2.2.3.3.2.

2.2.9.3 Morphology of osteogenic induced gBMSCs

The cell-cultured materials on day 28 were fixed with 1% gluteraldehyde in Sorensen phosphate buffer at 4℃ overnight. The specimens after thorough washing with PBS were evaluated under ESEM (ESEM- FEI Quanta 200).

2.2.9.4 Cell cycle analysis

The cell-cultured materials on day 28 were trypsinized with 0.25% trypsin-EDTA for 5 min and centrifuged at 2500 rpm for 10 min at 4℃. The cell pellet was fixed in 70% cold ethanol at 4℃ for 1h and washed twice with PBS and centrifugation at 4000 rpm for 5 min at 4℃. The cell pellet was treated with 250 µl ribonuclease in PBS (150 µg / mL PBS) (Imperial, India) for 45 min at 37℃ and added with propidium iodide (30 µg / mL PBS) (Sigma chemicals) for 5 min. The fluorescence were then recorded (20,000 events) using flow cytometer (Diva soft ware of BD Biosciences, FACS Aria).

2.2.9.5 Differentiation of gBMSCs into osteogenic lineage

2.2.9.5.1 Specific Alkaline Phosphatase activity – Biochemical estimation

The specific ALP activity of gOS+ cells after 7, 14, 21 and 28 days of cultivation was quantified, based on the hydrolysis of p-nitrophenyl phosphate (Sigma) to p-nitrophenol as described in section 2.2.1.5.

2.2.9.5.2 Alkaline Phosphatase activity - ELF-97 staining

The ALP activity of gOS+ cells on day 10 was confirmed using ELF-97 endogenous phosphatase detection kit (Invitrogen) as described in section 2.2.3.6.2 and

visualized through blue diode at 405 nm of cLSM (Carl Zeiss LSM 510 Meta).

2.2.9.5.3 Real-time PCR analysis

The expression of ALP, osteopontin and osteocalcin on gOS+ cells grown on 6 groups of materials was evaluated after 7, 14, 21 and 28 days of cultivation. The RNA was isolated by TRIzol reagent (Imperial, India) as per the manufacturer's instructions. To be in brief, the cell-cultured materials were treated with 500 µl TRIzol reagent for 10 min and kept at -80℃ until analysis. After thawing at room temperature, 100 µl of chloroform was added for 15 min followed by centrifugation at 12,000g for 15 min at 4℃. The clear supernatant (top layer) was transferred to a fresh tube and mixed with 250 µl of isopropyl alcohol for 10 min at room temperature for precipitating RNA followed by centrifugation at 12,000g for 8 min. The pellet was washed with 70% ethanol in RNase free water (Imperial, India) with centrifugation at 12,000g for 8 min. The pellet was air dried and added with 50 µl RNase fee water and incubated at 55℃ for 10 min. The yield of RNA was determined spectrophometrically.

The first strand cDNA was synthesized from 1 µg of total RNA, 5 µl MLV reverse transcriptase (50U / µl), 5 µl stratascript buffer (10x), 1 µl RNase inhibitor (40 U / µl), 4 µl random hexamer (10 pmole) and 2 µl dNTP mix (10 mM) (Imperial, India) for a 50 µl RT reaction using the Thermal cycler (Master Cycler, Eppendorf, USA). The real-time PCR was performed using a Chromo4 system (MJ Research, USA). All reactions were carried out in a total volume of 20 µl, containing 10 µl full velocity SYBR Green Master mix (Imperial, India), 1 µl forward and 1 µl reverse primer (10 picomole) and 8 µl cDNA at an annealing temperature of 50 - 55℃ (depending upon the primers) over 35 cycles. The primers that were designed are listed in Table 2 (Source: primer sequences of human alveolar bone cells were used due to non-availability of primer sequence of goat model). The annealing temperatures for β actin, ALP, osteopontin and osteocalcin gene are 54, 52, 52.5 and 53℃ respectively. For each gene, the quality and specificity was assessed by examining PCR melt-curves following real-time PCR. The results were normalized by being expressed relative to the amount of β-actin mRNA determined. The results of the expression of ALP, osteopontin and osteocalcin on day 7, 14, 21 and 28 was represented as fold increase with respect to the expression of gBMSCs at 24 h (gBMSCs do not express

osteogenic genes) cultured on six group of materials.

Gene	Forward primer	Reverse primer
ALP	CGTGGCTAAGAATGTCATCATGTT	TGGTGGAGCTGACCCTTGA
Osteopontin	ACATCCAGTACCCTGATGCTACAG	GGCCTTGTATGCACCATTCA
Osteocalcin	GCAAAGGTGCAGCCTTTGTG	GGCTCCCAGCCATTGATACAG
β actin	GCTCGTCGTCGACAACGGCTC	CAAACATGATCTGGGTCATCTTCTC

Table 2.2. Primer sequence designed for real-time PCR analysis of the expression of osteoblast specific genes of goat cells. (Reference: Xiao Y *et al.,* 2003).

2.2.10 Statistics

Three separate materials were used for every quantitative experiments in each group. Again from each material, all measurements were done in duplicate in order to confirm the repeatability. Each parameter was expressed as mean of all values ± standard deviations. Single factor analysis of variance (ANOVA) was employed to assess the statistical significance of results. P-values less than 0.01 were considered significant.

2.3 Extraskeletal implantation studies (*in vivo*)

The neo-osteogenesis and neo-vascularisation potential of tissue-engineered constructs in comparison with bare materials were evaluated at the extraskeletal site (muscle) in rat model.

2.3.1 Isolation of rat bone marrow-derived mesenchymal stem cells

As per the guidelines of IAEC and CPCSEA, rat bone marrow aspiration was conducted (Maniatopoulos C *et al.,* 1988). Wistar rats of average weight 200 - 300g were aseptically prepared and draped in a sterile fashion. After euthanizing by the

administration of chloroform, the muscles were separated. The bones like femur and tibia were retrieved and collected in PBS containing 200 units / ml of penicillin and 200 μg / ml of streptomycin – Gibco). After cutting two ends of the bone, the bone marrow was flushed using a syringe with 18 gauge needle having α-MEM with 10% FBS and antibiotics. The clumps of cells were gently broken and centrifuged at 500g for 10 min. The pellet was plated in 25 cm^2 TCPS flask (Nunc) containing 5 ml α-MEM with 10% FBS, 100 units / ml of penicillin and 100 μg / ml of streptomycin and incubated at 37°C in humid atmosphere and 5% CO_2. The medium was changed after 3 days to remove non-adherent cells and subsequently renewed twice a week. After 10 days in primary culture, the adherent rBMSCs were released with 0.25% trypsin-EDTA (Gibco, India) and centrifuged at 300g for 10 min. The cells were sub cultured and passaged. rBMSCs of passage number 2 to 5 were used for culturing on HA and HASi.

2.3.2 Culturing of osteogenic induced rBMSCs on bioactive ceramics

The behaviour of rat cells on HA and HASi was firstly determined *in vitro.* For this, the materials were polished in the form of discs having 5 mm diameter and 5 mm thickness. rBMSCs were seeded (1×10^5 cells / material as described in section 2.2.2) on all sides of conditioned HA and HASi (materials incubated in α-MEM with 10% FBS for 24 h at 37°C) placed in 48 well TCPS plates under static condition (Nunc). After being incubated at 37°C for 30 min to allow cell attachment, α-MEM with 10% FBS was added for 24 h, which was followed by osteogenic medium (α-MEM supplemented with 15% FBS, 10 mM β- glycerophosphate, 10^{-8} M dexamethasone and 0.05 mg / ml L-ascorbic acid – Sigma chemicals) to induce the differentiation of rBMSCs into osteogenic lineage (rOS+ cells). The medium change was done twice weekly.

2.3.3 Evaluation of osteogenic induced rBMSCs on bioactive ceramics *in vitro*

2.3.3.1 Viability of osteogenic induced rBMSCs

The viability of rOS+ cells after 3 and 7 days of cultivation was determined through the total activity of LDH in the cell lysate using LDH reaction buffer (Cytotox96 kit, Promega, USA) as discussed in section 2.2.3.2.3.

2.3.3.2 Differentiation of rBMSCs into osteogenic lineage

The specific ALP activity of rOS+ cells on HA and HASi was determined quantitatively after 3 and 7 days of cultivation, based on the hydrolysis of p-nitrophenyl phosphate to p-nitrophenol, as discussed in section 2.2.1.5.

2.3.4 Experimental Animal Groups

Care and management of animals were conducted as per the guidelines of IAEC and CPCSEA. For extraskeletal implantation studies, HA and HASi was polished in the dimension of 10 mm (length) x 1 mm (breadth) x 1 mm (thickness). Twenty four wistar rats with an average body weight of 200 – 300g and one defect per leg were divided into six groups as shown in Table 2.3 and 2.4. HA was implanted on the right leg while HASi on the left leg of each animal. Among six groups, Group II and Group V was included only in neo-osteogenesis studies, particularly, histological and histomorphometric evaluation at 4 weeks.

Period of study	**Group I (HASi)**	**Group II (HASi+C (OS-))**	**Group III (HASi+C)**
2 weeks	Bare HASi (without cells) (n=6)		rOS+ cells cultured on HASi for 7 days (osteogenic medium) (n=3)
4 weeks	Bare HASi (without cells) (n=6)	rBMSCs cultured on HASi for 7 days (α-MEM with 10% FBS) (n=3)	rOS+ cells cultured on HASi for 7 days (osteogenic medium) (n=3)

Table 2.3. Experimental animal groups for extraskeletal implantation with bare HASi and tissue-engineered HASi

Period of study	Group IV (HA)	Group V (HA+C (OS-))	Group VI (HA+C)
2 weeks	Bare HA (without cells) (n=6)		rOS+ cells cultured on HA for 7 days (osteogenic medium) (n=3)
4 weeks	Bare HA (without cells) (n=6)	rBMSCs cultured on HA for 7 days (α-MEM with 10% FBS) (n=3)	rOS+ cells cultured on HA for 7 days (osteogenic medium) (n=3)

Table 2.4. Experimental animal groups for extraskeletal implantation with bare HA and tissue-engineered HA

2.3.5 Animal surgical procedures

The surgical procedures were done according to the ISO standard 10993 – 6. The animals were anesthetized with ketamine (100 mg / kg) and xylazine (5 mg / kg) injection intramuscularly. The skin was shaved and disinfected with betadine-povidone iodine. 1 cm longitudinal skin incision was made and quadriceps muscle was exposed. The materials were then implanted deep into the muscle pouch and the wound was closed with 4.0 mer silk sutures. After closure, the sutured wound was swabbed with betadine and dressed with neosporin. The animals were kept in cages and fed with standard diet and water *ad libitum*. After two and four weeks, the animals were euthanized intraperitonially with excess thiopentone sodium.

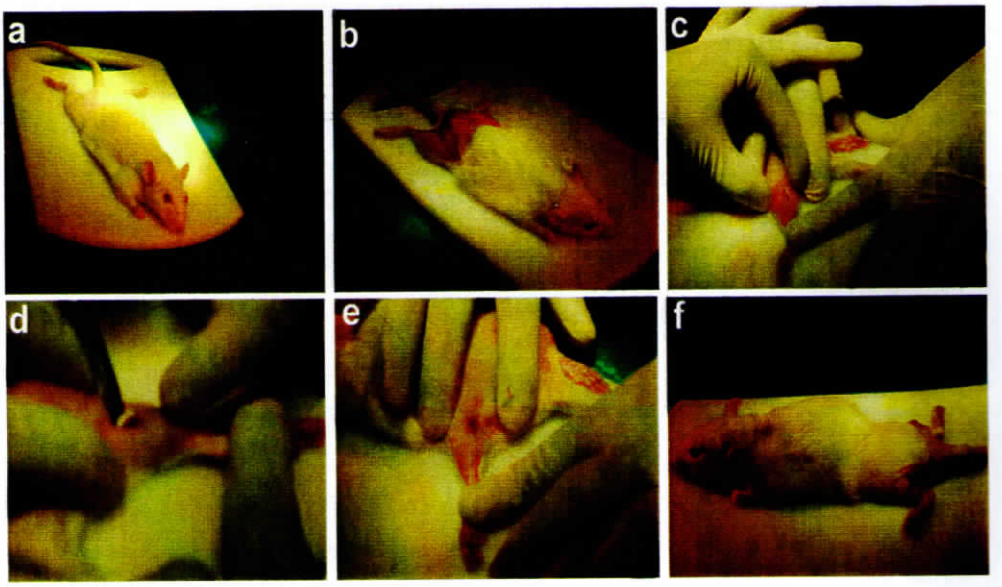

Figure 2.1. Surgical procedure of the implantation of bare and tissue-engineered HA and HASi at an extraskeletal site of rat model. As per ISO standard 10993 – 6. (a) Rat model prepared for surgery (b) Disinfection with betadine-povidone iodine (c) 1 cm longitudinal skin incision at the site (d) Material implantation deep into the muscle pouch (e) Suturing of the wound (f) Wound closure.

2.3.6 Evaluation of post-implanted tissues

2.3.6.1 Neo-vascularization studies

The implantation site along with material (12 mm length) x 2 mm breadth x 2 mm thickness) (Group I, III, IV and VI) after two and four weeks were fixed in 10% neutral buffered formalin in Sorensen phosphate buffer for 2 days. The materials were decalcified in 5% formic acid in formalin for two days. It was then washed with tap water; dehydrated in graded ascending series of acetone (30%, 50%, 70%, 90% and 100% acetone) for 20 min each; cleared in xylene I (10 min) and xylene II (15 min); infiltered in paraffin I (1 h); paraffin II (3h) and finally embedded in paraffin. Thin sections (5 µm) were then made using a microtome (Leica RM 2255).

The sections after heating in hot air oven for 60 min were deparaffinised with xylene (2 changes, 10 min each); rehydrated in descending grade of ethanol series (90% for 5 min, 70% for 5 min); washed in tap water for 3 min; stained with Harris's Hematoxylin for 30 min; washed in tap water for 3 min, differentiated in 1% acid alcohol for 30 sec and blued with 0.2% ammonia water for 30 sec. It was then washed with tap water for 5 min, counterstained with 1% eosin Y for 10 min;

dehydrated in ethanol (70% for 5 min, 100% ethanol for 5 min - 2 changes); cleared in xylene (2 changes, 10 min each); mounted in DPX and viewed under Light microscope (Leica DM 6000) (random selection of sections).

2.3.6.2 Neo-osteogenesis studies

2.3.6.2.1 Histological evaluation

The implantation site along with material (12 mm length) x 2 mm breadth x 2 mm thickness) (Group I, II, III, IV, V and VI) after four weeks of implantation were fixed in 10% neutral buffered formalin in Sorensen phosphate buffer for 2 days. The samples were dehydrated in graded ascending series of isopropyl alcohol (70% isopropyl alcohol for 4 days; 80% isopropyl alcohol for 4 days; 96% isopropyl alcohol for 4 days; 100% isopropyl alcohol for 2 days; isopropyl alcohol: acetone (1: 1 v/v) for 1 day; 100% isopropyl alcohol for 1 day), infiltered in PMMA (Merck, India) for 6 days (2 changes) and finally embedded in PMMA with 1% benzoyl peroxide (accelerator). The plastic sections of about 100 µm were sliced using high speed precision saw (Isomet ^{TM} 2000 Precision Saw, Buehler) and polished to get a thickness of 70 - 90 µm. The PMMA sections after washing with tap water were kept in Stevenal's blue solution at 60ºC for 15 min and counter stained with van Gieson's picrofuchsin for 5 min at room temperature. The sections were randomly viewed under Light microscope (Leica DM 6000). Stevenal's blue stains cells and extracellular structures in a subtle gradation of blue tones and van Gieson's picrofuchsin colours collagen fibres (green or green blue), bone (orange or purple) and osteoid matrix (yellow-green) (Maniatopoulos C *et al.,* 1986).

2.3.6.2.2 Histomorphometric analysis

The Stevenal's blue and van Gieson's picrofuchsin stained sections were scanned for determining (a) the area of cells infiltered around and within the pore of the materials and (b) the area of newly formed bone. Five sections were selected randomly and photographed with a charge-coupled device (CCD) camera. All the images were captured with 20X magnification lens and the images were suitably calibrated using an inbuilt image configuration. The area of cells (bluish colour) and the area of newly formed bone (yellowish colour) with respect to the total frame area in the image (356911.2 μm^2) was measured using the Quips programme of QWin soft ware of the microscope (Leica DM 6000).

2.3.6.2.3 Alkaline Phosphatase activity - ELF-97 staining

The retrieved tissues (Group III and VI) after four weeks of implantation were fixed in 10% formalin in Sorensen phosphate buffer for 2 days followed by decalcification and paraffin embedding (section 2.3.6.1). Thin sections (5 µm) were deparaffinised with xylene (2 changes, 10 min each); rehydrated in descending grade of ethanol series (90% for 2 min, 70% for 2 min); permeabilised with 1% Triton X-100 in PBS for 5 min and blocked with 3% BSA in PBS for 30 min. The staining was then performed with ELF 97 endogenous phosphatase detection kit (Invitrogen) for ALP activity and viewed with Hoechst filter of fluorescence microscope (Leica DM 6000).

2.3.6.2.4 Mineralization studies

High resolution x-ray micro-computed tomography (Micro-CT 40, SCANCO MEDICAL, Switzerland) was used to analyze the mineralization of 4 weeks post-implanted tissues (Group III and VI). The tissues were fixed in 10% formalin in Sorensen phosphate buffer for 2 days and scanned under micro-CT. The scanning parameters used: slice thickness and slice increment of 12 µm; energy of 70,000V and intensity of 114 µA. The density distribution graphs were plotted from 2D micro-CT images and compared with raw HA and HASi (before implantation).

2.4 Orthotopic implantation studies (*in vivo*)

The progress of bone regeneration and material degradation in a segmental defect (2 cm) created in goat femur was validated using tissue-engineered HASi in comparison with bare HASi.

2.4.1 Preparation of tissue-engineered groups

2.4.1.1 Culturing of osteogenic induced gBMSCs on HASi

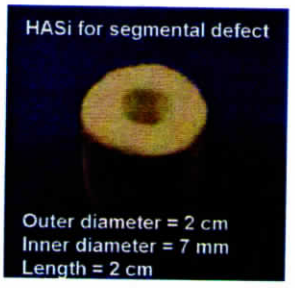

Figure 2.2. Gross view of HASi fabricated for segmental defect studies.

HASi was polished in the form of hollow cylinder having a length of 2 cm and an outer and inner diameter of 2 cm and 7 mm respectively. gBMSCs isolated (section 2.2.1.1) from the metaphyseal end of humerus of adult goats (n=8) were slowly seeded (passage 2 at a density of 1×10^5 cells per cm^2) on all sides of conditioned HASi scaffolds under static condition. After being incubated for 1 h to allow cell attachment, 35 mL of α-MEM with 10% FBS was added which was replaced by osteogenic medium after 24h as described in section 2.2.2. The constructs were then maintained in osteogenic medium for 7 days *in vitro*.

2.4.1.2 Separation of platelet-rich plasma from blood

PRP was obtained from the jugular vein of adult goats weighing around 23 - 25 kg (n=4) as described in section 2.2.7.1.1. Goat blood was centrifuged at 2500 rpm (1216g) for 5 min and the yellow plasma containing PRP fraction was separated and counted using a hematology analyzer (Sysmex K-4500).

2.4.2 Experimental Animal Groups

Care and management of animals were conducted as per the guidelines of IAEC and CPCSEA. Eighteen adult goats with an average body weight of 20 - 30 kg and one defect per animal were divided into three groups as shown in Table 5. Three groups were compared at 2 and 4 months, while the performance of bare HASi groups was evaluated for 6 and 12 months.

Period of study	Group I (HASi)	Group II (HASi+C)	Group III (HASi+CP)
2 months	Bare HASi (without cells or PRP)(n=2)	gOS+ cells cultured on HASi for 7 days (n=2)	gOS+ cells cultured on HASi for 7 days and PRP delivered at the defect site (n=2)
4 months	Bare HASi (without cells or PRP)(n=4)	gOS+ cells cultured on HASi for 7 days (n=2)	gOS+ cells cultured on HASi for 7 days and PRP delivered at the defect site (n=2)
6 months	Bare HASi (without cells or PRP) (n=2)	Nil	Nil
12 months	Bare HASi (without cells or PRP) (n=2)	Nil	Nil

Table 2.5. Experimental animal groups for orthotopic implantation in goat femur model

2.4.3 Animal surgical procedures

The animals were pre-medicated with intramuscular injection of atropine sulphate at 0.1 mg per kg body weight, xylazine hydrochloride at 0.22 mg per kg body weight and ketamine hydrochloride at 11 mg per kg body weight. Thiopentone sodium at 5 mg per kg body weight followed by succinyl choline at 0.02 mg per kg body weight intravenously was given for the induction of anesthesia and muscle relaxation respectively. The animals were intubated immediately with size 9 portex endotracheal tube and put on ventilator. Anesthesia was maintained with increments of 50 – 100 mg of thiopentone sodium and half the initial doses of succinyl choline every 30 – 40 minutes. The right femoral shaft was exposed through a 5 cm longitudinal incision using a standard lateral approach to the femur. The periosteum was elevated and 2 cm bone segment was excised from the mid diaphyseal region using a gigli saw. The bone ends were smoothened and made uniform using a bone file. The medullary canal was reamed with a hand reamer and its length was measured using a wire inserted intramedullary. A titanium nail used for human

humerus nailing with 6.7 mm in diameter and having three proximal locking holes and two distal locking holes were used for immobilization. After reaming the marrow cavity, the nail was introduced through the proximal fragment through the ceramic block into the distal fragments. Both distal and proximal ends were identified under an image intensifier (Siemens power Mobil, c-Arm). The distal locking was done with 2 static screws of appropriate length and the proximal locking with one static and one dynamic screw. The animals were sacrificed through the injection of high doses of thiopentone and 15% potassium chloride intravenously.

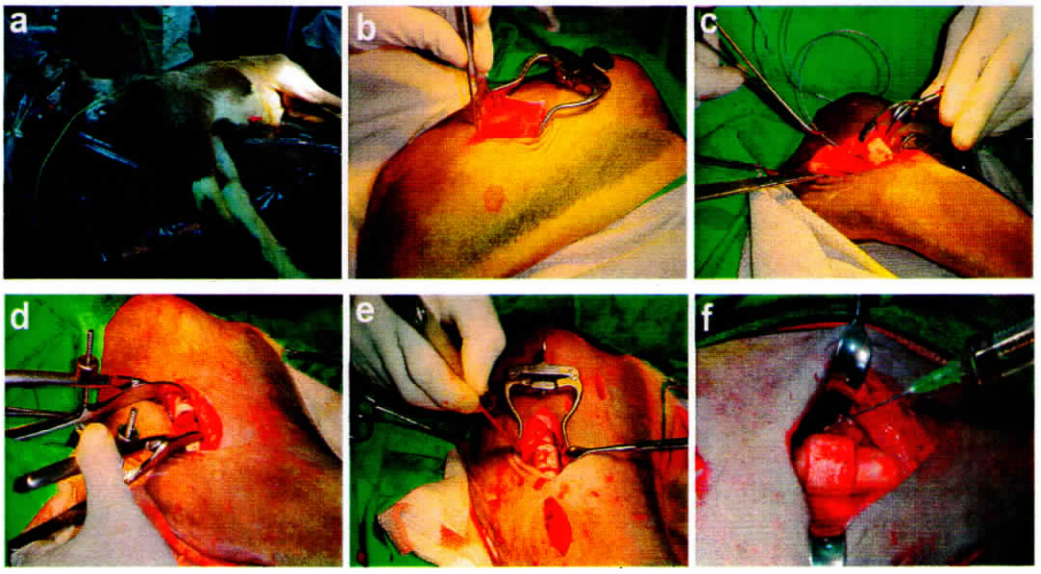

Figure 2.3. Surgical procedure of the implantation of bare and tissue-engineered HASi in segmental defect in the femur of goat model a) Goat prepared for the surgery (b) Exposition of right femoral shaft (c) Excision of bone segment (2 cm) from the mid diaphyseal region using a gigli saw (d) 2 cm segmental defect (e) Replacement of the defect with HASi / tissue-engineered HASi (f) Delivery of PRP at the defect site

2.4.4 Evaluation of post-implanted tissues

2.4.4.1 Gross evaluation

The femurs were dissected to remove any overlaying tissue and fixed in 10% neutral buffered formalin in Sorensen phosphate buffer for one month. The implant site (2 cm) along with the host bone (0.5 cm from either side) of each animal was resected (Total 3 cm) using a saw. The titanium intramedullary nail passing through the defect was carefully pulled out. The defect site was then cut longitudinally through the medullary canal using a High speed precision saw (Isomet ™ 2000 Precision Saw,

Buehler) and photographed with a digital camera (Nikon D705, Japan). To differentiate the new bone formed in the different regions of defect (2 cm), zones were defined as (a) Mid region (M) of the defect (1 cm) and (b) Peripheral region (P) of the defect = 0.5 cm on each side of the segmental defect.

2.4.4.2 Radiographic analysis

Radiographs were taken immediately after surgical implantation (Day 0) and at 6 weeks, 2, 4, 6 and 12 months post-implantation in standard projections on the operated limb using an image intensifier (Siemens power Mobil, c-Arm).

2.4.4.3 Histological evaluation

The retrieved tissues after fixing in 10% neutral buffered formalin were processed for Stevenal's blue and van Gieson's picrofuchsin staining as described in section 2.3.6.2.1. The sections were then viewed under Light microscope (Leica DM 6000).

2.4.4.4 Morphological evaluation

The retrieved tissues were fixed in 3% gluteraldehyde in Sorensen phosphate buffer at 4℃. After thorough washing with PBS, the specim ens were viewed under ESEM (FEI Quanta 200).

2.4.4.5 Histomorphometric evaluation

The Stevenal's blue and van Gieson's picrofuchsin stained sections were scanned for measuring the percentage of newly formed bone and the percentage of material degraded in the peripheral and mid region of the defect. Five sections were selected randomly and photographed with a charge-coupled device (CCD) camera. All the images were captured with 20X magnification lens and the images were suitably calibrated using an inbuilt image configuration. The area of newly formed bone (yellowish colour) and the area of material (greyish colour) degraded was measured using the Quips programme of QWin soft ware of the microscope (Leica DM 6000). The percentage of newly formed bone and material degraded was then calculated with respect to the total frame area in the image (356911.2μm^2).

Percentage of newly formed bone = Area of newly formed bone / 356911.2 x 100
Percentage of material degraded = Area of material degraded / 356911.2 x 100

2.4.4.6 Biochemical assays

2.4.4.6.1 Alkaline phosphatase activity

The blood was collected from post-implanted goats of each group and the serum was separated by centrifuging at 2500 rpm for 5 min. The ALP activity in the serum was determined based on the kinetic determination of p-nitrophenylphosphate to p-nitrophenol (Enzyme Technologies, India). The sample (1 µl) was mixed with 1 ml of substrate containing 1.0 mol / L diethanolamine buffer (pH 10.2), 0.5 mmol / L magnesium chloride, 10 mmol / L p-nitrophenylphosphate. It was then incubated for 1 min and the absorbance was read at 405 nm (Hitachi 220 spectrophotometer).

2.4.4.6.2 Tartrate Resistant Acid Phosphatase assay

The blood was collected from post-implanted goats of each groups and the serum was separated by centrifuging at 2500 rpm for 5 min. Tartrate Resistant Acid Phosphate (TRAP) activity in the serum was determined using acid phosphatase reagent kit (Enzyme Technologies, India). α-naphthol released from the substrate, α-naphthylphosphate, by acid phosphatase is coupled with Fast Red TR to produce a coloured complex, which absorbs light at 405 nm. L-Tartrate reagent specifically inhibits non-specific acid phosphatase activity other than TRAP. The acid phosphatase reagent (1 ml) was mixed with L-tartrate reagent (10 µl) and sample (100 µl) and incubated for 5 min. The absorbance was then read at 405 nm (Hitachi 220 spectrophotometer).

2.4.4.7 Mineralization studies

2.4.4.7.1 Energy dispersive x-ray spectroscopy

The retrieved tissues after fixing in 3% gluteraldehyde were viewed under ESEM (FEI Quanta 200). The elements present in the material, especially Ca, P and Si was plotted through EDS (OXFORD X-ray microanalysis software) and Ca / P ratio was calculated. The distribution of elements at the defect site was mapped by Line mapping in different fields.

2.4.4.7.2 Computed Tomography

The retrieved tissues were fixed in 10% neutral buffered formalin and thoroughly washed with PBS. The samples were then analyzed by CT scanner (Siemens syngo

soft ware) along sagittal planes. The scan parameters were 70 kV, 112 mA and an integration time of 3s. Total 30 slices were taken with 1 mm reconstruction interval. A colour-based density method was applied to represent the bone and the material (red colour - mineralized bone and green colour – material).

2.4.4.7.3 Micro-computed Tomography

The retrieved tissues were fixed in 10% neutral buffered formalin and thoroughly washed with PBS. The samples were centered in µCT machine (Micro-CT 40, SCANCO MEDICAL, Switzerland model) and scanned at 70 kV. The sections were scanned in z-axis to reconstruct regenerated bone in three dimensions. The backside (cortical region) and frontal side (medullary canal region) of the tissues was represented separately.

2.4.5 Characterization of post-implanted materials

2.4.5.1 X-ray diffraction technique

The phase analysis and crystallinity of 2 months post-implanted HASi was analyzed by XRD. The portion of implant remained in the mid region of the defect was collected, washed and sonicated with distilled water to remove the traces of fixative. It was then powdered and scanned between 20° and 40° 2 θ at a rate of 2° per minute under a step size of 0.02° using Cu-Kα1 radiation at a voltage of 40 kV and a current strength of 30 mA (Siemens D-5005).

2.4.5.2 Fourier Transform Infrared Spectroscopy

The functional groups present in 2 months post-implanted HASi was analyzed by FTIR. The samples were collected and powdered (section 2.4.5.1) and anlysed using Thermo Nicolet 5700 spectrometer (section 2.1.3.4).

2.4.6 Inductively Coupled Plasma spectroscopy

ICP analysis was done to quantity Si in different organs of body. For this purpose, different organs like kidney, lymph node, liver, heart, spleen and lungs were collected; dissected and dried at 60℃ overnight. T he samples were weighed and dissolved in aquaregia and made into 50 ml using HPLC grade water. It was then filtered and analyzed with ICP-AES system (IRIS INTREPID II XSP).

CHAPTER 3

PHYSICOCHEMICAL CHARACTERISATION OF BIOACTIVE CERAMICS

3.1 Abstract

Silica-based bioactive ceramics are characterized by superior biological activity and resorbability than calcium phosphate ceramics (Ning CQ *et al.,* 2004). These materials are prepared by melting and cooling (glass) or by melting and controlled crystallization (glass-ceramics) or by sol-gel method. Among these, sol-gel-derived bioactive ceramics are superior, which have been developed in order to obtain a material that would resorb at a similar rate as bone formation (Hamadouche M *et al.,* 2000). The advantages of these materials lie in their composition and structure (Hench LL *et al.,* 1990). In sol-gel process, SiO_2 is released via the thermal decomposition of metallorganic additive like TEOS or TPOS and allow the processing at lower temperature than melt-derived glasses (Langstaff S *et al.,* 1999). Sol-gel-derived glasses allow a control of pore structure and permit better control of bioactivity and biodegradability (Saravanapavan P *et al.,* 2004). The absence of Na_2O in sol-gel glasses avoid rapid change in interfacial pH in biological fluids, a greatest problem seen in Bioglass (Hench L *et al.,* 1990). An increase in the growth rate of HCA layer on the surface was also obtained with sol-gel-derived glasses when compared to melt-derived glasses (Vallet-Regi M *et al.,* 2000). In addition, the concentration of silica is higher in sol-gel glasses than in melt-derived glasses (Sepulveda P *et al.,* 2002).

In this study, sol-gel process was adopted in order to develop a silica-based HA, namely HASi, with the proposal of improving the bioactivity and the degradation of stoichiometric HA. For synthesizing HASi, HA was firstly prepared by wet

precipitation method and sintered between 1100℃ and 1300℃ for 1h. These blocks were dipped in silica sol (prepared by the hydrolysis of TEOS in ethanol-water system) for 1 min and again sintered at 1200°C for 2 h. This method was adopted with the hypothesis that silicon ions will incorporate into HA as an outer coating layer, while the main core of HASi remains as HA. Thus the goal was to utilize the dual properties of HA (osteoconduction, osteointegration) and silica (osteoconduction, osteointegration and degradation) in one product. HA without dipping in silica sol, but synthesized under the same conditions was used as the control.

The specific objectives of the first phase of the study were 1) To evaluate the physicochemical characteristics of HA and HASi 2) To evaluate the degradation of HA and HASi 3) To study the cytotoxicity and cytocompatibility of HA and HASi.

3.2 Physicochemical characterization of Materials

3.2.1 Microstructure of HASi

The coating of silica over HA was confirmed through ESEM (Fig. 3.1). For this, HASi was prepared and fractured in order to view the micro structural details in the outer and inner areas of the material. The core of HASi was polycrystalline and has clear grain boundary characteristics (Fig. 3.1b), while the outer coated layer was porous, less crystalline and has no clear grain and grain boundary (Fig. 3.1c). The porous structure together with the absence of clear gain and grain boundary in the outer coated layer of HASi is expected due to Si rich liquid phase formation which has penetrated to a depth of about 1 mm (John *et al.*, 2008).

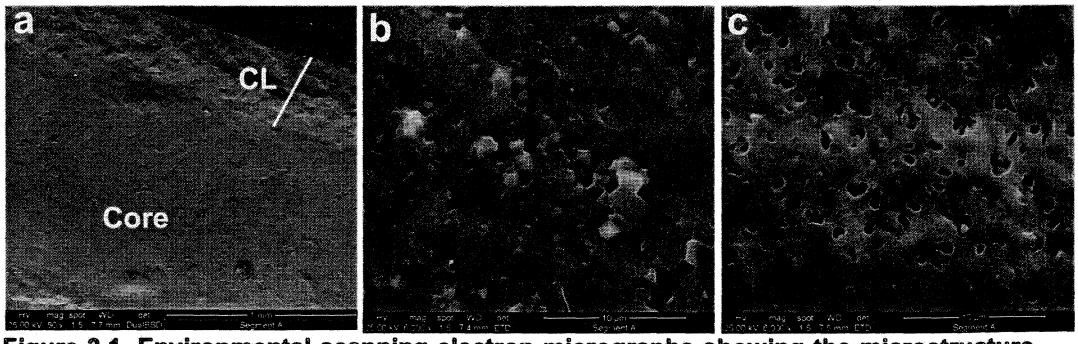

Figure 3.1. Environmental scanning electron micrographs showing the microstructure of HASi. a - Fractured HASi; b - Core of HASi, c – coated layer (CL) of HASi The bar line in Figure 3.1a shows the depth of silica coated layer.

3.2.2 Elemental Analysis

EDS spectra revealed that elements like Ca and P were present in the core of HASi (Fig. 3.2a) while the outer coated layer contained Si in addition to Ca and P (Fig. 3.2b). This confirmed that Si was present only on the surface and has not penetrated into the core of HASi.

The Ca / P ratio in the material decides whether pure HA or other phases has formed during the preparation. The Ca / P ratio of HA was 1.67, similar to theoretical ratio (Chai C *et al.,* 1994), However, the Ca / P ratio of HASi was 2.6, which established the presence of other phases in addition to HA. This observation was comparable to a previous report showing a higher Ca / P ratio in silicate-substituted HA (Hing KA *et al.,* 2006).

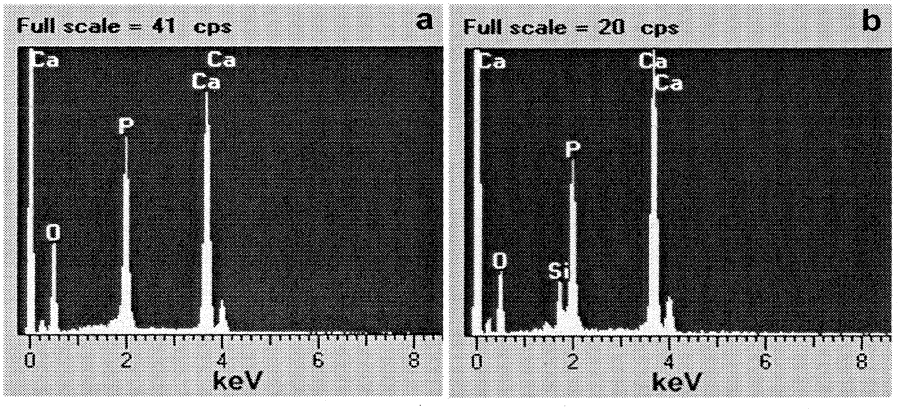

Figure 3.2. Energy dispersive x-ray spectra showing the elements present in the core and outer coated layer of HASi. a - Core of HASi. b - Outer coated layer of HASi

Element weight %	HA	HASi
Si	0	8.29
P	37.78	25.35
Ca	62.22	66.36
Total	100	100

Table 3.1. Weight percentage of elements (Ca, P and Si) present in HA and HASi, determined by energy dispersive x-ray spectroscopy

3.2.3 Phase analysis

Variations in the precise nature of calcium phosphate phases have strong effect on the cellular responses (Hing KA *et al.,* 1999). So the degree of crystallanity and phase purity are important parameters to characterize, which was analyzed by XRD.

The narrow peak in HA indicated high level of crystallinity. The only crystalline phase present was HA, which was in good agreement with ICDD (International Committee for Diffraction Data) standard pattern for HA (Fig. 3.3). This demonstrated that no other phases were present in HA with levels > 0.5 wt%.

HASi was also crystalline in nature, while the crystallinity was less when compared to HA. To differentiate the phases present in the core and outer coated layer, experiment was conducted with dense HASi made specifically for this study. Firstly, the surface of dense HASi was scanned for the identification of phases in the outer coated layer. Then the surface layer was removed by grinding and polishing and again subjected to XRD analysis. The results showed that the core of HASi contained HA phase only while the outer coated layer exhibited peaks for HA ($Ca_5(PO_4)_3(OH)$), β -TCP ($Ca_3 (PO_4)_2$) and calcium silicate (Ca_2SiO_4).

The crystallization and phase transformation is dependent on the chemical composition and sintering temperature. The dipping of HA in silica sol and sintering at high temperature (1200°C for 2 h) resulted in other phases like TCP and calcium silicate in HASi. It is assumed that during sol gel dipping, silicate ions (SiO_4^{4-}) entered into some of the sites of phosphates ions (PO_4^{3-}) in HA and the process may have accompanied by the reaction of silicate with Ca^{2+} to form calcium silicate phase. This may have reduced the calcium or Ca / P content in the material that resulted in the formation of TCP phase. It is proved that Ca-deficient HA can transform to TCP phase at temperatures above 800°C (Mavropoulos E *et al.,* 2003). Sinçe Si was introduced to already sintered HA, the resulting post-sintered phase is β-TCP (Langstaff S *et al.,* 1999). Similar to our data, Ruys *et al.,* (1993) demonstrated the presence of TCP phase and Ca-Si-P-O amorphous phase while increasing SiO_2 content in the system.

Earlier study reported that the maximal silica content that can be incorporated in HA without decomposing its structure is 3.32% (Ning *et al.,* 2004). Gibson *et al.,* (1998)

noted that no change took place in the symmetry of HA crystallographic unit cell while using up to 1.6 wt% SiO_2. However in our study, the core of HASi remained as HA without having alteration in its structure and Si in the form of calcium silicate was confined to the surface as a coating layer even if 15 -17 mass% silica was incorporated. This attainment is ascribed to the methodology adopted for synthesizing HASi, where sintered HA was dipped in silica sol only for 1 min. This duration is not adequate for the diffusion of silica throughout HA and changing its symmetry.

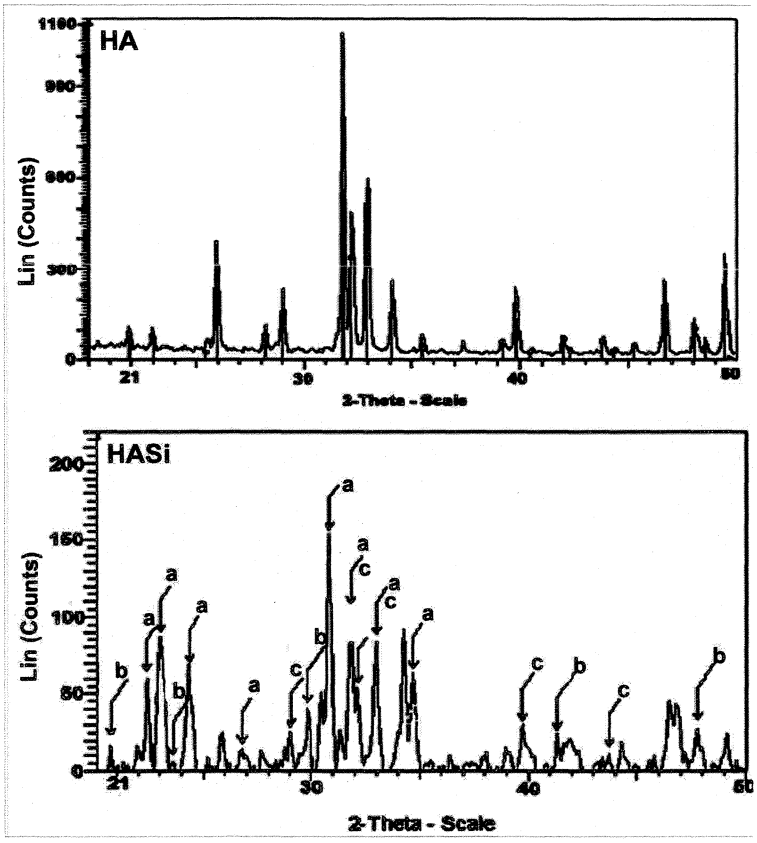

Figure 3.3. X-ray diffraction pattern of HA and HASi. HA contained hydroxyapatite phase only, while in HASi, hydroxyapatite (a), calcium silicate (b) and β-Tricalcium phosphate (c) phases were present.

3.2.4 Functional group studies

FTIR spectra obtained for HA demonstrated the characteristic triplet peak for phosphate at 962 cm^{-1}, 1054 cm^{-1} and 1088 cm^{-1} and hydroxyl groups at 3570 cm^{-1}, which was agreeable with the literature data (Walters MA *et al.*, 1990). The bands at

3570 cm^{-1} and 631 cm^{-1} was assigned to the stretching and vibrational modes respectively of the hydroxyl groups. The intense bands at 1088 cm^{-1}, 1054 cm^{-1} and 962 cm^{-1} was corresponded to the stretching vibration mode of P-O, whereas the doublet at 601 cm^{-1} and 573 cm^{-1} was assigned to the bending mode of the same bond. HASi also showed the bands assigned to HA phase, while the phosphate peak at 1088 cm^{-1} was absent and the intensity of hydroxyl peak (3570 cm^{-1}) was weak. Since phosphate and silicate shared similarly spaced vibrational modes due to their structural similarity, it was difficult to differentiate their peaks (Fig. 3.4).

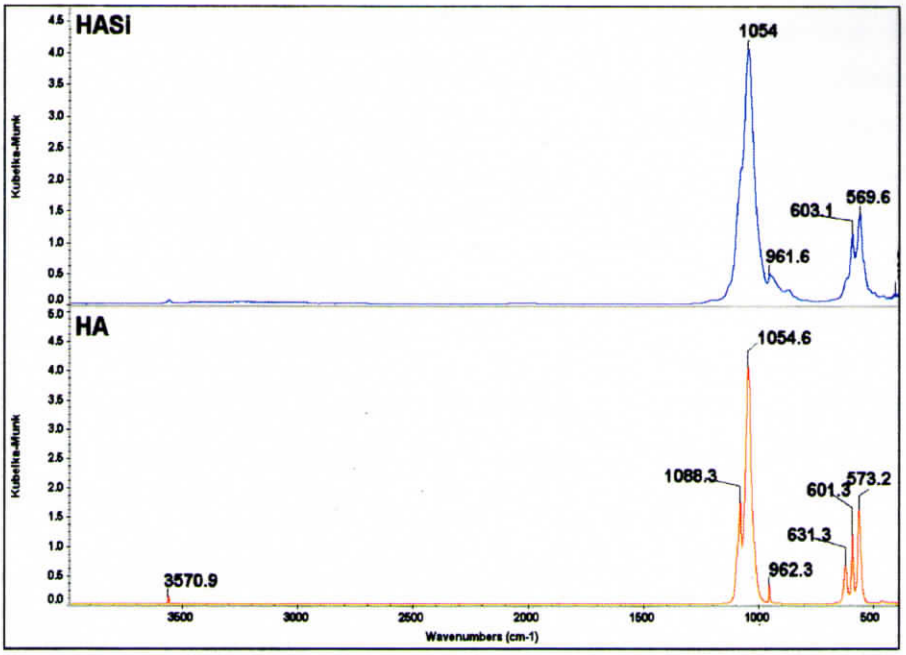

Figure 3.4. Fourier Transform Infrared spectra of HA and HASi.

The ionic radius of Si^{4+} suggest that Si^{4+} would enter either within P^{5+} sites or within PO_4^{3-} when incorporating Si in HA lattice (Langstaff S *et al.*, 1999). Rietveld structural refinements clearly illustrated the substitution of silicate ions for phosphate ions in HA lattice (Porter AE *et al.*, 2004a; Porter AE *et al.*, 2004b). According to Gibson's proposal (1999), Si was incorporated as tetrahedral silicate ions onto phosphate sites in HA lattice and the charge is maintained through the loss of hydroxyl ions as per the following equation.

$$Ca_{10}(PO_4)_6(OH)_2 + xSiO_4^{4-} \longrightarrow Ca_{10}(PO_4)_{6-x}(SiO_4)x(OH)_{2-x} + xPO_4^{3-} + xOH^-$$

Consistent with this mechanism, variation in the relative intensities of bands associated with phosphate stretches in HASi could be due to the substitution of silicate for phosphate species. Additionally, the weak relative intensity of OH^- band in HASi indicated a loss of occupancy of this site.

3.2.5 Porosity studies

Porosity is an important criterion that enables blood capillaries to provide nutrition, leading to bone growth and repair (Uchida A, *et al.,* 1984). The most common techniques used to create porosity in biomaterials are gas foaming, phase separation, mechanical stirring, freeze drying and sintering depending on the material used to fabricate the scaffold (Karageorgiou V *et al.,* 2005). Herein, the porosity was introduced by mechanical stirring method. The precipated HA powder was mixed and shaked vigrously with a binder (polyvinyl alcohol). The resulting frothy and viscous slurry were heated (300°C for 1h) to remove the binder that could leave voids (porosity) in the materials.

3.2.5.1 Scanning electron microscopy

SEM gave an insight into the ceramic structure with respect to porosity and morphology (Fig. 3.5). HA and HASi has an interconnecting pore system with pore size in the range of 50 – 500 µm.

The topography of the material is critical that profoundly affects the attachment and spreading of cells and finally other cellular activities like proliferation and differentiation (Gough JE *et al.,* 2004). Herein, HA displayed a rough surface whereas a smooth surface was noted on HASi, which may be due to silica coating.

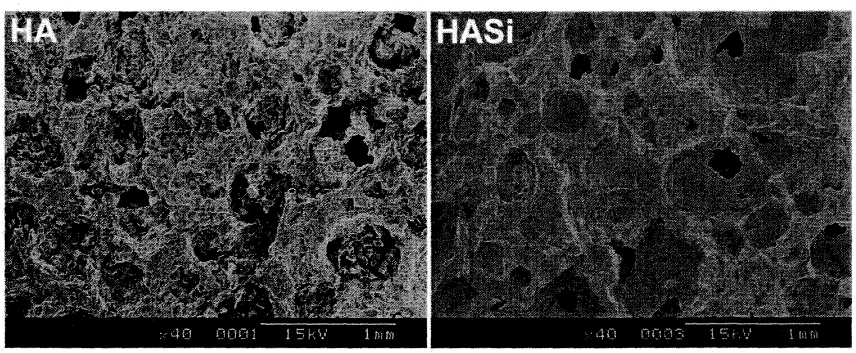

Figure 3.5. Scanning electron micrographs showing the porosity and morphology of HA and HASi.

3.2.5.2 Mercury Intrusion Technique

Mercury porosimeter is developed based on the physical principle that a non wetting liquid does not penetrate in pore until sufficient pressure is applied. The required pressure is inversely proportional to the size of the pores, according to Washburn equation, with the assumption that the pore is cylindrical and well interconnected (Washburn EW 1921). Therefore this method provides information on the pore size and overall interconnection of the pores of the materials.

The results depicted that HA and HASi has an open net work of pores and most of the pores were around 10 - 200 microns. The bulk density of HA was approximately 0.8 g / cc indicating 70% porosity, while the bulk density of HASi was approximately 1.04 g / cc representing 67% porosity. The skeletel density of HA and HASi was 2.8 g / cc, which showed that 85% of the pores were open. A plot of volume of Hg intruded as a function of pore size (pore size distribution) was shown in Fig. 3.6 and Fig. 3.7.

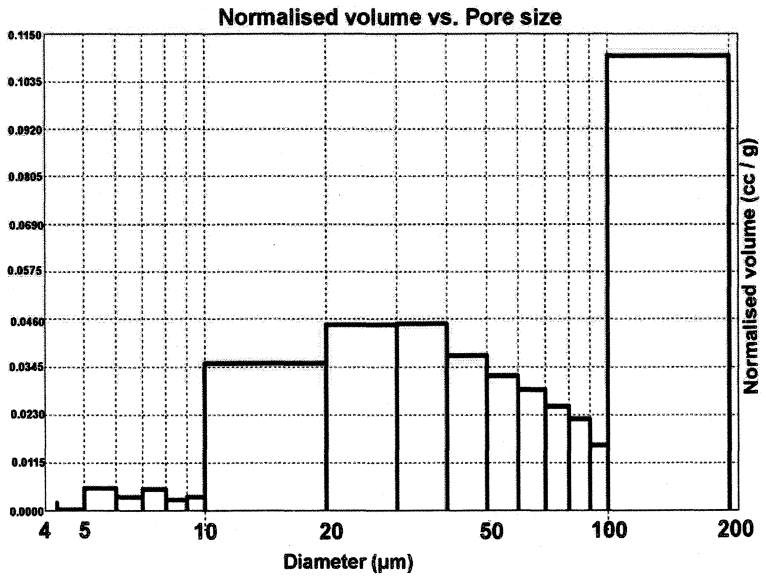

Figure 3.6. Porosity and pore size of HA determined by mercury intrusion porosimetry. Pore size ranges between 10 – 200 µm.

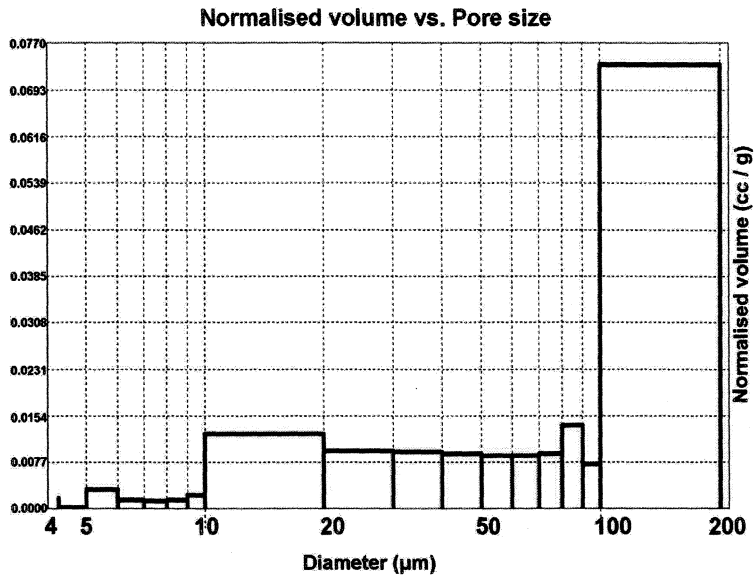

Figure 3.7. Porosity and pore size of HASi determined by mercury intrusion porosimetry. Pore size ranges between 10 – 200 µm.

SEM and mercury intrusion technique illustrated that most of the pores of HA and HASi was in the range of 50 – 500 µm, which is recommended for bone formation (Uchida A *et al.*, 1984). Trabecular bone comprise of 50 - 90% porosity (Kaplan FS *et al.*, 1994) and cortical bone consist of 3 - 12% porosity (Cooper DM *et al.*, 2004) suggesting that the porosity of HA (70%) and HASi (67%) is somewhere between cortical and cancellous bone. The interconnected porosity is an added advantage that can improve the fluid flow and nutrient supply both in an *in vitro* and *in vivo* environment (Hiu-Yan Y *et al.*, 2005).

3.2.6 Mechanical strength

Mechanical strength is an essential aspect to characterize for the use of materials in bone tissue engineering. The materials should have sufficient mechanical strength to withstand the hydrostatic pressure and to maintain the spaces required for cell ingrowth and ECM production. Compressive testing has been successfully used in the characterization of cancellous bone and has also been adopted in the testing of porous and dense HA (Hodgskinson R *et al.*, 1990). Herein the compressive strength of HA was 6.583 ± 1.856 MPa and that of HASi was 4.59 ± 1.44 MPa (Fig. 3.8). There was no significant difference in the compressive strength between these two

materials. These values are comparable to the compressive strength of trabecular bone of humans, which is in the range of 1.5 to 9.3 MPa, but not with load bearing sites like femur and tibia which showed a range of 90 – 215 MPa (Liebschner MA *et al.,* 2004). Since the degree of porosity (70% porosity - HA and 67% porosity - HASi) influences the mechanical property, a compromise between these two requirements is always needed for the fabrication of a successful tissue-engineered graft.

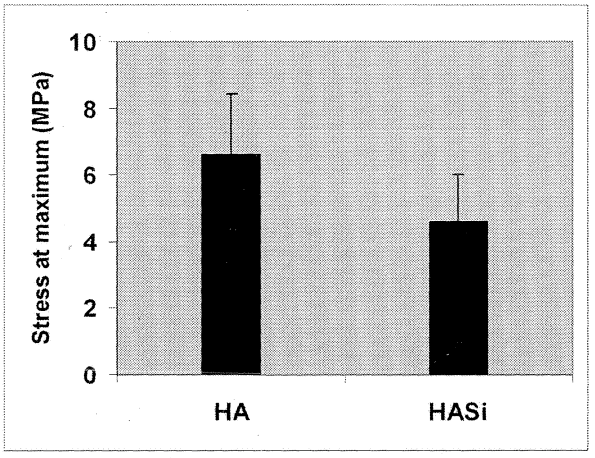

Figure 3.8. Compressive strength of HA and HASi.

3.3 *In vitro* degradation Studies

Biodegradable materials have been important in bone tissue engineering. These materials should be designed to degrade gradually in the body and replaced eventually by the newly formed tissue. The degradation of HA and HASi was characterized *in vitro* by accelerated (60°C) and real degradation (37°C) test as per ISO standard 10993 - 13. For this, the materials were immersed in PBS for 60 days and subjected to XRD and FTIR analysis and compared with raw materials (before immersing in PBS).

3.3.1 X-ray Diffraction technique

HASi block immersed in PBS showed peaks only for HA phase while TCP and calcium silicate phase present in the outer coated layer of raw HASi disappeared after 60 days, at 37°C and 60°C (Fig. 3.9). However , there was no difference in the XRD pattern between raw HA and HA immersed in PBS for 60 days at both the temperature (Fig. 3.10).

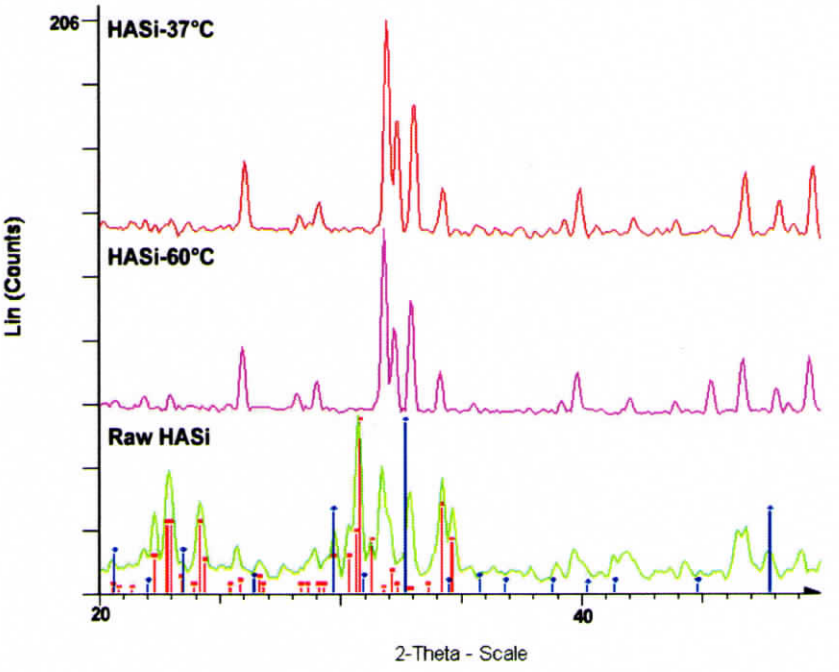

Figure 3.9. X-ray diffraction pattern of HASi after immersed in PBS for 60 days. Calcium silicate (blue line) and TCP phase (red line) disappeared when compared to raw HASi

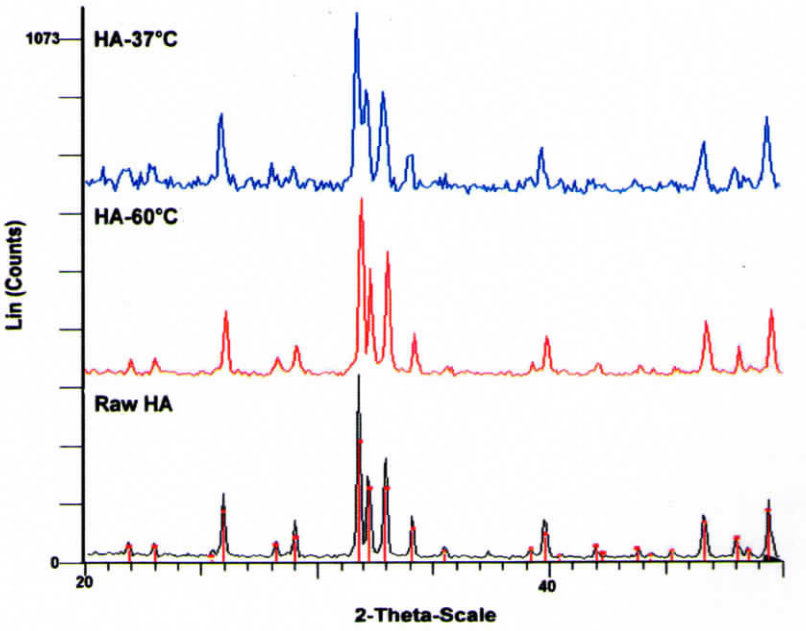

Figure 3.10. X-ray diffraction pattern of HA after immersed in PBS for 60 days. There was no significant change when compared to raw HA

3.3.2 Fourier transform Infrared spectroscopy

FTIR spectra showed that the characteristic hydroxyl peak at 3570 cm^{-1} together with the triplet peak for phosphate around 961 cm^{-1}, 1054 cm^{-1} and 1087 cm^{-1} appeared after immersing HASi in PBS for 60 days, at 37℃ and 60℃ (Fig. 3.11). This suggested that the material remained in PBS was HA, which is the core of HASi. However there was no change in the absorption band of HA at both the temperature (Fig. 3.12).

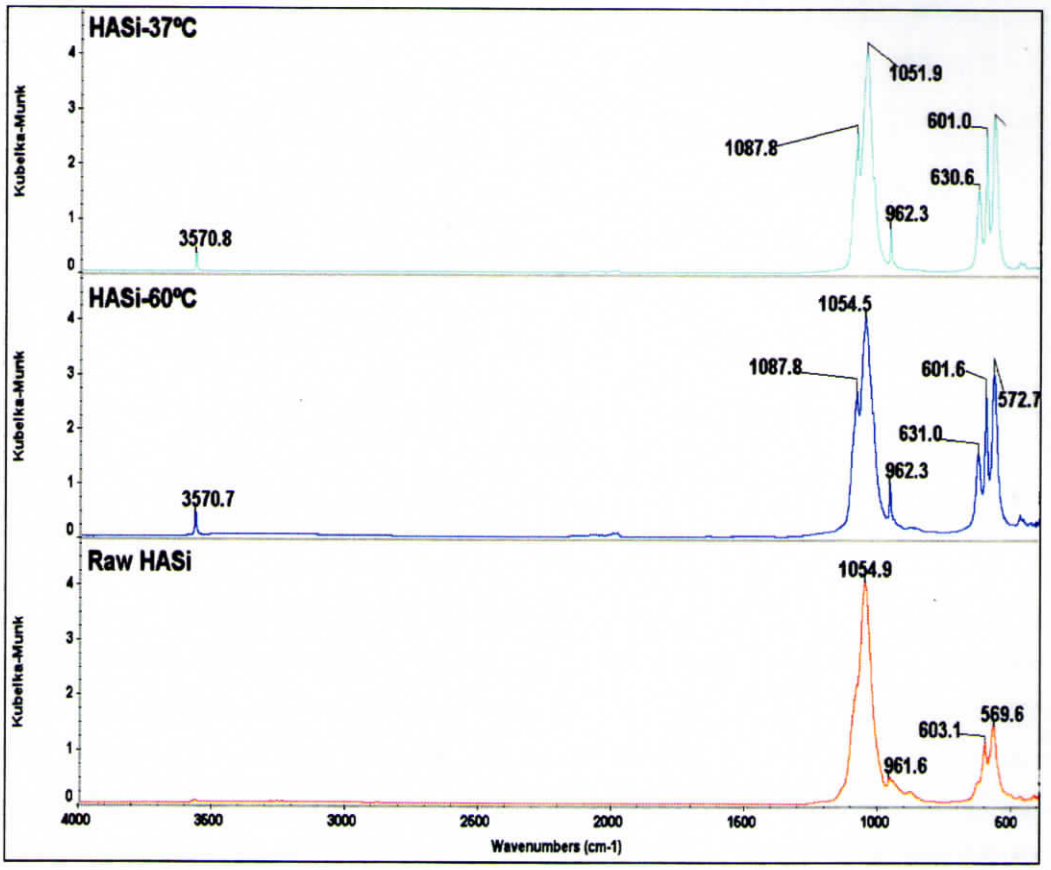

Figure 3.11. Fourier Transform Infrared spectra of HASi after immersed in PBS for 60 days.

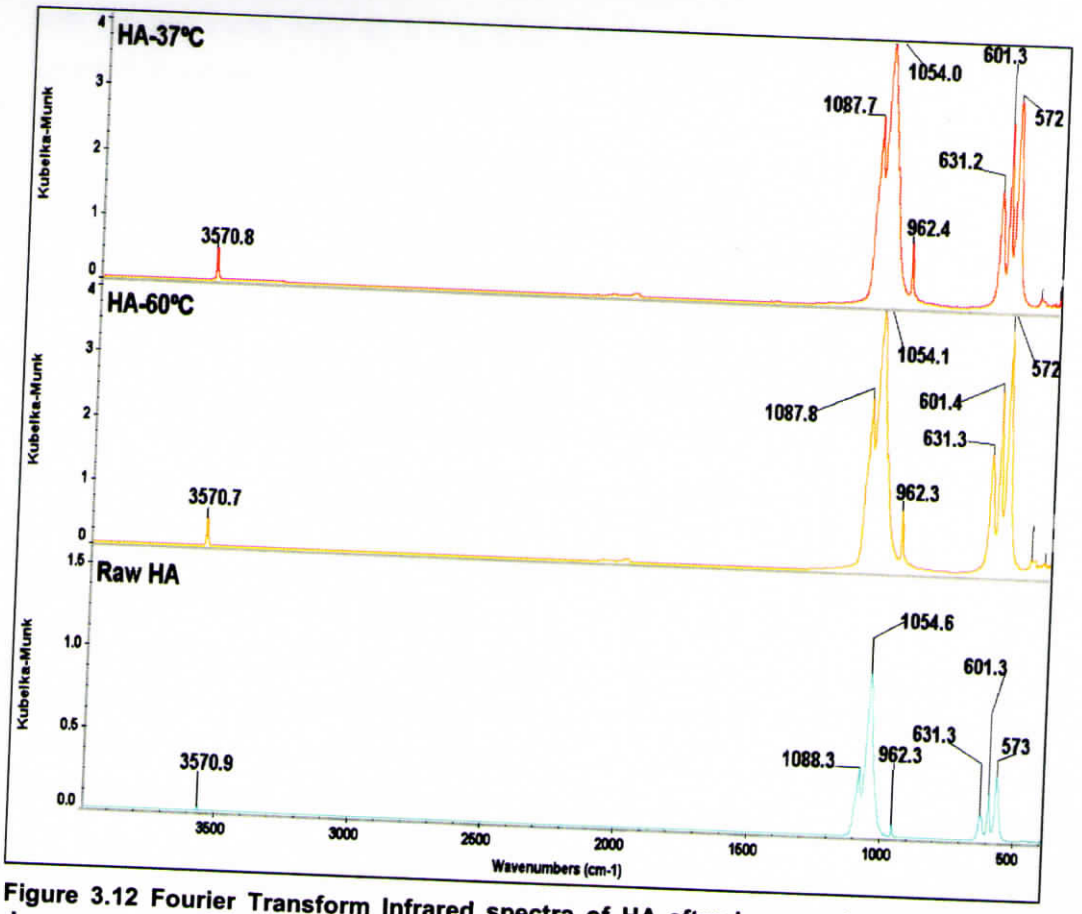

Figure 3.12 Fourier Transform Infrared spectra of HA after immersed in PBS for 60 days.

This study demonstrated the non-degradative nature of HA in PBS, which is comparable to a previous report where negligible dissolution of phase pure HA was observed after soaking in distilled water for 30 days at 37°C (Lin FH *et al.*, 1997). The slowest degradation rate may be due to high crystallinity of HA (Oonishi H *et al.*, 1995; Xue W *et al.*, 2005). On the other hand, in HASi, TCP and calcium silicate phase present in the outer coated layer dissoluted because of relatively less degree of crystallinity and less phase purity than HA. It has already been reported that TCP phase is highly soluble in biological media (Sanchez-Salcedo S *et al.*, 2006).

3.4 Cytotoxicity studies

As initial part of biocompatibility testing, cytotoxicity studies were done *in vitro* as per ISO standard 10993-5. L929 mouse fibroblast cells showed its characteristic spindle shaped appearance and spread to form a confluent monolayer after direct contact

with HA and HASi, after 48 h (Fig 3.13). This proved that HA and HASi is non-cytotoxic in nature.

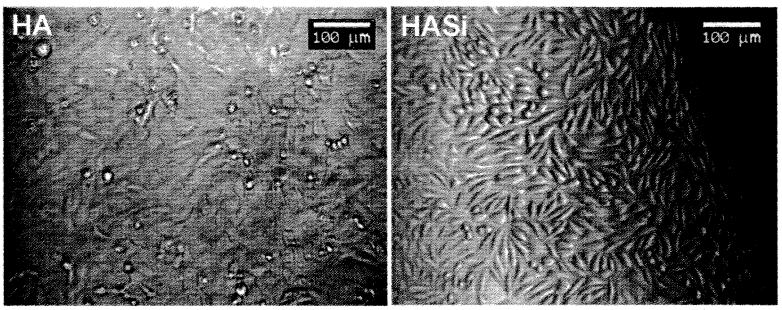

Figure 3.13. Phase contrast images showing non-cytotoxicity of HA and HASi. L929 mouse fibroblast cells were cultured in direct contact with the materials.

3.5 Cytocompatibility studies

SEM depicted that HOS cells adhered and spread on HA and HASi, with better spreading and interconnection with the adjacent cells on HASi (Fig. 3.14). It has been shown that silica rich layer formed on the surface of silica-based biomaterials can selectively adsorb higher amount of serum glycoproteins such as fibronectin (El-Ghannam A *et al.*, 1997; El-Ghannam A *et al.*, 1999; Phan PV *et al.*, 2003). Thus the local concentration of fibronectin and the presence of other bone building components like Ca, P and Si may preferentially enhance the adhesion of osteoblasts on HASi (Weiss RE *et al.*, 1981).

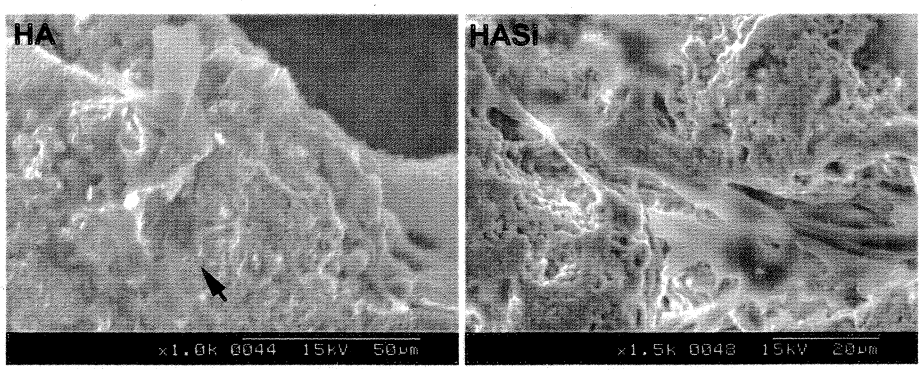

Figure 3.14. Scanning electron micrographs showing the compatibility of human osteoblast cell line on HA and HASi. Arrow- cells

CHAPTER 4

EVALUATION OF TISSUE-ENGINEERED CONSTRUCTS *IN VITRO* – PLATELET-RICH PLASMA / FIBRIN GLUE COATED AND UNCOATED BIOACTIVE CERAMICS IN CONJUNCTION WITH BMSCS

4.1 Abstract

The key component in tissue engineering is the scaffold that serves as the template for cell interactions and formation of ECM and provide the structural support for tissue regeneration. The performance of scaffolds must be examined initially in an *in vitro* cell culture system to ensure that the cells can attach and proliferate, before being implanted *in vivo.* It is proposed that coating of synthetic materials with a natural component, which mimics physiological environment like PRP or FG, can positively modulate the structural and functional properties of cells on synthetic scaffolds.

The specific objectives of the second phase of the study were 1) to expand and characterize gBMSCs 2) to study the capability of bioactive ceramics like HA and HASi to provide a microenvironment for adequate adherence, multiplication and osteogenic differentiation of BMSCs and OS+ cells (goat and human cells) separately 3) to study the effect of PRP and FG coated bioactive ceramics on the adhesion, proliferation and osteogenic differentiation of gOS+ cells.

4.2 Characterization of gBMSCs

MSCs can be enriched from whole bone marrow via their preferential attachment on TCPS (Friedenstein AJ *et al.*, 1970; Baddoo M *et al.*, 2003). The therapeutic potential of MSCs has been evaluated *in vivo* by administering the plastic adherent cell fraction of bone marrow to experimental animals (Pereira RF *et al.*, 1998). In this study as well, MSCs were isolated from the bone marrow of goat model based on their ability to adhere to TCPS flasks. Their characteristic fusiform spindle-shaped morphology was observed on day 5 (Fig. 4.1a). The cell density reached 80 - 90% confluence on day 10. The yield of cells after the isolation ranges from 1.5 to 5 x 10^5 cells / mL depending on the goat model (male or female).

A number of markers such as CD49e, CD44, CD90, CD105, CD73, STRO-1, vimentin and fibronectin are used to characterize MSCs (Zangi L *et al.*, 2006). Herein, gBMSCs were positive for vimentin staining (Fig. 4.1c). In addition, flow cytometric analysis showed that gBMSCs were negative for hematopoetic stem cell marker CD34, while the fluorescent intensity of CD44 increased when compared to unstained cells (Fig. 4.2). This confirmed the mesenchymal origin of gBMSCs.

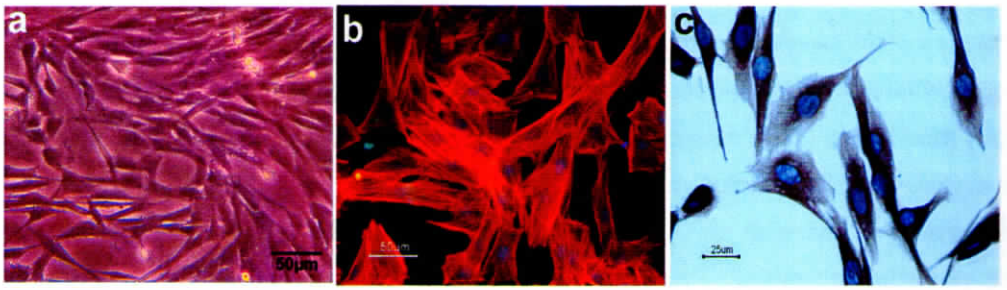

Figure 4.1. MSCs isolated from the bone marrow of goat model. (a) Phase contrast micrograph of gBMSCs on day 5; (b) Fluorescent micrograph showing cytoskeletal actin and nuclear pattern of gBMSCs through rhodamine-phalloidin (red) and Hoechst 33258 (blue) staining respectively; (c) Light micrograph showing vimentin (chromogen DAB - brown) and nuclear staining (hematoxylin - blue).

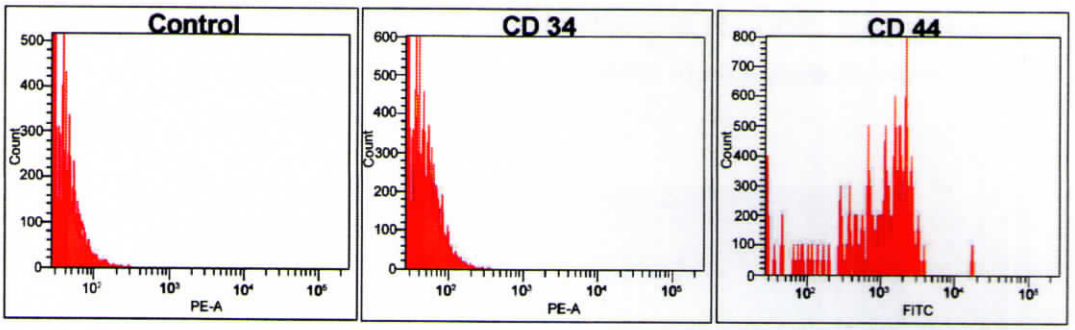

Figure 4.2. Flow cytometry analysis of the expression of CD34 and CD44 on gBMSCs - 48h. PE-A labelled CD34 (hematopoietic stem cell marker) and FITC labelled CD44 (mesenchymal stem cell marker) staining. gBMSCs without staining for these markers were used as the control.

4.3 Osteogenic differentiation of gBMSCs

Through the addition of osteogenic supplements, purified culture-expanded BMSCs can be differentiated into osteogenic lineage *in vitro,* as envisaged by the production of collagen-rich matrix, increased expression of non-collagenous proteins like ALP, osteocalcin and finally by the formation of mineralized matrix (Kern S *et al.,* 2006). Similarly, gBMSCs were induced to differentiate into the osteogenic lineage after 24 h of cell seeding by providing the osteogenic supplements like dexamethasone, L-ascorbic acid and β glycerophosphate in the medium. The activity of ALP, an early marker of osteoblasts, was found associated with the cellular regions after 48 h of cell seeding (Fig. 4.3 a). The formation of an intricate network of collagen fibers (Fig. 4.3b) and the deposition of abundant mineralized matrix composed of calcium and phosphorous (Fig. 4.3c-e) became evident on day 28. This reflected the extent of differentiation of gBMSCs towards the osteogenic lineage culminating in biomineralisation.

Earlier studies have shown that ascorbic acid is required for the synthesis of collagen and for osteogenesis *in vitro* (Maehata Y *et al.,* 2006). It also regulates ALP activity and protein synthesis in osteoblasts cultures (Son E *et al.,* 2007). The organic phosphate, β glycerophosphate, has often been used *in vitro* to provide a potential source of phosphate ions for mineralization (zur Nieden NI *et al.,* 2003). Dexamethasone, the key factor in producing bone-like nodules, is a synthetic glucocorticoid. One signal transduction pathway that has been associated with dexamethasone is the signaling of Wnt, which is a secreted glycoprotein that exerts

concentration-dependent effect on cell fate (de Boer J *et al.*, 2004). Wnt activates β-catenin resulting in its nuclear translocation that leads to an increased expression of Runx2 and ALP (Hamidouche Z *et al.*, 2008).

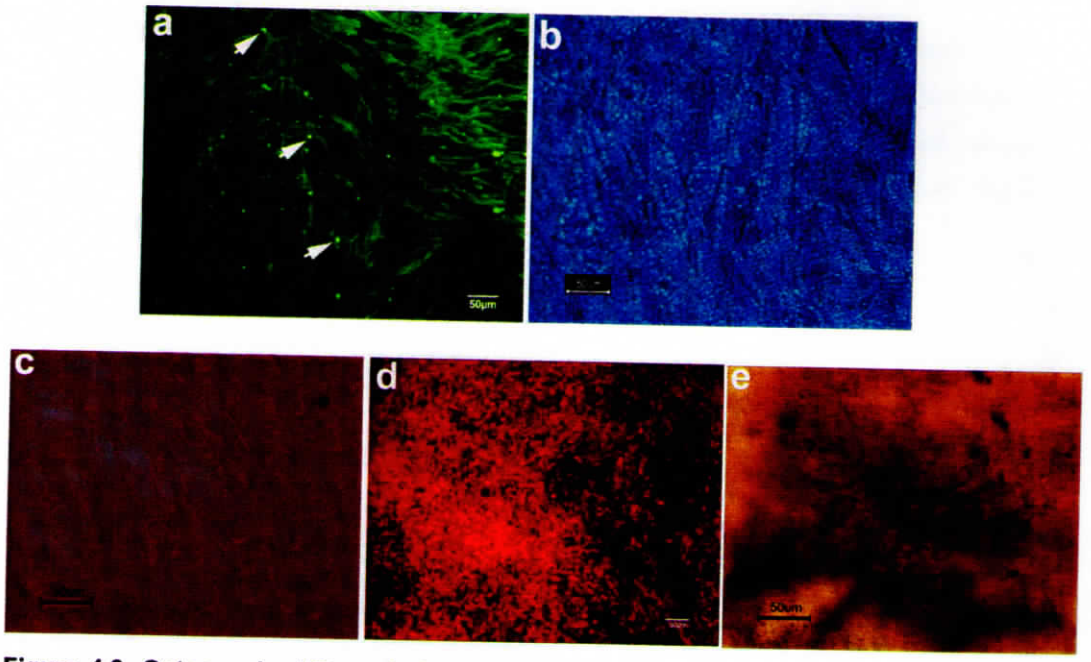

Figure 4.3. Osteogenic differentiation of gBMSCs. (a) Fluorescent image showing ALP activity (ELF-97 staining - yellowish green) and cytoskeletal actin organization (FITC phalloidin – green) after 48 h of cell seeding; (b) Light micrograph showing collagen deposition on day 28 (Masson's Trichrome staining); (c) - (e) Mineral deposition on day 28 (c) Fluorescent micrograph - Alizarin red S staining (d) Fluorescent micrograph -xylenol orange staining (e) Light micrograph - von Kossa staining

4.4 Proliferation and differentiation potential of gBMSCs

The cells may often be subcultured to generate necessary cell numbers to seed on the scaffolds for *in vivo* implantation, but it may alter the growth kinetics as well as phenotype of cells (Bruder SP *et al.*, 1997). The purpose of this study was to determine the effect of serial passaging on the proliferation and differentiation potential of gBMSCs. gBMSCs in passage 1 to 6 reached confluence on day 4 in 25 cm^2 TCPS flaks. While in later passages, the time required for the expansion of cells increased resulting in less number of cells on day 4, indicating a decline in growth rate (Fig. 4.4a). Similarly, the osteogenic differentiation potential of gBMSCs was depicted through specific ALP activity on day 7. The ALP activity was almost same for the cells in passage 2 to 5 (Fig. 4.4b), after which the activity declined.

Previous studies also demonstrated a decrease in calcium deposition and osteogenic potential of BMSCs after 3 - 4 passages (Ter Brugge PJ *et al.*, 2002; Sugiura F *et al.*, 2004). Serial passaging has been found to alter surface marker expression, which reflects a marked change in the response of MSCs to chemical stimuli that promote osteogenesis (Wall ME *et al.*, 2007). The reduction in expansion potential may be due to the progressive shortening of telomere during sub cultivation (Kobune M *et al.*, 2005). Since gBMSCs from passage 2 to 5 showed similar expansion and differentiation potential, these cells were used for further tissue engineering application.

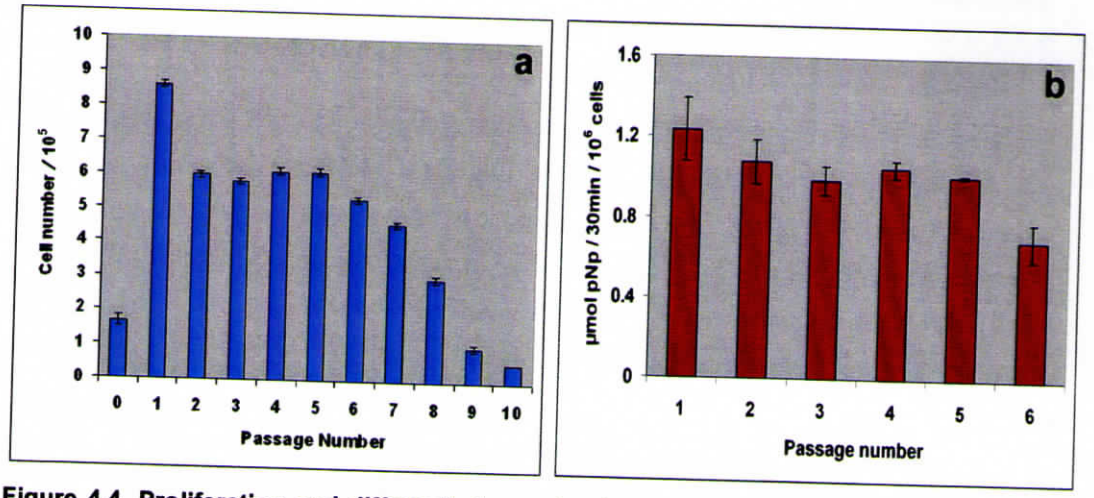

Figure 4.4. Proliferation and differentiation potential of gBMSCs in several passages. (a) The cell number obtained on day 4 after each passage (trypan blue staining and manual counting with hemocytometer); (b) The specific ALP activity on day 7, determined based on the hydrolysis of p-nitrophenyl phosphate to p-nitrophenol.

4.5 Evaluation of gBMSCs and osteogenic induced gBMSCs on bioactive ceramics

Tissue-engineered constructs were fabricated using HA and HASi in conjunction with gBMSCs and gOS+ cells separately. Prior to cell seeding, the materials were conditioned, which was done to improve the characteristics of material surface for contacting with cells. When the materials soak in the medium, an initial adsorption of serum proteins occur, after which a thin layer of amorphous calcium phosphate appear on the surface, which is effective for cell proliferation (Kizuki T *et al.*, 2003).

4.5.1 Adhesion of gBMSCs

The adhesion of cells on the material is very important, which influences their ability to proliferate and differentiate. Theoretically, the cells will be spherical initially, then flatten and later sufficiently spread out so that the nucleus becomes prominent (Malik MA *et al.,* 1992). Scanning electron micrographs revealed that gBMSCs attached and adhered on HA and HASi. Alike theoretical observation, the cells were spherical at 1 h and spread at 24 h, with better spreading on HASi (Fig. 4.5).

The adhesion of cells on the material depends on the initial adsorption of serum proteins like vitronectin and fibronectin (Anselme K 2000) whose strong affinity with ceramic substrates has been reported (Zreiqat H *et al.,*1996). gBMSCs were notably spread on HASi than HA that may be due to the silica content of HASi. The surface chemistry of silica-based materials is amenable to very strong irreversible adsorption of serum proteins, which is attributed to high negative surface-charge density generated by surface silinol (Si-OH) (Lobel KD *et al.,* 1998). Si-OH will bind to various functional groups of proteins via hydrogen bonding and electrostatic ionic amine bonds (Si-O– $+H_3N$-) that favor cell adhesion (Messing RA 1969). El-Ghannam *et al.,* (1999) reported selective and strong adsorption of fibronectin on silica-based materials than HA.

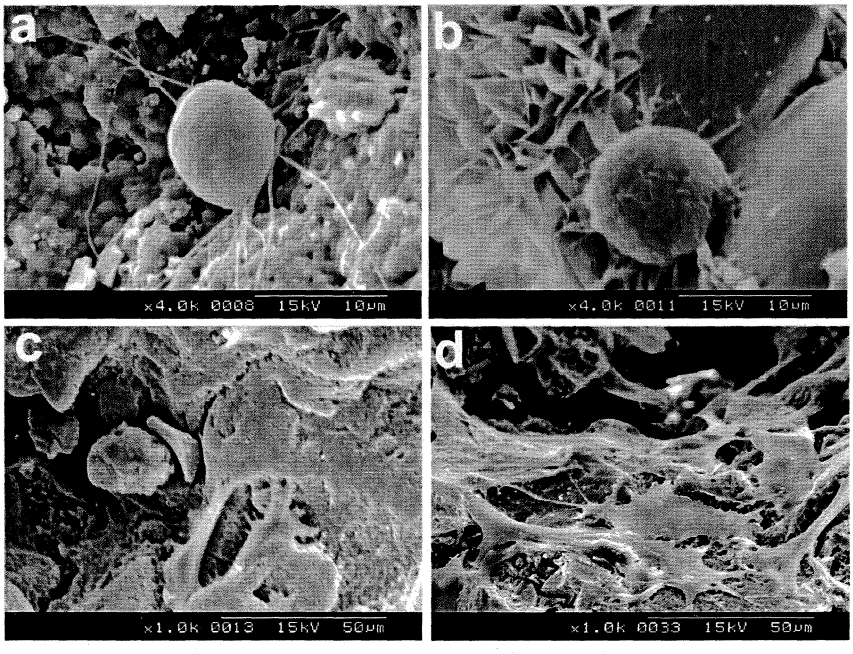

Figure 4.5. Scanning electron micrographs showing the adhesion of gBMSCs on HA and HASi (a) HA – 1h (b) HASi – 1h (c) HA – 24h (d) HASi – 24h

4.5.1 Adhesion of gBMSCs

The adhesion of cells on the material is very important, which influences their ability to proliferate and differentiate. Theoretically, the cells will be spherical initially, then flatten and later sufficiently spread out so that the nucleus becomes prominent (Malik MA *et al.,* 1992). Scanning electron micrographs revealed that gBMSCs attached and adhered on HA and HASi. Alike theoretical observation, the cells were spherical at 1 h and spread at 24 h, with better spreading on HASi (Fig. 4.5).

The adhesion of cells on the material depends on the initial adsorption of serum proteins like vitronectin and fibronectin (Anselme K 2000) whose strong affinity with ceramic substrates has been reported (Zreiqat H *et al.,*1996). gBMSCs were notably spread on HASi than HA that may be due to the silica content of HASi. The surface chemistry of silica-based materials is amenable to very strong irreversible adsorption of serum proteins, which is attributed to high negative surface-charge density generated by surface silinol (Si-OH) (Lobel KD *et al.,* 1998). Si-OH will bind to various functional groups of proteins via hydrogen bonding and electrostatic ionic amine bonds (Si-O– $+H_3N$-) that favor cell adhesion (Messing RA 1969). El-Ghannam *et al.,* (1999) reported selective and strong adsorption of fibronectin on silica-based materials than HA.

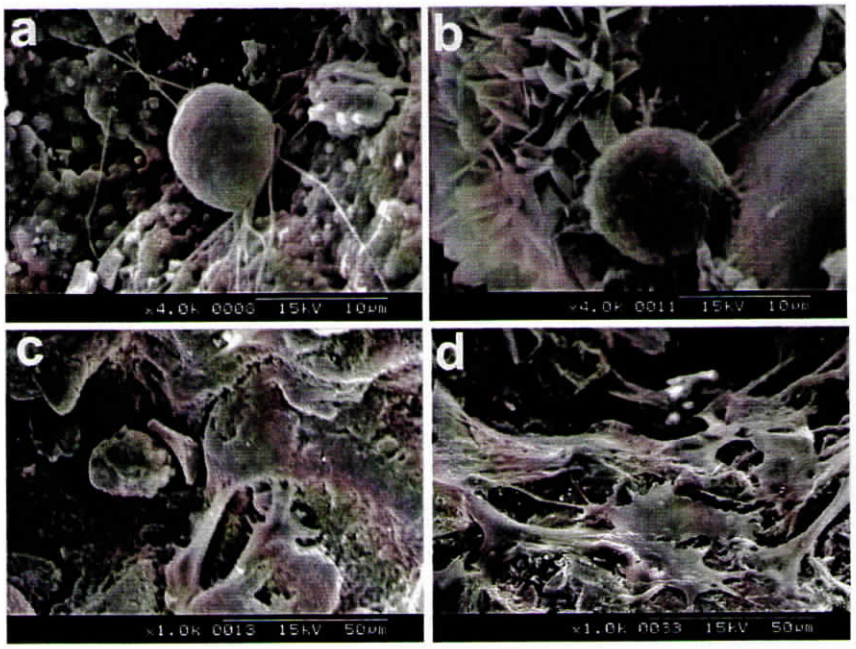

Figure 4.5. Scanning electron micrographs showing the adhesion of gBMSCs on HA and HASi (a) HA – 1h (b) HASi – 1h (c) HA – 24h (d) HASi – 24h

4.5.2 Viability of gBMSCs and osteogenic induced gBMSCs

Viability of cells on / in the scaffold was measured qualitatively and quantitatively by acridine orange and ethidium bromide staining and by LDH assay. Acridine orange is a green fluorescent dye that is permeant to living cell and intercalates between the base pairs in DNA while ethidium bromide fluoresces as orange and binds to DNA through its ability to enter damaged membranes and nucleus.

Confocal micrographs revealed that gBMSCs were homogenously adhered, distributed and rimmed around the macro pores of HA and HASi after 48 h, with slight increase in the number of viable cells on HASi (Fig. 4.6). Flow cytometric analysis supported this, which showed that about 75 - 80% of cells on HASi were positive for acridine orange staining, while on HA it was only about 60 - 65%. The remaining 20 - 25% cells were not dead but found in the quadrant, which was not emitting either acridine orange or ethidium bromide signals (Fig. 4.7).

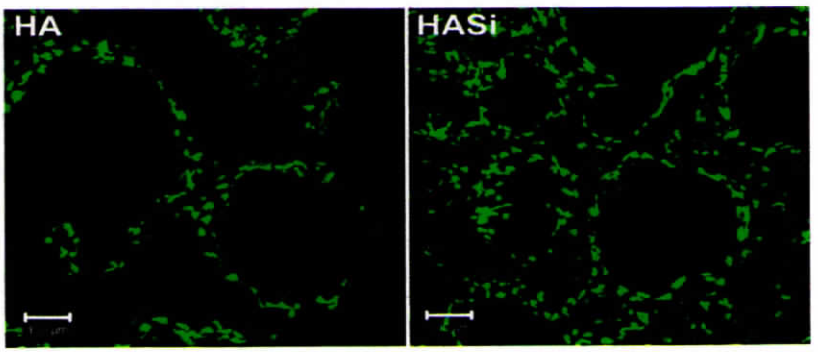

Figure 4.6. Confocal micrographs showing viable gBMSCs on HA and HASi. Acridine orange (green - live cells) and Ethidium bromide (red - dead cells) staining after 48h. The signals were collected through Argon / 2 laser (488 nm).

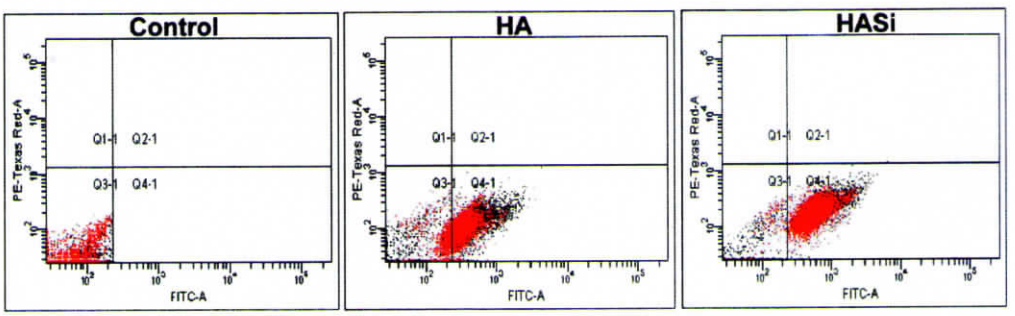

Figure 4.7. Flow cytometric analysis of the viability of gBMSCs cultured on HA and HASi. Acridine orange and Ethidium bromide staining after 48h. The cells without stain were taken as the control.

Since gBMSCs proved to be viable on HA and HASi up to 48h, LDH assay was done with gBMSCs and gOS+ cells by extending the cell culture period up to day 28. The conventional cytotoxicity detection protocols with LDH activity rely on the quantification of enzyme released into cell culture medium due to the damage of the cell membrane. In contrast, we have quantified the amount of LDH activity in undamaged cells after lysis (Sepp *et al.*, 1996), which is related to cell viability.

LDH assay showed good viability of cells on HA and HASi, which increased as the culturing period increased (Fig. 4.8). The cells cultured on HASi, both gBMSCs and gOS+ cells, had significantly higher viability ($p<0.001$) than on HA. The viability of gOS+ cells on HASi was maintained up to day 28, while on HA, it decreased after day 21. The improved performance of HASi may be attributed to the significant role of silica. Osteoblast-like cells treated with silica nanospheres have showed higher cell viability than cells without silica nanospheres (Jie Feng *et al.*, 2007). Increased viability of rat osteoblasts cultured in the presence of Si compared to that of biphasic calcium phosphate ceramic has been reported (Valerio *et al.* 2005).

While comparing two cell types, gOS+ cells were more viable than gBMSCs. The microenvironment similar to bone apatite created by HA and HASi may be more favourable for gOS+ cells than gBMSCs.

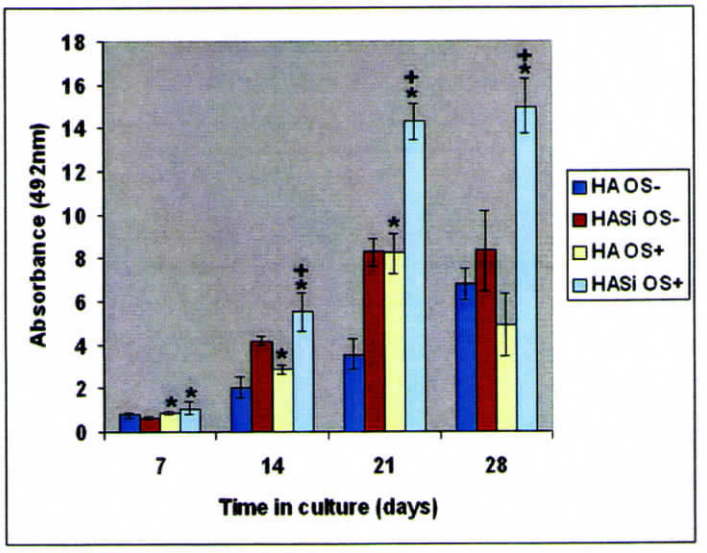

Figure 4.8. LDH assay for determining the viability of gBMSCs (OS-) and gOS+ cells cultured on HA and HASi. gOS+ cells showed significantly higher viability (*) than OS- cells and HASi significantly supported cell viability (+) than HA ($p<0.001$).

4.5.3 Proliferation of gBMSCs and osteogenic induced gBMSCs

The proliferation of cells on HA and HASi was evaluated with PCNA by flow cytometry and quantified by picogreen assay. The expression of PCNA will be elevated in the nucleus during the S-phase (replicative phase of DNA) of cell cycle and the positive cell for PCNA correlates directly with cell proliferation (Heron MI *et al.,* 1995). Similarly, picogreen is a very sensitive fluorescent dye that intercalate to DNA and is used effectively to evaluate cell proliferation (Kee WN *et al.,* 2005). More than 70 - 75% of gBMSCs on HASi were found to be positive for PCNA, while on HA the cells were less proliferative (45 - 50%) after 48 h (Fig. 4.9). In picogreen assay, gBMSCs and gOS+ cells were included and the culture period was extended up to day 28. The number of cells, both gBMSCs and gOS+ cells, were significantly increased ($p<0.001$) on HASi than HA. The proliferation of gOS+ cells on HASi was maintained up to day 28 whereas on HA it decreased after day 21 (Fig. 4.10).

The cell proliferation depends on appropriate porosity that can facilitate transport of oxygen and nutrients throughout the material (Karageorgiou V *et al.,* 2005). One study has compared goat bone marrow stromal cell proliferation on HA scaffolds of different porosities (70% porosity and 800 µm average pore size versus 60% porosity and 400 µm average pore size), which indicated that cells proliferated better on 60 / 400 scaffolds during a 6-day ex vivo culture (Kruyt MC *et al.,* 2003). The cell proliferation is also affected by sintering temperature of ceramics, which influences the crystal particle size. Report states that the proliferatrion rate of human osteoblast-like cells was higher on HA ceramics sintered above 1000℃ (Wang C *et al.,* 2004). Thus in this study, high sintering temperature in par with high porous nature of HA and HASi facilitated better cell proliferation on the materials.

The proliferation of gOS+ cells on HA was slower after 21 days of culture, which corroborated previous data with human trabecular osteoblast cells cultured on HA (Hott *et al.,* 1997). Neverthless, the cell proliferation was significant on HASi that can be accredited to its multiphase composition (HA, TCP and calcium silicate). One study reported that the presence of TCP plays an important role for the excellent response of osteoblast-like cells *in vitro.* β-TCP is highly soluble in cell cuture medium that can supply Ca^{2+} to the medium leading to improved bioactive behaviour (Sánchez-Salcedo S *et al.,* 2006). Furthermore, the silica content in HASi is a postive

factor, wherein improved cell adhesion and proliferation on silica based 2-hydroxyethylmethacrylate hydrogel when compared to pure poly (hydroxyethyl methacrylate) has been reported (Schiraldi C *et al.*, 2004). Another study reported that silica-containing bioactive glass can significantly increase cell proliferation, differentiation and viability of osteoblasts derived from rat calvaria in an *in vitro* culture condition (Valerio P *et al.*, 2004).

Similar to cell viability studies, the proliferation of gOS+ was higher than gBMSCs. Some studies have suggested a proliferation effect of osteogenic supplements like dexamethasone on cells, mediated through Wnt signalling (Jaiswal N *et al.*, 1997; De Boer J *et al.*, 2004).

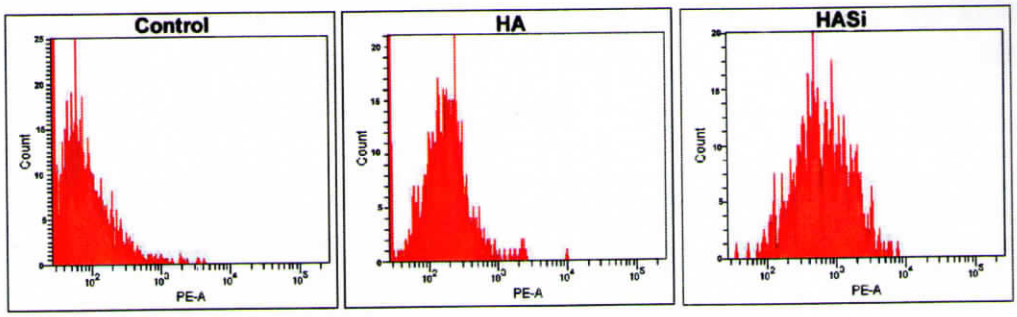

Figure 4.9. Flow cytometric analysis of the proliferation of gBMSCs cultured on HA and HASi – PCNA staining. PE-A labelled PCNA. The cells without stain were taken as control.

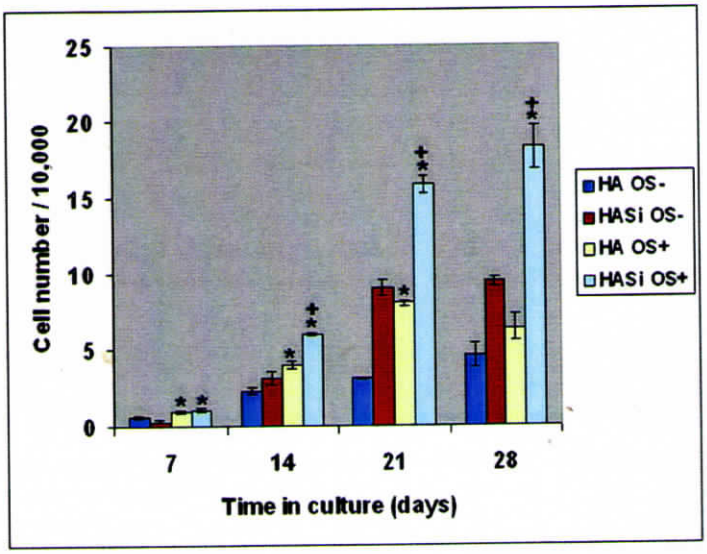

Figure 4.10. Picogreen assay for determining the proliferation of gBMSCs (OS-) and gOS+ cells cultured on HA and HASi. gOS+ cells showed significantly higher proliferation (*) than OS- cells. HASi significantly supported cell proliferation (+) than HA ($p<0.001$).

4.5.4 Morphology of osteogenic induced gBMSCs

The SEM study was performed to analyze the morphological behavior of gOS+ cells, where the cells were well spread on both HA and HASi on day 14 and 28. On HASi, the cell number was higher than HA, which morphed into a cell sheet-like canopy on day 14. On day 28, multilayers of cells were observed on HASi without pore bridging and occlusion (Fig. 4.11). Previous studies depicted that dexamethasone-treated MSCs exhibited a cuboidal phenotype in culture (Mauney JR *et al.,* 2004a), but herein the phenotype of individual cells were indistinguishable, particularly on HASi. The cell sheet-like structure supported the characterization of the population of cells as homogenous. It is reported that the spreading and continuous multilayer of osteoblasts is favored on smooth surfaces because focal contacts are uniformly distributed on smooth surfaces than rough surfaces (Anselme K *et al.,* 2000; Kieswetter K *et al.,* 1996). Thus smooth surface due to silica coating implicates HASi as a favorable substrate for the profuse proliferation of cells.

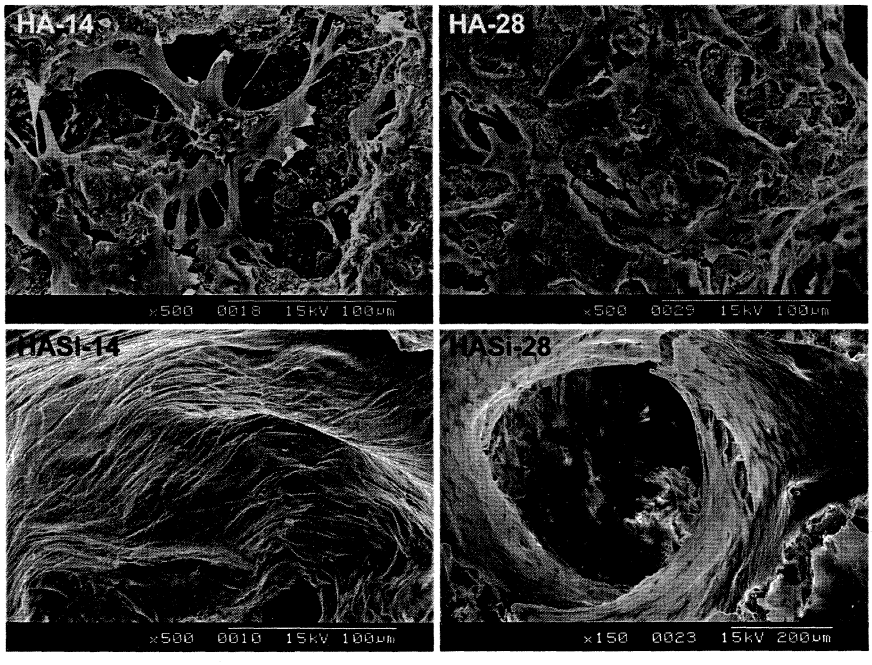

Figure 4.11. Scanning electron micrographs showing the morphology of gOS+ cells on HA and HASi - Day 14 and day 28.

4.5.5 In depth migration of osteogenic induced gBMSCs

The primary limitation of many culture systems, particularly static, is the depth of cell ingrowth. This is due to the diffusion limitation of cell culture media towards the centre of scaffold and the rapid formation of tissue on the outer surface of scaffold making the cells in the centre necrotic (Salgado AJ *et al.,* 2004). So in order to visualize the concealed distribution of cells lying within the internal voids of the material, cross sections of PMMA embedded tissue-engineered constructs were taken and stained on day 14 and day 28. On HA, most of the cells were seen on the periphery of the material and has penetrated only to a few millimeter depth (approximately up to 5 to 6 mm), whereas in HASi, the cells were able to migrate and invade the internal pores of the material. Patches of adhered and spread cells were distributed within the mid region of the material (Fig. 4.12). Confocal microscopy confirmed the firm lodging of viable cells in the internal niches of HASi through the scanning of multiple thin sections in z-axis direction (Fig. 4.13).

The spreading and migration of cells towards the mid region of HASi signifies the importance of the pore size of the scaffold. If the pores are small, pore occlusion will happen that will prevent cellular penetration and ECM production in the inner areas of the scaffold. Osteoblasts prefer pore size ranging from 200 - 400 µm in diameter that encourages migration, attachment and proliferation because the pore curvature provides optimum compression and tension on the cell's mechanoreceptors (Boyan BD *et al.,* 1996). When primary rat osteoblasts were seeded onto scaffolds with different pore sizes, cell migration was faster in larger pore scaffolds (100 µm) (Takahashi Y *et al.,* 2004). Thus the highly interconnected porous architecture with pore size in the range of 50 - 500 µm in HASi definitely improved the migration and distribution of cells through out the material.

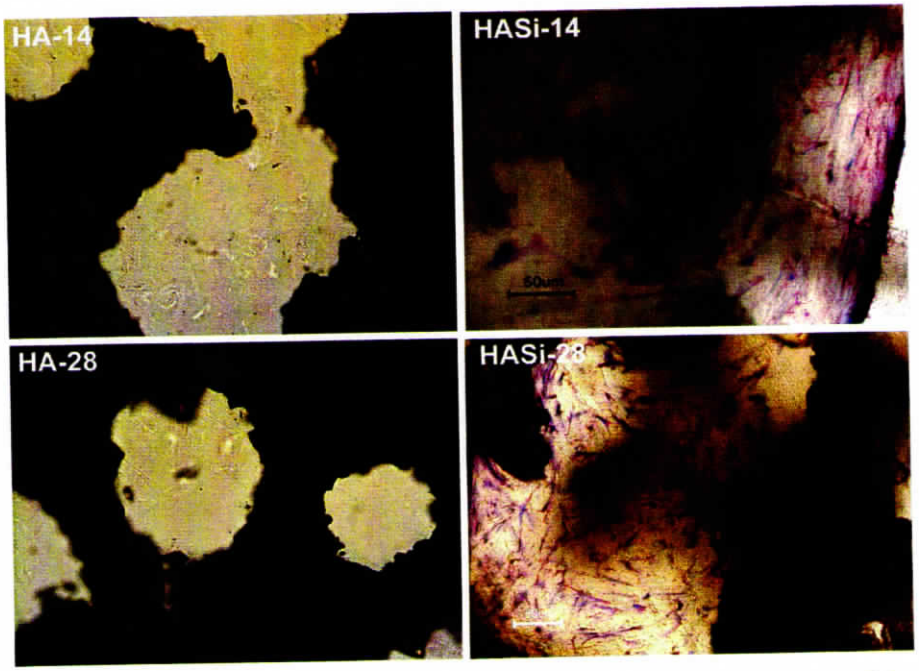

Figure 4.12. Light micrographs showing the migration and invasion of gOS+ cells towards the inner region of HA and HASi – Day 14 and day 28 (Size of the scaffold: 2cm).

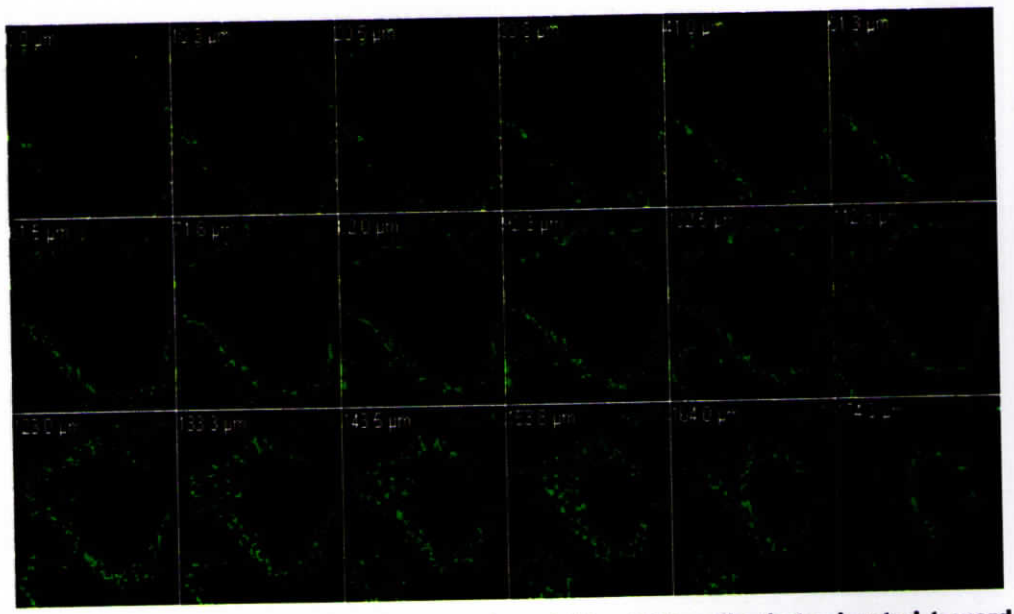

Figure 4.13. Confocal micrographs showing viable gOS+ cells that migrated towards the inner region of HASi. Acridine orange (green – live cells) and Ethidium bromide staining (red – dead cells) after 28 days. The signals were collected through Argon / 2 laser (488 nm). The sections were scanned up to 174 µm with a slice thickness of 10 µm.

4.5.6 Differentiation of gBMSCs into osteogenic lineage

The differentiation of gBMSCs into osteogenic lineage was confirmed through the presence of non-collagenous proteins like ALP, osteocalcin and osteopontin. The maturation of differentiated cells was validated through the level of their expression at each period.

4.5.6.1 Alkaline Phosphatase activity

ALP, an essential enzyme for the deposition of minerals, is present in pre-osteoblast s at an early stage of osteoblast differentiation and its level is found to be increased around the second week of *in vitro* culture (zur Nieden NI *et al.*, 2003; Stein GS *et al.*, 1990). Accordingly in this study, the specific ALP activity (ALP activity per cell) of gOS+ cells increased up to 14 days in culture after which the activity decreased. The activity was significantly higher on HASi when compared to HA ($p<0.001$) on day 7 and 14 (Fig. 4.14). gBMSCs showed low ALP activity, demonstrating that the differentiation towards osteoblastic lineage can happen only in the presence of osteogenic supplements in the cell culture medium. The ALP activity was further demonstrated through ELF-97 staining by confocal microscopy on day 10 and the results were correlated with biochemical data (Fig. 4.15).

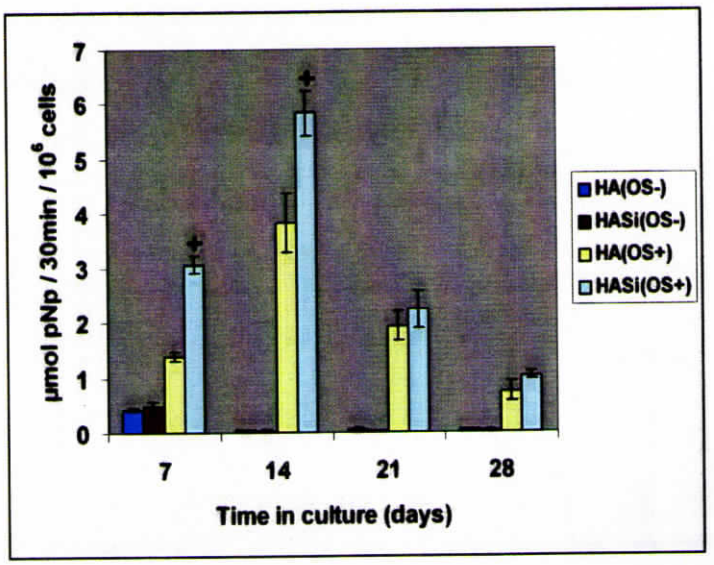

Figure 4.14. Specific ALP activity of gBMSCs and gOS+ cells cultured on HA and HASi - biochemical estimation. The ALP activity was determined based on the hydrolysis of p-nitrophenyl phosphate to p-nitrophenol. gBMSCs (OS-) cells showed low ALP activity. The activity was significantly higher on HASi (+) than HA ($p<0.001$).

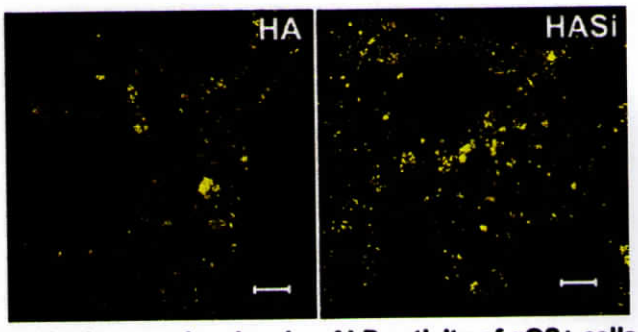

Figure 4.15. Confocal micrographs showing ALP activity of gOS+ cells on HA and HASi - ELF-97 staining. The signals were collected through blue diode (405 nm). Day 10

4.5.6.2 Osteopontin expression

Osteopontin, which is involved in binding calcium ions and HA during mineralization process is present in proliferating pre-osteoblasts and in mature osteoblasts. Its level is enhanced during the third week of culture (zur Nieden NI *et al.*, 2003; Lawton DM *et al.*, 1999). Herein, flow cytometric analysis showed a similar trend in gOS+ cells with the highest expression on day 21 on HA and HASi (Fig. 4.16). HASi showed significant increase in expression than HA. gBMSCs, which is taken as the control did not show any expression on both the substrates. The appreciable expression of osteopontin on HASi scaffolds was further confirmed with confocal microscopy on day 21 (Fig. 4.17).

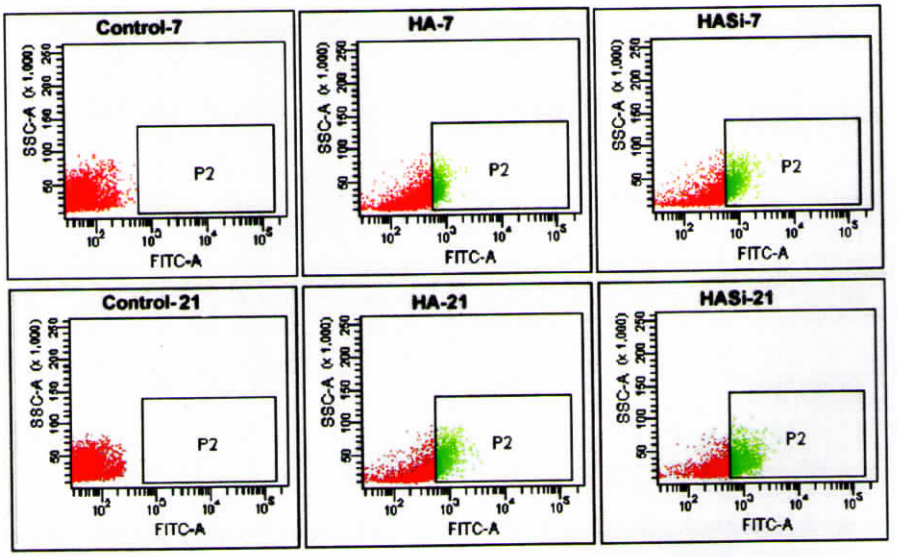

Figure 4.16. Flow cytometric analysis of the expression of osteopontin on gOS+ cells cultured on HA and HASi. Day 7 and day 21. FITC-labelled anti-osteopontin antibody was used for staining. gBMSCs were taken as the control.

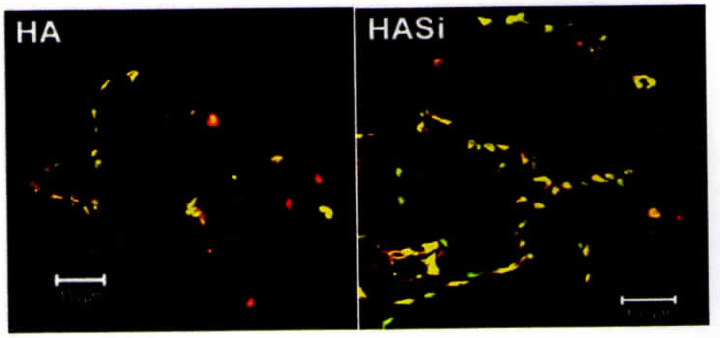

Figure 4.17. Confocal micrographs showing osteopontin expression on gOS+ cells cultured on HA and HASi. Day 21. FITC-labelled anti-osteopontin antibody for osteopontin (green) and rhodamine B phalloidin for actin (red). The signals were collected through Argon / 2 laser for FITC and HeNe 543 laser for rhodamine B.

4.5.6.3 Osteocalcin assay

Osteocalcin, a convenient marker for fully differentiated osteoblasts, is involved in the mineralization process, which shows increased expression during the fourth week of culture. (zur Nieden NI *et al.*, 2003; Weinreb M *et al.*, 1990). gOS+ cells on HASi significantly secreted osteocalcin into the medium than HA ($p<0.001$). The highest secretion was on day 28 on both the substrates establishing the transition to mature osteoblast phenotype during this period. gBMSCs, which was taken as the control, insignificantly secreted osteocalcin (Fig. 4.18).

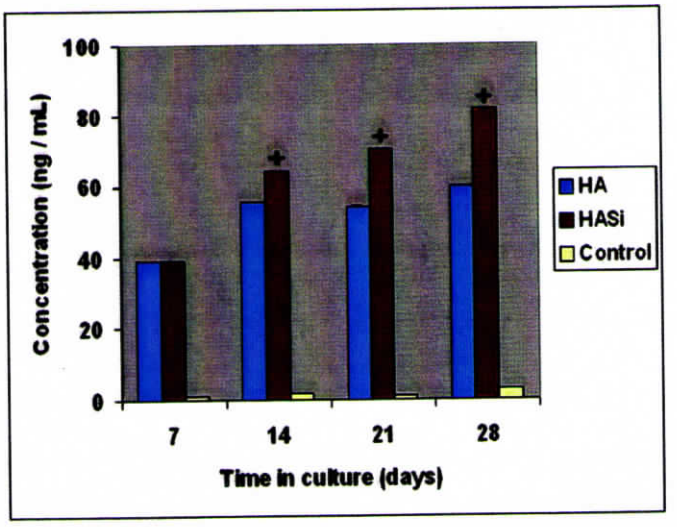

Figure 4.18. Graphs showing the concentration of osteocalcin in the medium secreted by gOS+ cells cultured on HA and HASi – ELISA technique. gBMSCs were taken as the control. The secretion was significantly higher with HASi (+) than HA ($p<0.001$).

Here gBMSCs differentiated to pre-osteoblasts and later to mature osteoblasts on both HA and HASi in the presence of osteogenic supplements, comparable to previous studies (Shu R *et al.,* 2003). However, an enhanced expression of non-collagenous proteins was observed on HASi than HA, which implies that osteoblasts respond to the difference in surface chemistry or topography. Although not a general rule, some studies have reported that the osteoblast differentiation is better on smooth than rough surfaces. This may validate the significant differentiation of gBMSCs on HASi (smooth) when compared to HA (rough). Human osteoblast-like cells (MG63) and adult jaw bone cells had lower proliferation and ALP activity on rough titanium disk and HA respectively when compared to smooth surface (Martin JY *et al.,* 1996; De Santis D *et al.,* 1996). Another explanation for the positive influence on osteogenic differentiation is the Si content in HASi (Xynos ID *et al.,* 2001; Loty C *et al.,* 2001). A better biological performance like proliferation and differentiation of mouse calvarial osteoblasts on PMMA / silica hybrid material was observed when compared to PMMA alone (Rhee S *et al.,* 2003). When ROS 17 / 2.8 cells (rat osteosarcoma cell line) were cultured on porous bioactive glass with 45% silica, high levels of ALP activity and maintenance of the osteoblastic phenotype was noticed (Kaufmann EA *et al.,* 2000). Thus the timely expression of ALP, osteopontin and osteocalcin indicated that HASi augmented osteoblast commitment and ultimately attained the phenotype of "mature osteoblasts or osteocytes" when compared to HA.

4.6 Evaluation of hBMSCs and osteogenic induced hBMSCs on bioactive ceramics

Tissue-engineered constructs were fabricated using HA and HASi in conjunction with hBMSCs and hOS+ cells separately. Prior to cell seeding, the materials were conditioned, which was done to improve the characteristics of material surface.

4.6.1 Adhesion of hBMSCs

The initial adhesion of hBMSCs on HA and HASi was evaluated by SEM which depicted round morphology for most of the cells on both the substrates after 1 h of cell seeding. However, few cells started spreading on HASi at this time. The adhesion and spreading became more obvious 4 h after seeding. After 24 h, the cells appeared well spread on both HASi and HA, with slightly more preference for the

silica coated surface (Fig. 4.19).

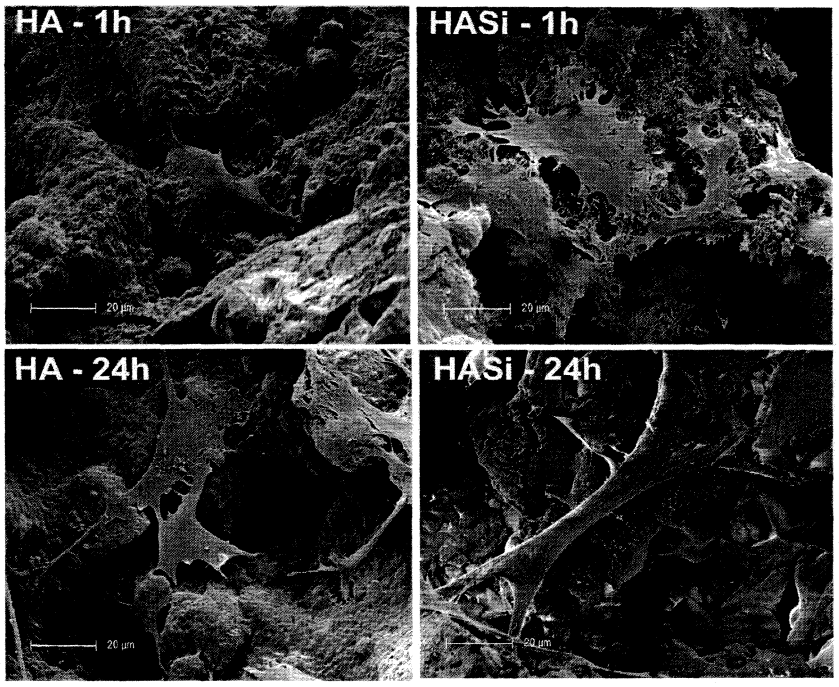

Figure 4.19. Scanning electron micrographs showing the adhesion of hBMSCs on HA and HASi. 1 h and 24 h

4.6.2 Viability of hBMSCs and osteogenic induced hBMSCs

Confocal images depicted a high ratio of living hBMSCs on HA and HASi at 24 h (Fig. 4.20). Since hBMSCs proved to be compatible with both the substrates, further studies were done by extending the culture period and by including hOS+ cells. LDH assay revealed a significantly higher rate of viability on HASi compared to HA ($p < 0.001$) particularly after the first week of culture (Fig. 21). While comparing the two cell types, the viability of hOS+ cells were significantly higher than hBMSCs.

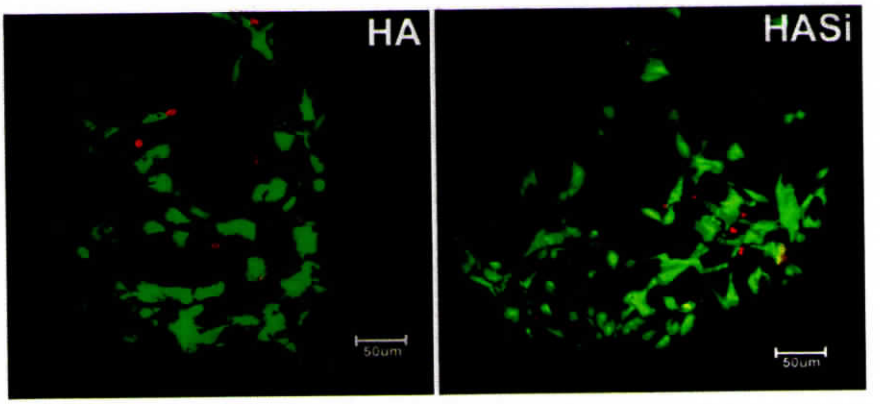

Figure 4.20. Confocal micrographs showing viable hBMSCs on HA and HASi. 4 mM calcein AM (green - viable) and 2 mM ethidium homodimer-1 staining (red- dead) staining after 24h. Ar^+ laser for calcein AM and HeNe laser 528 for ethidium homodimer.

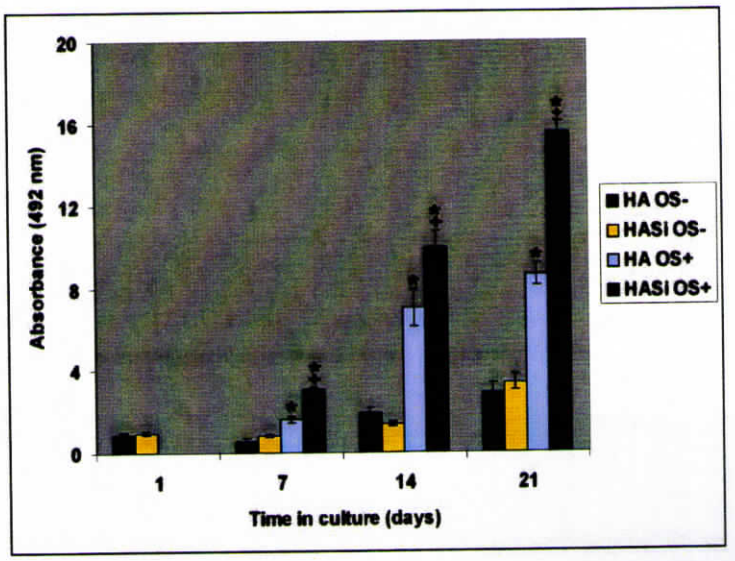

Figure 4.21. LDH assay for determining the viability of hBMSCs (OS-) and hOS+ cells cultured on HA and HASi. hOS+ cells showed significantly higher viability (*) than OS- cells and HASi significantly supported cell viability (+) than HA ($p<0.001$).

4.6.3 Proliferation of hBMSCs and osteogenic induced hBMSCs

Picogreen DNA assay revealed that the number of hOS+ cells on HASi was significantly higher than that on HA ($p<0.001$). The hOS+ cells also showed significantly higher proliferation when compared to hBMSCs on both HA and HASi (Fig. 4.22).

The considerable increase in spreading and proliferation of hOS+ cells on HASi was

further supported by SEM analysis, which showed that the cells appeared to be in a stage of confluency and formed a cell sheet-like canopy on day 14. On day 28, the cultures developed an interconnected network of ECM over the material without pore occlusion or pore bridging (Fig. 4.23).

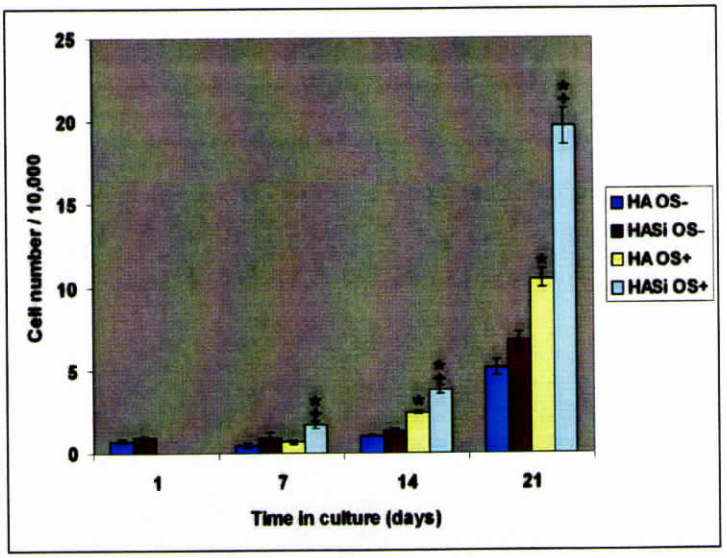

Figure 4.22. Picogreen assay for determining the proliferation of hBMSCs (OS-) and hOS+ cells cultured on HA and HASi. hOS+ cells showed significantly higher proliferation (*) than OS- cells and HASi significantly supported cell proliferation (+) than HA ($p<0.001$).

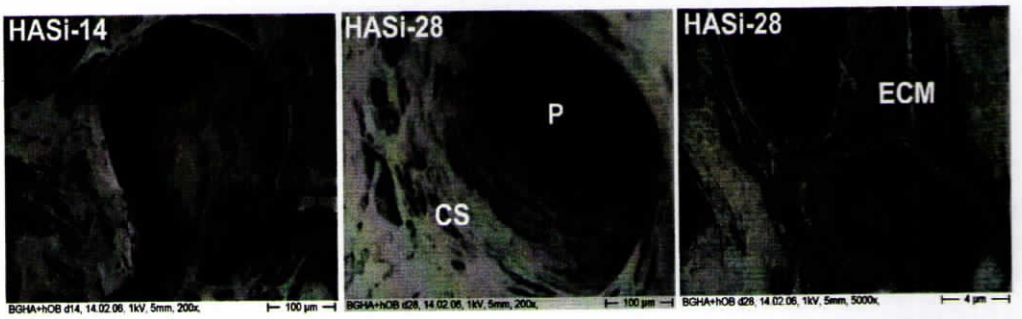

Figure 4.23. Scanning electron micrographs showing the morphology of hOS+ cells cultured on HA and HASi. Day 14 and Day 28. CS - cell sheet; P - pore; ECM - extracellular matrix.

The enhanced proliferation of hOS+ cells on HASi is consistent because previous studies have proved that human osteoblasts are influenced by the presence of silicon in HA substrate (Botelho *et al.*, 2006; Phan PV *et al.*, 2003). MC3T3-E1 cells seeded on Bioglass containing 45% silica exhibited higher proliferative capacity when compared to HA disks with zero silica. An increased synthesis of ECM was

also observed in that study (El- Ghannam *et al.*, 1997). Similar to goat cells, hOS+ cells also responded better than hBMSCs, both in terms of viability and proliferation.

4.6.4 Differentiation of hBMSCs into osteogenic lineage

4.6.4.1 Alkaline Phosphatase activity

The specific ALP activity of hOS+ cells were significantly higher on HASi on day 7 and 14 when compared to HA ($p<0.01$). The ALP activity of hBMSCs remain unchanged over the whole culture period of 21 days indicating that the differentiation of hBMSCs happens only in the presence of osteogenic supplements (Fig. 4.24). Confocal micrograph with ELF-97 staining also supported the biochemical data (Fig. 4. 25).

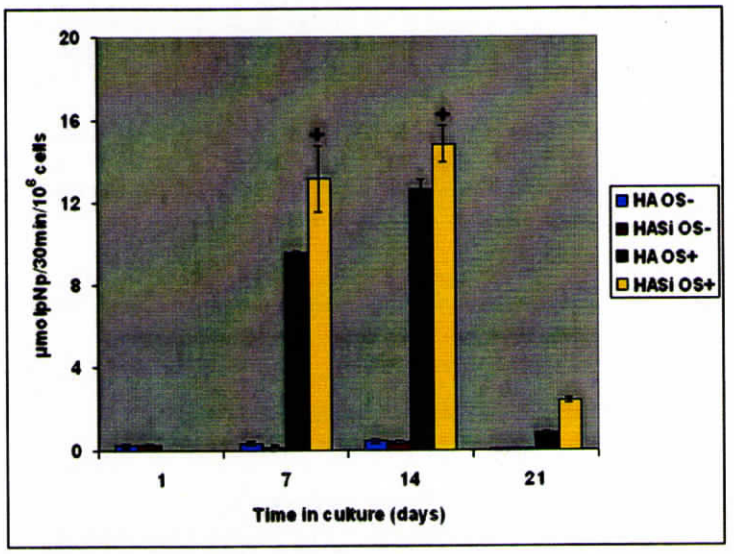

Figure 4.24. Specific ALP activity of hBMSCs and hOS+ cells cultured on HA and HASi – biochemical estimation. The activity was determined based on the hydrolysis of p-nitrophenyl phosphate to p-nitrophenol. The activity was significantly higher on HASi (+) than HA ($p<0.01$). hBMSCs (OS-) cells showed low ALP activity.

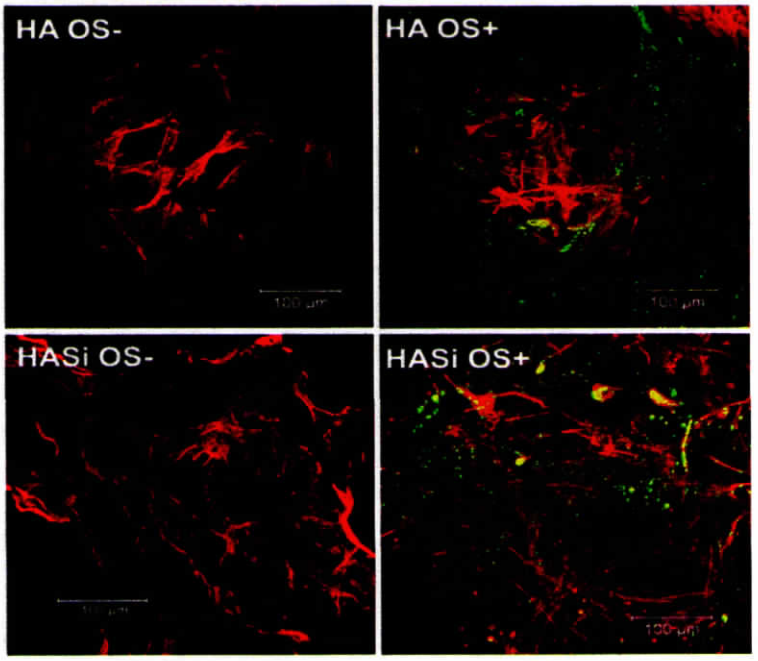

Figure 4.25. Confocal micrographs showing ALP activity of hBMSCs and hOS+ cells cultured on HA and HASi - ELF-97 staining. Rhodamine-phalloidin (actin - red) and ELF-97 (ALP activity - yellowish green) staining. The signals for ALP were collected through blue diode.

4.6.4.2 Expression of Alkaline Phosphatase and Bone sialo protein

Real-time PCR analysis of ALP and BSP II expression was done to confirm the differentiation of hBMSCs into the osteogenic lineage. The relative ALP expression was almost similar on HA and HASi on day 7, while on day 14, HASi showed a significant increase in the expression (Fig. 4.26). gBMSCs showed low ALP expression on all the days. Even though a significant difference in the ALP activity (protein level) between HA and HASi was noticed on day 7, there were no change in the ALP expression (mRNA level) on day 7. Silica may have a role in the post-translational level, but the real molecular mechanism has to be elucidated.

BSP II expression was insignificant on day 7 on HA and HASi, similar to the level of the expression shown by gBMSCs. However on day 14, HASi showed a significant increase in its expression than HA, which represented "mature osteoblast cells or osteocytes" on the materials by the second week of culture (4.27).

The promoting effect of ionic dissolution products of bioactive glass (mainly Si^{4+} and

Ca^{2+}) on the gene expression of human osteoblast involved in osteoblast proliferation and ECM remodeling has been reported (Phan PV *et al.*, 2003; Christodoulou I *et al.*, 2005). Another study depicted that by the supplementation of orthosilicic acid to human osteoblasts, an increase in ALP activity and osteocalcin has been observed (Reffitt DM *et al.*, 2003).

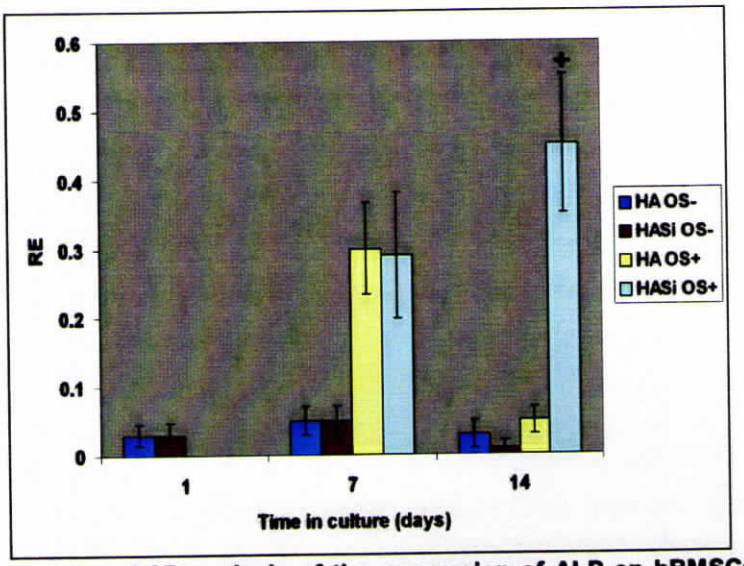

Figure 4.26. Real-time PCR analysis of the expression of ALP on hBMSCs and hOS+ cells cultured on HA and HASi. hBMSCs (OS-) showed low ALP expression. HASi showed significant increase in expression (+) than HA ($p<0.001$).

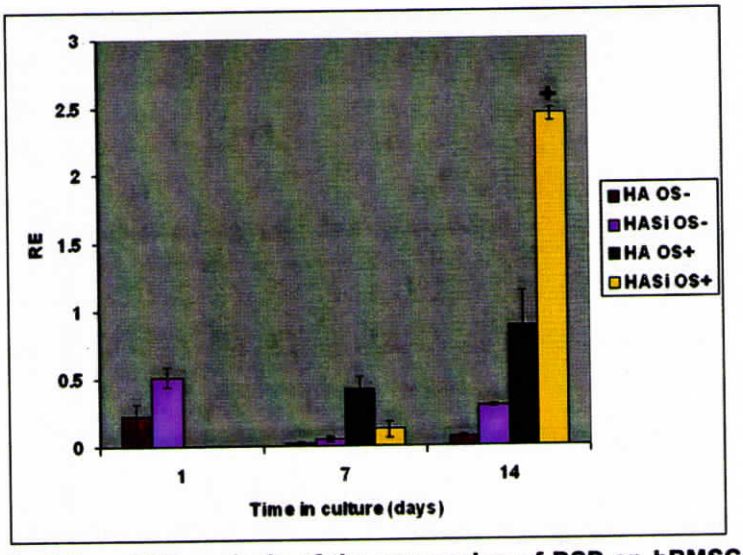

Figure 4.27. Real time PCR analysis of the expression of BSP on hBMSCs and hOS+ cells cultured on HA and HASi. hBMSCs (OS-) showed low BSP expression. HASi showed significant increase in expression (+) than HA ($p<0.001$).

The overall study showed that HA and HASi were capable of supporting the growth and functional activity of both goat and human cells. The stimulatory effect of HA on osteoblasts has already been reported (Xie J *et al.,* 2004), which is attributed to the presence of calcium and phosphorous, very similar to bone apatite. The increased level of extracellular calcium has been shown to induce osteoblast proliferation and chemotaxis through binding to a G-protein coupled extracellular calcium sensing receptor (Yamaguchi T *et al.,* 1998; Yamaguchi T *et al.,* 2000). The ability of osteoblasts to transport phosphorous is recognized as a requirement for the induction of gene expression. The influx of phosphorous into osteoblasts via the action of sodium-dependent phosphate cotransporter mechanism has been shown to trigger ECM proteins and subsequently mineralization (Beck GR Jr *et al.,* 2000). In addition to the prevalence of calcium and phosphorous, the highly interconnected porous architecture has also favoured the cellular function on HA and HASi.

The coating of HA with silica sol resulted in marked changes in cell behaviour, which confirms the importance of surface chemistry on osteoblast behaviour (Lossdörfer S *et al.,* 2004). Silica-based biomaterials can enhance biological activity through the (a) surface availability of Si and its influence on surface charge (b) local Si release (Hing KA *et al.,* 2006). In the first mechanism, an electronegative silanol (Si-OH) group will be generated on the surface of silica-based materials due to the ion exchange with H^+ and H_3O^+ (Lobel KD *et al.,* 1998). The ion exchange causes a rise in pH, thus influencing cell metabolism and function (Busa WB *et al.,* 1984). The process of ion exchange is followed by the formation of a silica-gel layer that can selectively and strongly adsorb serum glycoproteins and initiate cell adherence, therefore allowing for increased cell proliferation and differentiation. The second mechanism is the release of Si from silica-based biomaterials. Solutions of high silicon concentration induce osteoblasts and stimulate a subset of genes related to osteoblast function. One study reported that the ionic product of Bioglass with Si induced the expression of several growth factors and many kinases in signaling cascades like extracellular signal-regulated kinase (ERK) and mitogen-activated proteins kinases (MAPKs) pathways (Xynos *et al.,* 2001).

The response of goat and human cells on HA and HASi in terms of viability,

morphology and proliferation was approximately same with no significant difference, which implies the comparability between these two species for *in vivo* studies. However, the ALP activity of goat cells was significantly lower than human cells in this study, which may be probably species related. This data is comparable to a previous study where the ALP activity of human cells was 10 - 20 times higher than goat cells (Kruyt *et al.,* 2004).

Generally, the cell proliferation and differentiation are two interdependent processes having a counteracting relationship. When the cells go through differentiation lineage with subsequent induction of genes associated with matrix maturation and mineralization, a decline in cell proliferation is reported on TCPS plates (Stein GS *et al.,* 1990). A similar phenomenon was observed on HA, where the cell proliferation was decreased after the third week of culture. On the other hand, interestingly, HASi was capable of maintaining the cell proliferation and osteogenic maturation in a parallel relationship. Recently, results with human MSCs and human fibroblasts indicated that the growth on denatured collagen matrix resulted in the reduction of the rate of cellular aging with simultaneous increase in the retention of osteogenic-specific functions and markers (Mauney JR *et al.,* 2004b). Rat calvarial osteoblasts showed an enhanced proliferation and differentiation on *O*-phospho-L-serine modified calcium phosphate bone cement (Reinstorf A *et al.,* 2004). Thus the ultimate fortune of cells is determined by the respective matrix / substratum.

4.7 Evaluation of osteogenic induced gBMSCs on fibrin glue and platelet-rich plasma coated bioactive ceramics

The reponse of gOS+ cells on six group of materials were included in the study. The group were (1) uncoated HA (HA) (2) uncoated HASi (HASi) (3) PRP coated HA (PHA) (4) PRP coated HASi (PHASi) (5) Fibrin glue coated HA (FHA) (6) Fibrin glue coated HASi (FHASi) was included in the study.

4.7.1 PRP separation and platelet coating

PRP was separated from the blood by centrifuging at 2500 rpm for 5 min. The platelet count of goat blood was approximately 400 x 10^6 platelets / mL whereas for PRP, it was about 600 x 10^6 platelets / mL (1.5 fold increase). Similarly, the platelet count of human blood was about 200 x 10^6 platelets / mL and for PRP, it was about

400 x 10^6 platelets / mL (2 fold increase).

The coating of platelets on HA and HASi was performed by immersing these materials in PRP for 1h with agitation. The percentage reduction of platelets in PRP was higher with HA than HASi, indicating more adsorption of platelets on HA (Fig. 4. 28a). There were no significant differences in the adsorption between goat and human platelets. These results were further confirmed by LDH assay (Fig. 4.28b). The greater adsorption of platelets on HA may be due to its rough surface when compared to HASi. It has been reported that rough surfaces display an increase in fibrinogen adsorption and platelet adhesion at early blood contact times (Nygren H *et al.*,1997).

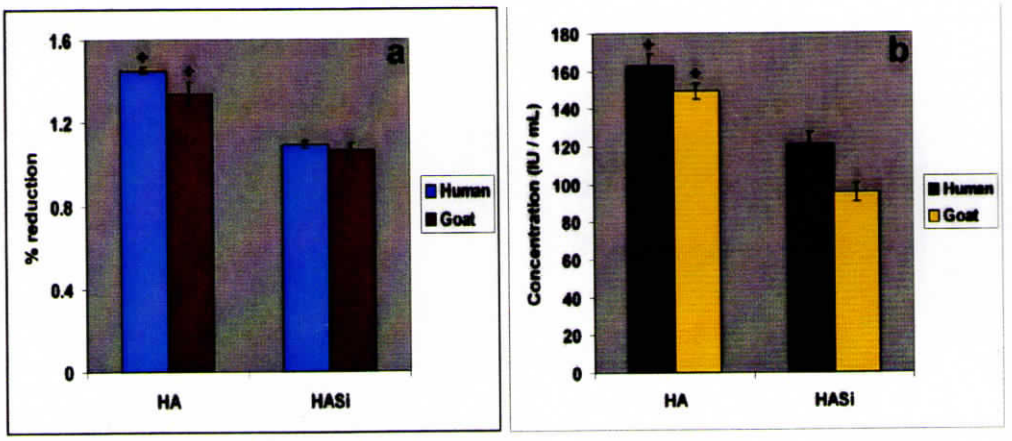

Figure 4.28. The adhesion of goat and human platelets on HA and HASi (a) The percentage reduction of platelets in PRP after agitation with HA and HASi separately (b) LDH assay. HA showed significant increase (+) in adhesion than HASi ($p < 0.01$).

4.7.2 Platelet activation

It is comprehended that bovine thrombin or calcium trigger the activation of platelets to secrete growth factors. However, there is evidence that exposure to bovine thrombin can result in the development of autoimmune antibodies, usually against factor V, which can lead to a profound coagulopathy (Landesberg R *et al.*, 1998). At the same time, HA and HASi contained calcium as the main element, which can induce platelet aggregation (Kamath S *et al.*, 2001). So the activation of platelets without using any triggering agents was proposed. P-selectin is an adhesion molecule expressed on activated platelets and PF4 secreted by the platelets is an index of platelet aggression (Kawabata K *et al.*, 1998).

Flow cytometric analysis showed that P-selectin expression was significantly higher when exposed to HASi than HA. Four well TCPS plate (control) always showed low expression of P-selectin than HA and HASi (Fig. 4.29).

The concentration of PF4 release was determined by ELISA technique. At 1 min, there were no significant change in PF4 release between HA and HASi, while at 60 min, HASi performed significantly better than HA. Four well TCPS plate (control) always showed low release of PF4 at both the time points (Fig. 4.29). These results reflected that with out the addition of any triggering factors, HA and HASi can activate platelets. Even though the platelet adhesion was higher on HA, the activation was significantly enhanced on HASi than HA where the chemical composition, particularly silica may have played an important role (Nemmar A *et al.*, 2005).

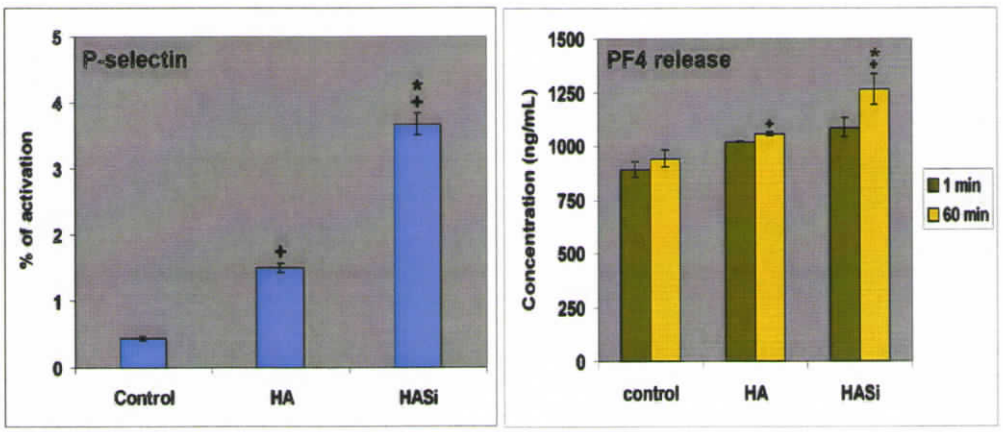

Figure 4.29. The activation of human platelets exposed to HA and HASi. P-selectin expression was determined by flow cytometry (60 min) and PF4 release by ELISA (1 min and 60 min). P-selectin expression and PF4 release was significantly higher with HASi than HA (*) than control (+). Four well TCPS plate was taken as the control ($p < 0.01$).

4.7.3 Fibrin glue coating

The coating of FG on HA and HASi was determined through SEM-EDS and Raman spectroscopy. SEM revealed a uniform coating of FG with smooth appearance on HA and HASi. EDS of FG coated materials showed an additional element of carbon along with the main elements in HA and HASi (HA - Ca and P; HASi - Ca, P and Si) (Fig. 4.30). Raman spectroscopic analysis confirmed the coating where an addition band of primary amine at 1590 cm^{-1} was observed in FHA and FHASi (Fig. 4.31).

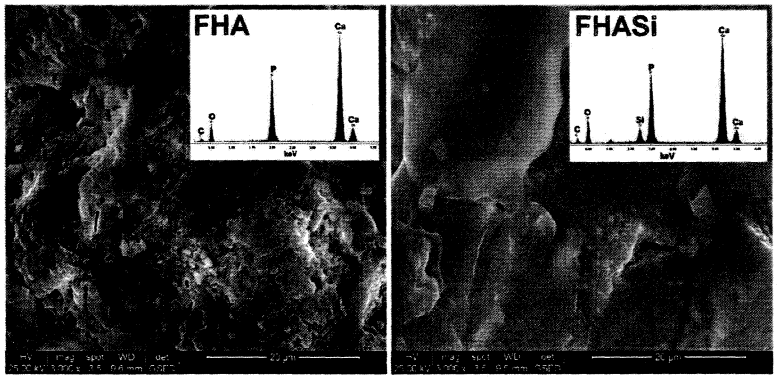

Figure 4.30. ESEM-EDS of FG coated HA and HASi. FHA – C, Ca, P and O & FHASi - C, Ca, P, O and Si

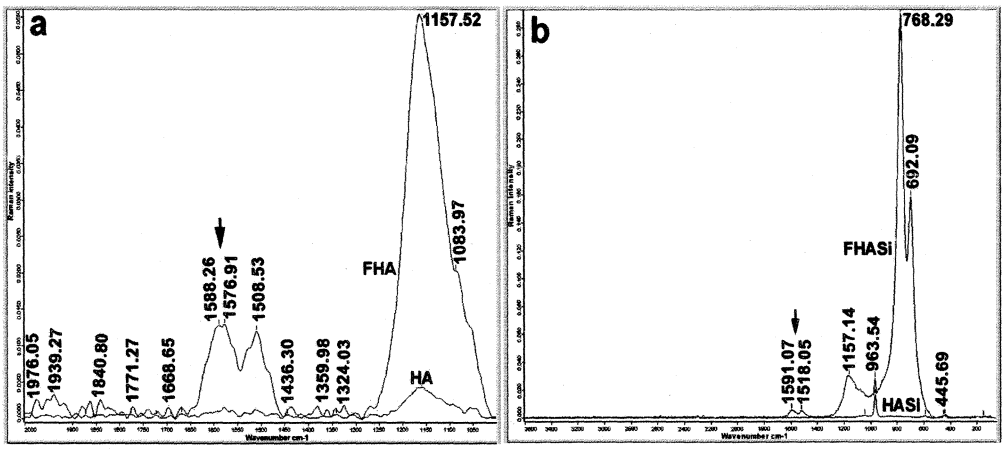

Figure 4.31. Raman spectroscopic analysis of FG coated HA and HASi in comparison with uncoated HA and HASi (a) Overlay of uncoated HA and FHA (b) Overlay of uncoated HASi and FHASi.

4.7.4 Viability of osteogenic induced gBMSCs

Confocal micrographs depicted that gOS+ cells were abundant, homogenous and occupied a wider area reaching confluence throughout the entire volume of PRP and FG coated HA and HASi. The morphology of cells also differed in coated groups where the cells exhibited a spindle shaped appearance with conspicuous cytoplasmic extensions. HASi showed better performance than HA, in uncoated and PRP / FG coated groups (Fig. 4.32).

LDH assay depicted that the viability of gOS+ cells increased with incubation time in all the groups except uncoated HA (Fig. 4.33). On uncoated HA, the cell viability

decreased after day 21, but on PHA and FHA, the viability significantly sustained up to day 28 ($p < 0.001$). During the first week of culture, PRP and FG coated HA and HASi performed better than uncoated groups, with preference for HASi than HA groups. But after day 7, the viability of cells on FHA and PHA reduced, so that the performance was in the order of FHASi > PHASi > HASi > FHA > PHA > HA among the groups. The decrease in viability in HA groups (uncoated and PRP / FG coated) was significantly higher ($p < 0.001$) on day 21 and day 28 as compared to PRP and FG coated HASi groups and even than on uncoated HASi. This emphasizes that the strong stimulus emanated perhaps from the silica content in HASi groups to sustain cell viability was even higher than the stimulus offered by PRP and FG in HA groups.

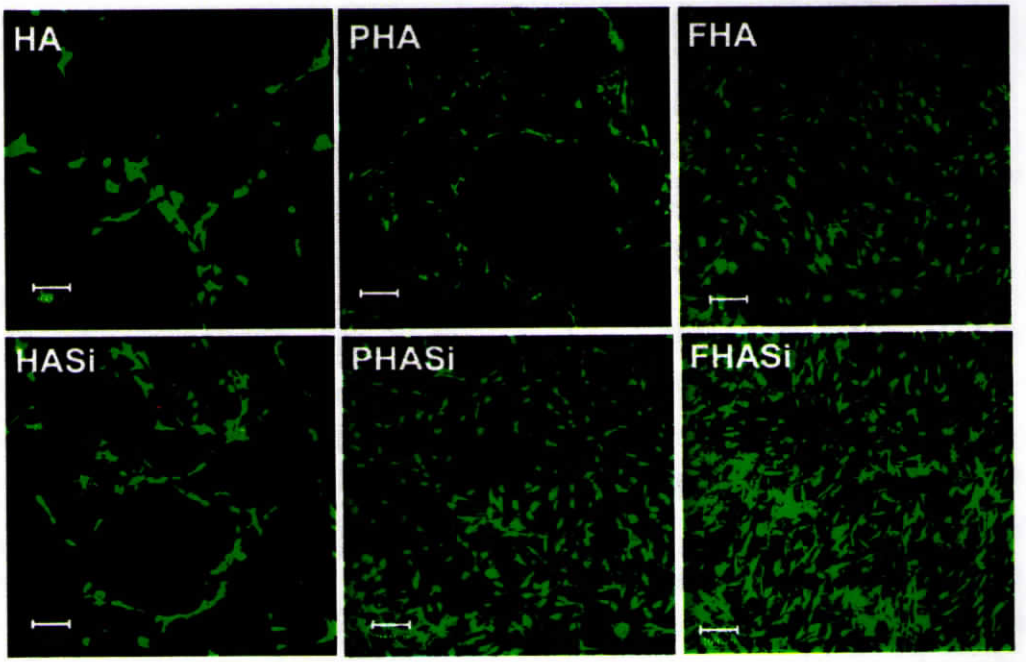

Figure 4.32. Confocal micrographs showing viable gOS+ cultured on PRP and FG coated HA and HASi. Acridine orange (viable cells - green) and ethidium bromide staining (dead cells – red) after 28 days in culture. The signals were collected through 488 nm Argon / 2 laser.

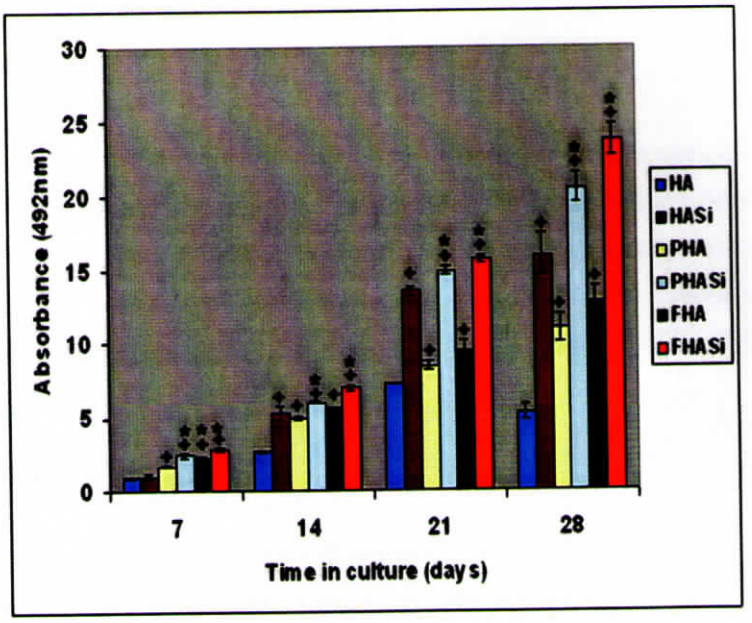

Figure 4.33. LDH assay for determining the viability of gOS+ cells cultured on PRP and FG coated HA and HASi. The viability was significantly enhanced on PRP and FG coated matrices when compared to uncoated HA (+) and uncoated HASi (*) ($p < 0.001$).

This study proved that PRP and FG coated HA and HASi can enhance cell viability. Activated PRP has a favorable effect on osteoblasts as they can release multifaceted blend of growth factors that has stimulatory effects on MSCs (Graziani F *et al.*, 2006; Slapnicka J *et al.*, 2008). But these activities are dependent on the concentration of PRP. The viability and proliferation of osteoblasts were stimulated by low PRP concentrations (1 - 5%) and were suppressed by high PRP concentrations (Choi B *et al.*, 2005; Graziani F *et al.*, 2006). Based on these previous reports, it is hypothesized that the activation of platelets exposed to HA and HASi without the addition of any triggering factors may be satisfactory to stimulate gOS+ cells. Similarly, FG proved to support cells as it contains arginine-glycine-asparagine (RGD) motifs, which bind to cell receptors (predominately integrins) very firmly and sustain cellular viability (Seelich T 1982; Sierra DH 1993).

It is well established that the cell spreading, viability and proliferation is dependent on the quality of initial cell adhesion on a substrate. So the proposition is that the growth factors released by PRP and the temporary ECM created by FG have facilitated the initial cell adhesion firmly that lead to enhanced cell viability. This also gave an explanation for a different morphology for the cells cultured on PRP and FG coated

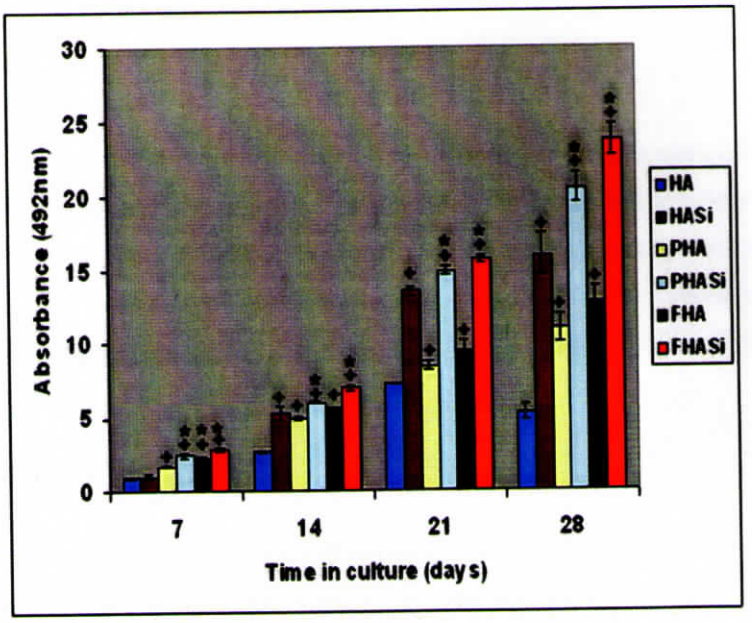

Figure 4.33. LDH assay for determining the viability of gOS+ cells cultured on PRP and FG coated HA and HASi. The viability was significantly enhanced on PRP and FG coated matrices when compared to uncoated HA (+) and uncoated HASi (*) ($p < 0.001$).

This study proved that PRP and FG coated HA and HASi can enhance cell viability. Activated PRP has a favorable effect on osteoblasts as they can release multifaceted blend of growth factors that has stimulatory effects on MSCs (Graziani F *et al.*, 2006; Slapnicka J *et al.*, 2008). But these activities are dependent on the concentration of PRP. The viability and proliferation of osteoblasts were stimulated by low PRP concentrations (1 - 5%) and were suppressed by high PRP concentrations (Choi B *et al.*, 2005; Graziani F *et al.*, 2006). Based on these previous reports, it is hypothesized that the activation of platelets exposed to HA and HASi without the addition of any triggering factors may be satisfactory to stimulate gOS+ cells. Similarly, FG proved to support cells as it contains arginine-glycine-asparagine (RGD) motifs, which bind to cell receptors (predominately integrins) very firmly and sustain cellular viability (Seelich T 1982; Sierra DH 1993).

It is well established that the cell spreading, viability and proliferation is dependent on the quality of initial cell adhesion on a substrate. So the proposition is that the growth factors released by PRP and the temporary ECM created by FG have facilitated the initial cell adhesion firmly that lead to enhanced cell viability. This also gave an explanation for a different morphology for the cells cultured on PRP and FG coated

matrices when compared to bare materials.

4.7.5 Proliferation of osteogenic induced gBMSCs

DNA results proved that the cell number increased as the culture period increased in all the groups, except on uncoated HA on which the cell proliferation decreased after day 21. However, PRP and FG coated HA has stimulated the cell growth significantly up to day 28. The results of cell proliferation was in par with cell viability and here as well, the performance among the groups was in the order of FHASi > PHASi > HASi > FHA > PHA > HA after day 7 (Fig. 4.34).

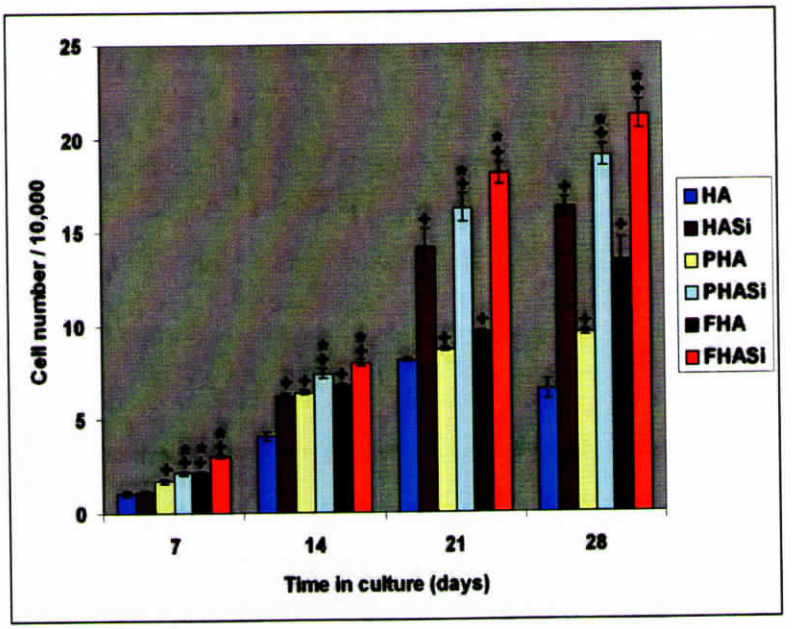

Figure 4.34. Picogreen assay for determining the proliferation of gOS+ cells cultured on PRP and FG coated HA and HASi. The proliferation was significantly enhanced on PRP and FG coated matrices when compared to uncoated HA (+) and uncoated HASi (*) ($p < 0.001$).

The mitogenic effects of PRP on BMSCs and osteoblasts have been reported which is mediated through PDGF and TGF-β (Lucarelli E *et al.*, 2003; van den Dolder J *et al.*, 2006; Slapnicka J *et al.*, 2008). Some studies have showed that PRP mediated induction of osteoblast proliferation can happen even without FBS, a major source of growth factors, emphasizing the beneficial abilities of PRP (Ferreira CF *et al.*, 2006). Similar to PRP, gOS+ cells proliferated appreciably on FG coated matrices. It is reported that the rate of proliferation of MSCs on FG is dependent on the ratio of

fibrinogen complex to thrombin (Ho W *et al.*, 2006). In addition, the fibropeptides released during the formation of fibrin is also mitogenic for various cells (Sporn LA *et al.*, 1995).

When the cells enter into the differentiation lineage, the proliferation rate declines (Stein GS *et al.*,1990). The proliferation of cells slowed down on uncoated and PRP / FG coated HA groups after day 7. On the contrary, the cells continued to proliferate on HASi, both in uncoated and PRP / FG coated groups, which indicated the inherent influence of silica on cellular activities.

4.7.6 Morphology of osteogenic induced gBMSCs

The efficiency of cell adhesion and spreading on PRP and FG coated HA and HASi was determined through SEM on day 28. The cell body with anchoring filopodia was clearly seen on uncoated HA, but the cell number was low. On bare HASi, the cells were uniformly spread to form a cell sheet-like structure. Interestingly, HA and HASi coated with PRP and FG had more cell densities and ECM deposition (Fig. 4. 35).

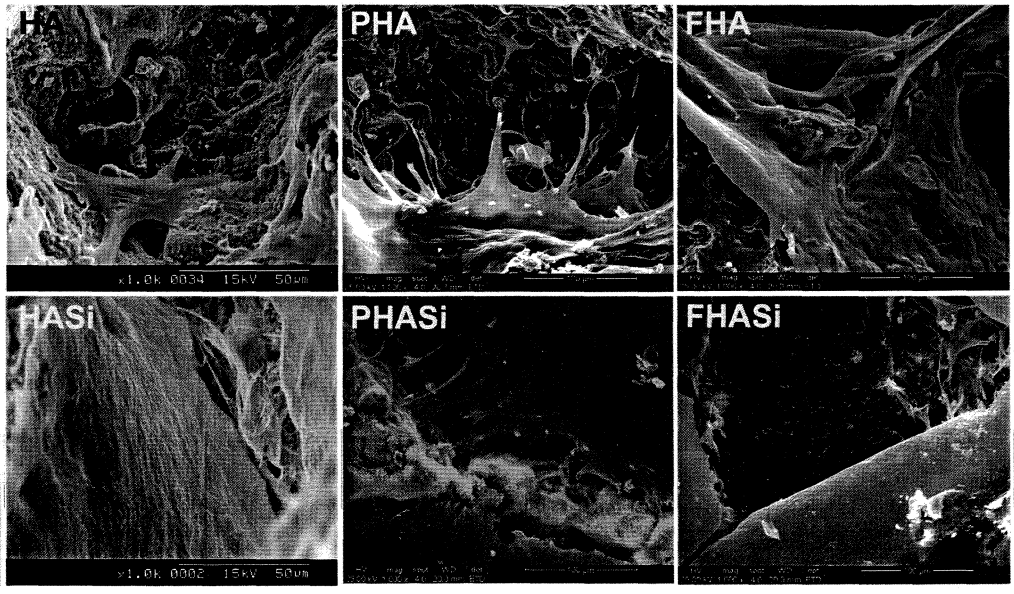

Figure 4.35. Scanning electron micrographs showing the morphology of gOS+ cells cultured on PRP and FG coated HA and HASi - Day 28.

4.7.7 Cell cycle analysis

The cell cycle analysis was done through propidium iodide staining by flow cytometry

on day 28. The cell doublets were excluded through pulse width versus pulse area so that the single cells passing through the beam was taken into consideration. More emphasis was given to S-phase and apoptotic phase of the cell cycle in order to know the influence of scaffolds on the cells to undergo replication and apoptosis. The percentage of cells in replicative phase were more on HASi groups including uncoated / PRP / FG coated HASi groups. Similarly, the performance of substrates with cells in apoptotic-phase was in the order of HA > HASi > PHA = FHA = PHASi = FHASi. This emphasised the significance of PRP and FG coating in reducing the apoptosis of cells when compared to uncoated groups (Fig. 4.36).

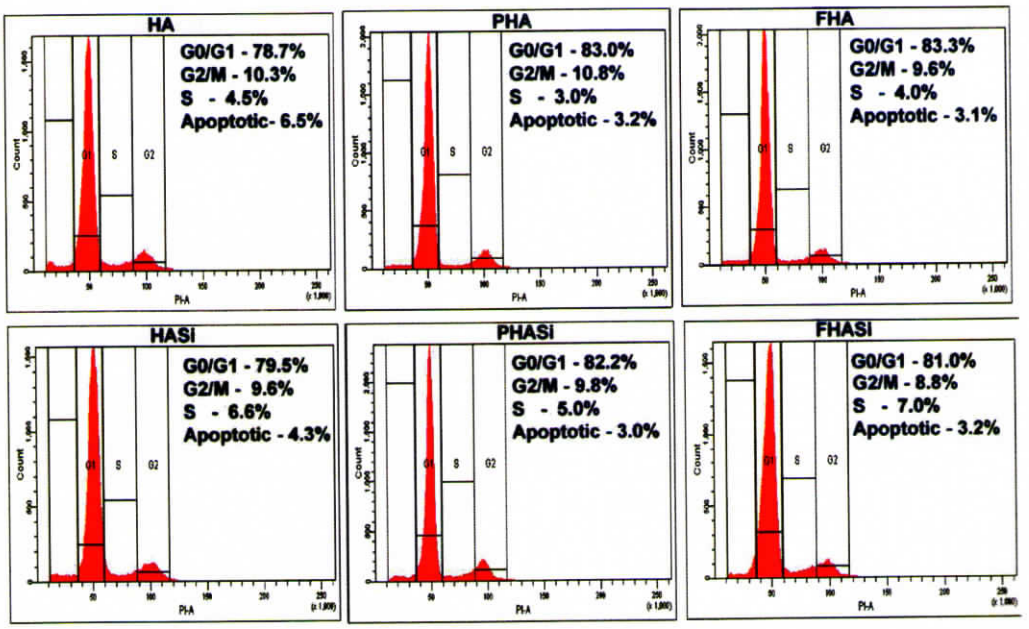

Figure 4.36. Cell cycle analysis of gOS+ cells cultured on PRP and FG coated HA and HASi. Propidium iodide staining by flow cytometry on day 28

4.7.8 Differentiation of gBMSCs into osteogenic lineage

The differentiation of gBMSCs into osteogenic lineage was confirmed through ALP activity and real time PCR analysis of ALP, osteopontin and osteocalcin expression. The results of real time-PCR were represented as fold increase with respect to gBMSCs at 24 h.

4.7.8.1 Alkaline Phosphatase activity

Biochemical data showed a gradual increase in the ALP activity during the culture

period, with a peak on day 14, followed by decreasing values in all the groups. The performance among the six groups was in the order of FHASi > FHA > PHASi = HASi > PHA = HA on day 7 and 14. Thus there were no significant difference in the ALP activity between uncoated and PRP coated HA and HASi. However, FHA and FHASi showed enhanced ALP activity on all days ($p<0.001$) and among all, FHASi depicted maximum ALP activity on day 14 (Fig. 4.37). The results were further confirmed through ELF 97 staining by confocal microscope on day 10 (Fig. 4.38).

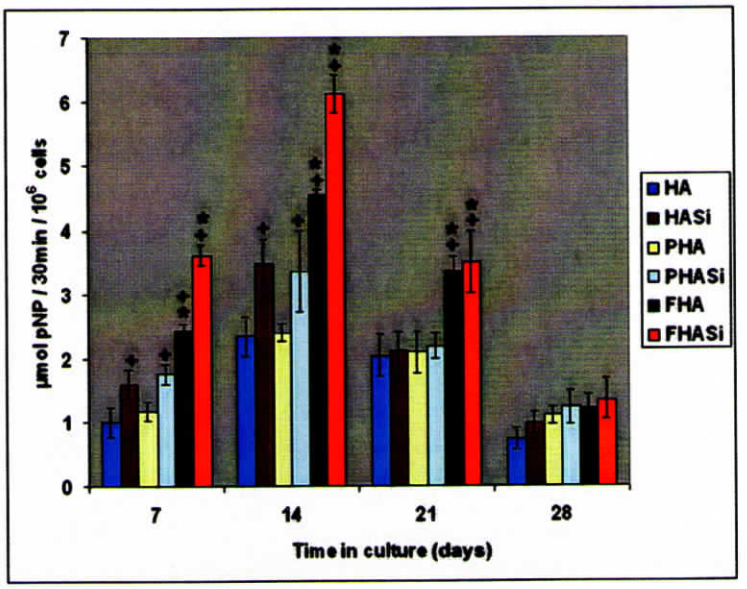

Figure 4.37. Specific ALP activity of gOS+ cells cultured on PRP and FG coated HA and HASi – biochemical estimation. The ALP activity was significantly enhanced on FG coated matrices when compared to uncoated HA (+) and uncoated HASi (*) ($p< 0.001$).

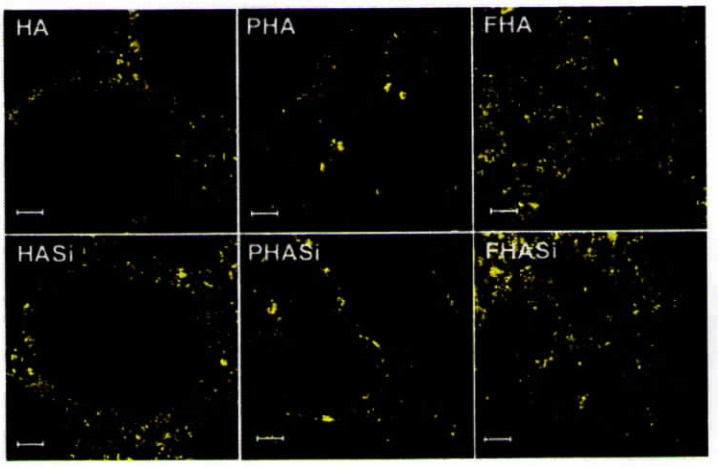

Figure 4.38. Confocal micrographs showing ALP activity of gOS+ cells cultured on PRP and FG coated HA and HASi - ELF-97 staining - Day 10. The signals were collected through Hoechst long pass filter.

4.7.8.2 ALP expression

Real time data of ALP was comparable to biochemical data. The expression of ALP was in the order of FHASi > FHA > PHASi = HASi > PHA = HA on day 7 and 14. The highest expression was on day 14. There was no significant difference in ALP expression between uncoated and PRP coated HA and HASi. However, FG coated matrices showed improved ALP expression with the highest expression on FHASi on all the days (Fig. 4.39).

Similar to our data, previous studies have also reported that PRP has no effect on the ALP activity of osteogenic induced rat BMSCs (Kanno T *et al.*, 2005; van den Dolder J *et al.*, 2006). In another study, PRP enhanced the proliferation of rat BMSCs but it decreased ALP activity significantly (Ogino Y *et al.*, 2005). The real molecular mechanism behind the suppressive or null effect of PRP on ALP is not yet elucidated.

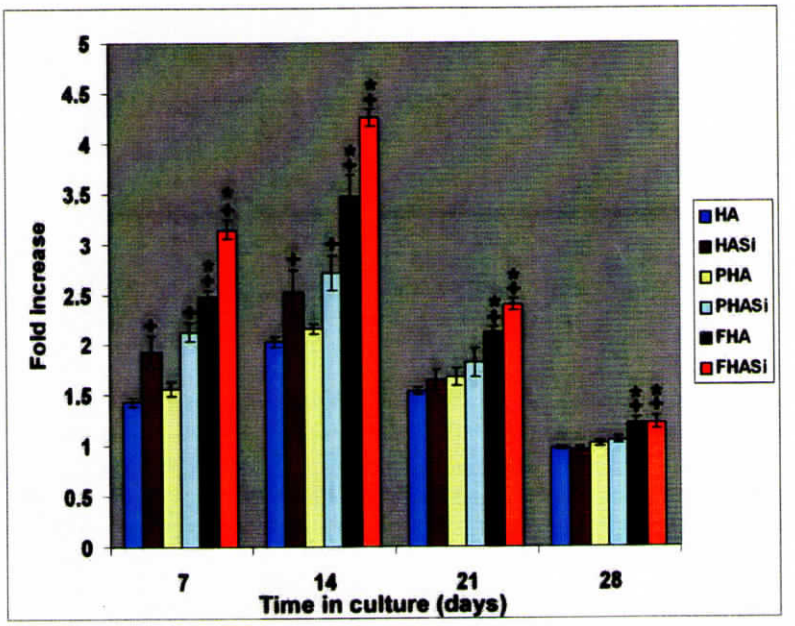

Figure 4.39. Real-time PCR analysis of the expression of ALP on gOS+ cells cultured on PRP and FG coated HA and HASi. The ALP expression was significantly enhanced on FG coated matrices when compared to uncoated HA (+) and uncoated HASi (*) ($p < 0.001$).

4.7.8.3 Osteopontin expression

The expression of osteopontin gradually augmented during the culture period with a peak on day 21, followed by a decline in expression, indicating that the osteoblast

cells attained maturity by third week of culture. PRP and FG coated HA and HASi significantly performed better than uncoated groups, with preference for HASi groups (Fig. 4.40).

4.7.8.4 Osteocalcin expression

The expression of osteocalcin was highest on day 28 on all the substrates, which indicated that osteoblasts became matured and has undergone mineralization during the fourth week of culture. The performance of osteocalcin among the groups was in the order of FHASi > FHA = PHASi > PHA = HASi > HA on all the days except on day 28 (Fig. 4.41).

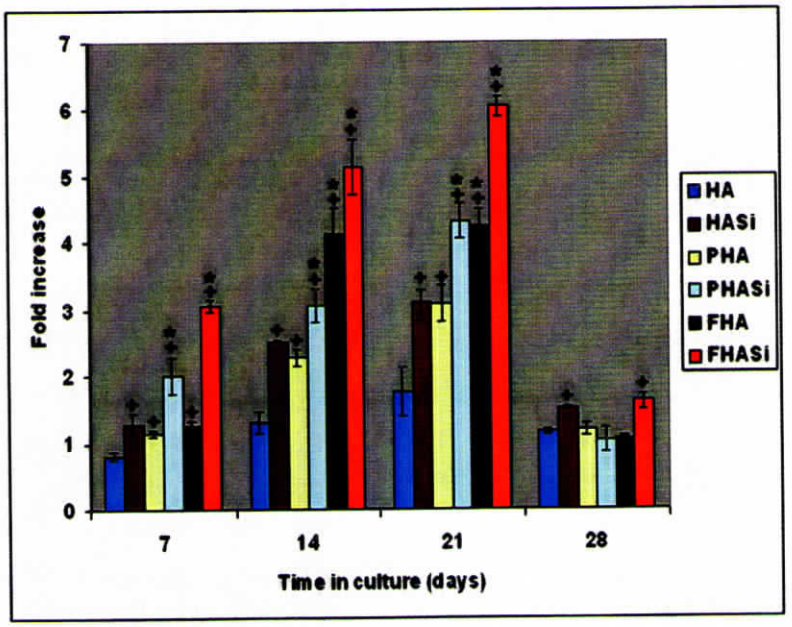

Figure 4.40. Real-time PCR analysis of the expression of osteopontin on gOS+ cells cultured on PRP and FG coated HA and HASi. The expression was significantly enhanced on PRP and FG coated matrices when compared to uncoated HA (+) and uncoated HASi (*) ($p < 0.001$).

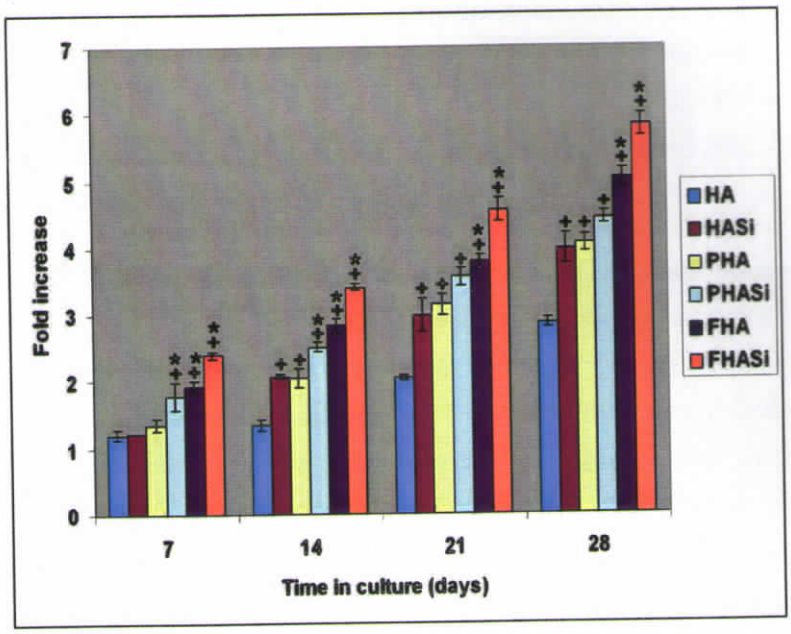

Figure 4.41. Real-time PCR analysis of the expression of osteocalcin on gOS+ cells cultured on PRP and FG coated HA and HASi. The expression was significantly enhanced on PRP and FG coated matrices when compared to uncoated HA (+) and uncoated HASi (*) ($p < 0.001$).

Even though PRP has no effect on ALP, the osteopontin and osteocalcin expression was significantly enhanced on PRP coated HA and HASi, comparable to previous reports where PRP enhanced the levels of osteopontin mRNA in human osteosarcoma cell lines like HOS and SaOS-2 (Kanno T *et al.*, 2005). In another study, PRP stimulated cell proliferation and upregulated the expression of osteocalcin at a platelet concentration of 2.5x than baseline whereas increased concentrations resulted in a reduction in proliferation and a suboptimal effect on osteoblast function (Graziani F *et al.*, 2006). The differentiation of gBMSCs on FG coated matrices was also enhanced, even better than PRP coated matrices. It was reported that FG has great influence on the differentiation of MSCs into osteoblasts and can induce differentiation even in the absence of any osteogenic inducing factors (Catelas I *et al.*, 2006).

The present study revealed that PRP and FG have a stimulating effect on the growth and differentiation of gOS+ cells. PRP is a rich source of many growth factors and the period of the direct influence of growth factors is said to be less than 3 days. For example, the release of PDGF was highest during the first 24 h of culture and TGF-

β_1 during the first 48 h (Zagai U *et al.,* 2003). Similarly, fibrin matrix is maintained only for few days (in the order of days to few weeks) and the degradation occurs subsequently (Ho W *et al.,* 2006). Within this short time scale, both PRP and FG act as a positive stimulant for the proliferation of the cells and to form their own ECM, leading to a long-lasting effect on cellular responses.

Compared to all the substrates, FHASi was the excellent substrate because of the communal action of the stimulus emanated by the silica content and the temporary ECM provided by FG. However some of the features of PRP are attractive in their use for further *in vivo* studies. These include (a) they can be easily obtained from patient's blood after a simple centrifugation step (b) PRP contains high concentration of platelets and a native concentration of fibrinogen. Thus, the effect of FG also will be attained in the presence of indigenous thrombin when PRP is delivered to the defect site (Yamada Y *et al.,* 2004) (c) PRP preparation is cheap while the cost of commercially available FG like Tisseel is exorbitant for its price (about $300 for a total volume of 4 mL) (Alving BM *et al.,* 1995, Alving B *et al.,* 1999).

CHAPTER 5

EVALUATION OF TISSUE-ENGINEERED BIOACTIVE CERAMICS *IN VIVO* – EXTRASKELETAL AND ORTHOTOPIC IMPLANTATION

5.1 Abstract

The treatment of segmental bone defects resulting from trauma or surgical resection of bone tumors is a formidable clinical challenge nowadays. An ideal bone substitute should simulate an autograft in its characteristics of being osteoconductive and osteointegrative, so that it can unite with host bone without fibrous tissue formation and inflammation. In addition, autograft contains viable osteoprogenitor cell pool that makes it osteoinductive. Thus the current strategy is focused on tissue-engineered constructs, where an osteoconductive material seeded with cells may provide necessary osteoinductive signals for the regeneration of bone. However, the cells in construct should survive and function after implantation, which in turn is dependent on the vascularisation potential of material at the vicinity of defect site.

The specific objectives of the third phase of study were: 1) To evaluate the vascularisation potential of bare HA and HASi (without cells) in comparison with tissue-engineered HA and HASi (with rOS+ cells) at an extraskeletal site in rat model 2) To evaluate the osteoinductive potential of bare HA and HASi (without cells) in comparison with tissue-engineered HA and HASi (with rBMSCs / rOS+ cells) at an extraskeletal site in rat model 3) To evaluate the potential of bare HASi (without cells or PRP) in comparison with tissue-engineered HASi (with gOS+ cells and PRP) to regenerate bone and to undergo degradation in a segmental defect (2 cm) created in the femur of goat model.

5.2 Extraskeletal implantation studies

5.2.1 Evaluation of osteogenic induced rBMSCs on bioactive ceramics *in vitro*

The duration of culturing of cells on the materials *in vitro* prior to implantation is an imperative aspect that ensures the success of tissue-engineered constructs. A previous study with rBMSCs examined this effect and established that the bone formation was generated more effectively by a short *in vitro* culture period (day 1-8) (van den Dolder J *et al.*, 2002). Therefore herein, the cells were cultured on HA and HASi for a period of 7 days. LDH assay (Fig. 5.1a) and specific ALP activity, (Fig 5.1b) proved that rOS+ cells were viable and manitained their osteogenic phenotype when used for extraskeletal implantations. The cellular reponses were significantly high on HASi than HA.

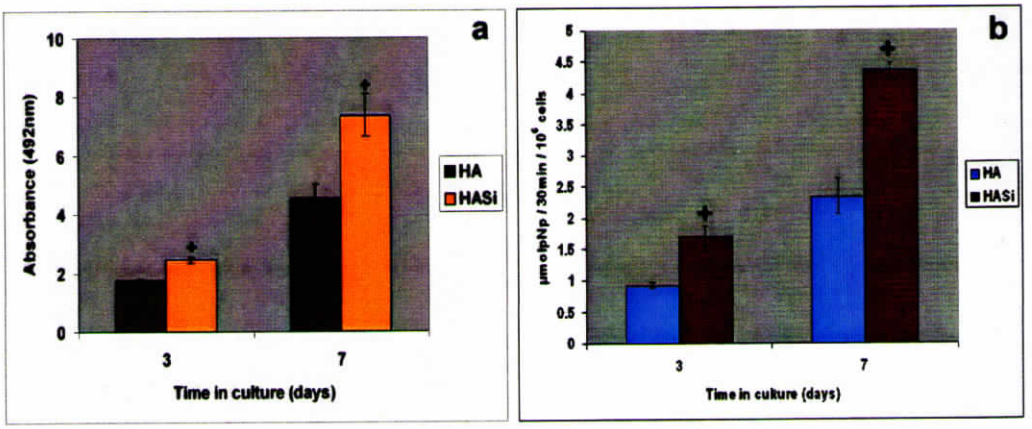

Figure 5.1. Viability and osteogenic differentiation of rOS+ cells cultured on HA and HASi (a) LDH assay – viability (b) specific ALP activity – osteogenic differentiation. HASi showed significant increase (+) in performance than HA ($p<0.001$).

5.2.2 Experimental groups

Six groups were included in the study. Group I: Bare HASi (HASi); Group II: rBMSCs cultured HASi (HASi+C (OS-); Group III: rOS+ cells cultured HASi (HASi+C); Group IV: Bare HA (HA); Group V: rBMSCs cultured HA (HASi+C (OS-); Group VI: rOS+ cells cultured HA (HA+C). Group II and Group IV was included only in neo-osteogenesis studies, particularly, histological and histomorphometric evaluation.

5.2.3 Evaluation of post-implanted tissues

5.2.3.1 Gross observation

All rats showed an undisturbed wound healing without any clinical signs of inflammation at the surgical site. The materials in all the groups showed intimate contact with the surrounding muscles depicting proper stationing of the materials in the implantation bed.

5.2.3.2 Neo-vascularization studies

The cells within the tissue-engineered constructs can survive by diffusion of nutrients and oxygen from blood vessels, but it is limited to a diffusion depth of 300 μm (Kruyt MC *et al.,* 2004a; Kruyt MC *et al.,* 2004b). Therefore sequential growth and spread of a vascular system within the tissue-engineered constructs particularly in larger defects is imperative.

Herein, neo-vascularisation at the implant site was determined by H & E staining for 2 and 4 weeks. The vascular invasion was very low in bare HA groups, while a notable increase in blood capillaries together with small blood vessels could be seen in bare HASi groups at 2 weeks. HA+C and HASi +C groups showed a prominent increase in performance when compared to bare HA and HASi groups (Fig. 5.2).

At 4 weeks, the vascular invasion with the formation of blood capillaries was improved in bare HA groups when compared to 2 weeks. Interestingly, in bare HASi groups, the implantation site was well vascularised with profuse ingrowth of blood capillaries together with numerous thin and thick walled blood vessels. HA+C and HASi+C groups showed an excellent response when compared to bare HA and HASi groups (Fig. 5.3).

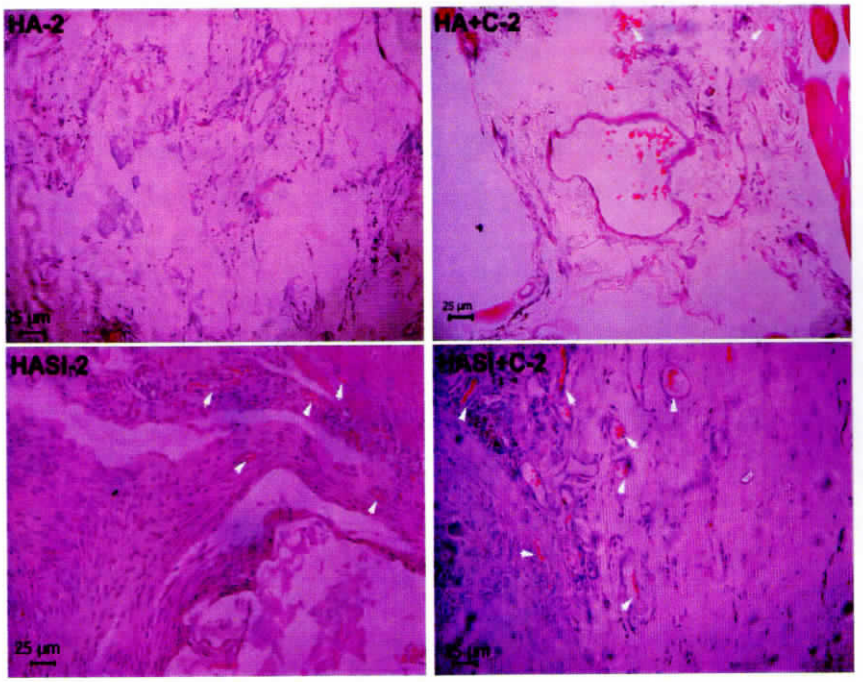

Figure 5.2. Light micrographs showing neo-vascularisation at an extraskeletal site at 2 weeks post-implantation. H & E staining. Arrow - Blood capillaries and blood vessels. Magnification: 20X

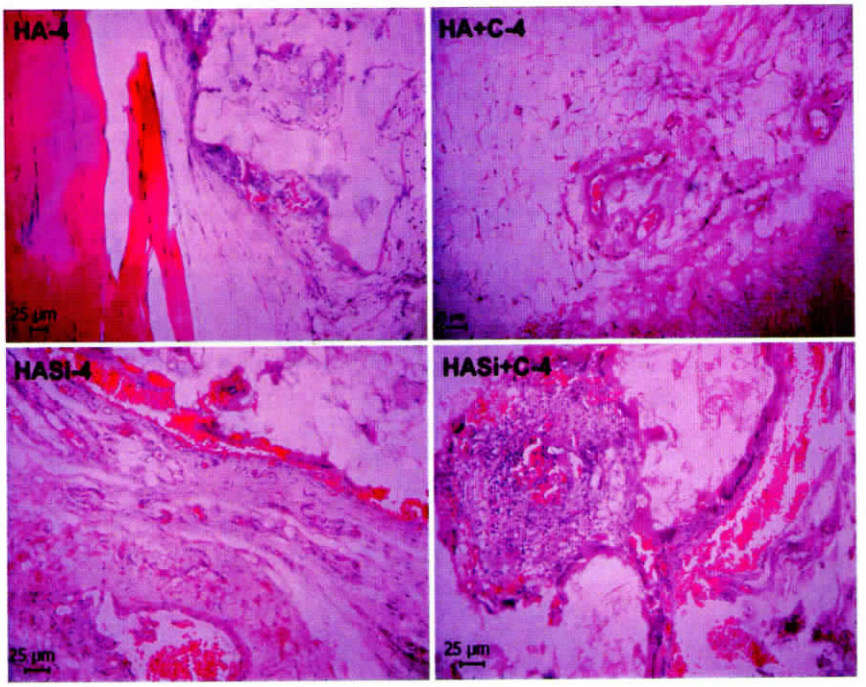

Figure 5.3. Light micrographs showing neo-vascularisation at an extraskeletal site at 4 weeks post-implantation. H & E staining. Magnification: 20X

In most cases after transplantation, the grafts are exposed to the harsh environment of a hematoma and may be deprived of vascular supply for weeks, which results in graft failure (Hartman ED *et al.,* 2004). Scaffolds with pore size above 100 μm and having pore interconnections can facilitate the intrusion of cells and blood vessels from the host tissue (Karageorgiou V *et al.,* 2005). Accordingly, the highly porous structure of HA and HASi has improved vascular invasion in this study. However, the neo-vascularisation was significantly enhanced in HASi, which may be ascribed to the presence of Si that has been supported by other studies. One study reported that the increased presence of ionic dissolution products of 45S5 Bioglass (mainly Si) can stimulate the expression and release of VEGF and bFGF that can induce neo-vascularization (Richard MD 2005). In another study, bioactive glass coating on polymeric substrate enhanced angiogenesis through the mitogenic stimulation of endothelial cells (Leach JK *et al.,* 2006).

The engineering of materials with cells is an added benefit because these cells secrete many inductive factors that due to their autocrine effects quickly enhance neo-vascularisation. It is reported that osteopontin play an important role in angiogenesis by facilitating endothelial cell migration in cooperation with the up regulation of VEGF (Senger DR *et al.,* 1996; Takahashi F *et al.,* 2002). Our *in vitro* studies showed good expression of osteopontin on HA and HASi, which may be accountable for enhanced neo-vascularisation in HA+C and HASi+C groups.

5.2.3.3 Neo-osteogenesis studies

Neo-osteogenesis was evaluated through histology (Stevenal's blue and van Gieson's picrofuchsin staining), histomorphometry, ALP activity and micro-CT.

5.2.3.3.1 Histological evaluation

Bare HA and HASi groups did not reveal any active site of osteoid deposition or bone mineralization, which is in agreement with previous data demonstrated that ceramics did not induce any bone formation (Yoshikawa T *et al.,* 1992; Yuan H *et al.,* 2006). Bare HA was lined by thin connective tissue of fibroblast-like cells. The majority of osteoblast-like cells was seen along the margin of bare HA and was occasional on the surface or within the pores. However, in bare HASi groups, the cells were visible not only at the periphery but also within the internal pores and on the surface of the

implant without fibrous tissue formation and inflammation. The cellular ingrowth towards the internal pores accentuates higher osteoconductive potential of HASi than HA (Fig. 5.4).

In tissue-engineered groups, a notable difference was seen not only between HA and HASi groups, but also among rBMSCs and rOS+ cells cultured materials. In HA+C (OS-) and HASi+C (OS-) groups, the ingrowth of numerous osteoblast-like cells was seen around and within the pores of the materials without fibrous tissue formation and inflammation. On the other hand, there was no osteoid deposition in those groups. Similar results were obtained for HA+C groups, where also osteoblast-like cells were visualized without osteoid deposition. Nevertheless, in HASi+C groups, immature woven bone with osteoblast-like cells infiltered around and within the pores of the material was observed (Fig. 5.4). The positive impact in forming bone is more attributable to the scaffold and not to the cells alone, because both HA and HASi were engineered simultaneously with the cells from the same source and same passage.

The presence of numerous osteoblast-like cells in tissue-engineered groups demonstrated metabolically active tissue within the materials. The cells cultured on the scaffolds prior to implantation stimulate the recruitment and proliferation of indigenous stem cells after implantation (Kruyt MC *et al.,* 2004a). However, the tissue-specific differentiation of MSCs is dependent on the local microenvironment in which these cells reside and their interactions with the host tissue (Harris CT *et al.,* 2004). Thus in the absence of any bony environment (extraskeletal site), rBMSCs on the scaffolds may have needed some more time to reach their osteogenic potential to fabricate bone. We anticipate that HA+C (OS-) and HASi+C (OS-) groups may be able to form bone while increasing the implantation period for over 4 weeks.

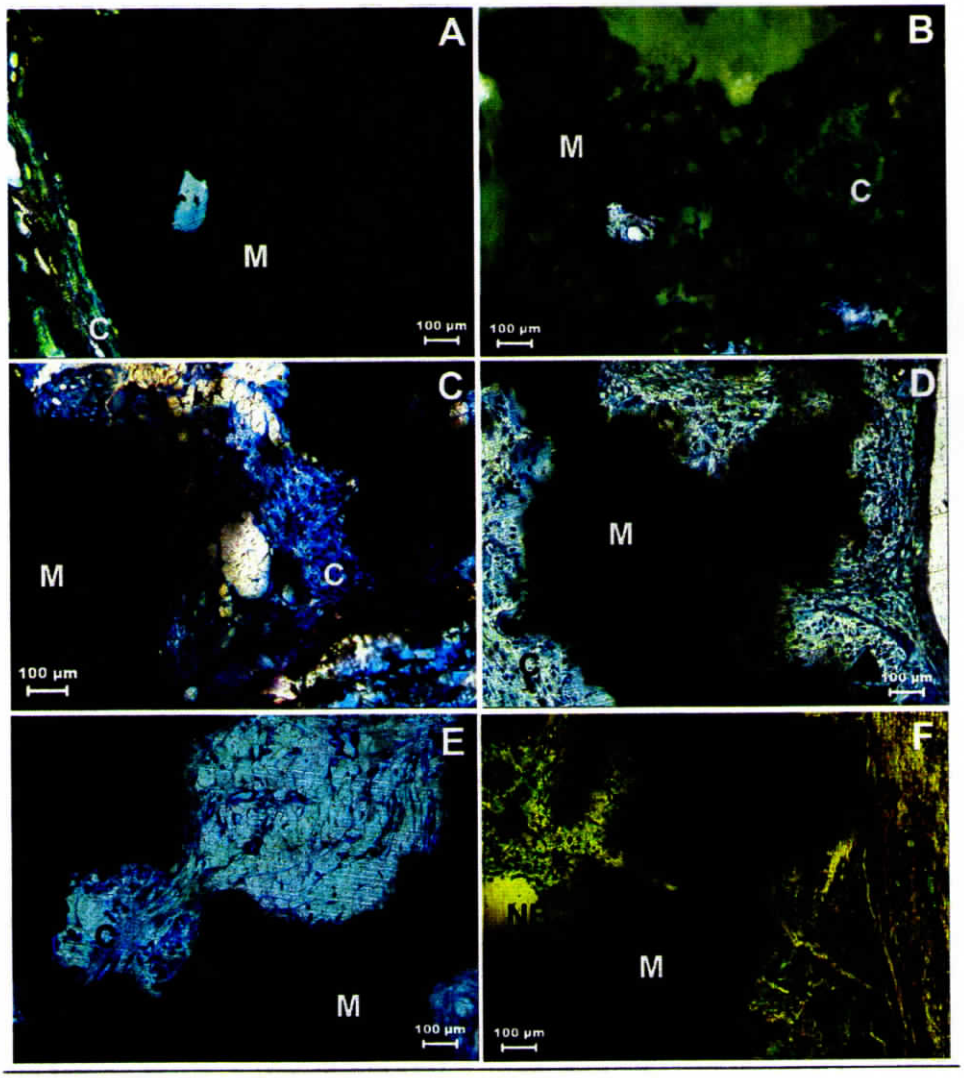

Figure 5.4. Histological evaluation of neo-osteogenesis at an extraskeletal site at 4 weeks post-implantation. Stevenal's blue and van Gieson's picrofuchsin staining. A -HA; B – HASi; C - HA+C (OS-); D - HASi+C (OS-); E - HA+C; F- HASi+C. M - material; NB - New bone; C - cells. Stevenal's blue stains osteoblast-like cells (blue) and van Gieson's picrofuchsin stains osteoid matrix (yellow). Magnification: 20X

5.2.3.3.2 Histomorphometric evaluation

The image analysis of the stained sections (Stevenal's blue and van Gieson's picrofuchsin staining) were carried out to quantify (a) the area of cells infiltered around and within the pore of the materials and (b) the area of newly formed bone. Generally, HASi illustrated an increase in cellular ingrowth when compared to HA, both in bare and tissue-engineered groups. Among the groups, the area of cells

infiltered around and within the pores of the materials was in the order of HA < HASi < HASi+C < HA+C (OS-) < HASi+C (OS-)< HA+C. There were no significant differences between all these groups except for bare HA groups where the cellular ingrowth was comparatively low. The new bone formation was observed only in HASi+C groups which showed that about 40 - 50% of the pores were filled with newly formed bone (Fig. 5.5).

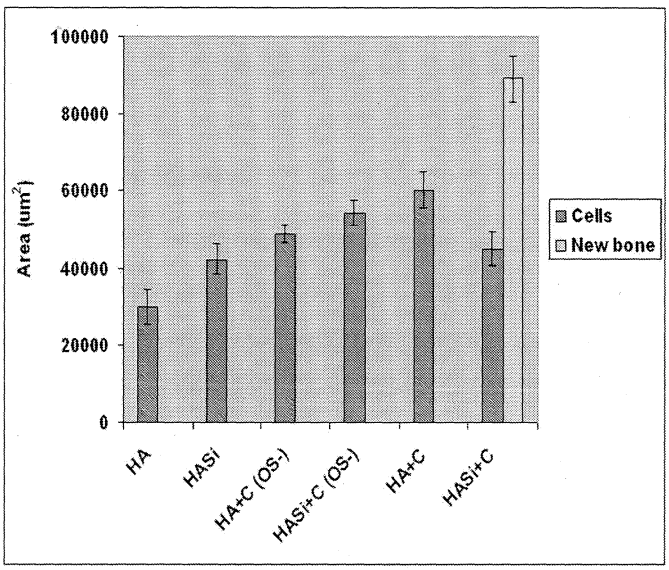

Figure 5.5. Histomorphometric evaluation of the area of cellular infiltration and new bone formation at an extraskeletal site 4 weeks post-implantation. The area was measured using the Quips programme of QWin soft ware of the microscope (Leica DM 6000).

5.2.3.3.3 Alkaline Phosphatase activity

The activity of ALP, a known biomarker for osteoinductive cells, (Wlodarski KH *et al.,* 1986) at the implanted site was observed 2 weeks post-implantation through ELF-97 staining by fluorescence microscopy (Fig. 5.6). HA+C and HASi+C groups were only included in this study to confirm the histology data concerning new bone formation. The ALP activity was observed in both the groups, with significant enhancement on HASi. Muscle cells taken as negative control showed no ALP activity.

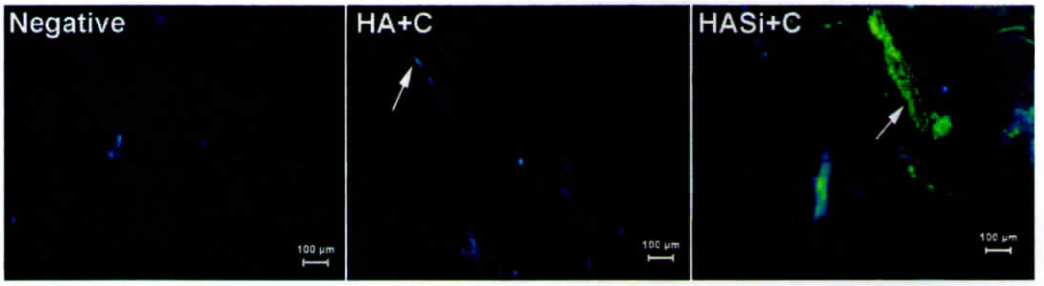

Figure 5.6. Fluorescent micrographs depicting ALP activity at an extraskeletal site 2 weeks post-implantation. ELF-97 staining for ALP activity (yellowish green). Arrow – ALP activity. Magnification: 20X

5.2.3.3.4 Mineralization studies

The newly formed bone undergoes mineralization which was verified through the density distribution graph plotted from 2D micro-CT images 4 weeks post-implantation (Fig. 5.7). Micro-CT imaging is an efficient, non-destructive tool to measure the amount and distribution of mineralised matrix throughout 3D constructs *in vitro* and *in vivo* (Cartmell S *et al.*, 2004).

The density of raw HA and HASi (before implantation) was compared with HA+C and HASi+C groups. The density of raw HA and HASi was approximately 2293 mgHA / ccm and 1657 mgHA / ccm respectively. Following implantation, HA+C groups did not show any remarkable change in the density (approximately 2000 mgHA / ccm), while a detectable increase in the density was observed in HASi+C groups (approximately 2100 mgHA / ccm). This specified an increase in total matrix mineralization in HASi+C groups.

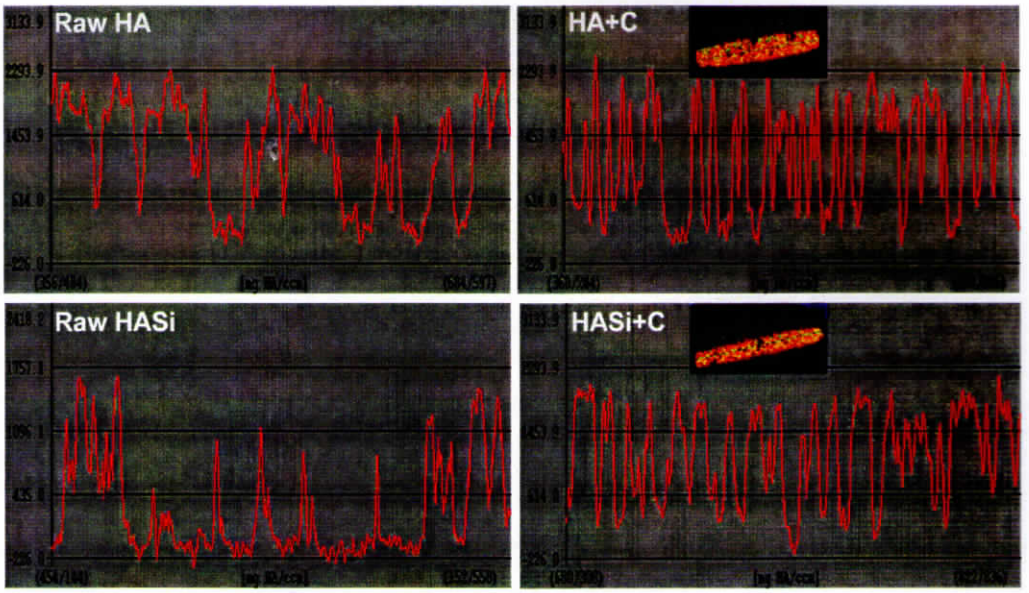

Figure 5.7. Density distribution graphs showing mineralization of newly formed bone at an extraskeletal site 4 weeks post-implantation. The graphs were plotted from 2D micro-CT image. mgHA / ccm denotes milligram of hydroxyapatite per cubic centimeter. The inset image shows the retrieved tissues from the implanted site.

These studies confirmed new bone formation in tissue-engineered conditions, with an obvious preference for HASi scaffolds and the cells cultured in presence of osteogenic supplements. It is well recognized that the rate of bone regeneration and its quality is related to porosity (Karageorgiou V *et al.*, 2005). When ceramics with different pore sizes were compared, the new bone formation was higher for 300 - 400 µm pore size and this was the critical size above which blood capillaries could be observed when implanted subcutaneously in rats (Kuboki *et al.*, 2001; Tsuruga *et al.*, 1997). Even though the pore size of HA and HASi ranged between 50 – 500 µm, new bone formation was observed only in HASi+C groups. This emphasized that apart from porosity, the surface chemistry of material, particularly the presence of Si, plays an important role in inducing and accelerating bone formation. A previous study supported this hypothesis where the new bone formation was accelerated when calcium phosphate calcium silicate system in combination with FG was used at an extraskeletal site of mice model. At the same time, HA did not induce bone formation in the same condition (Abiraman S *et al.*, 2002). Another study reported that the activity of silica-based bioactive materials can overshadow the effect of even BMP 2 gene therapies and induce local bone turnover (Välimäki VV *et al.*, 2006).

The vascularity of the defect site is an important parameter for osteoinduction and for osteogenesis to occur (Ripamonti U 2006). When fresh marrow cells or cultured BMSCs were combined with ceramic as the delivery vehicle, bone was formed in close association with host vasculature (Goshima J *et al.,* 1991a; Goshima J *et al.,* 1991b). Hartman *et al.,* (2004) found that muscle recipient site could favor bone formation in a cell-based bone graft substitute compared to subcutaneous recipient site due to high vascularity of the muscle tissue. In HASi+C groups, the neo-vascularisation was significantly enhanced that lead to neo-osteogenesis.

The new bone formation in HASi+C groups was occurred by intramembranous ossification, since no cartilage was observed. It is reported that small pores of the materials favor hypoxic conditions and induce osteochondral formation before osteogenesis, while large pores that are well vascularised leads to direct osteogenesis without preceding cartilage formation (Jin QM *et al.,* 2000).

5.3 Orthotopic implantation studies

Herein we focused on the progress of bone regeneration in par with material degradation in a segmental defect (2 cm) in goat femur. All the *in vitro* studies and extraskeletal implantation studies proved HASi is a better substrate than HA. So we have selected HASi as bone substitute in this study.

5.3.1 Experimental groups

Three experimental groups were included for implantation. Group I: Bare HASi (HASi); Group II: gOS+ cells cultured HASi (HASi+C). Group III: gOS+ cells cultured HASi together with the delivery of PRP to the defect site (HASi+CP). Three groups were compared at 2 and 4 months while the studies with bare HASi were continued for 6 and 12 months.

5.3.1.1 Post-operative management

All goats were self standing and took feed normally even on the first post-operative day. It gradually gained weight and socialized within the groups in which they were kept. All the 18 goats survived the study period without any evidence of inflammation or infection at the implantation site.

5.3.2 Evaluation of post-implanted tissues

5.3.2.1 Gross evaluation

No gross failure or other post operative complications occurred in any of the animals. The bone had regenerated to bridge the defect and the integration of the material with host bone on either side was observed in all the animals at 6 weeks

Bare HASi groups – New bone formation was observed in the peripheral region of the defect, while the mid region was identifiable with a portion of the material at 2 months. The material was well incorporated with newly regenerated tissue, demonstrating its osteointegrative nature. At 4 months, new bone formation in par with the degradation of material was almost achieved throughout the defect. The original cross circular shape of normal femur with the regeneration of medullary canal was evident at 6 months and the complete bone remodeling at 1 year (Fig. 5.8).

HASi+C and HASi+CP groups - In both the groups, new bone formation was observed through out the defect at 2 months. Only few residues of the materials were seen, indicating the degradation. The regeneration of medullary canal with the circular shape of normal femur was achieved at 2 months in HASi+CP groups, while a similar progress was seen in HASi+C groups at 4 months only (Fig. 5.8).

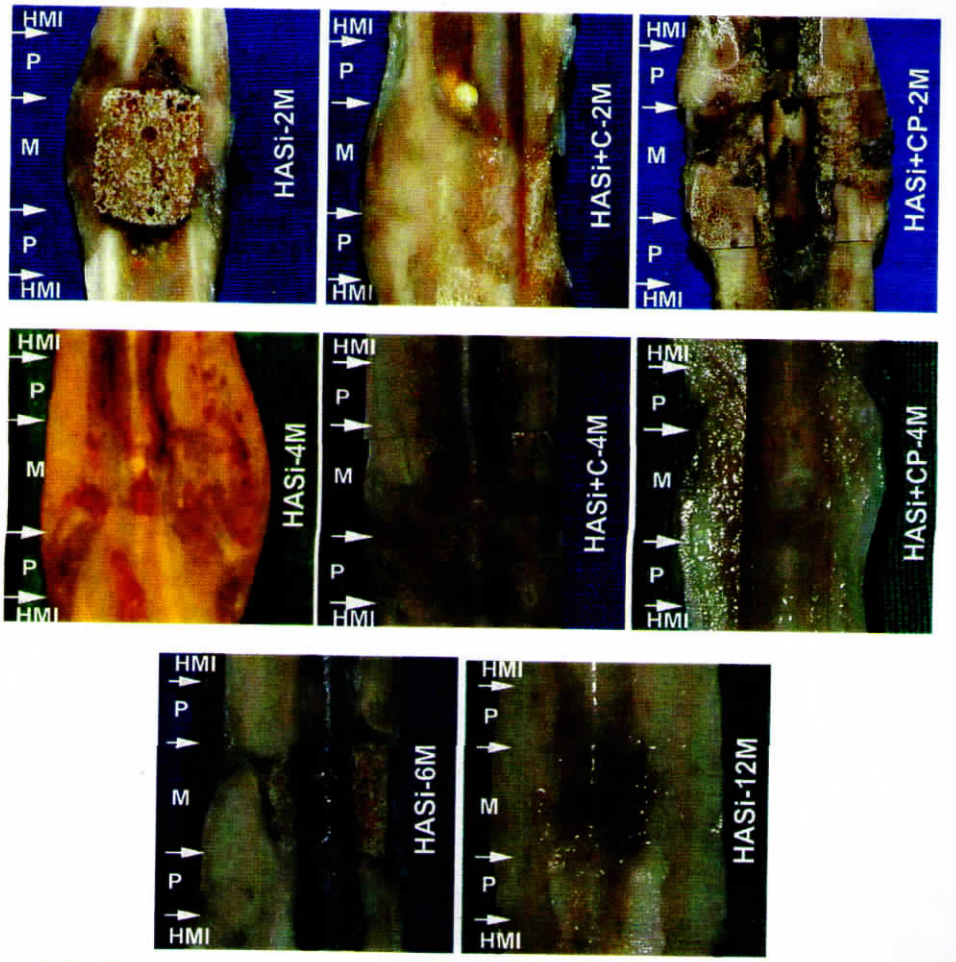

Figure 5.8. Gross view of newly regenerated bone in segmental defect post-implantation. 2M (2 months); 4M (4 months); 6M (6 months); 12M (12 months). The area between arrows shows mid region (M) (1 cm) and peripheral regions (P) (0.5 cm on each side) of the segmental defect. HMI denotes host bone-material interface (approximately 0.5 cm on each side).

5.3.2.2 Radiographic analysis

The ceramics could be visualized easily because of the radio opacity of the material (Bruder *et al.*, 1998). A distinct radiolucent zone at the interface between the material

and the host bone was visible immediately after the surgery. The absence of this radiolucent zone is considered to be an indication of "union" between the material and the host bone. Accordingly, this union was observed at 6 weeks in all the groups demonstrating the osteoconductive and osteointegrative nature of HASi. In addition, an osseous callus had developed around the periphery of material as well as around the adjacent host bone at 6 weeks in all the groups, depicting indirect or secondary bone healing at the defect site. Since ceramics are much more radio opaque than bone, a decrease in radio opacity was considered as new bone regeneration and material degradation (Fig. 5.9).

Bare HASi groups - New bone was regenerated at the interfacial area between the material and host bone as well as along the edges of intramedullary nail within the defect at 2 months. The material was still visible in the mid region of the defect during this period. At 4 months, a decrease in radio opacity related to new bone formation and material degradation was observed throughout the defect. The newly formed bone integrated completely with host bone and underwent mineralization at 6 months. The density of mineralized new bone was similar to host bone at 12 months so that the defect region was difficult to distinguish from the host bone. The thickening of *de novo* cortical bone similar to normal femur was also achieved during this period.

HASi+C and HASi+CP groups - A decrease in radio opacity of implant indicating new bone formation and material degradation was noticed throughout the defect at 2 months. The newly formed bone has undergone mineralization and the density of mineralized region was almost comparable to the host bone at 4 months. The newly formed bone integrated completely with host bone and the cortical bone thickening similar to normal femur and remodeling was also achieved during this period. HASi+C and HASi+CP groups showed comparable temporal response, while a slightly faster response was seen in HASi+CP groups.

Radiographic results depicted that the fixation of porous HASi cylinders using titanium intramedullary nail and inter fragmentary screws to the proximal and distal diaphysis were stable and pertinent. Porous ceramics are brittle and tend to fracture in the centre (Moore DC *et al.,* 1987; Grundel *et al.,* 1991). So it is necessary to avoid excessive load on the ceramic materials during the early stages of healing to

prevent collapse and fracture of the implant (Zhang C *et al.,* 2001).

Although the fixation system is needed for the stabilization of porous materials, some mechanical stress should pass through the bone, which optimizes ultimate bone architecture as per Wolff's law (Frost HM 1994). Thus in order to provide mechanical stress through the defect, some studies showed the removal of intramedullary nails or screws as bone regenerated and grew into the pores of the material (Zhu *et al.,* 2006). However the removal of fixation devices requires an additional surgery after few months of implantation. So herein, in order to avoid an extra surgery and to provide reasonable mechanical stress or motion through bone-implant interface throughout the implantation period, one of the proximal locking was done with dynamic screw system. This micro motion has led to indirect or secondary healing with osseous callus, which was evident at 6 weeks of post implantation. Finally, the thickening of newly regenerated bone matching the architecture of host bone suggested an appropriate stress transfer along HASi during the repair of segmental defect.

Faster consolidation and mineralization was observable in HASi+C and HASi+CP groups. This indicated that gOS+ cells cultured on HASi scaffolds and PRP delivered at the defect site was efficient in restoring the continuity of implant and the normal architecture of bone in an effective and easiest manner. These results were comparable to previous reports using resorbable scaffolds with BMSCs and PRP (Petite H *et al.,* 2000; Zhang CQ *et al.,* 2004).

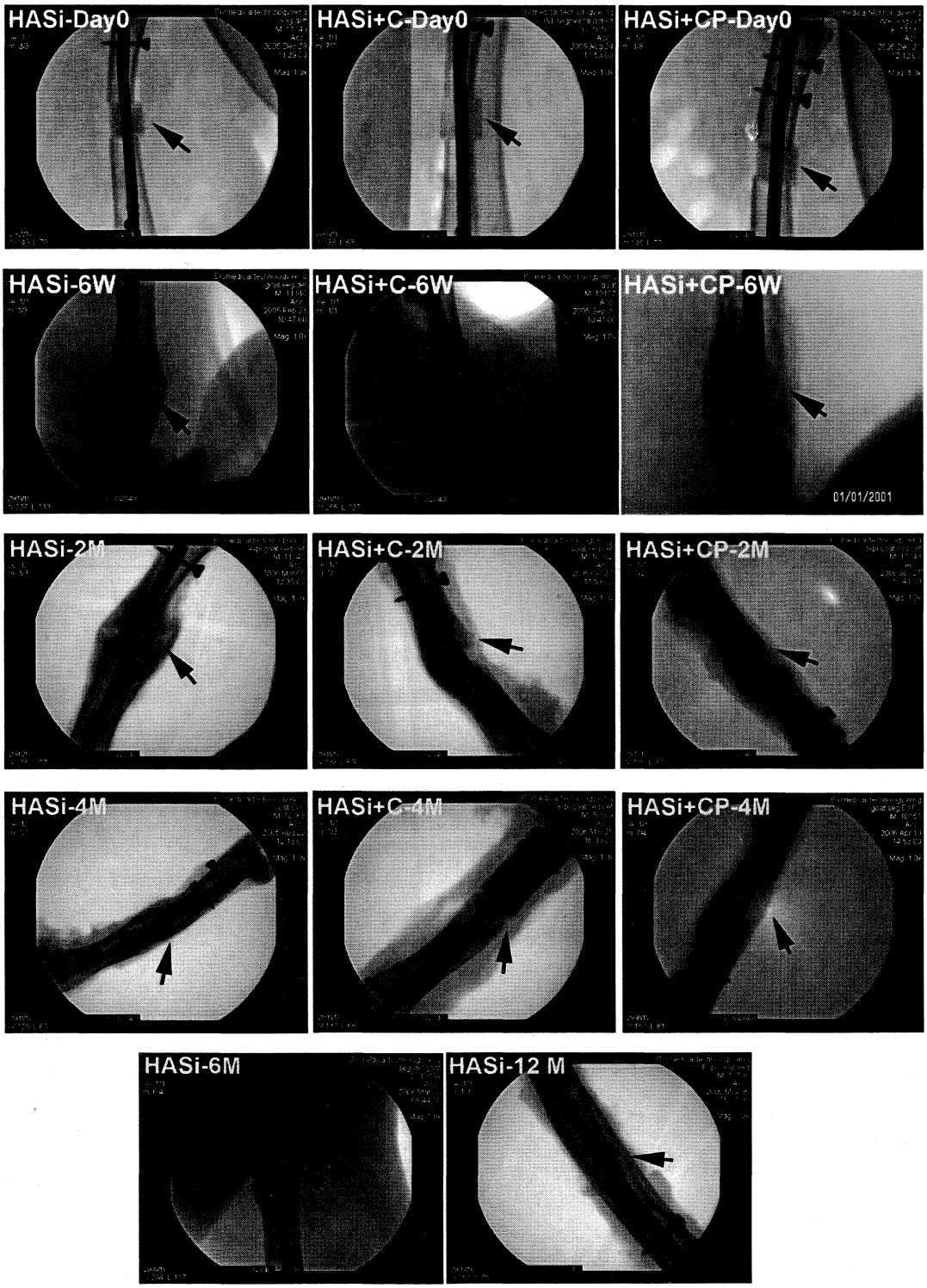

Figure 5.9. Radiographs of newly regenerated bone in segmental defect post-implantation. Day 0 (Immediately after surgery); 6W (6 weeks); 2M (2 months); 4M (4 months); 6M (6 months); 12M (12 months). Arrow - segmental defect site.

5.3.2.3 Histological evaluation

Histological examination demonstrated an unevenful healing of the defect without any signs of inflammatory response or fibrous tissue formation. Bridging of the defect and union of the material with host bone on either side was observed in all the groups. The peripheral and mid region of the defect was validated separately.

In bare HASi groups, new bone deposition and material degradation was advanced in peripheral region as compared to mid region of the defect. The osteoblasts colonized and formed bone matrix and osteocytes were encased in the bone matrix mainly in the form of mature lamellar or Haversian structure in the peripheral region of the defect at 2 months. Moreover, the material was almost degraded leaving behind a few ghost structures of HASi. However, in the mid region of defect at 2 months, newly formed trabeculae were scanty and most of the area was occupied by the material. Numerous osteoblast-like cells were seen in and around the material without fibrous tissue formation and inflammation (Fig. 5.10). At 4 months, new bone deposition and material degradation was achieved throughout the defect, but a qualitative difference was observed in the bone formed between peripheral and mid region of the defect. A well organized mature lamellar pattern of bone was visualized in the peripheral region while immature woven bone lined with a seam of osteoblast cells was seen in the mid region of defect. The material was not completely resorbed but existed as small islands embedded in newly formed bone (Fig. 5.11). At 6 and 12 months, newly formed bone was organized in the form of mature lamellar pattern through out the defect. A complete bone remodeling was achieved at 12 months (Fig. 5.12).

In HASi+C and HASi+CP groups, new bone formation and material degradation was faster and superior. At 2 months, newly formed bone was seen throughout the defect with a qualitative difference between peripheral and mid region of the defect. A mature lamellar pattern of newly formed bone was observed in the peripheral region, while immature woven bone was seen in the mid region of defect. Only few remnants of the material were seen throughout the defect, which was in direct contact with osteoblast-like cells without the interposition of fibrous tissue (Fig. 5.10). At 4 months, mature lamellar bone organizations were seen throughout the defect where osteocyte-like cells were arranged around the Haversian canal. There were no traces

of material at the defect site (Fig. 5.11). HASi+C and HASi+CP groups did not show any noticeable difference between them.

Many osteoclast-like cells were also found close to the material in HASi+C and HASi+CP groups at 2 months, demonstrating osteoclast-mediated degradation of materials in these groups (Fig. 5.13 and Fig. 5.14).

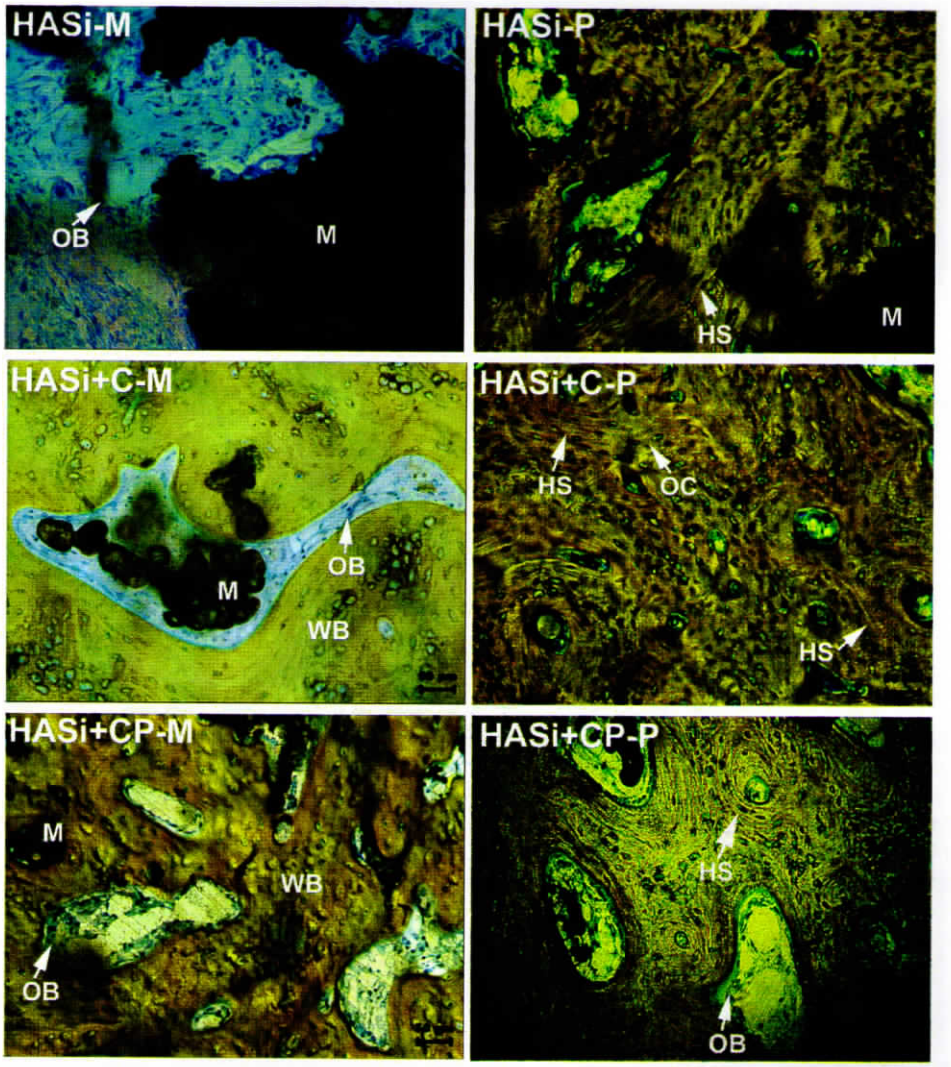

Figure 5.10. Light micrographs of newly formed bone in the peripheral and mid region of segmental defect - 2 months post-implantation. M-Mid region of the defect; P-peripheral region of the defect; OB-osteoblast-like cells; M – material; WB – woven bone; HS – Haversian system; OC – osteocyte-like cells. Stevenal's blue (osteoblast-like cells - blue) and van Gieson's picrofuchsin (osteoid matrix – yellow) staining. Magnification: 20X

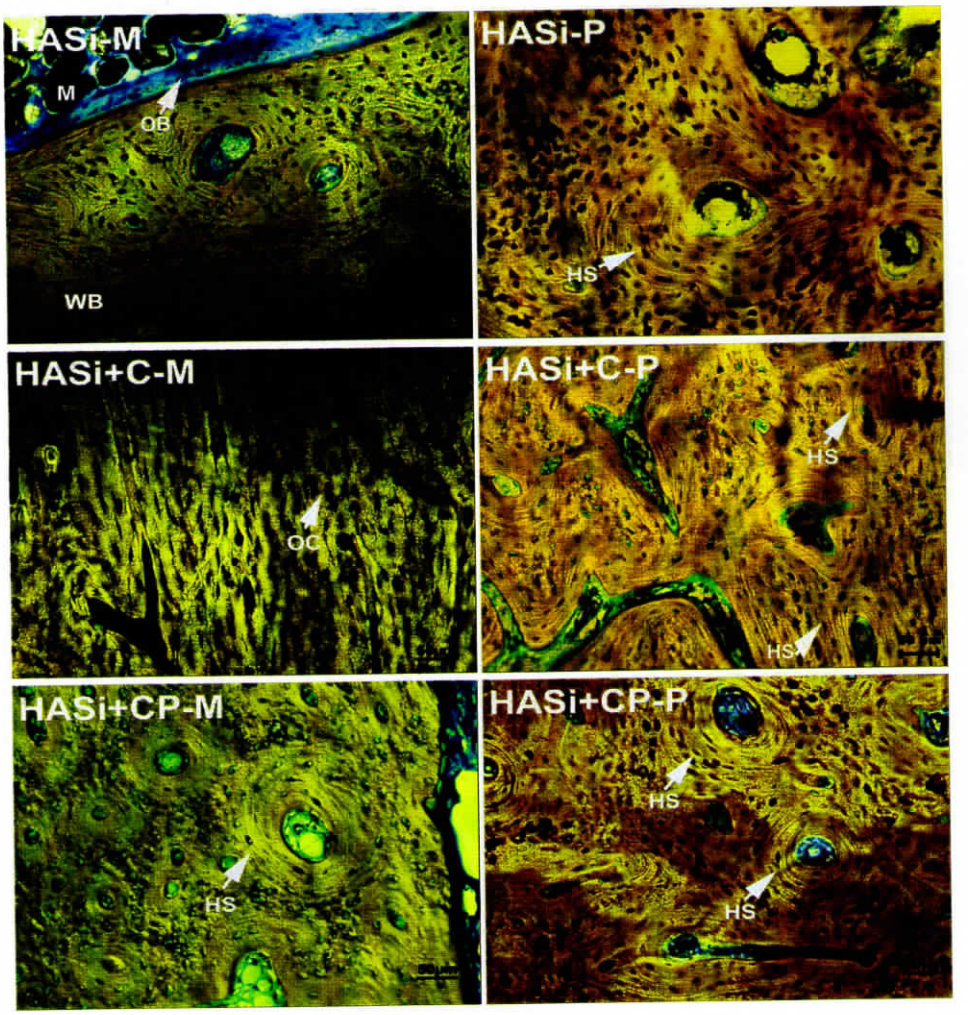

Figure 5.11. Light micrographs of newly formed bone in the peripheral and mid region of segmental defect - 4 months post-implantation. M-Mid region of the defect; P-peripheral region of the defect; OB-osteoblast-like cells; M – material; WB – woven bone; HS – Haversian system; OC – osteocyte-like cells. Stevenal's blue (osteoblast-like cells – blue) and van Gieson's picrofuchsin (osteoid matrix – yellow) staining. Differential coloring of van Gieson's picrofuchsin indicate difference in the organization level of osteoid matrix. Magnification: 20X

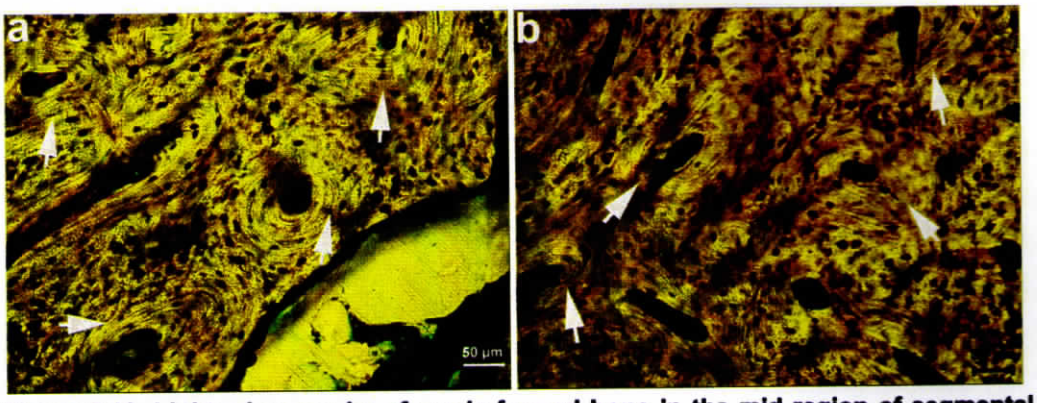

Figure 5.12. Light micrographs of newly formed bone in the mid region of segmental defect – 6 and 12 months post-implantation. (a) 6 months (b) 12 months. Stevenal's blue (osteoblast-like cells – blue) and van Gieson's picrofuchsin (osteoid matrix – yellow) staining. Arrow -Haversian pattern. Magnification: 20X

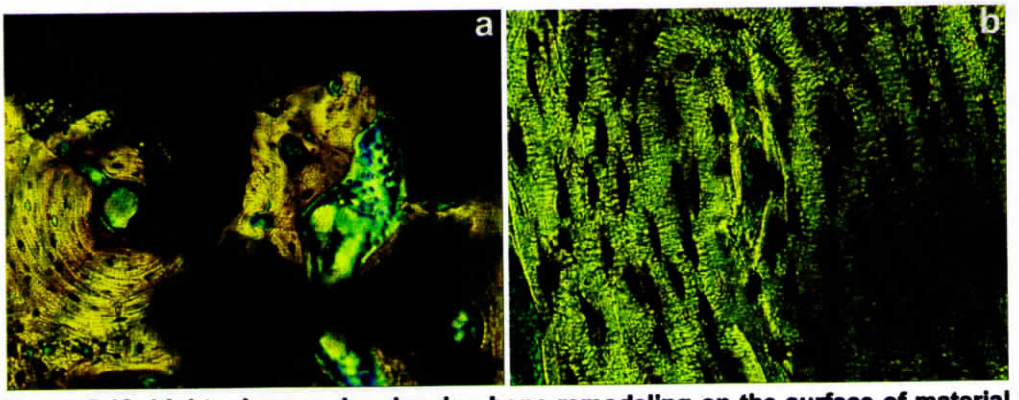

Figure 5.13. Light micrographs showing bone remodeling on the surface of material 2 months post-implantation - HASi+C group (a) 20X (b) Typical Haversian structure (50X). Stevenal's blue and van Gieson's picrofuchsin staining.

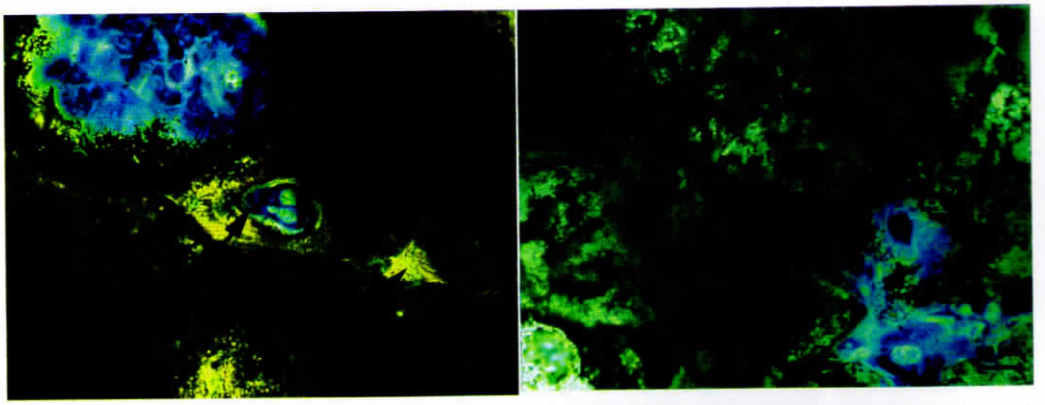

Figure 5.14. Light micrographs showing the association of osteoclast-like cells and material 2 months post- implantation - HASi+C group (Stevenal's blue and van Gieson's picrofuchsin staining). (a) 50x (b) 100x. M-material; OCL-osteoclast-like cells; WB – woven bone.

Studies have reported the use of materials like HA-βTCP, coral and polylactide membranes for the repair of segmental defects where the union mainly appeared at the host bone-implant interface while the mid portion of these defects showed fibrous tissue deposition (Bruder *et al.,* 1998; Meinig RP *et al.,* 2002; Zhu *et al.,* 2006). When porous ceramic cylinders consisting of HA and β-TCP were used for the healing of canine segmental defect (2.1 cm), trabecular bone was formed only at the cut ends of the cortex of host bone and most of the pores were filled with fibrous tissue (Bruder *et al.,* 1998). The use of coral as a scaffold material was ineffective in the healing of goat femur segmental defect (2.5 cm) (Zhu *et al.,* 2006). When β-TCP was used for 3 cm mandibular segmental defect, minimal bone formation with almost fibrous connection was observed (Yuan *et al.,* 2007). In all these cases with bare material group, native cells could migrate into the scaffold to generate new tissues and achieve bony union. However, if the migration rate of native cells is not fast enough to match the degradation rate of scaffold, fibrous union will be formed. Interestingly in this study, besides the union at host bone-implant interface, new bone was seen in the mid region of defect without the intervention of fibrous tissue. Thus the capability of HASi to facilitate the migration and proliferation of native cells and to undergo degradation was almost similar. Periosteum may significantly contribute for improving the repair process with bare HASi. The role of periosteum-derived cells in the bone repair process was assessed in live bone grafts harvested from Rosa 26A mice. In this model, approximately 70% of the osteogenesis on the graft was attributed to the expansion and differentiation of donor periosteal progenitors (Zhang X *et al.,* 2005).

It is decisive to note that the process of bone regeneration occurred by direct conversion of MSCs into osteoblasts (intramembranous ossification) rather than through cartilagenous intermediate (endochondral ossification), which may be imputed to neo-vascularisation at the defect site (Thompson TJ *et al.,* 1989). Extraskeletal implantation studies in rat model confirmed the vascularisation potential of HASi that leads to direct bone formation. The vasculature provide a portal for the entry and establishment of host-derived MSCs and pre-osteoblasts. These cells can arrive and establish initially in the peripheral region while more time is required for the cells to reach the mid region of the defect site. This could be the possible explanation why new bone formation in the mid region was slowed down when

compared to the peripheral region of defect in bare HASi groups.

An improved and faster osteogenesis in HASi+C and HASi+CP groups was due to its osteoinductive nature (confirmed through extraskeletal implantation studies) in addition to its osteoconductive and osteointegrative property, which is critical for augmenting the healing of segmental defects (Habibovic P *et al.,* 2006). Many studies reported the promising approach of culture-expanded osteoprogenitors for the significant improvement of the repair of long bone defects (Ohgushi H *et al.,* 2003; Kruyt MC *et al.,* 2003; Kon E *et al.,* 2000). The growth factors released through the delivery of PRP can further improve the expansion of native MSCs at the defect site, leading to faster bone regeneration (Vogel JP *et al.,* 2006).

An ideal scaffold after providing an initial support for the bone depositing cells should be resorbed with the same kinetics of new bone formation in order to obtain a constantly stabilized repair. Even though HA facilitates bony ingrowth onto its surface, the slow resorption rate is a serious problem, which delays complete bone remodeling (Vuola J *et al.,* 1998). However in this study, a progressive complete degradation of HASi scaffolds was observed that provide platforms for the growth and remodeling of new bone tissue. The process was enhanced when used in conjunction with OS+ cells and PRP, highlighting the dependency of the material upon cell and ECM to undergo degradation (Mastrogiacomo M *et al.,* 2007).

5.3.2.4 Morphological evaluation

Scanning electron micrographs demonstrated the union of material with host bone on either side as well as the formation of new bone without any intervening fibrous connective tissue, which was similar to histology data (Fig. 5.15).

Bare HASi groups - At 2 months, new bone formation together with material degradation was observed in the peripheral region of defect while in the mid region, the material was still visible embedded in the osteoid matrix secreted by osteoblast-like cells. At 4 months, newly formed bone was seen throughout the defect, which organized and displayed a regular architecture at 6 months and the complete bone remodeling at 12 months.

HASi+C and HASi+CP groups – The defect area was almost completely occupied by newly formed bone tissue in par with material degradation at 2 months. This newly

formed bone displayed a regular architecture at 4 months. There was no observable difference between HASi+C and HASi+CP groups except for some vacuolar spaces in HASi+CP groups at 2 months.

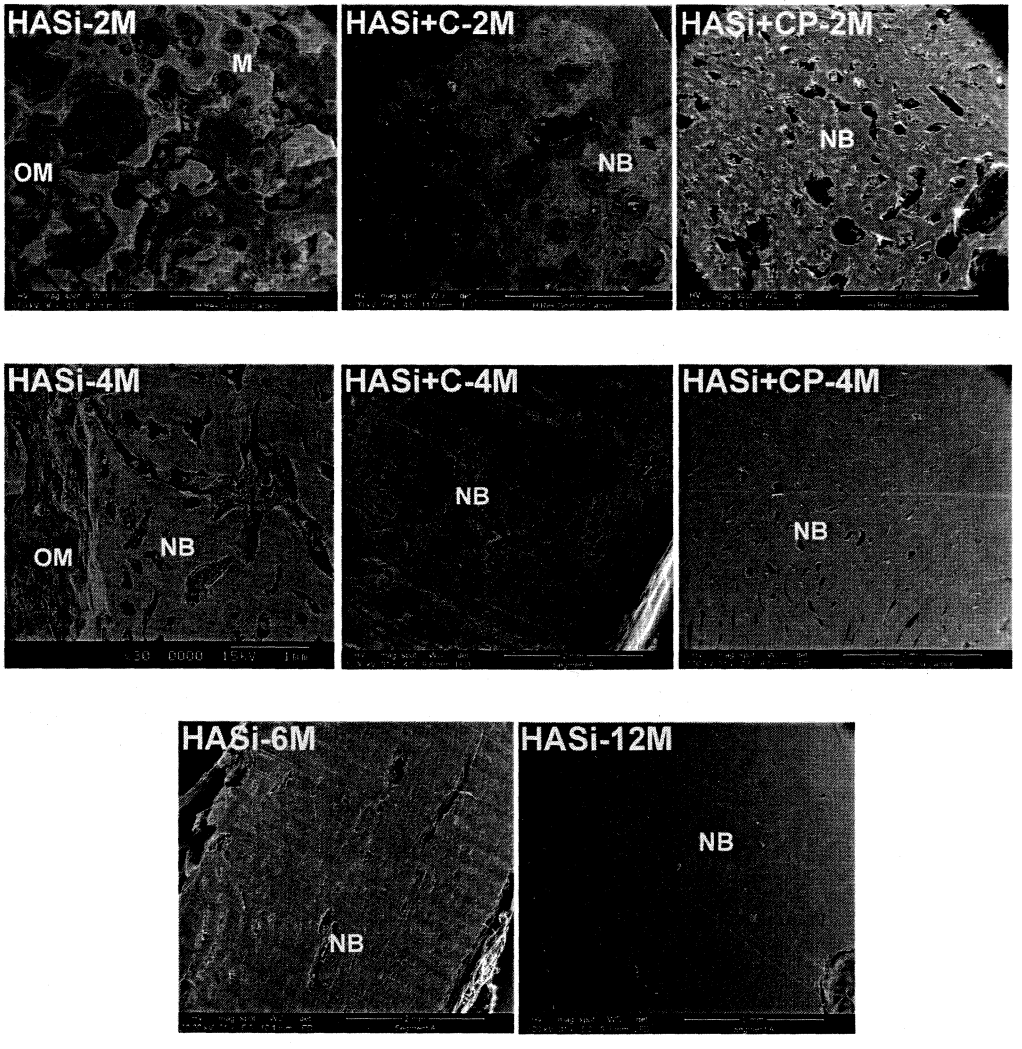

Figure 5.15. Scanning electron micrographs of newly formed bone in the mid region of segmental defect - 2, 4, 6 and 12 months post implantation; NB - new bone; OM – osteoid matrix.

5.3.2.5 Histomorphometric evaluation

The results of the percentage of newly formed bone and material degraded in the peripheral and mid region of defect is summarized here. The percentage of newly formed bone and material degraded was calculated with respect to total frame area (356911.2μm^2).

At 2 months, neo-osteogenesis was significantly greater in HASi+CP groups (76.7% ± 10.1%) and HASi+C groups (61.6 ± 4.8%) when compared to bare HASi groups (36.2 ± 10.16%) in the mid region of the defect. However, there were no significant differences between the groups (67 ± 9.6% for bare HASi groups, 80.9 ± 4.2% for HASi+C groups and 84.5 ± 4.5% for HASi+CP groups) in the peripheral region of the defect. At 4 months, there were no significant differences between three groups both in the peripheral region (78.2 ± 6.3% for bare HASi groups, 79 ± 9.7% for HASi+C groups and 83.1± 7.9% in HASi+CP groups), as well as in the mid region of the defect (62.5 ± 10.9% for bare HASi groups, 78.8 ± 3.7% for HASi+C groups and 85.2 ± 5.8% in HASi+CP groups. As the implantation period escalated, bare HASi groups performed well both in the mid and peripheral regions and achieved approximately 97.5 ± 1.9% new bone at 12 months (Fig. 5.16).

The material degradation also followed the similar trail in three groups during the implantation period. The material degradation was significantly greater in HASi+CP groups (70.4 ± 1.3%) and HASi+C groups (55.2 ± 7.4%) when compared to bare HASi groups (20.1 ± 9.9%) in the mid region of the defect at 2 months. Whereas, the peripheral regions showed no statistically significant differences between the groups (77.9 ± 0.81% for bare HASi groups; 83.4 ± 1.6% for HASi+C groups and 84.3 ± 1.7% for HASi+CP groups). At 4 months, there were no significant differences between three groups both in the peripheral regions (75.2 ± 8.4% for bare HASi groups; 95.4 ± 1.8% for HASi+C groups and 94.4 ± 0.6% for HASi+CP groups) as well as in the mid region of the defect (88.5 ± 7.9% for bare HASi groups; 97.4 ± 4.3% for HASi+C groups and 97.4 ± 4.1% in HASi+CP groups). At 12 months, the material was completely degraded to 99.6 ± 0.33% (Fig. 5.17).

Thus among the groups, the performance in terms of bone regeneration as well as material degradation was in the order of bare HASi < HASi+C < HASi+CP. The results demonstrated that the material was degraded progressively at a rate commensurate with the formation of new bone. The premature degradation of material destroy the tissue structure if new bone has not generated yet, while a lingering degradation of material affect the repairing process, such as tissue structure and remodeling. Thus the ability of HASi to undergo degradation and to regenerate bone uniformly is a positive impact in bone tissue engineering studies.

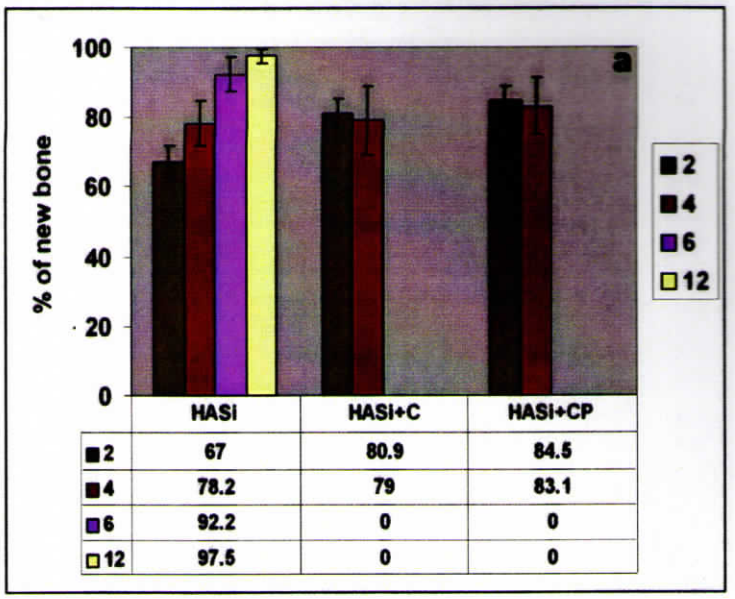

	HASi	HASi+C	HASi+CP
2	67	80.9	84.5
4	78.2	79	83.1
6	92.2	0	0
12	97.5	0	0

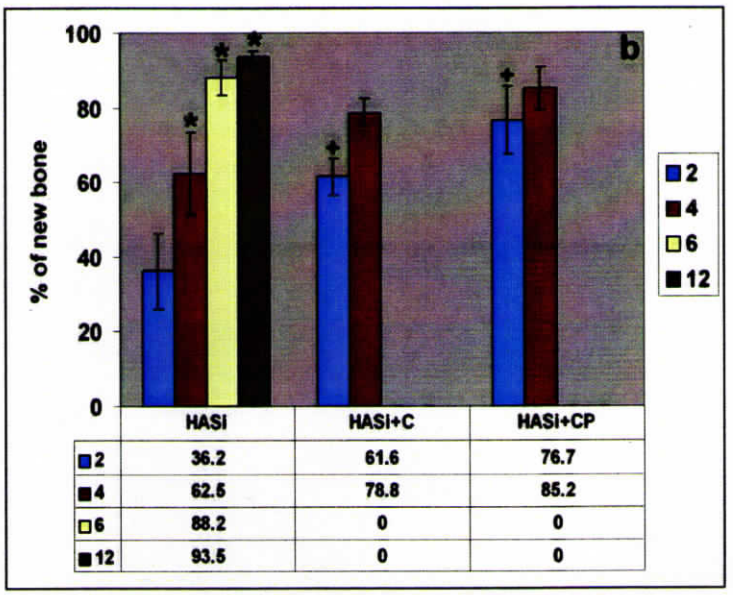

	HASi	HASi+C	HASi+CP
2	36.2	61.6	76.7
4	62.5	78.8	85.2
6	88.2	0	0
12	93.5	0	0

Figure 5.16. Histomorphometric evaluation of the percentage of newly formed bone in segmental defect (a) Peripheral region of the defect site (b) Mid region of the defect site. Bare HASi groups showed significant increase in performance (*) at 4, 6 and 12 months when compared to 2 months. The percentage of newly formed bone was significantly enhanced in HASi+C (+) and HASi+CP groups (+) when compared to bare HASi groups at 2 months.

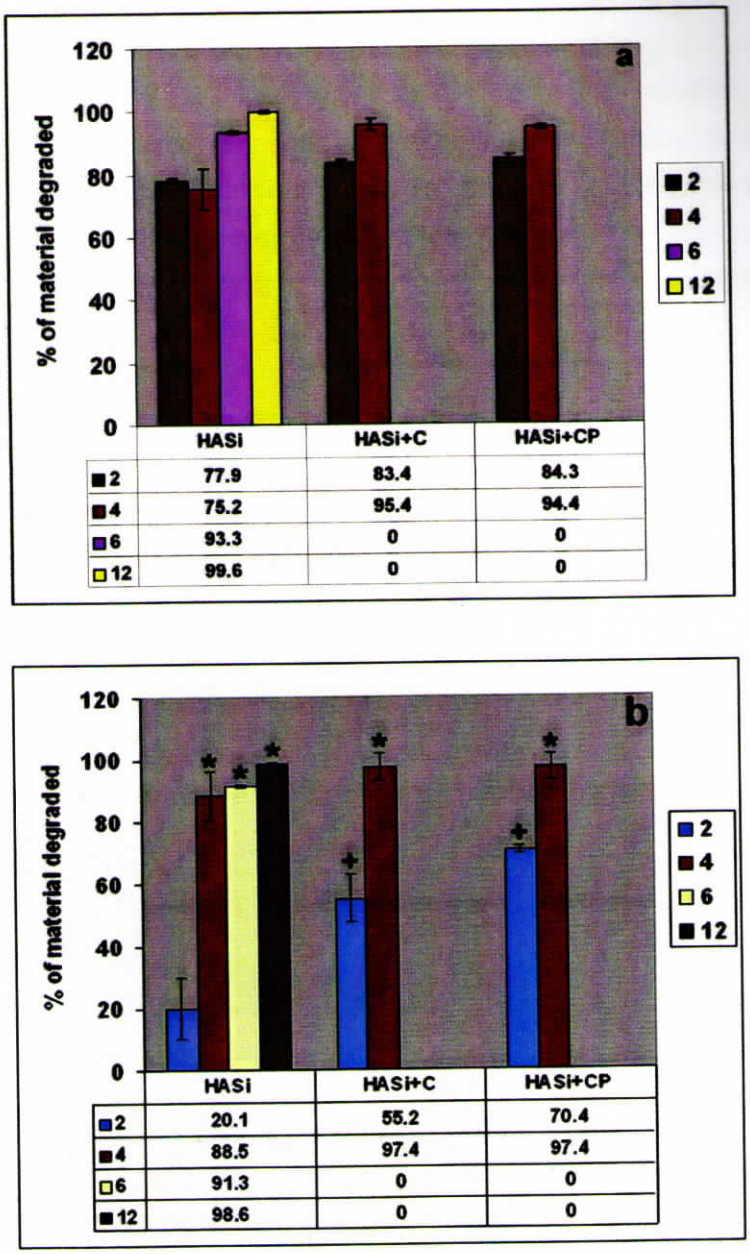

Figure 5.17. Histomorphometric evaluation of the percentage of material degraded in segmental defect (a) Peripheral region of the defect site (b) Mid region of the defect site. Three groups showed a significant increase in performance (*) at 4, 6 and 12 months as compared to 2 months. The percentage of material degraded was significantly enhanced in HASi+C (+) and HASi+CP (+) groups when compared to bare HASi groups at 2 months.

5.3.2.6 Biochemical assays

It has been reported that serum or urine can be utilized for the evaluation of bone metabolic indices in humans and animals. ALP is the marker of osteoblasts and its activity can be correlated with new bone formation. Similarly, TRAP is the marker of osteoclasts and its activity can be considered as the degradation of bone or material (Sato J *et al.*, 2002). So herein, ALP and TRAP activity in serum was determined to confirm the bone regeneration and material degradation.

5.3.2.6.1 ALP activity

ALP activity was significantly higher in HASi+C and HASi+CP groups at 2 months, which slowed down at 4 months when compared to bare HASi. In bare HASi groups, the activity was significantly higher at 4 months (Fig. 18).

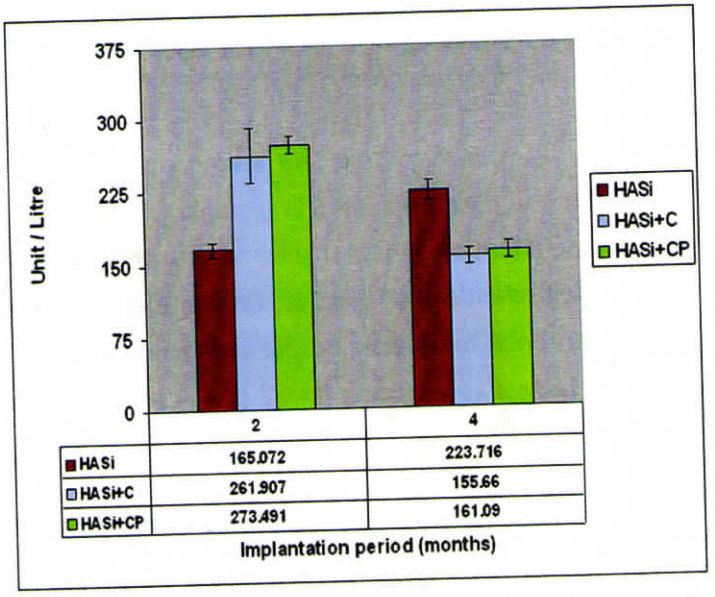

Figure 5.18. ALP activity in the serum of goat model. The activity was significantly higher in HASi+C (+) and HASi+CP (+) groups at 2 months, while it was higher in bare HASi groups (*) at 4 months as compared to bare HASi groups at 2 months. The reference values of ALP activity in adult ranges between 100 - 275 unit / L at 37℃.

5.3.2.6.2 TRAP activity

TRAP activity was significantly higher in HASi+C and HASi+CP groups at 2 months which slowed down at 4 months. In bare HASi groups, the activity was significantly higher at 4 months (Fig. 19).

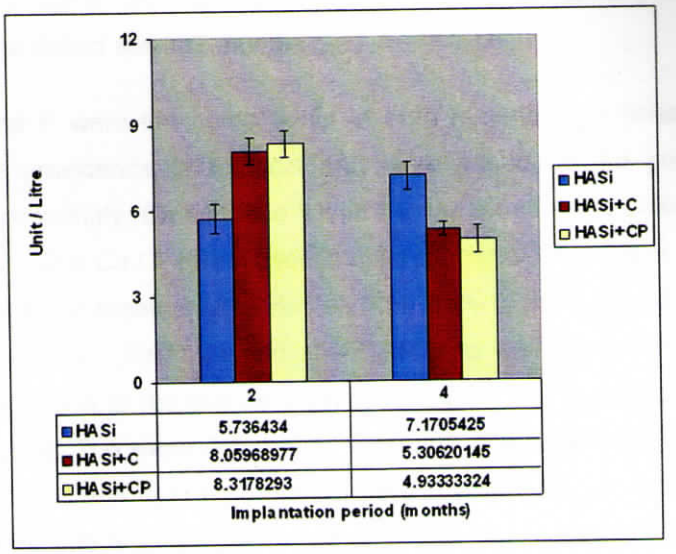

Figure 5.19. TRAP activity in the serum of goat model. The activity was significantly higher in HASi+C (+) and HASi+CP (+) groups at 2 months, while it was higher in bare HASi groups (*) at 4 months as compared to bare HASi groups at 2 months. The theoretical value for acid phosphatase ranges between 0 - 9 unit / L.

ALP and TRAP activity confirmed that HASi cultured with gOS+ cells can provide better conditions for the functioning of both osteoblast and osteoclast cells leading to faster bone regeneration in par with material degradation. In bare HASi groups, indigenous osteoclast and osteoblast cells has to make their way to the defect site and therefore requires more time for the process of bone remodeling. That is why in bare HASi groups, the ALP and TRAP activity was less at 2 months followed by a significant increase in its activity.

5.3.2.7 Mineralization studies

5.3.2.7.1 Energy Dispersive x-ray spectroscopy

The degree of mineralization of newly formed bone and the degradation of material from the defect site was determined through line mapping of ESEM-EDS system (Fig. 5.20). The main elements investigated at the defect site include Ca, P and Si. Line mapping revealed the very less Si distribution together with the uniform distribution of Ca and P in HASi+C and HASi+CP groups at 2 months. This showed that the degradation of material from the defect site (Si is present only in material) and the mineralization of newly formed bone (Ca and P were uniformly distributed rather than localized). However, in bare HASi groups, the level of Si was

comparatively higher and Ca and P were localized, representing the occurrence of material at the defect site at 2 months.

Since Ca and P were the constituents of both material and bone, it was hard to interpret the providence of material and bone based on the presence of these elements. Accordingly, Ca / P ratio within the defect site was calculated (Fig. 5.21 and Fig. 5.22). The Ca / P ratio varies in different parts of the same bone and also in different bones and theoretically it ranges from 1.8% to 3.2% (Fountos G *et al.,* 1997, Tzaphlidou M *et al.,* 2003). Herein, the Ca/P ratio was similar to theoretical value (approximately 2) in all the groups, both in peripheral and mid region of the defect at 2 and 4 months. The exceptional case was shown only by bare HASi groups at 2 months, particularly in the mid region of defect, where Ca / P ratio attained was 4. The reason for this greater ratio is not apparent. The contributions of Ca from the material side (a portion of material was present in the mid region of defect in bare HASi groups) as well as from the bony site may be accountable for this large Ca / P ratio.

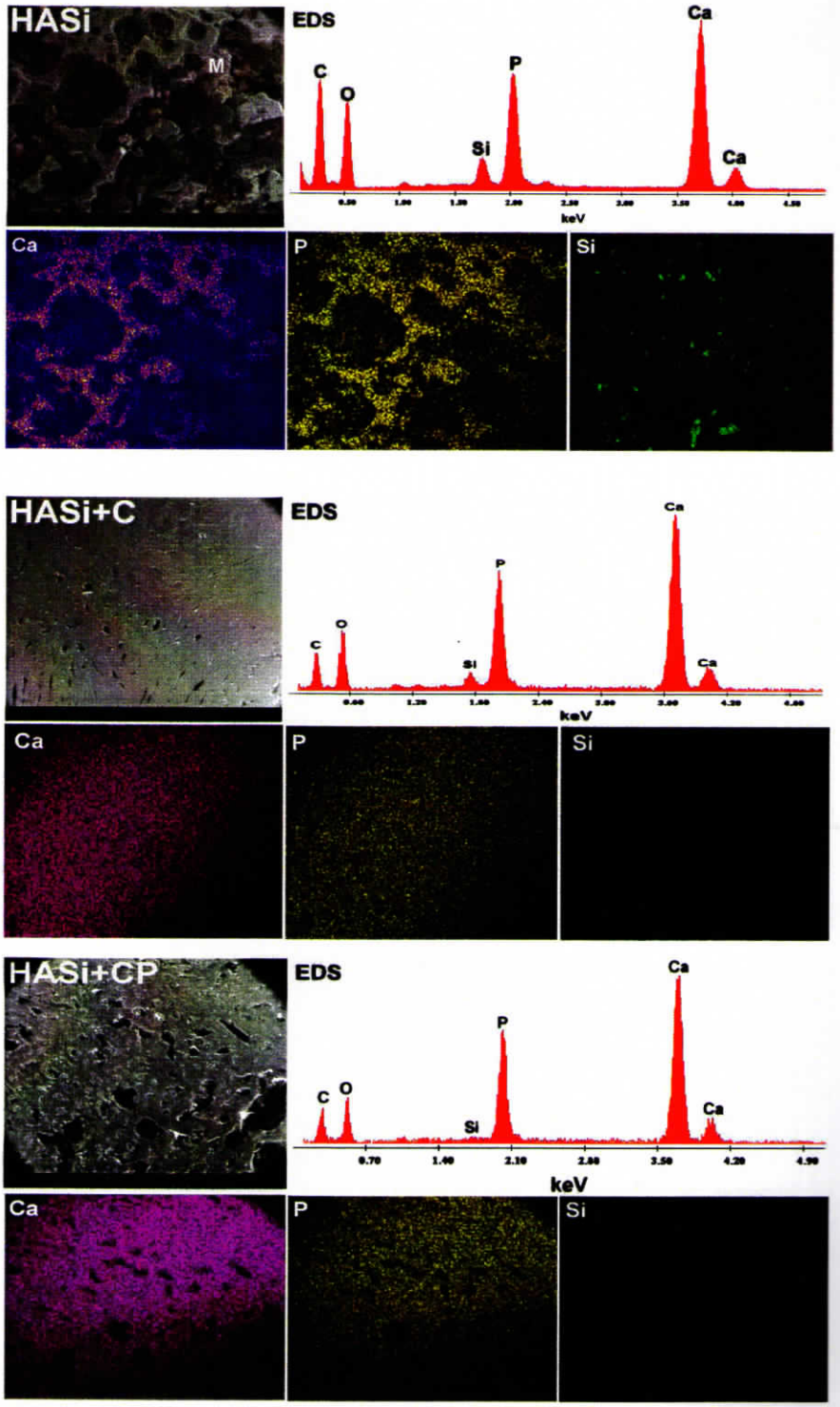

Figure 5.20. ESEM-EDS showing the distribution of elements like Ca, P and Si in the mid region of segmental defect 2 months post-implantation. Line mapping was done to determine the distribution of elements in the region.

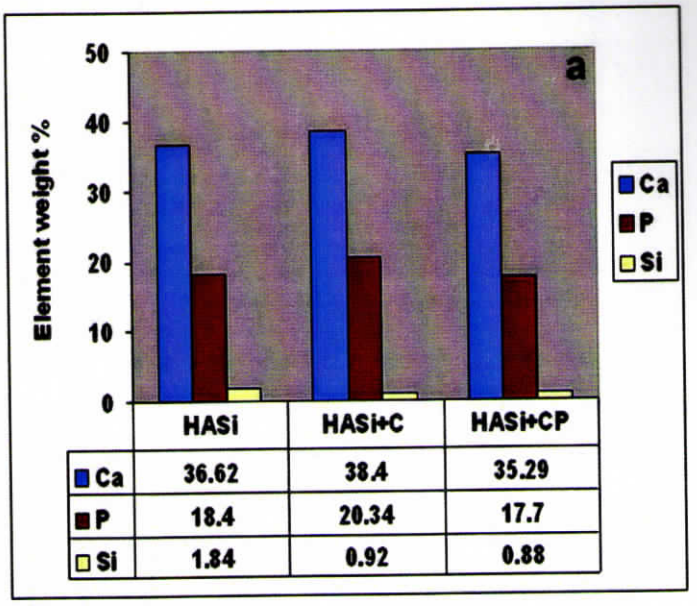

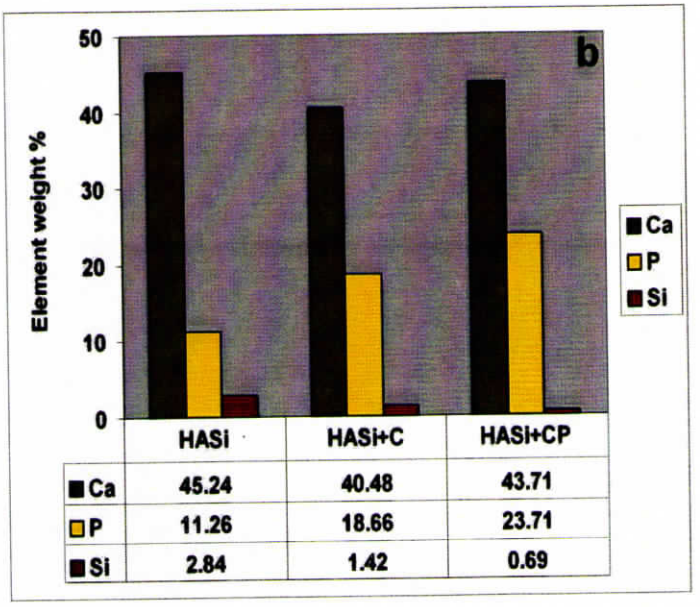

Figure 5.21. Histogram of the weight percentage of elements like Ca, P and Si in segmental defect 2 months post-implantation. (a) Peripheral region of the defect (b) Mid region of the defect.

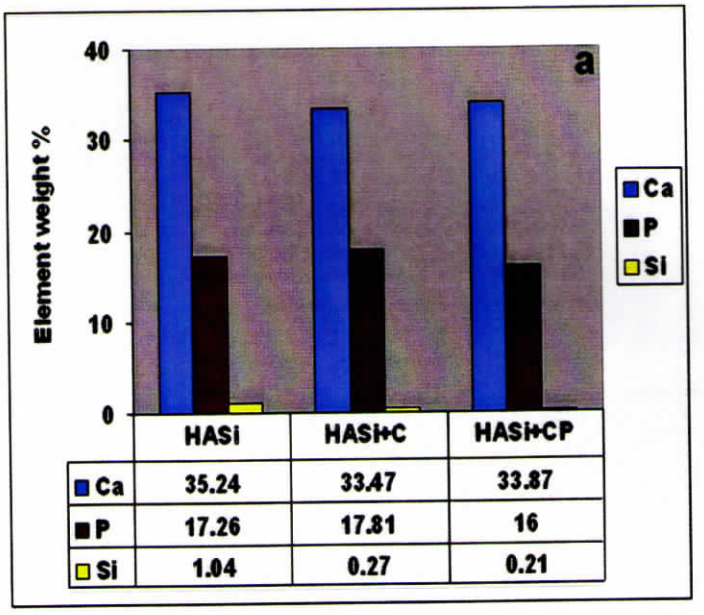

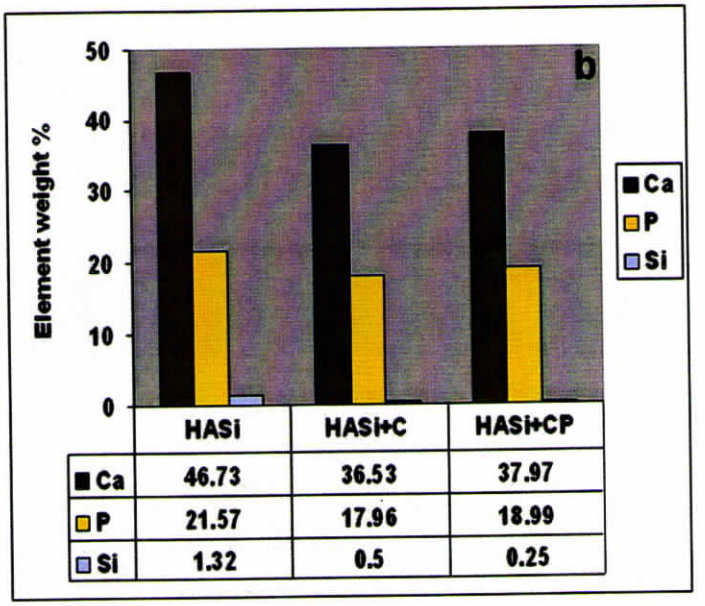

Figure 5.22. Histogram of the weight percentage of elements like Ca, P and Si in segmental defect 4 months post-implantation. (a) Peripheral region of the defect (b) Mid region of the defect.

5.3.2.7.2 Computed Tomography

The mineralization of newly formed bone in par with material degradation was confirmed through computed tomography, based on their density difference. A conspicuous difference between three groups was observed only in 2 months, which is represented here.

A colour-based density method was applied to all the three groups using Syngo software of Siemens CT scanner (Fig. 5.23). Accordingly, red colour represent the mineralized bone phase and green colour represent the material phase. In bare HASi groups, the mineralized bone phase was found only in the peripheral region of defect while the mid region was almost occupied by the material. On the contrary, in HASi+C and HASi+CP groups, a uniform distribution of red colour related to the mineralization of newly formed bone was observed. Qualitatively there was no noticeable difference between HASi+C and HASi CP groups.

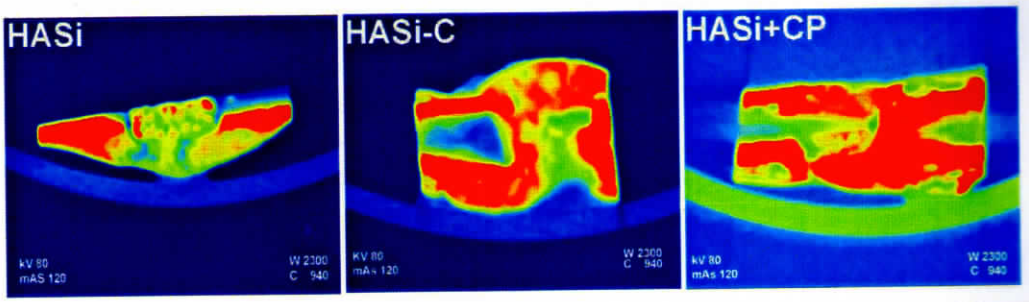

Figure 5.23. Computed Tomographs showing the mineralization of newly formed bone in segmental defect 2 months post-implantation. CT image of longitudinally cut portion of the femur of goat model (middle view in sagittal plane) (Model: Siemens syngo soft ware).

5.3.2.7.3 Micro-computed Tomography

The mineralization of newly formed bone was once again confirmed through micro-CT based on its density difference, which provides optimal isotropic resolution around 10 μm^3 (Gauthier O *et al.*, 2005). In addition to mineralization, micro-CT is a non-destructive technique for the analysis of 3D trabecular bone micro architecture *in vivo* (Kuhn JL *et al.*, 1990).

The retrieved tissue was scanned in z-axis to get 3D view of micro structural pattern and mineralization of the defect. The backside (cortical region) and frontal side

(medullary canal region) of 2 and 12 months post-implanted bone tissue is represented here (Fig. 5.24).

Bare HASi groups - New bone has bridged across the defect at 2 months. New bone with normal femoral contour was achieved throughout the cortical region of defect, while the frontal side towards the mid region of defect showed the existence of material. A line of crack in one side of the cortical region of defect was seen, which may be the region where the material has already degraded and the new bone was started to form. The density of bone, which is related to mineralization, was found to be advanced in the cortical region of defect. At 12 months, a completely mineralized bone having the thickness of a normal femur was achieved, both in the cortical and medullary region of bone tissues.

HASi+C and HASi+CP groups - The new bone has formed in perfect continuity with surrounding host bone and almost attained the appearance of the original cortex of femoral diaphysis at 2 months. 3D images demonstrated newly developed trabecular bone and its homogenous interconnectivity throughout the entire defect. In addition, the density of newly formed bone was advanced in entire z-stacked images, representing the uniformity of mineralisation all over the tissue constructs. There was no observable difference between HASi+C and HASi+CP groups.

Mineralization of bone matrix implies two successive steps: a rapid primary mineralization on the calcification front followed by a slow process of secondary mineralization progressively adding about one-half of the mineral content on bone matrix. Element weight percentage analysis, CT and micro-CT showed that HASi+C and HASi+CP groups were capable of generating mineralized matrix through out the defect in a rapid manner within 2 months. In addition, Ca / P ratio was within the theoretical range of bone. The reason is that the culturing of cells in osteogenic medium can create mineralized template under *in vitro* culture conditions that dramatically enhance subsequent *in vivo* mineralized tissue formation (Bielby RC *et al.,* 2004). Previous studies reported that the impact of changes in bone remodeling rate is dependent on the degree of mineralization of bone (Boivin G *et al.,* 2000; Boivin G *et al.,* 2002). This proposal is factual in our studies because the bone remodeling was earlier in HASi+C and HASi+CP groups, where the mineralization was also far in advance.

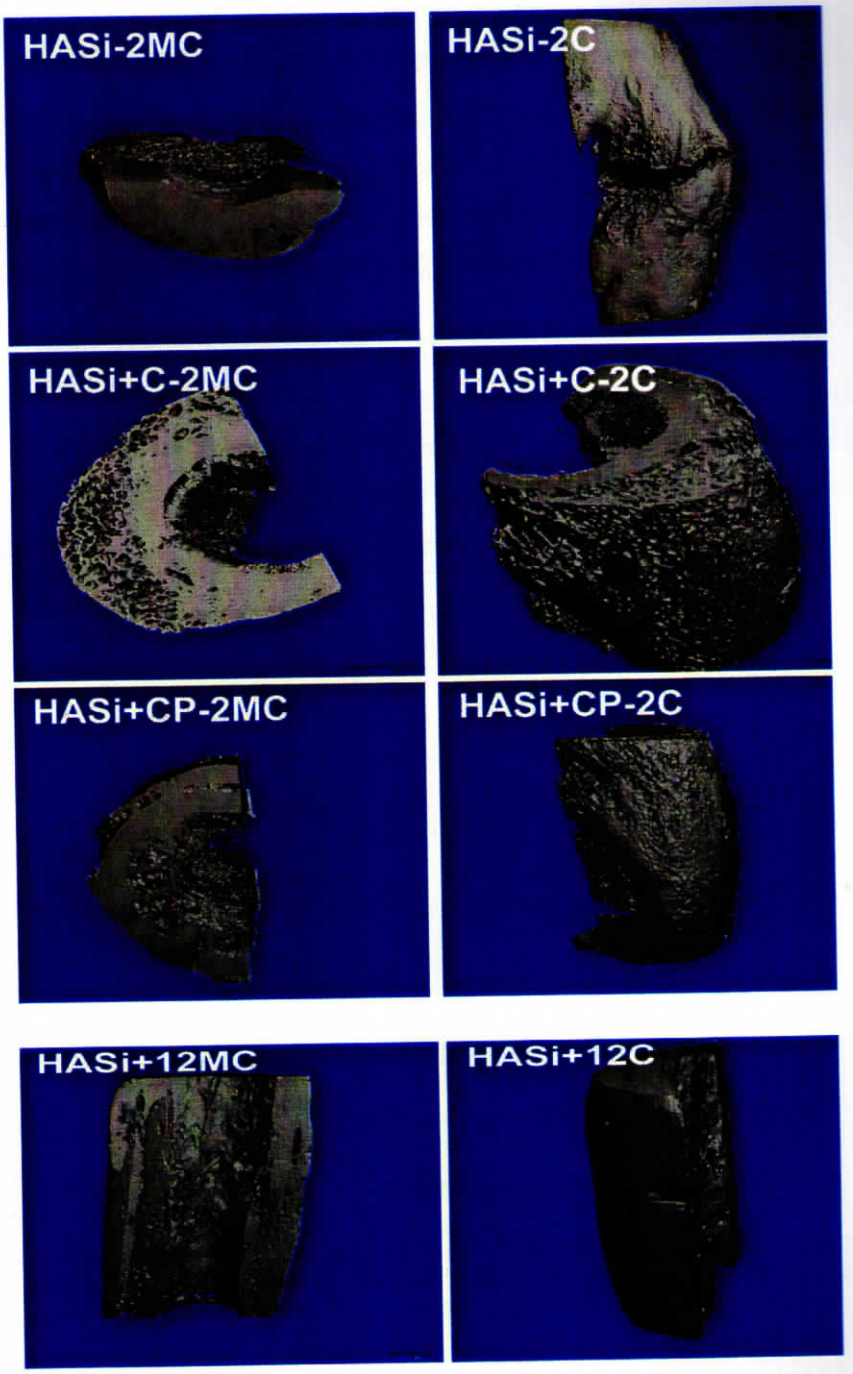

Figure 5.24. Micro-computed tomographs showing new bone formation and its mineralization in segmental defect. 2 months and 12 months post-implantation. The frontal side (towards the medullary canal) (MC) and the back side (towards the cortical region) (C) is represented here.

5.3.2.8 Characterization of HASi post implantation

All the studies demonstrated a progressive degradation of HASi from the defect site. So it is necessary to characterize the material in order to know the fate of material after implantation. The material that remained in the mid region of defect site in bare HASi groups at 2 months was collected and analyzed for XRD and FTIR.

5.3.2.8.1 X-ray diffraction technique

XRD revealed that the major phase of material that remained in the defect site was HA. Moreover, there were no peaks for calcium silicate and TCP, which were present in raw HASi. The XRD spectra were broad and less intense when compared to raw HASi, related to less crystallinity of the material (Fig. 5.25).

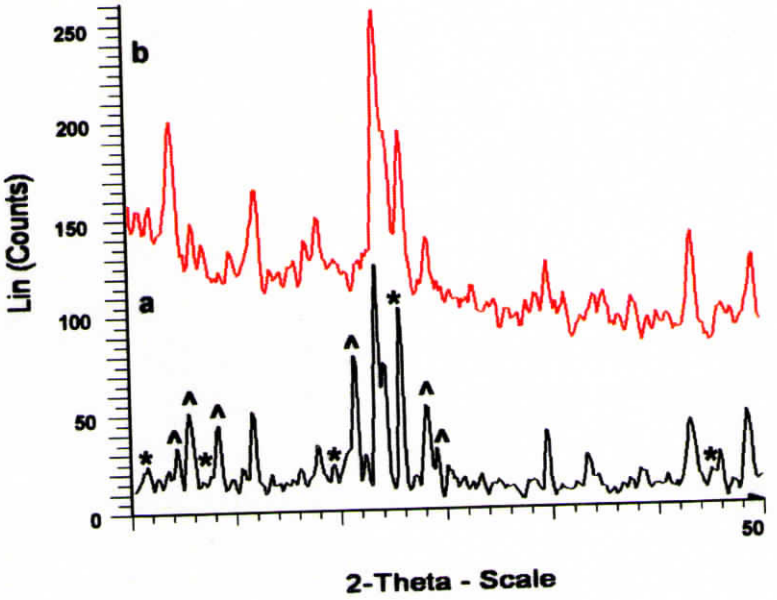

Figure 5.25. X-ray diffraction pattern of HASi remained in the defect site 2 months post-implantation (a) Raw HASi (before implantation) (b) HASi 2 months post-implantation. * shows calcium silicate and ^ shows TCP phase.

5.3.2.8.2 Fourier Transform Infrared spectroscopy

FTIR spectra showed the characteristic OH^- band at 3570 cm^{-1} and PO_4^{3-} bands at 1051 cm^{-1} and 961 cm^{-1}, confirming that the material remained in the defect site was HA. The intensity of phosphate peak at 961 cm^{-1} was comparatively less than raw HASi. In addition, a peak associated with CO_2^{3-} vibration mode (1652 cm^{-1} and 871

cm^{-1}) appeared, which was not present in raw HASi (Fig. 5.26).

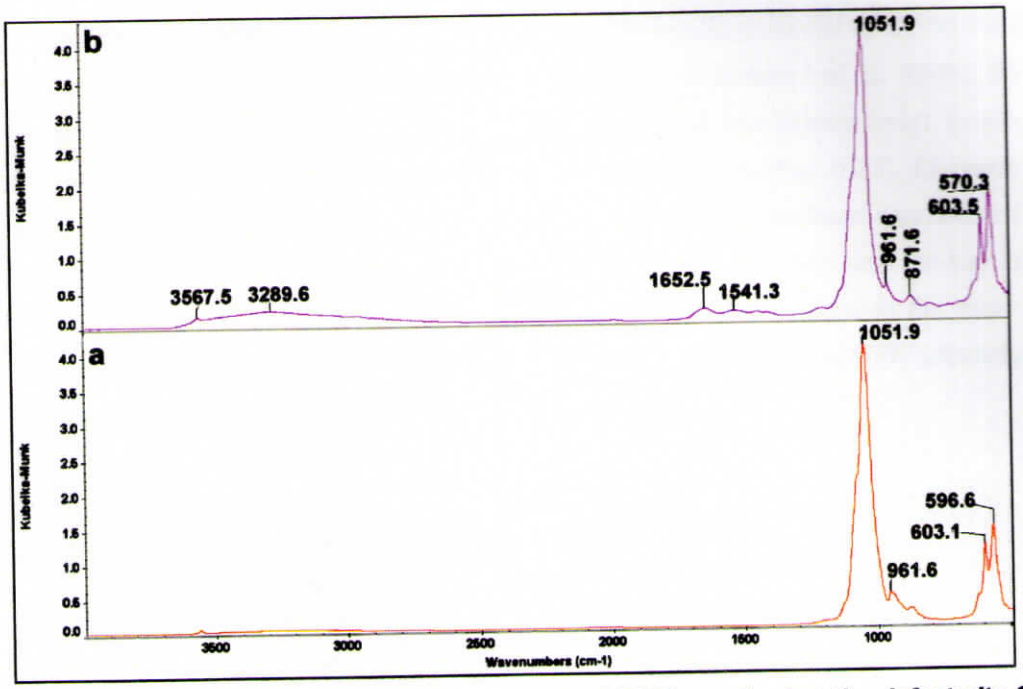

Figure 5.26. Fourier Transform Infrared spectra of HASi remained at the defect site 2 months post-implantation. a) Raw HASi (before implantation) (b) HASi 2 months post-implantation.

These studies depicted that TCP and calcium silicate present in the outer coating layer of raw HASi disappeared and the material remained in the defect site is a carbonate substituted HA. The carbonate groups may have substituted at the site of phosphate groups of raw HASi, which can be correlated with less intense phosphate band (961 cm^{-1}) following implantation. It is reported that the bone mineral exhibits calcium, phosphate and hydroxyl deficiency, internal crystal disorder and contains various cationic and anionic constituents, principally carbonate (up to 8 wt%) making it more like an A-B type carbonate-substituted apatite (Boskey A *et al.*, 2007; Elliot JC 1994). XRD showed a transient amorphous phase that seems to be an essential step because the formation of calcium apatite in bone is preceded by a transient amorphous phase (Pek`ounov Y *et al.*, 2008). Thus it is interpreted that the physico-chemical characteristics of HASi is changing slowly following implantation, making it more similar to bone apatite.

5.3.2.9 Distribution of Si in principal organs

Besides the positive impact, the inflammatory and fibrogenic potential of Si followed by exposure at high dose has been reported in rat lungs (Lemaire I *et al.*, 1989). So the accumulation of Si, if any, in different organs of the body like kidney, heart, lymph node, liver, spleen and lung was determined by ICP analysis (Fig. 5.27). All these organs showed ppm levels of Si at 2 months, except heart whose level was too low to be detected. At 4 and 6 months, the level of Si in kidney and lungs was too low to detect. ICP analysis confirmed that Si has not accumulated anywhere in the body, which may be excreted as metabolic waste. Si was found to leave the body primarily through the urine at an average rate of 1.8 mg / day (Lai W *et al.*, 2005).

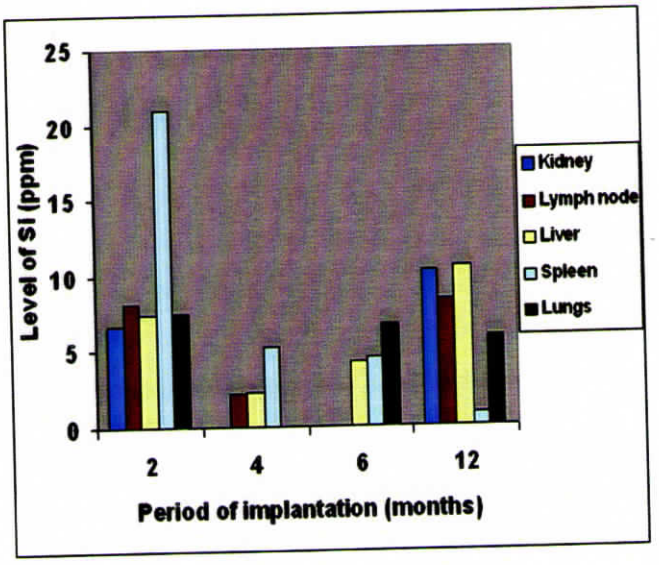

Figure 5.27. Inductively coupled plasma spectroscopic analysis of the distribution of Si in different organs of goat model.

All our orthotopic experiments revealed that HASi is osteoconductive, osteointegrative and degradative in nature during the repair of segmental defect in the femur of goat model and the process was enhanced with the supplementation of gOS+ cells and PRP. HASi was replaced by natural bone during the course of the implantation period which may be owed to its (1) highly interconnected porous structure and (2) chemical composition (silica).

Generally, biomaterials having pore size above 100 μm are required for bone repair that facilitate the ingrowth of cells and blood capillaries (Hench LL *et al.*, 1993).

Pioneering studies showed that pore size less than 15 – 50 µm result in fibrovascular ingrowth, pore size of 50 -150 µm encourage osteoid formation and pore size greater than 150 µm encourage the ingrowth of mineralized bone (Petite H *et al.,* 2000). To be specific, better bone ingrowth (osteoconduction) was observed in bioceramics with larger pore size ranging between 200 µm and 400 µm in diameter as a result blood vessel formation (Hiu-Yan Y *et al.,* 2005). The bone regeneration study in segmental defect in rat femur showed that polycaprolactone-TCP scaffolds with a pore size of 400 – 600 µm and porosity of 70% allowed the infiltration of blood vessels and new bone formation deep within and on the outer surface of the material (Rai B *et al.,* 2007). The pore interconnectivity is another important criterion that can offer intercellular communication among osteogenic cells inside the bioceramics by improving the fluid flow and nutrient supply (Bignon A *et al.,* 2003). In addition, the porous material improves mechanical interlocking between the implant and the surrounding natural bone (bone ingrowth), thereby providing greater mechanical stability at the critical interface (Karageorgiou V *et al.,* 2005). The highly interconnected porous structure (50 - 500 µm) of HASi is a positive factor that permit the ingrowth of cells and blood vessels, leading to enhanced bone regeneration. Apart from porosity, the chemical composition of materials, particularly the presence of silica, has a beneficial role to enhance the bone repair (Hing K *et al.,* 2006). It plays a critical role in the development and structural integrity of connective tissue (Seaborn CD *et al.,* 2002). The role of silica has been implicated in the hydroxylation of proline intracellularily during collagen synthesis, in forming cross links at hydroxylysine / lysine sites (Reiser KM *et al.,* 1986) and in stabilizing the glycosaminoglycan network (Schwarz K 1973).

The second focus of our study was related to the degradation of HASi with time. Generally the mechanism of bioceramic degradation is known to involve two kinds of processes: solution-mediated degradation and cell-mediated degradation (Jarcho M 1981) and whatever the mechanism, appropriate porosity and chemical composition of the material has an important role. It is reported that the rate of degradation depends on implant microporosity (de Groot 1980). The dense material without macro or micro pores rarely showed any degradation (Kotani S *et al.,* 1991). In addition to porosity, the silica content of HASi has also played a major role to undergo degradation (Hing KA *et al.,* 2005). The osteoclast response to carbonate-

substituted and stoichiometric HA demonstrated that the osteoclast attachment and activity were sensitive to surface energy (Redey SA *et al.,* 1999). Measurement of the point of zero charge (PZC) and zeta potential have shown that the surface charge on silicate-substituted apatite was more electronegative than stoichiometric HA with its near neutral PZC of 7.3 ± 0.1 (Harding IS *et al.,* 2005; Botelho CM *et al.,* 2002), which is responsible for increased osteoclast activity when exposed to silica-based biomaterials. *In vitro* experiments with aqueous Si derived from Si-TCP materials showed a dose dependent effect of Si on osteoblast and osteoclast cells (Pietak AM *et al.,* 2007). Another study reported that the progressive resorption of silicon-stabilized TCP ceramics was mediated through phagocytosis by macrophages and osteoclast activity (Mastrogiacomo M *et al.,* 2006a).

The process of bone formation, mineralisation and material degradation was enhanced and faster in HASi+C and HASi+CP groups due to the promotive effect of osteoconductive and osteoinductive stimuli The performance of three groups in terms of new bone formation and material degradation, particularly in the mid region of the defect can be compared as:

At 2 months, cellular ingrowth + bulk of material in bare HASi groups = mineralized woven bone + few remnants of material in HASi+C groups = mineralized woven bone + few remnants of material in HASi+CP groups.

At 4 months, mineralized woven bone in bare HASi groups + few remnants of material = mineralized lamellar bone + very few remnants of material in HASi+C groups = mineralized lamellar bone + very few remnants of material in HASi+CP groups

Thus what ever the qualities that have attained in tissue-engineered groups at 2 months was achievable only at 4 months in bare HASi groups.

Previous studies demonstrated that the application of MSCs combined with synthetic materials allowed complete closure of defect and stimulated the vascularisation process when compared to material alone (Schantz JT *et al.,* 2003; Bruder SP *et al.,* 1998b; Zhu L *et al.,* 2006). The outcome in these studies was better because culturing of OS+ cells on the scaffold prior to implantation minimize the necessity for the migration and expansion of indigenous osteoprogenitors. The cells could

efficiently proliferate and produce their own matrix on the scaffold that can decrease the *in situ* interval between implantation and their biosynthetic activity. These cells can also secrete inductive factors that recruit new MSCs into osteogenic lineage and produce mature bone matrix quickly (Xie H *et al.,* 2007). Moreover, these cells are the targets for endogenous osteoinductive molecules such as BMPs, which are released during normal bone healing. Thus the combined contributions of cells on the scaffolds and host-derived MSCs and biomolecules can advance osteogenesis in the defect site. Goshima J *et al.,* (1991b) reported that the bone formation in ceramic grafts is a biphasic phenomenon with the initial bone formation being of "donor origin". When this donor-derived bone has partially filled the pores of the ceramics, host-derived cells begin remodeling the donor bone, thus beginning the second phase or "host-derived" bone formation.

Many studies demonstrated that the formation of bone is directly related to the number of BMSCs seeded on the scaffold. Bruder *et al.,* 1998 suggested that excessively high concentrations of BMSCs are disadvantageous in their adherence to scaffold. Herein, 1 x 10^5 cells / cm^2 of scaffold was chosen as the seeding concentration and our *in vitro* studies proved that the cells spread and deposit ECM in this concentration. Apart from cell number, the *in vitro* culture period of tissue-engineered constructs also influences their ability to regenerate bone when implanted in segmental defects. One study reported that sintered titanium fiber meshes seeded with cells that have been cultured in osteogenic media for 4 days revealed the highest bone formation when implanted in cranial defect of Fisher rats and lowest bone formation was obtained when it was cultured for 16 days *in vitro* (Castano-Izquierdo H *et al.,* 2007). In this study, we have cultured gOS+ cells on HASi for 7 days, which was able to enhance bone formation in segmental defect.

A problem encountered while using tissue-engineered constructs for large segmental defects is the impaired cell survival following implantation (Rose FR *et al.,* 2002) and the potential reason is delayed revascularization (Kruyt MC *et al.,* 2003). The acceptable distance for diffusion of oxygen and nutrients, which is indispensable for cell survival and maintenance of their biological functions, is limited to a depth of 300 µm (Kruyt MC *et al.,* 2004a; Kruyt MC *et al.,* 2004b; Muschler GF *et al.,* 2004). The large size of clinically applied bone grafts exceeds this size (300 µm), result in hypoxia. Herein, the faster and superior performance with tissue-engineered groups

demonstrated that OS+ cells cultured on HASi have survived satisfactorily on these scaffolds and contributed towards new bone formation.

Similar to bone regeneration, the material resorption was also superior in HASi+C and HASi+CP groups, mainly mediated through osteoclast cells. Several hypothesis can be proposed to exploit the role of OS+ cells in facilitating the degradation of material. One suggestion is that these cells may stimulate host-derived cells by expressing or releasing biological factors. For example, osteoblasts express a membrane-associated factor called receptor activator of nuclear factor-κB ligand (RANKL), which binds to RANK, a receptor located on osteoclast membrane. The interaction of RANKL-RANK initiates a cascade of events resulting in the activation and differentiation of osteoclast cells (Katagiri T *et al.,* 2002).

Second hypothesis is that OS+ cells cultured on HASi create an ECM that can favor the successive migration of osteoclasts. Among many ECM proteins, osteopontin has an important role in promoting the adhesion of osteoclasts to the scaffold surface through their arginine-glycine-aspartic acid sequence (Mastrogiacomo M *et al.,* 2006a). Osteopontin is an acidic protein, which exhibits several conserved elements including a stretch of 7 to 9 Asp or Glu residues that represent calcium or HA binding site and RGD cell adhesion site (Gilbert M *et al.,* 2000). Our *in vitro* studies with RT-PCR and flow cytometry showed that the expression of osteopontin was significantly enhanced on HASi than HA. Thus the combined effects of the characteristics of material (porosity and silica content) and the ability of OS+ cells to attract osteoclasts have improved cell-mediated resorption in HASi+C and HASi+CP groups.

Quantitatively, there were no significant difference between HASi+C and HASi+CP groups in bone regeneration and material degradation. Still, HASi+CP groups showed a slightly better and quicker response where the delivery of PRP to the defect site could release numerous growth factors into the immediate local environment. The life span of a platelet and the period of direct influence of its growth factors are less than 5 days in an *in vivo* situation (Marx RE *et al.,* 1998). After the initial burst of growth factors, these platelets synthesize and secrete additional growth factors for the remaining days of their life span to stimulate the proliferation and differentiation of stem cells in the defect site.

An important parameter for the performance of PRP is the method of its preparation, since this can significantly influence the concentration of platelets and growth factors and consequently their osteogenic capacity (Weibrich G *et al.,* 2003). A platelet count of 1000 x 10^6 / mL measured in a volume of 5 mL plasma is considered as the "therapeutic dose" of PRP (Landesberg R *et al.,* 2000; van den Dolder J *et al.,* 2006). Platelet concentration of less than 1000 x 10^6 / mL were not reliable to enhance wound healing, whereas higher concentrations also did not show any further enhancement of wound healing (Marx RE *et al.,* 2001). In this study, about 9 mL of PRP having a count of 600 x10^6 / mL platelets was added so that a therapeutic dose (5400 x 10^6 / 9 mL) can be expected at the defect site

Some reports showed that PRP did not influence bone healing (Choi BH *et al.,* 2004; Roldán JC *et al.,* 2004; Mooren RE *et al.,* 2007). In general, it is said that PRP does not have any strong osteogenic effect so that filling a defect with PRP alone will not allow osteogenesis to occur. At the same time, PRP has an osseopromotive effect and can enhance bone regeneration in the presence of osteogenic precursor cells by encouraging their proliferation and differentiation (Schlegel KA *et al.,* 2004). Additionally, MSCs associated with PRP are potent angiogenic inducers proven to release VEGF leading to faster bone regeneration and remodeling (Yamada Y *et al.,* 2004; Lucarelli E *et al.,* 2005). Kitoh *et al.,* (2004 and 2007) observed that transplantation of bone marrow cells and PRP shortened treatment period and reduced associated complications by accelerating new bone formation in distraction osteogeneis. Reducing the time needed for optimal bone and soft tissue regeneration will have major impact since it reduce treatment time and costs, accelerate patient's recovery time-period and improve patient's life quality.

Generally PRP is applied as gel by combining with calcium chloride and bovine thrombin. Recently some studies have reported the negative effect of PRP gel when compared to PRP liquid. An explanation projected is that PRP gel has a viscous jelly-like consistency, which can result in additional pressure on the drill walls of already tightly fitted implant. This might cause an additional trauma during its installation and as a result, the healing process at bone-implant interface might become disturbed (Nikolidakis D *et al.,* 2006). Significantly more interfacial bone-to-implant contact was attained while using PRP in liquid form than in the form of gels (Nikolidakis D *et al.,* 2006). A study by Zechner *et al.,* in 2003 in a mini pig model failed to show any

statistically significant effect of PRP gel on peri-implant bone formation after 6 weeks healing period. In another study, Weibrich *et al.,* (2004) analyzed the influence of PRP gel on bone regeneration around self tapping titanium screw implants inserted in the femoral bone of rabbits. After 4 weeks healing period, no advantageous effect on bone-implant contact rate was seen. Based on these reports and *in vitro* studies with PRP (HASi can activate platelets in the absence of triggering agents), herein we have focused on the delivery of PRP liquid rather than going for PRP gel with calcium chloride and thrombin.

It is difficult to compare the results that we have obtained with previous results particularly, the rate of bone formation and material degradation and the time required for the healing of bone. This is because the results may vary significantly with respect to animal model (dog, sheep, goat); treated bone (femur, tibia, mandible); chemical composition; geometry and resorbability of the biomaterial used. Therefore herein, a comparison was made with the current treatment methods for the repair of segmental defect like distraction osteogenesis and autograft (DeCoster TA *et al.,* 2004). In distraction osteogenesis, after a 5 days latent period, the segment produced by osteotomy of the metaphysis can be transported approximately 1 mm per day to eliminate the diaphyseal segmental bone defect. Two to three days of consolidation are required for each day of distraction. Thus for a 2 cm segmental defect, approximately 65 – 70 days (two and half months) are required to achieve union as per theoretical calculation. Similarly with autograft, approximately 1.5 months are needed for every centimeter of defect in addition to the usual time for the fracture to heal (about 1.6 months). Thus about 3 months are needed for the treatment of a 2 cm segmental defect. Based on these, it can be concluded that repairing segmental defect with HASi+C and HASi+CP was superior (union and bone regeneration achieved in 2 months) to the treatment offered by distraction osteogenesis and autografts. The performance of bare HASi groups was little bit slower (union achieved in 2 months, but complete bone regeneration at 4 months) when compared to these treatment methods.

CHAPTER 6

SUMMARY AND CONCLUSION

6.1 Restatement of the problem

The segmental bone defect caused by tumor resection, trauma and skeletal abnormalities like osteomyelitis is still a major problem in orthopaedics due to the lack of predictability in attaining functional bone after the treatment (Ip WY 2002). Autografts, either vascularised or nonvascularised is the preferred treatment approach, but is related with complications such as infections or nonunion, especially in larger shaft reconstructions. Furthermore, harvesting of healthy tissue can result in donor site morbidity. Allografts as the second option face problems like disease transmission and graft immune rejection. Distraction osteogenesis or bone transportation method relies on the bone regeneration potential, thus avoiding concerns related to graft integration, but it is often associated with problems like high chance of traction injury to nerves and soft tissues and long term hospitalization (Green SA *et al.,* 1992).

An ideal bone substitute would approximate an autograft, in being biocompatible; osteoconductive; osteogenic and osteoinductive, to enhance bone repair. Bone tissue engineering has the potential to become an alternative to autografts, which involves the association of cells or growth factors with a natural or synthetic porous biomaterial (scaffold) to produce a three-dimensional living, implantable construct (Langer R *et al.,* 1993). The selection of the biomaterial component is a critical step that determines the ultimate success of the engineered graft. The scaffold must provide an appropriate environment (porosity, chemical composition, surface topography, degradation etc.) for the attachment, proliferation and function of cells. It should have an appropriate interconnected pore network to facilitate the ingrowth of vascular tissue that nourishes the cells implanted within the tissue-engineered construct or that invaded from local host environment. Finally it should be

biodegradable and tissue regeneration should be in par with material degradation (Ishaug SL *et al.,* 1997).

Bioactive calcium-phosphate ceramics have proven to be of great interest in bone tissue engineering applications because of their osteoconductivity and the ability to integrate with bone tissue. Among these, HA has shown the most promising results due to their osteoconductive properties, unlimited availability and absence of immune response. However, low degradation rate of HA may prevent the proper remodeling of newly formed bone, resulting in significant reduction in its strength. One promising way to cope with this problem is to modify the chemical composition of HA. The incorporation of silicate ions into phase pure HA has been shown to have the potential to increase the rate of bone apposition and material degradation (Mastrogiacomo M *et al.,* 2007). In addition, a link between Si and connective tissue health has been proposed, suggesting a manifold role of Si in bone healing through direct physiological action on vascularisation, bone metabolism, and bone quality (matrix organization and mineralization) (Hing KA *et al.*, 2006). Thus it was hypothesized that the combination of silica and HA may enhance the bone ingrowth within the scaffold in par with material degradation.

As classified, the first approach of tissue engineering is to repair bone defects using osteoconductive scaffolds alone. But this grafting procedure remains a challenge in the treatment of large bone defects where the bone regeneration depends solely on the migration and proliferation of indigenous cells into the scaffold. A second approach is to culture osteogenic cells on the scaffold *in vitro* so that a living construct with cellular ingrowth and ECM can be implanted. There are such reports of a number of cell sources potentially suitable for bone repair in association with porous ceramics scaffolds (Maniatopoulos C *et al.,*1988; Bruder SP *et al.,* 1998a). The most desirable source would be to obtain osteoblast precursor cells or MSCs from bone marrow. BMSCs grown *in vitro* are capable of self-renewal for many passages without any significant loss of their characteristics (Pittenger MF *et al.,* 1999). They can be induced to differentiate into osteoblasts by providing biochemical supplements (dexamethasone, L-ascorbic acid and β glycerophosphate) in defined concentrations in their external milieu (Jaiswal N *et al.,* 1997). If these cells are of autogenous origin, there would be no risk of immune rejection or pathogen transfer.

The third approach in tissue engineering is the sustained delivery of multiple growth factors, which closely mimics the natural regenerative processes. PRP serves as a potential source of growth factors like PDGF, TGF-β, IGF, VEGF etc. Activation of platelets will result in the release of these factors into the immediate local environment and has favourable effect on bone healing. Several studies highlight the merits of the use of PRP in vascularisation, safety and cost effectiveness. Furthermore, PRP can easily be obtained on the day of surgery by a simple centrifugation method from autogenous blood (Anitua E *et al.,* 2007).

The objective of this study was to propose a novel 3D biomaterial for the repair of segmental defects. An indigenous porous bioactive ceramic, silica coated HA (HASi) was selected and characterized as the material of choice. Tissue-engineered constructs were fabricated using these materials in combination with BMSCs / OS+ cells and PRP. The focus was on assuring the cytocompatibility and functionality of cells on the materials *in vitro* followed by their ability to facilitate vascularisation, osteoconduction, osteoinduction and osteointegration *in vivo*.

6.2 Description of procedures

The whole study was divided into three phases.

The objective of first phase was to evaluate the physicochemical characteristics of bioactive ceramics like Hydroxyapatite (HA) and Triphasic ceramic coated hydroxyapatite (HASi), which was gifted by Bioceramics Laboratory, SCTIMST. HA powder was synthesized by wet precipitation method, mixed with binder and sintered at high temperature to get porous ceramics. For synthesizing HASi, HA blocks prepared by the above process were dipped in silica sol for 1 min (sol gel method) and sintered at 1200°C. The coating of silica (15 - 17 mass%) over HA was confirmed by ESEM-EDS. The phase composition and functional groups on the materials were determined by XRD and FT-IR respectively. The porosity of HA and HASi was assessed by SEM and mercury intrusion technique. The compressive strength of the materials was evaluated by Universal testing machine. The degradation of HA and HASi was determined *in vitro* as per ISO standard 10993 – 13. For this, the materials were immersed in PBS for 60 days and analyzed for any change in phase composition and functional groups. The cytotoxicity and cytocompatibility of HA and HASi was assessed using L929 mouse fibroblast cell

lines and HOS cell lines respectively.

The objective of second phase was to evalute tissue-engineered constructs *in vitro* - platelet-rich plasma / fibrin glue coated and uncoated bioactive ceramics in conjunction with BMSCs. HA and HASi were polished in the form of discs of 5 mm diameter and 5 mm thickness for fabricating tissue-engineered constructs *in vitro*. In the first part of experiments, BMSCs and OS+ cells of goat and human origin were cultured separately on HA and HASi. In the second part of experiments, HA and HASi was coated with PRP and FG separately and cultured with gOS+ cells. The mesenchymal origin of stem cells isolated from bone marrow was determined through markers like vimentin, CD34, CD44 and also through their ability to differentiate into osteoblasts. The proliferation (trypan blue staining) and osteogenic differentiation (ALP activity) potential of gBMSCs in different passages were studied in order to choose suitable cells for tissue-engineered constructs. The cellular responses in these constructs (PRP / FG coated and uncoated HA and HASi) were evaluated in terms of adhesion (SEM); viability (acridine orange / ethidium bromide staining by cLSM and flow cytometry and by LDH assay); proliferation (PCNA staining by flow cytometry and picogreen assay); morphology (SEM); in depth migration of cells towards the centre of the materials (Stevenal's blue / van Gieson's picrofuchsin staining; and acridine orange / ethidium bromide staining by cLSM); Cell cycle analysis (propidium iodide staining by flow cytometry) and differentiation of BMSCs into osteogenic lineage (ALP activity – biochemical assay and ELF-97 staining by cLSM; osteocalcin measurement – ELISA; expression of osteopontin by flow cytometry and cLSM; real-time PCR analysis of the expression of ALP, osteopontin, osteocalcin, bone sialoprotein II).

The objective of third phase was to evaluate tissue-engineered bioactive ceramics *in vivo* - extraskeletal and orthotopic implantation. Care and management of animals were conducted as per the guidelines of IAEC and CPCSEA. In the first part of experiments, the tissue-engineered constructs in comparison with bare materials (without cells) were validated at an extraskeletal site (muscle) in rat model. The tissue-engineered constructs were fabricated by culturing rBMSCs and rOS+ cells separately on HA and HASi for 7 days. Twenty four wistar rats with an average body weight of 200 – 300g with one defect per leg were divided into six groups for implantation (Group I: bare HASi; Group II: rBMSCs cultured HASi; Group III: rOS+

cells cultured HASi; Group IV: bare HA; Group V: rBMSCs cultured HA; Group VI: rOS+ cells cultured HA, which were implanted deep into the muscle. The neo-vascularisation (Group I, III, IV and VI) after two and four weeks of implantation was determined through H & E staining. The neo-osteogenesis after four weeks of implantation (six groups) was evaluated through histology (Stevenal's blue and van Gieson's picrofuchsin staining); histomorphometry (Quips programme of Leica DM 6000); ALP activity (EL-97 staining by fluorescent microscopy) and mineralization studies (density distribution graph of micro-CT).

In the second part of experiments, the progress of bone regeneration and material resorption in segmental defects (2 cm) created in the femur of goat model was validated using tissue-engineered constructs in comparison with bare materials (without cells or PRP). Eighteen adult goats with an average body weight of 20 – 30 kg with one defect per animal were divided into three groups for implantation. Group I: Bare HASi (HASi group); Group II: gOS+ cells cultured HASi (HASi+C group); Group III: gOS+ cells cultured HASi together with the delivery of PRP to the defect site (HASi+CP groups). Three groups were compared at 2 and 4 months, while the performance of bare HASi groups was evaluated for 6 and 12 months. The retrieved tissues were assessed through gross view (Nikon D70S); radiography (image intensifier); histology (Stevenal's blue and van Gieson's picrofuchsin staining); morphology (SEM) and histomorphometry. The serum was separated from the blood of post-implanted goats and measured for ALP activity and TRAP activity. The mineralization of newly formed bone was confirmed through EDS, CT and micro-CT. The phase composition and functional groups of 2 months post-implanted HASi was analyzed by XRD and FT-IR respectively. The accumulation of Si in different organs of the implanted goats (kidney, lymph node, liver, heart, spleen and lungs) was determined through ICP analysis.

6.3 Major Findings

HASi was synthesized with the hypothesis that the main core of material remains as HA while silicon ions will incorporate only as an outer coating layer so that the dual properties of HA (osteoconduction, osteointegration) and silica (osteoconduction, osteointegration and degradation) can be utilized in one product. As per the hypothesis, the core of HASi was polycrystalline while the outer coated layer was

porous and less crystalline due to Si rich liquid phase formation. SiO_2 (15-17 mass%) was restricted on the surface as a coating layer and has not penetrated into the core of HASi. The only phase of HA was hydroxyapatite while in HASi, apart from hydroxyapatite as the main or core phase, the outer coated layer showed peaks for calcium silicate and TCP phases. SEM and mercury intrusion technique depicted the interconnected porous nature of HA and HASi and pore size in the range of 50 – 500 µm. HASi was degradative when compared to HA when immersed in PBS for 60 days. With cell lines after 48 h in culture, HA and HASi proved to be non-cytotoxic and cytocompatible.

The stem cells isolated from the bone marrow of goat model were of mesenchymal origin and have the ability to differentiate into osteoblasts by providing osteogenic supplements. The proliferation and osteogenic differentiation potential of gBMSCs from passages 2 to 5 was almost similar and selected for further tissue engineering applications. Studies with HA and HASi in combination with goat / human BMSCs and OS+ cells depicted HASi as a better substrate than HA for enhancing cellular activities, with their first choice for OS+ cells than BMSCs. HASi was capable of inducing cell proliferation while undergoing osteogenic maturation and mineralization, but on HA, the cell proliferation declined as the cells enter into differentiation lineage. Studies with PRP showed that HA and HASi can activate platelets with out the addition of any triggering factors. When HA and HASi was coated with PRP or FG, the cellular viability, growth and spreading was improved. The viability and proliferation of gOS+ cells on uncoated HASi was significantly greater than PRP and FG coated HA at a later culture period of day 21 and 28. Cell cycle studies showed that the cells in replicative phase were more and the cells in apoptotic phase were less on PRP / FG coated materials. The osteopontin and osteocalcin expression was significantly enhanced on PRP and FG coated HA and HASi, but PRP had neither effect on ALP expression nor ALP activity. In all the studies, HASi was better than HA both in uncoated and PRP / FG coated groups and the best performance was displayed by FG coated HASi. Eventhough the signal generated by FG was more encouraging to cells than PRP, a few attractive features like ease of availability and cost effectiveness prompted the use of PRP for orthotopic implantation studies.

H & E staining depicted neo-vascularisation in muscle implanted with bare HA and HASi and the process was improved when rOS+ cells cultured materials were

implanted. The neo-vascularisation was significantly enhanced in bare and tissue-engineered HASi groups as compared to HA. In addition, rOS+ cells cultured HASi could induce the bone formation in muscle while on HA, the osteoblast-like cells were seen within and around the pore of materials without depositing much osteoid matrix. Since osteoinductive property was shown only by HASi cultured with OS+ cells group, further orthotopic implantation studies were done only with HASi groups.

Orthotopic implantation studies showed that HASi was able to regenerate bone in segmental defect in the femur of goat model and has undergone degradation. The process was enhanced in combination with cells and PRP. The new bone formation, organization and mineralisation was similar and advanced in the peripheral region of defect in all the three groups. However in the mid region of defect, the new bone formation and mineralisation was faster and enhanced in HASi+C and HASi+CP groups than bare HASi groups and best performance was shown by HASi+CP groups. Si has not accumulated in the principal organs of goat model. HASi was degradative in nature, mainly through cell-mediated mechanism, which was apparent and superior in HASi+C and HASi+CP groups.

6.4 Conclusions

- ✓ The coating of silica over HA is noteworthy in facilitating solution-mediated degradation of HASi when compared to HA.
- ✓ The growth and osteogenic differentiation potential of gBMSCs decreased after passage 5, signifying the importance of the selection of cells in correct passage for bone tissue engineering applications.
- ✓ The cellular activities (rat, goat and human cells), mainly OS+ cells, were significantly enhanced on HASi than HA, showing the influence of surface chemistry on osteoblast behaviour.
- ✓ The interconnected porous structure and chemical composition of HASi was suitable in facilitating the migration and distribution of cells towards the internal voids of material, which is a major limitation in many static culture systems.

- ✓ The ability of HASi to maintain cell proliferation and osteogenic differentiation in a parallel relationship indicate that the ultimate fortune of cells is determined by the respective matrix / substratum.

- ✓ The response of goat and human cells in terms of viability, morphology and proliferation was almost same on HA and HASi, implying the comparability between these two species for *in vivo* studies.

- ✓ The coating of PRP and FG on HA and HASi have significant positive effects on the performance of gOS+ cells, suggesting the possibility of using these combination products in bone tissue engineering applications.

- ✓ Bare HASi and Tissue-engineered HASi (with OS+ cells) could augment neo-vascularisation at an extraskeletal site in rat model as compared to HA. This indicate that the chemical composition and the internal porous architecture of HASi is favourable for the ingrowth of blood vessels.

- ✓ Tissue-engineered HASi (with OS+ cells) could induce bone formation at an extra skeletal site in rat model. The osteoinductive property has much relevance for augumenting the healing of large defects.

- ✓ HASi was able to regenerate and remodel bone in segmental defect (2 cm) in the femur of goat model without fibrous tissue formation and inflammation, owing to its osteoconductive and osteointegrative nature.

- ✓ The process of bone regeneration in segmental defect was faster and superior in tissue-engineered HASi groups (with OS+ cells and PRP). Reducing the time needed for bone regeneration and remodeling will have major impact since it reduce treatment time and costs and accelerate patient's quality of life, particularly geriatric patients.

- ✓ The delivery of PRP liquid directly to segemental defect site (without the addition of any triggering agents) could enhance healing in segmental defect, giving a hope for simulating similar simple procedures on clinical bed.

- ✓ An ideal material should have a proper balance between bone formation and degradability and at the same time remaining osteoconductive. As per the

rule, HASi degraded progressively at a rate proportionate with the formation of new bone, mainly through osteoclast-mediated mechanism. The process of degradation was advanced and faster in tissue-engineered groups.

6.5 Tissue-engineering approach in clinical practice – Case studies

The repair of massive bone defects in humans (4-8 cm) by means of implantation of a porous ceramic scaffold seeded with *in vitro* expanded autologous BMSCs has been reported (Quarto R *et al.,* 2001; Marcacci M *et al.,* 2007). Four patients with age ranging from 16 to 41 years were selected for this treatment after the failure of conventional surgical therapies. Complete fusion between the implant and the host bone occurred 5 – 7 months after surgery. A good integration of the implants was verified at the latest follow-up, which happened 6-7 years post surgery for two of the patients.

Distraction osteogenesis with contemporary transplantation of autologous BMSCs and PRP were performed in three femora and two tibia of two patients suffering from achondroplasia and one patient with congenital pseudoarthrosis of the tibia (Kitoh H *et al.,* 2004). Autologous cells and PRP were injected into the distracted callus. However, the contribution of the injected cells to the bone formation was difficult to evaluate due to the lack of a control group of patients (without cells / PRP injection).

The treatment of benign bone tumors in three patients using tissue-engineered HA ceramic scaffold has been reported (Morishita T *et al.,* 2006). *In vitro* expanded BMSCs obtained from each patient's bone marrow were induced to differentiate into osteoblasts and to secrete bone matrix on HA ceramic scaffolds. Immediate healing potential was found with no adverse reactions.

Gronthos S (2004) reported the reconstruction of a human mandible by bone-muscle-flap *in vivo* prefabrication technique in a 56 year old patient. A titanium mesh was chosen as the external scaffold, which was loaded with HA blocks coated with recombinant BMP-7 and BMSCs. The patient served as his own bioreactor as the scaffold was implanted into his latissimus dorsi muscle to allow for the growth of heterotopic bone and ingrowth of vessel from the thoracodorsal artery. After 7 weeks, the mandible replacement was transplanted along with the adjacent vessel

pedicle, into the mandibular defect. During the first 6 months, the patient reported a continuous improvement both in the quality of life and in self-confidence. Between 7 and 13 months, a fracture of the external titanium mesh scaffold, the patient's bad habits such as drinking and active smoking and a partial infection of the regenerated bone with oral flora partially compromised the initial good clinical results. Unfortunately, the patient died by a cardiac arrest 15 months after implantation of the mandible replacement.

The tissue-engineering approach in clinical cases showed successful outcome where it has been attempted (Cancedda R *et al.,* 2007). These studies established that even though a staggering array of biomaterials portrayed as "ideal" scaffolds in pre-clinical studies in the past 10 years, very few have reached clinical usefulness. Regardless of the source or type of biomaterials, i.e. natural or synthetic, they have to be biocompatible, ideally osteoinductive, osteoconductive and osteointegrative. These materials must provide cell anchorage sites, mechanical stability and structural guidance within an *in vivo* milieu; provide the interface to respond to physiological and biological changes and to remodel the ECM in order to integrate with the surrounding native tissues. In this study, we have successfully demonstrated that HASi can fulfill many of these requirements of prospective candidates for bone tissue engineering applications. However the ultimate success of any biomaterial can be judged only from the final good clinical results. In this context, the feasibility of tissue-engineered HASi will be investigated in 'Clinical Translational' studies in future.

6.6 Future investigations

Bone tissue engineering has the potential to become a real alternative to autologous bone grafts. But before this could be approved as a standard treatment, it is a dire necessity to solve many of the associated problems, which includes:

- With regard to the *in vitro* expansion of cells, the introduction of serum free media will certainly represent a big advantage over the potential risk of viral or bacterial infections associated with the use of fetal bovine serum.

- BMSCs can escape immuno rejection after their incorporation within the implant. But these immuno-modulatory properties are lost upon their

differentiation. So the dream of all orthopaedic surgeons is a cell product ready "off the shelf" to be used for bone regeneration in all patients.

- Several approaches to improve the oxygen and nutrient supply to tissue-engineered constructs will be further investigated. One approach is to stimulate blood vessel growth by supplementing angiogenic growth factors or co-culturing endothelial cells in tissue-engineered constructs. A second method is bone muscle-flap *in vivo* prefabrication technique, but the method may be uncomfortable for the patients.

- An alternative direction for bone tissue engineering is not to involve pre-operative use of stem cells and / or angiogenic factors, but uses appropriate scaffolds that attract and stimulate patient's own stem cells post-implantation.

- Biological issues specific to the person undergoing the reconstruction play a part in the success of bone regeneration. Host comorbidities such as diabetes, inflammatory arthritis or the presence of infection may have an effect on the process of incorporating the bone graft. So the bone regenerations studies in diseased models are critical which needs surveillance and understanding.

- Medical Regulatory laws for the application of tissue-engineered products in clinical situations must be implemented.

BIBLIOGRAPHY

Abdollahi K, Kumar PJ, Shepherd L, Patzakis MJ. Estimation of defect volume in segmental defects of the tibia and femur. J Trauma. **1999**; 46(3): 413-6.

Abiraman S, Varma HK, Umashankar PR, John A. Fibrin glue as an osteoinductive protein in a mouse model. Biomaterials **2002**; 23(14): 3023-31.

Albala DM. Fibrin sealants in clinical practice. Cardiovasc Surg. **2003**; 11 Suppl 1: 5-11.

Alving B, Alcorn K. How to Improve Transfusion Medicine A Treating Physician's Perspective. Arch Pathol Lab Med. **1999**; 123(6): 492-5.

Alving BM, Weinstein MJ, Finlayson JS, Menitove JE, Fratantoni JC. Fibrin sealant: summary of a conference on characteristics and clinical uses. Transfusion. **1995**; 35(9): 783-90.

Anitua E, Sánchez M, Nurden AT, Nurden P, Orive G, Andía I. New insights into and novel applications for platelet-rich fibrin therapies. Trends Biotechnol. **2006**; 24(5): 227-34.

Anitua E, Sánchez M, Orive g, Andía I. The potential impact of the preparation rich in growth factors (PRGF) in different medical fields. Biomaterials **2007**; 28(31): 4551-60.

Anselme K, Bigerelle M, Noel B, Dufresne E, Judas D, Iost A, Hardouin P. Qualitative and quantitative study of human osteoblast adhesion on materials with various surface roughness. J Biomed Mater Res. **2000**; 49(2): 155-66.

Anselme K. Osteoblast adhesion on biomaterials. Biomaterials **2000**; 21(7): 667-81.

Arinzeh TL, Peter SJ, Archambault MP, van den Bos C, Gordon S, Kraus K, Smith A, Kadiyala S. Allogeneic mesenchymal stem cells regenerate bone in a critical-sized canine segmental defect. J Bone Joint Surg Am. **2003**; 85-A(10): 1927-35.

Attias N, Lindsey RW. Case reports: management of large segmental tibial defects using a cylindrical mesh cage. Clin Orthop Relat Res. **2006**; 450: 259- 66.

Baddoo M, Hill K, Wilkinson R, Gaupp D, Hughes C, Kopen GC, Phinney DG. Characterization of mesenchymal stem cells isolated from murine bone marrow by negative selection. J Cell Biochem. **2003**; 89(6): 1235-49.

Balçik C, Tokdemir T, Senköylü A, Koç N, Timuçin M, Akin S, Korkusuz P, Korkusuz F. Early weight bearing of porous HA/TCP (60/40) ceramics in vivo: a longitudinal study in a segmental bone defect model of rabbit. Acta Biomater. **2007**; 3(6): 985-96.

Barrilleaux B, Phinney DG, Prockop DJ, O'Connor KC. Review: ex vivo engineering of living tissues with adult stem cells. Tissue Eng. **2006**; 12(11): 3007-19.

Beck GR Jr, Zerler B, Moran E. Phosphate is a specific signal for induction of

osteopontin gene expression. Proc Natl Acad Sci U S A **2000**; 97(15): 8352-7.

Bensaïd W, Triffitt JT, Blanchat C, Oudina K, Sedel L, Petite H. A biodegradable fibrin scaffold for mesenchymal stem cell transplantation. Biomaterials **2003**; 24(14): 2497-502.

Bielby RC, Boccaccini AR, Polak JM, Buttery LD. In vitro differentiation and in vivo mineralization of osteogenic cells derived from human embryonic stem cells. Tissue Eng. **2004**; 10(9-10): 1518-25.

Bignon A, Chouteau J, Chevalier J, Fantozzi G, Carret JP, Chavassieux P, Boivin G, Melin M, Hartmann D. Effect of micro- and macroporosity of bone substitutes on their mechanical properties and cellular response. J Mater Sci Mater Med. **2003**; 14(12): 1089-97.

Blokhuis TJ, Wippermann BW, den Boer FC, van Lingen A, Patka P, Bakker FC, Haarman HJ. Resorbable calcium phosphate particles as a carrier material for bone marrow in an ovine segmental defect. J Biomed Mater Res. **2000**; 51(3): 369-75.

Boivin G, Meunier PJ. Changes in bone remodeling rate influence the degree of mineralization of bone. Connect Tissue Res. **2002**; 43(2-3): 535-7.

Boivin G, Meunier PJ. The degree of mineralization of bone tissue measured by computerized quantitative contact microradiography. Calcif Tissue Int. **2000**; 70(6): 503-11.

Bonnevialle P, Cariven P, Bonnevialle N, Mansat P, Martinel V, Verhaeghe L, Mansat M. Segmental tibia fractures: a critical retrospective analysis of 49 cases. Rev Chir Orthop Reparatrice Appar Mot. **2003**; 89(5): 423-32.

Boskey A, Pleshko Camacho N. FT-IR imaging of native and tissue-engineered bone and cartilage. Biomaterials. **2007**; 28(15): 2465-78.

Botelho CM, Brooks RA, Spence G, McFarlane I, Lopes MA, Best SM, Santos JD, Rushton N, Bonfield W. Differentiation of mononuclear precursors into osteoclasts on the surface of Si-substituted hydroxyapatite. J Biomed Mater Res. A **2006**; 78(4): 709-20.

Botelho CM, Lopes MA, Gibson IR, Best SM, Santos JD. Structural analysis of Si-substituted hydroxyapatite: zeta potential and X-ray photoelectron spectroscopy. J Mater Sci Mater Med. **2002**; 13(12): 1123-7.

Boyan BD, Hummert TW, Dean DD, Schwart Z. Role of material surfaces in regulating bone and cartilage cell response. Biomaterials **1996**; 17(2):137-46.

Boyce T, Edwards J, Scarborough N. Allograft bone. The influence of processing on safety and performance. Orthop Clin North Am. **1999**; 30(4): 571-81.

Brodke D, Pedrozo HA, Kapur TA, Attawia M, Kraus KH, Holy CE, Kadiyala S, Bruder SP. Bone grafts prepared with selective cell retention technology heal canine segmental defects as effectively as autograft. J Orthop Res. **2006**; 24(5): 857-66.

Bruder SP, Jaiswal N, Haynesworth SE. Growth kinetics, self-renewal, and the osteogenic potential of purified human mesenchymal stem cells during extensive subcultivation and following cryopreservation. J Cell Biochem. **1997**; 64(2): 278-94.

Bruder SP, Jaiswal N, Ricalton NS, Mosca JD, Kraus KH, Kadiyala S. Mesenchymal stem cells in osteobiology and applied bone regeneration. Clin Orthop Relat Res. **1998a**; 355 Suppl: S247-56.

Bruder SP, Kraus KH, Goldberg VM, Kadiyala S. The effect of implants loaded with autologous mesenchymal stem cells on the healing of canine segmental bone defects. Bone Joint Surg Am. **1998b**; 80(7): 985-96.

Bruder SP, Kurth AA, Shea M, Hayes WC, Jaiswal N, Kadiyala S. Bone regeneration by implantation of purified, culture-expanded human mesenchymal stem cells. J Orthop Res. **1998c**; 16(2): 155-62.

Buckwalter JA, Glimcher MJ, Cooper RR, Recker R. Bone biology. I: Structure, blood supply, cells, matrix, and mineralization. Instr Course Lect. **1996**; 45: 371-86.

Busa WB, Nuccitelli R. Metabolic regulation via intracellular pH. Am J Physiol. **1984**; 246(4 Pt 2): R409-38.

Butler WT. Noncollagenous proteins of bone and dentin: a brief overview. In: Goldberg M, Boskey A, Robinson C, editors. Chemistry and biology of mineralized tissue. Rosemont, IL: AAOS, **2000**. p.137-41.

Calabresi PA, Fields NS, Maloni HW, Hanham A, Carlino J, Moore J, Levin MC, Dhib-Jalbut S, Tranquill LR, Austin H, McFarland HF, Racke MK. Phase 1 trial of transforming growth factor beta 2 in chronic progressive MS. Neurology. **1998**; 51(1): 289-92.

Camerson DA. The ultra structure of bone. In: Bourne GH, editor. The biochemistry and physiology of bone. Academic Press, New York, **1972**. p. 191-236.

Cancedda R, Giannoni P, Mastrogiacomo M. A tissue engineering approach to bone repair in large animal models and in clinical practice. Biomaterials **2007**; 28(29): 4240-50.

Caplan AI. Mesenchymal stem cells. J. Orthop Res. 1991; 9(5): 641-650.

Caplan AI. Mesenchymal Stem Cells: Cell based reconstructive therapy in orthopaedics. Tissue Eng. **2005**; 11(7-8): 1198-211.

Carlisle EM. Silicon: A Possible Factor in Bone Calcification. Science **1970**; 167(916): 279-80.

Carlisle EM. Biochemical and morphological changes associated with long bone abnormalities in silicon deficiency. J Nutr. **1980**; 110(5):1046-56.

Carlisle EM. Silicon: An Essential Element for the Chick. Science **1972**; 178(61): 619-21.

Cartmell S, Huynh K, Lin A, Nagaraja S, Guldberg R. Quantitative microcomputed tomography analysis of mineralization within three-dimensional scaffolds in vitro. J Biomed Mater Res. A **2004**; 69(1): 97-104.

Castano-Izquierdo H, Alvarez-Barreto J, van den Dolder J, Jansen JA, Mikos AG, Sikavitsas VI. Pre-culture period of mesenchymal stem cells in osteogenic media influences their in vivo bone forming potential. J Biomed Mater Res. A **2007**; 82(1): 129-38.

Catelas I, Sese N, Wu BM, Dunn JC, Helgerson S, Tawil B. Human mesenchymal stem cell proliferation and osteogenic differentiation in fibrin gels in vitro. Tissue Eng. **2006**; 12(8): 2385-96.

Cattaneo R, Catagni M, Johnson EE. The treatment of infected nonunions and segmental defects of the tibia by the methods of Ilizarov. Clin Orthop Relat Res. **1992**; 280: 143-52.

Centers for Disease Control and Prevention. Septic arthritis following anterior cruciate ligament reconstruction using tendon allografts-Florida and Louisiana, **2000**. MMWR Morb Mortal Wkly Rep. 2001; 50(48): 1081-3.

Centers for Disease Control and Prevention. Update: allograft-associated bacterial infections-United States, 2002. MMWR Morb Mortal Wkly Rep. **2002**; 51(10): 207-10.

Chai C, Ben-Nissan B. Source: International Ceramic Monographs. **1994**; 1(1): 79-85.

Chang DW, Weber KL. Use of a vascularized fibula bone flap and intercalary allograft for diaphyseal reconstruction after resection of primary extremity bone sarcomas. Plast Reconstr Surg. **2005**; 116(7): 1918-25.

Choi BH, Im CJ, Huh JY, Suh JJ, Lee SH. Effect of platelet-rich plasma on bone regeneration in autogenous bone graft. Int J Oral Maxillofac Surg. **2004**; 33(1): 56-9.

Choi BH, Zhu SJ, Kim BY, Huh JY, Lee, S. H., and Jung, J. H. Effect of platelet-rich plasma (PRP) concentration on the viability and proliferation of alveolar bone cells: an in vitro study. Int J Oral Maxillofac Surg. **2005**; 34(4): 420-4.

Christodoulou I, Buttery LD, Saravanapavan P, Tai G, Hench LL, Polak JM. Dose- and time-dependent effect of bioactive gel-glass ionic-dissolution products on human fetal osteoblast-specific gene expression. J Biomed Mater Res B Appl Biomater. **2005**; 74(1): 529-37.

Cockin J. Autologous bone grafting - complications at the donor site. J. Bone Jt. Surg. **1971**; 53B: 153.

Cole ZA, Dennison EM, Cooper C. Osteoporosis epidemiology update. Curr Rheumatol Rep. **2008**; 10(2): 92-6.

Collier JP, Colligan GA, Brown SA. Bone ingrowth into dynamically loaded porous-

coated intramedullary nails. J Biomed Mater Res. **1976**; 10(4): 485-92.

Connolly JF, Guse R, Tiedeman J, Dehne R. Autologous marrow injection as a substitute for operative grafting of tibial nonunions. Clin Orthop Relat Res. **1991**; 266: 259-70.

Constantino PD, Friedman CD. Synthetic bone graft substitutes. Otolaryngol Clin North Am **1994**; 27: 1037-73.

Cooper DM, Matyas JR, Katzenberg MA, Hallgrimsson B. Comparison of microcomputed tomographic and microradiographic measurements of cortical bone porosity. Calcif Tissue Int. **2004**; 74(5): 437-47.

Copcu E, Sivrioglu N, Aksoy B, Oztan S. Long Term Results of the Reconstruction of Maxillofacial Segmental Bone Defects with bioactive glass: Presentation of six cases. The Internet Journal of Plastic Surgery **2007**.

Daculsi G, LeGeros RZ, Deudon C. Scanning and transmission electron microscopy, and electron probe analysis of the interface between implants and host bone. Osseo-coalescence versus osseo-integration. Scanning Microsc. **1990**; 4(2): 309-14.

D'Agostino P, Stassen P, Delloye C. Post-traumatic bone loss of the femur treated with segmental bone allograft and bone morphogenetic protein: a case report. Acta Orthop Belg. **2007**; 73(3): 396-9.

Damen JJ, Ten Cate JM. Silica-induced precipitation of calcium phosphate in the presence of inhibitors of hydroxyapatite formation. J Dent Res. **1992**; 71(3): 453-7.

Damien CJ, Parsons JR. Bone graft and bone graft substitutes: a review of current technology and applications J Appl Biomater. **1991**; 2(3): 187-208.

De Boer J, Wang HJ, Van Blitterswijk C. Effects of Wnt signaling on proliferation and differentiation of human mesenchymal stem cells. Tissue Eng. **2004**; 10(3-4): 393-401.

de Groot K. Bioceramics consisting of calcium phosphate salts. Biomaterials **1980**; 1(1): 47-50.

De Santis D, Guerriero C, Nocini PF, Ungersbock A, Richards, Gotte P, Armato U. Adult human bone cells from jaw bones cultured on plasma-sprayed or polished surfaces of titanium or hydroxylapatite. J Mater Sci Mater Med. **1996**; 7(1): 21-8.

DeCoster TA, Gehlert RJ, Mikola EA, Pirela-Cruz MA. Management of posttraumatic segmental bone defects. J Am Acad Orthop Surg. **2004**: 12(1): 28-38.

den Boer FC, Wippermann BW, Blokhuis TJ, Patka P, Bakker FC, Haarman HJ. Healing of segmental bone defects with granular porous hydroxyapatite augmented with recombinant human osteogenic protein-1 or autologous bone marrow. J Orthop Res. **2003**; 21(3): 521-8.

D'Ippolito G, Schiller PC, Ricordi C, Roos BA, Howard GA. Age-related osteogenic potential of mesenchymal stromal stem cells from human vertebral bone marrow. J Bone Miner Res. **1999**; 14(7): 1115-22.

Duffy GP, Wood MB, Rock MG, Sim FH. Vascularized free fibular transfer combined with autografting for the management of fracture nonunions associated with radiation therapy. J Bone Joint Surg Am. **2000**; 82(4): 544-54.

Eanes E. Dynamics of calcium phosphate precipitation. In: Bonucci E. editor. Calcification in biological systems CRC Press, London, **1992**. p. 2-17.

Egrise D, Martin D, Vienne A, Neve P, Schoutens A. The number of fibroblastic colonies formed from bone marrow is decreased and the in vitro proliferation rate of trabecular bone cells increased in aged rats. Bone **1992**; 13(5): 355-61.

Einhorn TA. Clinically applied models of bone regeneration in tissue engineering research. Clin Orthop Relat Res. **1999**; 367 Suppl: S59-67.

El-Ghannam A, Ducheyne P, Shapiro IM. Effect of serum proteins on osteoblast adhesion to surface-modified bioactive glass and hydroxyapatite. J Orthop Res. **1999**; 17(3): 340-5.

El-Ghannam A, Ducheyne P, Shapiro IM. Porous bioactive glass and hydroxyapatite ceramic affect bone cell function in vitro along different time lines. J Biomed Mater Res. **1997**; 36(2): 167-80.

El-Ghannam A. Bone reconstruction: from bioceramics to tissue engineering. Expert Rev Med Devices. **2005**; 2(1): 87-101.

Elliot J. Structure and chemistry of the apatites and other calcium orthophosphates. **1994**. Elsevier, New York. p. 389.

Evans CE, Galasko CS, Ward C. Effect of donor age on the growth in vitro of cells obtained from human trabecular bone. J Orthop Res. **1990**; 8(2): 234-7.

Feng J, Yan W, Gou Z, Weng W, Yang D.Stimulating effect of silica-containing nanospheres on proliferation of osteoblast-like cells. J Mater Sci Mater Med. **2007**; 18(11): 2167-72.

Ferreira CF, Carriel Gomes MC, Filho JS, Granjeiro JM, Oliveira Simões CM, Magini Rde S. Ferreira CF, Carriel Gomes MC, Filho JS, Granjeiro JM, Oliveira Simões CM, Magini Rde S. Platelet-rich plasma influence on human osteoblasts growth. Oral Surg Oral Med Oral Pathol Oral Radiol Endod. **2006**; 101(6): 724-9.

Fialkov JA, Holy CE, Shoichet MS, Davies JE. In vivo bone engineering in a rabbit femur. J Craniofac Surg. **2003**; 14(3): 324-32.

Fountos G, Yasumura S, Glaros D. The skeletal calcium/phosphorus ratio: a new in vivo method of determination. Med Phys. **1997**; 24(8): 1303-10.

Fréchette JP, Martineau I, Gagnon G. Platelet-rich plasmas: growth factor content

and roles in wound healing. J Dent Res. **2005**; 84(5): 434-9.

Friedenstein AJ, Chailakhjan RK, Lalykina KS. The development of fibroblast colonies in monolayer cultures of guinea-pig bone marrow and spleen cells. Cell Tissue Kinet. **1970**; 3(4): 393-403.

Frost HM. Wolff's Law and bone's structural adaptations to mechanical usage: an overview for clinicians. Angle Orthod. **1994**; 64(3): 175-88.

Fu YC, Nie H, Ho ML, Wang CK, Wang CH. Optimized bone regeneration based on sustained release from three-dimensional fibrous PLGA/HAp composite scaffolds loaded with BMP-2. Biotechnol Bioeng. **2008**; 99(4): 996-1006.

Fujibayashi S, Neo M, Kim HM, Kokubo T, Nakamura T. A comparative study between in vivo bone ingrowth and in vitro apatite formation on Na_2O-CaO-SiO_2 glasses. Biomaterials **2003**; 24(8): 1349-56.

Gao TJ, Lindholm TS, Kommonen B, Ragni P, Paronzini A, Lindholm TC. Microscopic evaluation of bone-implant contact between hydroxyapatite, bioactive glass and tricalcium phosphate implanted in sheep diaphyseal defects. Biomaterials **1995**; 16(15): 1175-9.

Gao TJ, Tuominen TK, Lindholm TS, Kommonen B, Lindholm TC. Morphological and biomechanical difference in healing in segmental tibial defects implanted with Biocoral or tricalcium phosphate cylinders. Biomaterials **1997**; 18(3): 219-23.

Gauthier O, Müller R, von Stechow D, Lamy B, Weiss P, Bouler JM, Aguado E, Daculsi G. In vivo bone regeneration with injectable calcium phosphate biomaterial: a three-dimensional micro-computed tomographic, biomechanical and SEM study. Biomaterials **2005**; 26(27): 5444-53.

Giannoudis PV, Hinsche AF, Cohen A, Macdonald DA, Matthews SJ, Smith RM. Segmental tibial fractures: an assessment of procedures in 27 cases. Injury **2003**; 34(10): 756-62.

Gibson IR, Best SM, Bonfield W. Chemical characterization of silicon-substituted hydroxyapatite. J Biomed Mater Res. **1999**; 44(4): 422-8.

Gibson IR, Jha LJ, Santos JD, Best SM, Bonfield W. Effect of silicon content on the chemical and phase composition of novel silicon substituted hydroxyapatite. In: LeGeros RZ, LeGeros JP, editors. Bioceramics. World Scientific, Singapore **1998**, p. 105-8.

Gilbert M, Shaw WJ, Long JR, Nelson K, Drobny GP, Giachelli CM, Stayton PS. Chimeric peptides of statherin and osteopontin that bind hydroxyapatite and mediate cell adhesion. J Biol Chem. **2000**; 275(21): 16213-8.

Gitelis S, Cole BJ. The use of allografts in orthopaedic surgery. Instr Course Lect. **2002**; 51: 507-20.

Gogolewski S, Pineda L, Büsing CM. Bone regeneration in segmental defects with

resorbable polymeric membranes: IV. Does the polymer chemical composition affect the healing process? Biomaterials. **2000**; 21(24): 2513-20.

Goshima J, Goldberg VM, Caplan AI. Osteogenic potential of culture-expanded rat marrow cells as assayed in vivo with porous calcium phosphate ceramic. Biomaterials **1991a**; 12(2): 253-8.

Goshima J, Goldberg VM, Caplan AI. The osteogenic potential of culture-expanded rat marrow mesenchymal cells assayed in vivo in calcium phosphate ceramic blocks. Clin Orthop Relat Res. **1991b**; 262: 298-311.

Gough JE, Notingher I, Hench LL. Osteoblast attachment and mineralized nodule formation on rough and smooth 45S5 bioactive glass monoliths. J Biomed Mater Res. A **2004**; 68(4): 640-50.

Graziani F, Ivanovski S, Cei S, Ducci F, Tonetti M, Gabriele M. The in vitro effect of different PRP concentrations on osteoblasts and fibroblast. Clin Oral Implants Res. **2006**; 17(2): 212-9.

Green SA, Jackson JM, Wall DM, Marinow H, Ishkanian J. Management of segmental defects by the Ilizarov intercalary bone transport method. Clin Orthop Relat Res. **1992**; 280: 136-42.

Greenbaum MA, Kanat IO. Current concepts in bone healing. Review of the literature. J Am Podiatr Med Assoc. **1993**; 83(3): 123-129.

Gronthos S. Reconstruction of human mandible by tissue engineering. Lancet. **2004**; 364(9436): 735-6

Grundel RE, Chapman MW, Yee T, Moore DC. Autogeneic bone marrow and porous biphasic calcium phosphate ceramic for segmental bone defects in the canine ulna. Clin Orthop Relat Res. **1991**; 266: 244-58.

Gugala Z, Gogolewski S. Regeneration of segmental diaphyseal defects in sheep tibiae using resorbable polymeric membranes: a preliminary study. J Orthop Trauma **1999**; 13(3): 187-95.

Guo X, Zheng Q, Kulbatski I, Yuan Q, Yang S, Shao Z, Wang H, Xiao B, Pan Z, Tang S. Bone regeneration with active angiogenesis by basic fibroblast growth factor gene transfected mesenchymal stem cells seeded on porous beta-TCP ceramic scaffolds. Biomed Mater. **2006**; 1(3): 93-9.

Habibovic P, Yuan H, van den Doel M, Sees TM, van Blitterswijk CA, de Groot K. Relevance of osteoinductive biomaterials in critical-sized orthotopic defect. J Orthop Res. **2006**; 24(5): 867-76.

Hagino T, Hamada Y. Accelerating bone formation and earlier healing after using demineralized bone matrix for limb lengthening in rabbits. J Orthop Res. **1999**; 17(2): 232-7.

Hamadouche M, Meunier A, Greenspan DC, Blanchat C, Zhong JP, La Torre GP,

Sedel L. Bioactivity of sol-gel bioactive glass coated alumina implants. J Biomed Mater Res. **2000**; 52(2): 422-9.

Hamidouche Z, Haÿ E, Vaudin P, Charbord P, Schüle R, Marie PJ, Fromigué O. FHL2 mediates dexamethasone-induced mesenchymal cell differentiation into osteoblasts by activating Wnt/β-catenin signaling-dependent Runx2 expression. The FASEB Journal. **2008**; 22: 3813-22.

Harding IS, Rashid N, Hing KA. Surface charge and the effect of excess calcium ions on the hydroxyapatite surface. Biomaterials **2005**; 26(34): 6818-26.

Harris CT, Cooper LF. Comparison of bone graft matrices for human mesenchymal stem cell-directed osteogenesis. J Biomed Mater Res A. **2004**; 68(4): 747-55.

Hartman EH, Vehof JW, de Ruijter JE, Spauwen PH, Jansen JA. Ectopic bone formation in rats: the importance of vascularity of the acceptor site. Biomaterials **2004**; 25(27): 5831-7.

Hassan MH. Predicting graded young modulus values of Ti alloys modified by ion implantation. Med J Malaysia. **2004**; 59 Suppl B: 164-5.

Haynesworth SE, Goshima J, Goldberg VM, Caplan AI. Characterization of cells with osteogenic potential from human marrow. Bone **1992**; 13(1): 81-8.

He Y, Zhang ZY, Zhu HG, Qiu W, Jiang X, Guo W. Experimental study on reconstruction of segmental mandible defects using tissue engineered bone combined bone marrow stromal cells with three-dimensional tricalcium phosphate. J Craniofac Surg. **2007**; 18(4): 800-5.

Heath CA. Cells for tissue engineering. Trends in Biotechnology **2000**; 18(1): 17-19.

Heise U, Osborn JF, Duwe F. Hydroxyapatite ceramic as a bone substitute. International Orthopaedics **1990**; 14(3): 329-38.

Hench LL and Wilson J. An Introduction to Bioceramics. Advanced Series in Ceramics - Vol 1, World Scientific, USA, **1993**, p.1-24.

Hench LL, West J. The sol-gel process. Chem Rev **1990**; 90: 33-72.

Hernigou P, Mathieu G, Poignard A, Manicom O, Beaujean F, Rouard H. Percutaneous autologous bone-marrow grafting for nonunions. Surgical technique. J Bone Joint Surg Am. **2006**; 88 Suppl 1 Pt 2: 322-7.

Heron MI, Rakusan K. Proliferating cell nuclear antigen (PCNA) detection of cellular proliferation in hypothyroid and hyperthyroid rat hearts. J Mol Cell Cardiol **1995**; 27(7): 1393-403.

Hill NM, Horne JG, Devane PA. Donor site morbidity in the iliac crest bone graft. Aust N Z J Surg. **1999**; 69(10): 726-8.

Hing KA, Best SM, Bonfield W. Characterization of porous hydroxyapatite. J Mater

Sci Mater Med. **1999**; 10(3): 135-45.

Hing KA, Revell PA, Smith N, Buckland T. Effect of silicon level on rate, quality and progression of bone healing within silicate-substituted porous hydroxyapatite scaffolds. Biomaterials **2006**; 27(29): 5014-26.

Hing KA. Bioceramic Bone Graft Substitutes: Influence of Porosity and chemistry. International Journal of Applied Ceramic Technology **2005**; 2(3): 184-99.

Hing KA. Bone repair in the twenty-first century: biology, chemistry or engineering? Philos Transact A Math Phys Eng Sci. **2004**; 362(1825): 2821-50.

Hiu-Yan Y, Ling Q, Kwong-Man L, Ming Z, Kwok-Sui L, Chun-yiu CJ. Novel approach for quantification of porosity for biomaterial implants using microcomputed tomography (microCT). J Biomed Mater Res B Appl Biomater. **2005**; 75(2): 234-42.

Ho W, Tawil B, Dunn JC, Wu BM. The behavior of human mesenchymal stem cells in 3D fibrin clots: dependence on fibrinogen concentration and clot structure. Tissue Eng. **2006**; 12(6): 1587-95.

Hodgskinson R, Currey JD. The effect of variation in structure on the Young's modulus of cancellous bone: a comparison of human and non-human material. Proc Inst Mech Eng [H]. **1990**; 204 (2): 115-21.

Høl PJ, Mølster A, Gjerdet NR. Should the galvanic combination of titanium and stainless steel surgical implants be avoided? Injury **2008**; 39(2): 161-9.

Hollinger JO, Brekke J, Gruskin E, Lee D. Role of bone substitutes. Clin Orthop Relat Res. **1996**; 324: 55-65.

Hollinger JO, Kleinschmidt JC. The critical size defect as an experimental model to test bone repair materials. J Craniofac Surg. **1990**; 1(1): 60-8.

Holmes RE. Bone Regeneration within a Coralline Hydroxyapatite Implants. Plast. Reconstr. Surg. **1979**; 63(5): 626-33.

Holy CE, Fialkov JA, Shoichet MS, Davies JE. In vivo models for Bone Tissue-Engineering constructs. In: Davies JE, editor. Bone Engineering. Em squared incorporated, **2000**, p.496-8.

Hopp SG, Dahners LE, Gilbert JA. A study of the mechanical strength of long bone defects treated with various bone autograft substitutes: an experimental investigation in the rabbit. J Orthop Res. **1989**; 7(4): 579-84.

Hott M, Noel B, Bernache-Assolant D, Rey C, Marie PJ. Proliferation and differentiation of human trabecular osteoblastic cells on hydroxyapatite. J Biomed Mater Res. **1997**; 37(4): 508-16.

Huang SC. Comparison of bone transport and bone graft methods in the experimental treatment of bone defects. J Formos Med Assoc. **1997**; 96(1): 23-9.

Hulbert SF, Morrison SJ, Klawitter JJ. Tissue reaction to three ceramics of porous and non-porous structuresJ Biomed Mater Res. **1972**; 6(5): 347-74.

Hurley MM, Marie P, Florkiewicz R. Fibroblast growth factor (FGF) and FGF receptor families in bone. In: Bilezikian PJ, Raisz GL, Rodan AG, editors. Principles of Bone Biology, Academic Press, New York, **2002**, p. 825-51.

Hutmacher DW. Scaffolds in tissue engineering bone and cartilage. Biomaterials **2000**; 21(24): 2529-43.

Ilizarov GA, Lediaev VI, Shitin VP. The course of compact bone reparative regeneration in distraction osteosynthesis under different conditions of bone fragment fixation (experimental study) Eksp Khir Anesteziol. **1969**; 14(6): 3-12.

Ip WY. Polylactide membranes and sponges in the treatment of segmental defects in rabbit radii. Injury **2002**; 33: S-B-66 – 70.

Ishaug SL, Crane GM, Miller MJ, Yasko AW, Yaszemski MJ, Mikos AG. Bone formation by three-dimensional stromal osteoblast culture in biodegradable polymer scaffolds. J Biomed Mater Res. **1997**; 36(1): 17-28.

Isobe M, Yamazaki Y, Mori M, Amagasa T. Bone regeneration produced in rat femur defects by polymer capsules containing recombinant human bone morphogenetic protein-2. J Oral Maxillofac Surg. **1999**; 57(6): 695-8.

Isogai N, Landis WJ, Mori R, Gotoh Y, Gerstenfeld LC, Upton J, Vacanti JP. Experimental use of fibrin glue to induce site-directed osteogenesis from cultured periosteal cells. Plast Reconstr Surg. **2000**; 105(3): 953-63.

Jackson MR. Fibrin sealants in surgical practice: An overview. Am J Surg. **2001**; 182(2 Suppl): 1S-7S.

Jadlowiec JA, Celil AB, Hollinger JO. Bone tissue engineering: recent advances and promising therapeutic agents. Expert Opin Biol Ther. **2003**; 3(3): 409-23.

Jaiswal N, Haynesworth SE, Caplan AI, Bruder SP. Osteogenic differentiation of purified, culture-expanded human mesenchymal stem cells in vitro. J Cell Biochem. **1997**; 64(2): 295-312.

Jansen JA, Vehof JW, Ruhé PQ, Kroeze-Deutman H, Kuboki Y, Takita H, Hedberg EL, Mikos AG. Growth factor-loaded scaffolds for bone engineering. J Control Release. **2005**; 101(1-3): 127-36.

Jarcho M. Calcium phosphate ceramics as hard tissue prosthetics. Clin Orthop Relat Res. **1981**; 157: 259-78.

Jie Feng, Weiqi Yan, Zhongru Gou, Wenjian Weng and Disheng Yang. Stimulating effect of silica-containing nanospheres on proliferation of osteoblast-like cells. J Mater Sci Mater Med **2007**; 18 (11): 2167-72.

Jin QM, Takita H, Kohgo T, Atsumi K, Itoh H, Kuboki Y. Effects of geometry of

hydroxyapatite as a cell substratum in BMP-induced ectopic bone formation. J Biomed Mater Res. **2000**; 51(3): 491-9.

John A, Nair MB, Bernhardt A, Varma H, Gelinsky M. Biodegradation and cytocompatibility studies of a triphasic ceramic coated porous hydroxyapatite for bone substitute applications. Int. J. Appl. Ceram. Technol. **2008**; 5(1): 11-19.

Jugdaohsingh R, Tucker KL, Qiao N, Cupples LA, Kiel DP, Powell JJ. Dietary silicon intake is positively associated with bone mineral density in men and premenopausal women of the Framingham Offspring cohort. J Bone Miner Res. **2004**; 19(2): 297-307.

Kadyala S, Jaiswal N, Bruder SP. Culture-expanded, bone marrow-derived mesenchymal stem cells can regenerate a critical-sized segmental bone defect. Tissue Eng. **1997**, 3(2): 173-85.

Kamath S, Blann AD, Lip GY. Platelet activation: assessment and quantification. Eur Heart J. **2001**; 22(17): 1561-71.

Kanno T, Takahashi T, Tsujisawa T, Ariyoshi W, Nishihara T. Platelet-rich plasma enhances human osteoblast-like cell proliferation and differentiation. J Oral Maxillofac Surg. **2005**; 63(3): 362-9.

Kaplan FS, Hayes WC, Keaveny TM, Boskey A, Einhorn TA, Lannotti JP. Form and function of bone. In: Simon SP, editor. Orthopaedic basic science. American Academy of Orthopaedic Surgeons, Columbus, **1994**. p. 127-185.

Karageorgiou V, Kaplan D. Porosity of 3D biomaterial scaffolds and osteogenesis. Biomaterials **2005**; 26(27): 5474-91.

Katagiri T, Takahashi N. Regulatory mechanisms of osteoblast and osteoclast differentiation. Oral Dis. **2002**; 8(3): 147-59.

Kaufmann EA, Ducheyne P, Shapiro IM. Effect of varying physical properties of porous, surface modified bioactive glass 45S5 on osteoblast proliferation and maturation. J Biomed Mater Res. **2000**; 52(4): 783-96.

Kawabata K, Nagake Y, Shikata K, Fukuda S, Nakazono H, Takahashi M, Ichikawa H, Makino H. Soluble P-selectin is released from activated platelets in in vivo during hemolysis. Nephron **1998**; 78: 148-155.

Kee WN, David TWL, Dietmar WH. The challenge to measure cell proliferation in two and three dimension. Tissue Eng. **2005**; 11(1-2): 182-91.

Kern S, Eichler H, Stoeve J, Klüter H, Bieback K. Comparative analysis of mesenchymal stem cells from bone marrow, umbilical cord blood, or adipose tissue. Stem Cells. **2006**; 24(5): 1294-301.

Khan S, Bostrom M, Lane J. BONE GROWTH FACTORS. Orthopedic Clinics of North America **2000**; 31(3): 375-87.

Kieswetter K, Schwartz Z, Hummert TW, Cochran DL, Simpson J, Dean DD, Boyan BD. Surface roughness modulates the local production of growth factors and cytokines by osteoblast-like MG-63 cells. J Biomed Mater Res. **1996**; 32(1): 55-63.

Kitoh H, Kitakoji T, Tsuchiya H, Katoh M, Ishiguro N. Transplantation of culture expanded bone marrow cells and platelet rich plasma in distraction osteogenesis of the long bones. Bone **2007**; 40(2): 522-8.

Kitoh H, Kitakoji T, Tsuchiya H, Mitsuyama H, Nakamura H, Katoh M, Ishiguro N. Transplantation of marrow-derived mesenchymal stem cells and platelet-rich plasma during distraction osteogenesis-a preliminary result of three cases. Bone **2004**; 35(4): 892-8.

Kitsugi T, Yamamuro T, Kokubo T. Bonding behavior of a glass-ceramic containing apatite and wollastonite in segmental replacement of the rabbit tibia under load-bearing conditions. J Bone Joint Surg Am. **1989**; 71(2): 264-72.

Kizuki T,Ohgaki M, Kastura M, Nakamura S, Hashimoto K, Toda Y, Udagawa, S, Yamashita K. Effect of bone-like layer growth from culture medium on adherence of osteoblast-like cells. Biomaterials **2003**; 24 (6): 941-7.

Kobune M, Kato J, Chiba H, Kawano Y, Tanaka M, Takimoto R, Hamada H, Niitsu Y. Telomerized human bone marrow-derived cell clones maintain the phenotype of hematopoietic-supporting osteoblastic and myofibroblastic stromal cells after long-term culture. Exp Hematol. **2005**; 33(12): 1544-53.

Kocaoglu M, Eralp L, Rashid HU, Sen C, Bilsel K. Reconstruction of segmental bone defects due to chronic osteomyelitis with use of an external fixator and an intramedullary nail. J Bone Joint Surg Am. **2006**; 88(10): 2137-45.

Kokubo S, Fujimoto R, Yokota S, Fukushima S, Nozaki K, Takahashi K, Miyata K. Bone regeneration by recombinant human bone morphogenetic protein-2 and a novel biodegradable carrier in a rabbit ulnar defect model. Biomaterials. **2003**; 24(9): 1643-51.

Komlev VS, Peyrin F, Mastrogiacomo M, Cedola A, Papadimitropoulos A, Rustichelli F, Cancedda R. Kinetics of in vivo bone deposition by bone marrow stromal cells into porous calcium phosphate scaffolds: an X-ray computed microtomography study. Tissue Eng. **2006**; 12(12): 3449-58.

Kon E, Muraglia A, Corsi A, Bianco P, Marcacci M, Martin I, Boyde A, Ruspantini I, Chistolini P, Rocca M, Giardino R, Cancedda R, Quarto R. Autologous bone marrow stromal cells loaded onto porous hydroxyapatite ceramic accelerate bone repair in critical-size defects of sheep long bones. J Biomed Mater Res. **2000**; 49(3): 328-37.

Kotani S, Fujita Y, Kitsugi T, Nakamura T, Yamamuro T, Ohtsuki C, Kokubo T. Bone bonding mechanism of beta-tricalcium phosphate. J Biomed Mater Res. **1991**; 25(10): 1303-15.

Krebsbach PH, Kuznetsov SA, Bianco P, Robey PG. Bone marrow stromal cells: characterization and clinical application. Crit Rev Oral Biol Med. **1999**; 10(2): 165-81.

Kruyt MC, de Bruijn JD, Wilson CE, Oner FC, van Blitterswijk CA, Verbout AJ, Dhert WJ. Viable osteogenic cells are obligatory for tissue-engineered ectopic bone formation in goats. Tissue Eng. **2003**; 9(2): 327-36.

Kruyt MC, Dhert WJ, Oner C, van Blitterswijk CA, Verbout AJ, de Bruijn JD. Osteogenicity of autologous bone transplants in the goat. Transplantation **2004a**; 77(4): 504-9.

Kruyt MC, Dhert WJ, Yuan H, Wilson CE, van Blitterswijk CA, Verbout AJ, de Bruijn JD. Bone tissue engineering in a critical size defect compared to ectopic implantations in the goat. J Orthop Res. **2004b**; 22(3): 544-51.

Kuboki Y, Jin Q, Takita H. Geometry of carriers controlling phenotypic expression in BMP-induced osteogenesis and chondrogenesis. J Bone Joint Surg Am. **2001**; 83-A Suppl 1(Pt 2): S105-15.

Kuhn JL, Goldstein SA, Feldkamp LA, Goulet RW, Jesion G. Evaluation of a microcomputed tomography system to study trabecular bone structure. J Orthop Res. **1990**; 8(6): 833-42.

Lai W, Garino J, Flaitz C, Ducheyne P. Excretion of resorption products from bioactive glass implanted in rabbit muscle. J Biomed Mater Res. A **2005**; 75(2): 398-407.

Landesberg R, Moses M, Karpatkin M. Risks of using platelet rich plasma gel. J Oral Maxillofac Surg. **1998**; 56(9): 1116-7.

Landesberg R, Roy M, Glickman RS. Quantification of growth factor levels using a simplified method of platelet-rich plasma gel preparation. J Oral Maxillofac Surg. **2000**; 58(3): 297-300.

Langer R, Vacanti JP. Tissue Engineering. Science **1993**; 260(5110):920-6.

Langstaff S, Sayer M, Smith TJ, Pugh SM, Hesp SA, Thompson WT. Resorbable bioceramics based on stabilized calcium phosphates. Part I: rational design, sample preparation and material characterization. Biomaterials **1999**; 20(18): 1727-41.

Lawton DM, Andrew JG, Marsh DR, Hoyland JA and Freemont AJ. Expression of the gene encoding the matrix gla protein by mature osteoblasts in human fracture non-unions. Mol Pathol. **1999**; 52(2): 92-6.

Le Guéhennec L, Layrolle P, Daculsi G. A review of bioceramics and fibrin sealant. Eur Cell Mater. **2004**; 8: 1-10.

Leach JK, Kaigler D, Wang Z, Krebsbach PH, Mooney DJ. Coating of VEGF-releasing scaffolds with bioactive glass for angiogenesis and bone regeneration. Biomaterials **2006**; 27(17): 3249-55.

Lemaire I, Dionne PG, Nadeau D, Dunnigan J. Rat lung reactivity to natural and man-made fibrous silicates following short-term exposure. Environ Res. **1989**; 48(2): 193-210.

Li Z, Yang Y, Wang C, Xia R, Zhang Y, Zhao Q, Liao W, Wang Y, Lu J. Repair of sheep metatarsus defects by using tissue-engineering technique. J Huazhong Univ Sci Technolog Med Sci. **2005**; 25(1): 62-7.

Liebschner MA. Biomechanical considerations of animal models used in tissue engineering of bone. Biomaterials **2004**; 25(9): 1697-714.

Lin FH, Liao CJ, Chen KS, Sun JS, Liu HC. Degradation behaviour of a new bioceramic: Ca_2P2O_7 with addition of $Na_4P_2O_710H_2O$. Biomaterials **1997**; 18(13): 915-21.

Liu G, Zhao L, Zhang W, Cui L, Liu W, Cao Y. Repair of goat tibial defects with bone marrow stromal cells and beta-tricalcium phosphate. J Mater Sci Mater Med. **2008**; 19(6): 2367-76.

Lobel KD, Hench LL. In vitro adsorption and activity of enzymes on reaction layers of bioactive glass substrates. J Biomed Mater Res. **1998**; 39(4): 575-9.

Lossdörfer S, Schwartz Z, Lohmann CH, Greenspan DC, Ranly DM, Boyan BD. Osteoblast response to bioactive glasses in vitro correlates with inorganic phosphate content. Biomaterials **2004**; 25(13): 2547-55.

Loty C, Sautier JM, Tan MT, Oboeuf M, Jallot E, Boulekbache H, Greenspan D, Forest N. Bioactive glass stimulates in vitro osteoblast differentiation and creates a favorable template for bone tissue formation. J Bone Miner Res. **2001**; 16(2): 231-9.

Lucarelli E, Beccheroni A, Donati D, Sangiorgi L, Cenacchi A, Del Vento AM, Meotti C, Bertoja Z, Giardino R, Fornasari PM, Mercuri M, and Picci P. Platelet-derived growth factors enhance proliferation of human stromal stem cells. Biomaterials **2003**; 24(18): 3095-100.

Lucarelli E, Fini M, Beccheroni A, Giavaresi G, Di Bella C, Aldini NN, Guzzardella G, Martini L, Cenacchi A, Di Maggio N, Sangiorgi L, Fornasari PM, Mercuri M, Giardino R, Donati D. Stromal stem cells and platelet-rich plasma improve bone allograft integration. Clin Orthop Relat Res. **2005**; 435: 62-8.

Maehata Y, Takamizawa S, Ozawa S, Kato Y, Sato S, Kubota E, Hata R. Both direct and collagen-mediated signals are required for active vitamin D3-elicited differentiation of human osteoblastic cells: roles of osterix, an osteoblast-related transcription factor. Matrix Biol. **2006**; 25(1): 47-58.

Malik MA, Puleo DA, Bizios R, Doremus RH. Osteoblasts on hydroxyapatite, alumina and bone surfaces in vitro: morphology during the first 2 h of attachment. Biomaterials **1992**; 13(2): 123-8.

Maniatopoulos C, Rodriguez A, Deporter DA, Melcher AH. An improved method for preparing histological sections of metallic implants. Int J Oral Maxillofac Implants. **1986**; 1(1): 31-7.

Maniatopoulos C, Sodek J, Melcher AH. Bone formation *in vitro* by stromal cells obtained from bone marrow of young adult rats. Cell Tissue Res. **1988**; 254(2): 317-30.

Marcacci M, Kon E, Moukhachev V, Lavroukov A, Kutepov S, Quarto R, Mastrogiacomo M, Cancedda R. Stem cells associated with macroporous bioceramics for long bone repair: 6- to 7-year outcome of a pilot clinical study. Tissue Eng. **2007**; 3(5): 947-55.

Marcacci M, Kon E, Zaffagnini S, Giardino R, Rocca M, Corsi A, Benvenuti A, Bianco P, Quarto R, Martin I, Muraglia A, Cancedda R. Reconstruction of extensive long-bone defects in sheep using porous hydroxyapatite sponges. Calcif Tissue Int. **1999**; 64(1): 83-90.

Marrini E, Valdinucci F, Silvestrini G, Moretti S, Carlesimo M, Poggio,C Bonnuci E. Morphological investigations on bone formation in hydroxyapatite fibrin implants in human maxillary and mandibular bone. Cells and Materials **1994**; 4: 231-46.

Martin JY, Dean DD, Cochran DL, Simpson J, Boyan BD, Schwartz Z. Proliferation, differentiation, and protein synthesis of human osteoblast-like cells (MG63) cultured on previously used titanium surfaces. Clin Oral Implants Res. **1996**; 7(1): 27-37.

Marx RE, Carlson ER, Eichstaedt RM, Schimmele SR, Strauss JE, Georgeff KR. Platelet-rich plasma: Growth factor enhancement for bone grafts. Oral Surg Oral Med Oral Pathol Oral Radiol Endod. **1998**; 85(6): 638-46.

Marx RE. Platelet-Rich Plasma (PRP): What is PRP and what is Not PRP? Implant Dent. **2001**; 10(4): 225-8.

Mastrogiacomo M, Corsi A, Francioso E, Di Comite M, Monetti F, Scaglione S, Favia A, Crovace A, Bianco P, Cancedda R. Reconstruction of extensive long bone defects in sheep using bioresorbable bioceramics based on silicon stabilized Tricalcium phosphate. Tissue Eng. **2006a**; 12(5): 1261-73.

Mastrogiacomo M, Papadimitropoulos A, Cedola A, Peyrin F, Giannoni P, Pearce SG, Alini M, Giannini C, Guagliardi A, Cancedda R. Engineering of bone using bone marrow stromal cells and a silicon-stabilized tricalcium phosphate bioceramic: evidence for a coupling between bone formation and scaffold resorption. Biomaterials **2007**; 28(7): 1376-84.

Mastrogiacomo M, Scaglione S, Martinetti R, Dolcini L, Beltrame F, Cancedda R, Quarto R. Role of scaffold internal structure on in vivo bone formation in macroporous calcium phosphate bioceramics. Biomaterials **2006b**; 27(17): 3230-7.

Mathias B, Xu Y, Lakovos K. Current Opinion in Orthopedics **2000**; 11(5): 403-12.

Mauney JR, Blumberg J, Pirun M, Volloch V, Vunjak-Novokovic G, Kaplan DL Osteogenic differentiation of human bone marrow stromal cells on partially demineralised bone scaffolds in vitro. Tissue Eng. **2004a**; 10(1-2): 81-92.

Mauney JR, Kaplan DL, Volloch V. Matrix-mediated retention of osteogenic differentiation potential by human adult bone marrow stromal cells during ex vivo expansion. Biomaterials **2004b**; 25(16): 3233-43.

Mauney JR, Volloch V, Kaplan DL. Role of adult mesenchymal stem cells in bone

tissue engineering applications: current status and future prospects. Tissue Eng. **2005**; 11(5-6): 787-802.

Mavropoulos E, Ross AM, da Rocha NCC, Soares GA, Moreira JC, Moure GT. Dissolution of calcium-deficient hydroxyapatite synthesized at different conditions. Mater Charact. **2003**; 50 (2-3): 203-207.

Meana A, Iglesias J, Del Rio M, Larcher F, Madrigal B, Fresno MF, Martin C, San Roman F, Tevar F. Large surface of cultured human epithelium obtained on a dermal matrix based on live fibroblast-containing fibrin gels. Burns **1998**; 24(7): 621-30.

Meinig RP. Polylactide membranes in the treatment of segmental diaphyseal defects: Animal model experiments in the rabbit radius, sheep tibia, yucatan mini pig radius, and goat tibia. Injury. **2002**; 33 Suppl 2: B58-65.

Messing RA. Molecular inclusions. Adsorption of macro molecules on porous glass membranes. J. Am. Chem. Soc. **1969**; 91(9): 2370-1.

Minami A, Kimura T, Matsumoto O, Kutsumi K. Fracture through united vascularised bone grafts. J Reconstr Microsurg **1993**; 9: 227-32.

Moore DC, Chapman MW, Manske D. The evaluation of a biphasic calcium phosphate ceramic for use in grafting long-bone diaphyseal defects. J Orthop Res. **1987**; 5(3): 356-65.

Mooren RE, Merkx MA, Bronkhorst EM, Jansen JA, Stoelinga PJ. The effect of platelet-rich plasma on early and late bone healing: an experimental study in goats. Int J Oral Maxillofac Surg. **2007**; 36(7): 626-31.

Morishita T, Honoki K, Ohgushi H, Kotobuki N, Matsushima A, Takakura Y. Tissue engineering approach to the treatment of bone tumors: three cases of cultured bone grafts derived from patients' mesenchymal stem cells. Artif Organs. **2006**; 30(2): 115-8.

Morsi E. Tibial reconstruction using a non-vascularised fibular transfer. Int Orthop. **2002**; 26(6): 377-80.

Muschler GF, Nakamoto C, Griffith LG. Engineering principles of clinical cell-based tissue engineering. J Bone Joint Surg Am. **2004**; 86-A (7): 1541-58.

Nandi SK, Kundu B, Datta S, De DK, Basu D. The repair of segmental bone defects with porous bioglass: An experimental study in goat. Res Vet Sci. **2008** Jul 2 .

Nemmar A, Nemery B, Hoet PH, Van Rooijen N, Hoylaerts MF. Silica particles enhance peripheral thrombosis: key role of lung macrophage-neutrophil cross-talk. Am J Respir Crit Care Med. **2005**; 171(8): 872-9.

Nicolas V, Prewett A, Bettica P, Mohan S, Finkelman RD, Baylink DJ, Farley JR. Age-related decreases in insulin-like growth factor-I and transforming growth factor-beta in femoral cortical bone from both men and women: implications for bone loss with aging. J Clin Endocrinol Metab. **1994**; 78(5): 1011-6.

Nielsen F, Poellot R. Dietary silicon affects bone turnover differently in ovariectomized and sham-operated growing rats. J. Trace Elem. Exp. Med. **2004**; 17(3): 137-149.

Nikolidakis D, van den Dolder J, Wolke JG, Stoelinga PJ, Jansen JA. The effect of platelet-rich plasma on the bone healing around calcium phosphate-coated and non-coated oral implants in trabecular bone. Tissue Eng. **2006**; 12(9): 2555-63.

Ning CQ, Greish Y, El-Ghannam A. Crystallization behavior of silica-calcium phosphate biocomposites: XRD and FTIR studies. J Mater Sci Mater Med. **2004**; 15(11): 1227-35.

Nordström EG, Sánchez Muñoz OL. Physics of bone bonding mechanism of different surface bioactive ceramic materials in vitro and in vivo. Biomed Mater Eng. **2001**; 11(3): 221-31.

Nygren H, Tengvall P, Lundstrom I. The initial reactions of TiO_2 with blood. J Biomed Mater Res. **1997**; 34(4): 487-92.

Ogino Y, Ayukawa Y, Tsukiyama Y, Koyano K. The effect of platelet-rich plasma on the cellular response of rat bone marrow cells in vitro. Oral Surg Oral Med Oral Pathol Oral Radiol Endod. **2005**; 100(3): 302-7.

Ohgushi H, Miyake J, Tateishi T. Mesenchymal stem cells and bioceramics: strategies to regenerate the skeleton. Novartis Found Symp. **2003**; 249: 118-27.

Oliva A, Salerno A, Locardi B, Riccio V, Della Ragione F, Iardino P, Zappia V. Behaviour of human osteoblasts cultured on bioactive glass coatings. Biomaterials **1998**; 19(11-12): 1019-25.

Oonishi H, Kushitani S. Iwaki H. Comparative bone formation in several kinds of bioceramic granules. In: Wilson J, Hench LL, Greenspan D. editors. Eighth international symposium on ceramics in medicine. Tokyo. Japan: Elsevier Science Ltd: **1995**. p.137 - 44.

Patel N, Best S, Bonfield W, Gibson I, Hing K, Damien E, Revell PA. A comparative study on the in vivo behaviour of hydroxyapatite and silicon substituted hydroxyapatite granules. J Mater Sci Mater Med. **2002**; 13(12): 1199-206.

Pekounov Y, Petrov OE. Bone resembling apatite by amorphous-to-crystalline transition driven self-organisation. J Mater Sci Mater Med. **2008**; 19(2): 753-9.

Pelled G, G T, Aslan H, Gazit Z, Gazit D. Mesenchymal stem cells for bone gene therapy and tissue engineering. Curr Pharm Des. **2002**; 8(21): 1917-28.

Pereira RF, O'Hara MD, Laptev AV, Halford KW, Pollard MD, Class R, Simon D, Livezey K, Prockop DJ. Marrow stromal cells as a source of progenitor cells for nonhematopoietic tissues in transgenic mice with a phenotype of osteogenesis imperfecta. Proc Natl Acad Sci U S A **1998**; 95(3): 1142-7.

Petite H, Viateau V, Bensaïd W, Meunier A, de Pollak C, Bourguignon M, Oudina K,

Sedel L, Guillemin G. Tissue engineered bone regeneration. Nature Biotechnology **2000**; 18: 959-62.

Petrakova KV. Heterotopic ossification in the rat kidney in ischemia. Arkh Anat Gistol Embriol. **1963**; 44: 112-116.

Phan PV, Grzanna M, Chu J, Polotsky A, el-Ghannam A, Van Heerden D, Hungerford DS, Frondoza CG. The effect of silica-containing calcium-phosphate particles on human osteoblasts in vitro. J Biomed Mater Res. A **2003**; 67(3): 1001-8.

Pietak AM, Reid JW, Stott MJ, Sayer M. Silicon substitution in the calcium phosphate bioceramics. Biomaterials **2007**; 28(28): 4023-32.

Pietrzak WS, Sarver D, Verstynen M. Bioresorbable implants-practical considerations Bone **1996**; 19(1 Suppl): 109S-119S.

Pittenger MF, Mackay AM, Beck SC, Jaiswal RK, Douglas R, Mosca JD, Moorman MA, Simonetti DW, Craig S, Marshak DR. Multilineage potential of adult human mesenchymal stem cells Science. **1999**; 284(5411): 143-7.

Porter AE, Best SM, Bonfield W. Ultrastructural comparison of hydroxyapatite and silicon-substituted hydroxyapatite for biomedical applications. J Biomed Mater Res A. **2004a**; 68(1): 133-41.

Porter AE, Botelho CM, Lopes MA, Santos JD, Best SM, Bonfield W. Ultra structural comparison of dissolution and apatite precipitation on hydroxyapatite and silicon-substituted hydroxyapatite in vitro and in vivo. J Biomed Mater Res. A **2004b**; 69(4): 670-9.

Prolo DJ, Rodrigo JJ. Contemporary bone graft physiology and surgery. Clin Orthop Relat Res. **1985**; 200: 322-42.

Quarto R, Mastrogiacomo M, Cancedda R, Kutepov SM, Mukhachev V, Lavroukov A, Kon E, Marcacci M. Repair of large bone defects with the use of autologous bone marrow stromal cells. N Engl J Med. **2001**; 344(5): 385-6.

Quarto R, Thomas D, Liang CT. Bone progenitor cell deficits and the age-associated decline in bone repair capacity. Calcif Tissue Int. **1995**; 56(2): 123-9.

Rai B, Oest ME, Dupont KM, Ho KH, Teoh SH, Guldberg RE. Combination of platelet-rich plasma with polycaprolactone-tricalcium phosphate scaffolds for segmental bone defect repair. J Biomed Mater Res. A **2007**; 81(4): 888-99.

Redey SA, Razzouk S, Rey C, Bernache-Assollant D, Leroy G, Nardin M, Cournot G. Osteoclast adhesion and activity on synthetic hydroxyapatite, carbonated hydroxyapatite, and natural calcium carbonate: relationship to surface energies. J Biomed Mater Res. **1999**; 45(2): 140-7.

Reffitt DM, Ogston N, Jugdaohsingh R, Cheung HF, Evans BA, Thompson RP, Powell JJ, Hampson GN. Orthosilicic acid stimulates collagen type I synthesis and osteoblastic differentiation in human osteoblast-like cells in vitro. Bone **2003**; 32(2):

127-35.

Reinstorf A, Ruhnow M, Gelinsky M, Pompe W, Hempel U, Wenzel KW, Simon P. Phosphoserine-a convenient compound for modification of calcium phosphate bone cement collagen composites. J Mater Sci Mater Med. **2004**; 15(4): 451-455.

Reiser KM, Last JA. Collagen cross linking in lungs of rats with experimental silicosis. Coll Relat Res. **1986**; 6(4): 313-23.

Rhee S, Hwang M, Si HJ, Choi JY. Biological activities of osteoblast on poly (methyl methacrylate) / silica hybrid containing calcium salt. Biomaterials **2003**; 24(6): 901-6.

Richard MD. Bioactive glass stimulates the secretion of angiogenic growth factors and angiogenesis in vitro. Tissue Eng. **2005**; 11(5/6): 768-77.

Ripamonti U. Soluble osteogenic molecular signals and the induction of bone formation. Biomaterials **2006**; 27(6): 807-22.

Rivron NC, Liu J J, Rouwkema J, de Boer J, van Blitterswijk CA. Engineering vascularised tissues in vitro. Eur Cell Mater. **2008**; 15: 27-40.

Robey PG. Bone matrix proteoglycans and glycoproteins. In: Bilezikian JP, Raisz LG, Rodan GA, editors. Principles of Bone Biology. Academic press, San Diego, **1996**. p. 235.

Roldán JC, Jepsen S, Miller J, Freitag S, Rueger DC, Açil Y, Terheyden H. Bone formation in the presence of platelet-rich plasma vs. bone morphogenetic protein-7. Bone **2004**; 34(1): 80-90.

Rose FR, Oreffo RO. Bone tissue engineering: hope vs hype. Biochem Biophys Res Commun. **2002**; 292(1):1-7.

Rosen V, Thies RS. The BMP proteins in bone formation and repair. Trends Genet. **1992**; 8(3): 97-102.

Ruys AJ. Silicon-doped hydroxyapatite. J Aust Ceram Soc. **1993**; 29: 71-80.

Salgado AJ, Coutinho OP, Reis RL. Bone Tissue Engineering: State of the art and future trends. Macromol. Biosci. **2004**; 4(8): 743-65.

Sánchez-Salcedo S, Izquierdo-Barba I, Arcos D, Vallet-Regí M. In vitro evaluation of potential calcium phosphate scaffolds for tissue engineering. Tissue Eng. **2006**; 12(2): 279-90.

Saravanapavan P, Jones JR, Verrier S, Beilby R, Shirtliff VJ, Hench LL, Polak JM. Binary $CaO-SiO_2$ gel-glasses for biomedical applications. Biomed Mater Eng. **2004**; 14(4): 467-86.

Sato J, Okada K, Fukuda S, Sato R, Yasuda J, Naito Y. Serum activities of tartrate-resistant acid phosphatase and bone specific alkaline phosphatase as indices of bone metabolism in the cow. J Vet Med Sci. **2002**; 64(7): 653-5.

Scaglione S, Ilengo C, Fato M, Quarto R. Hydroxyapatite-Coated Polycaprolacton Wide Mesh as a Model of Open Structure for Bone Regeneration. Tissue Eng Part A **2008**. DOI: 10.1089=ten.tea.2007.0410.

Schantz JT, Hutmacher DW, Lam CX, Brinkmann M, Wong KM, Lim TC, Chou N, Guldberg RE, Teoh SH. Repair of calvarial defects with customised tissue-engineered bone grafts II. Evaluation of cellular efficiency and efficacy in vivo. Tissue Eng. **2003**; 9 Suppl 1: S127-39.

Schiraldi C, D'Agostino A, Oliva A, Flamma F, De Rosa A, Apicella A, Aversa R, De Rosa M. Development of hybrid materials based on hydroxyethylmethacrylate as supports for improving cell adhesion and proliferation. Biomaterials **2004**; 25(17): 3645-53.

Schlegel KA, Donath K, Rupprecht S, Falk S, Zimmermann R, Felszeghy E, Wiltfang J. De novo bone formation using bovine collagen and platelet-rich plasma. Biomaterials **2004**; 25(23): 5387-93.

Schwarz K, Milne DB. Growth-promoting effects of silicon in rats. Nature **1972**; 239(5371): 333-4.

Schwarz K. A bound form of silicon in glycosaminoglycans and polyuronides. Proc Natl Acad Sci USA. **1973**; 70(5): 1608-12.

Seaborn CD, Nielsen FH. Silicon deprivation decreases collagen formation in wounds and bone, and ornithine transaminase enzyme activity in liver. Biol Trace Elem Res. **2002**; 89(3): 251-61.

Seelich T. Biochemistry and methods of application. J Head Neck Pathol **1982**; 365–9.

Seiler JG, Johnson J. Iliac Crest Autogenous Bone Grafting: Donor Site complications. J. South Orthop. Assoc. **2000**; 9(2): 91-97.

Senger DR, Ledbetter SR, Claffey KP, Papadopoulos-Sergiou A, Peruzzi CA, Detmar M. Stimulation of endothelial cell migration by vascular permeability factor/vascular endothelial growth factor through cooperative mechanisms involving the alphavbeta3 integrin, osteopontin, and thrombin. Am J Pathol. **1996**; 149(1): 293-305.

Sepp A, Binns RM, Lechler RI. Improved protocol for colorimetric detection of complement-mediated cytotoxicity based on the measurement of cytoplasmic lactate dehydrogenase activity. J Immunol Methods **1996**; 196(2): 175-180.

Sepulveda P, Jones JR, Hench LL. In vitro dissolution of melt-derived 45S5 and sol-gel derived 58S bioactive glasses. J Biomed Mater Res. **2002**; 61(2): 301-11.

Shimazaki K, Mooney V. Comparative study of porous hydroxyapatite and tricalcium phosphate as bone substitute. J Orthop Res. **1985**; 3(3): 301-10.

Shu R, McMullen R, Baumann MJ, McCabe LR. Hydroxyapatite accelerates

differentiation and suppresses growth of MC3T3-E1 osteoblasts. J Biomed Mater Res A. **2003**; 67(4):1196-204.

Fujibayashi S, Kim HM, Neo M, Uchida M, Kokubo T, Nakamura T.. Repair of segmental long bone defect in rabbit femur using bioactive titanium cylindrical mesh cage. Biomaterials **2003**; 24(20): 3445-51.

Sierra DH. Fibrin sealant adhesive systems: A review of their chemistry, material properties and clinical applications. J Biomater Appl. **1993**; 7(4): 309-52.

Sikavitsas VI, Temenoff JS, Mikos AG. Biomaterials and bone mechanotransduction. Biomaterials. **2001**; 22(19): 2581-93.

Simmons DJ. Comparative physiology of bone. In: Bourne GH, editor. The biochemistry and physiology of bone, Academic Press, New York, **1976**, p. 445-516.

Simon JA, Ricci JL, Di Cesare PE. Bioresorbable fracture fixation in orthopedics: a comprehensive review. Part I. Basic science and preclinical studies. Am J Orthop. **1997**; 26(10): 665-71.

Singh R, Dahotre NB. Corrosion degradation and prevention by surface modification of biometallic materials. J Mater Sci Mater Med. **2007**; 18(5): 725-51.

Slapnicka J, Fassmann A, Strasak L, Augustin P, Vanek J. Effects of activated and nonactivated platelet-rich plasma on proliferation of human osteoblasts in vitro. J Oral Maxillofac Surg. **2008**; 66(2): 297-301.

Son E, Do H, Joo HM, Pyo S. Induction of alkaline phosphatase activity by L-ascorbic acid in human osteoblastic cells: a potential role for CK2 and Ikaros. Nutrition **2007**; 23(10): 745-53.

Sporn LA, Bunce LA, Francis CW. Cell proliferation on fibrin: modulation by fibrinopeptide cleavage. Blood **1995**; 86(5): 1802-10.

Stein GS, Lian, JB, Owen TA. Relationship of cell growth to the regulation of tissue-specific gene expression during osteoblast differentiation. The FASEB Journal **1990**; 4(13): 3111-23.

Sugiura F, Kitoh H and Ishiguro N. Osteogenic potential of rat mesenchymal stem cells after several passages. Biochem Biophys Res Commun. **2004**; 316(1): 233-9.

Tachibana Y, Ninomiya S, Kim YT, Sekikawa M. Tissue response to porous hydroxyapatite ceramic in the human femoral head. J Orthop Sci. **2003**; 8(4): 549-53.

Takahashi F, Akutagawa S, Fukumoto H, Tsukiyama S, Ohe Y, Takahashi K, Fukuchi Y, Saijo N, Nishio K. Osteopontin induces angiogenesis of murine neuroblastoma cells in mice. Int J Cancer. **2002**; 98(5): 707-12.

Takahashi Y, Tabata Y. Effect of the fiber diameter and porosity of non-woven PET fabrics on the osteogenic differentiation of mesenchymal stem cells. J Biomater Sci Polym Ed. **2004**; 15(1): 41-57.

Tanizawa Y, Suzuki T. Effects of silicate ions on the formation and transformation of calcium phosphorus in neutral aqueous solutions. J Chem Soc Faraday Trans **1995**; 91: 3499-503.

Tementoff JS, Lu L, mikos AG. Bone tissue engineering using syntheic biodegrdable polymer scaffolds. In: Davies JE, editor. Bone Engineering. Em squared incorporated, **2000**. p. 454-9.

Ter Brugge PJ, Jansen JA. In vitro osteogenic differentiation of rat bone marrow cells subcultured with and without dexamethasone. Tissue Eng. **2002**; 8(2): 321-31.

Thompson TJ, Owens PD, Wilson DJ. Intramembranous osteogenesis and angiogenesis in the chick embryo. J Anat. **1989**; 166:55-65.

Tomford WW. Transmission of disease through transplantation of musculoskeletal allografts. J Bone Joint Surg Am. 1995; 77(11): 1742-54.

Tomić S, Bumbasirević M, Lesić A, Mitković M, Atkinson HD. Ilizarov frame fixation without bone graft for atrophic humeral shaft nonunion: 28 patients with a minimum 2-year follow-up. J Orthop Trauma. **2007**; 21(8): 549-56.

Tsuruga E, Takita H, Itoh H, Wakisaka Y, Kuboki Y. Pore size of porous hydroxypatite as the cell-substratum controls BMP-induced osteogenesis. J Biochem. **1997**; 121(2): 317-24.

Turgeman G, Pittman DD, Müller R, Kurkalli BG, Zhou S, Pelled G, Peyser A, Zilberman Y, Moutsatsos IK, Gazit D. Engineered human mesenchymal stem cells: a novel platform for skeletal cell mediated gene therapy. J Gene Med. **2001**; 3(3): 240-51.

Tzaphlidou M, Zaichick V. Calcium, phosphorus, calcium-phosphorus ratio in rib bone of healthy humans. Biol Trace Elem Res. **2003**; 93(1-3): 63-74.

Uchida A, Nade SM, McCartney ER, Ching W. The use of ceramics for bone replacement. A comparative study of three different porous ceramics. J Bone Joint Surg Br. **1984**; 66(2): 269-75.

Urist MR. Bone: formation by autoinduction. 1965. Clin Orthop Relat Res. **2002**; 395: 4-10.

Vail TP, Urbaniak JR. Donor site morbidity with use of vascularised autogenous fibular grafts. J. Bone Joint Surg Am **1996**; 78: 204-11.

Valerio P, Guimaraes MH, Pereira MM, Leite MF, Goes AM. Primary osteoblast cell response to sol-gel derived bioactive glass foams. J Mater Sci Mater Med. **2005**; 16(9): 851-6.

Valerio P, Pereira MM, Goes AM, Leite MF. The effect of ionic products from bioactive glass dissolution on osteoblast proliferation and collagen production. Biomaterials **2004**; 25(15): 2941-8.

Välimäki VV, Aro HT. Molecular basis for action of bioactive glasses as bone graft substitute. Scand J Surg. **2006**; 95(2): 95-102.

Vallet-Regi M, Ramilla A. New bioactive glass and changes in porosity during the growth of a carbonate hydroxyapatite layer on glass surfaces. Chem. Mater. **2000**; 12(4): 961-65.

van den Dolder J, Mooren R, Vloon AP, Stoelinga PJ, Jansen JA. Platelet-rich plasma: quantification of growth factor levels and the effect on growth and differentiation of rat bone marrow cells. Tissue Eng. **2006**; 12(11): 3067-73.

van den Dolder J, Vehof JW, Spauwen PH, Jansen JA. Bone formation by rat bone marrow cells cultured on titanium fiber mesh: effect of in vitro culture time. J Biomed Mater Res. **2002**; 62(3): 350-8.

Vehof JW, Haus MT, de Ruijter AE, Spauwen PH, Jansen JA. Bone formation in transforming growth factor beta-I-loaded titanium fiber mesh implants. Clin Oral Implants Res. **2002**; 13(1): 94-102.

Vogel JP, Szalay K, Geiger F, Kramer M, Richter W, Kasten P. Platelet-rich plasma improves expansion of human mesenchymal stem cells and retains differentiation capacity and in vivo bone formation in calcium phosphate ceramics. Platelets **2006**; 17(7): 462-9.

Volkmer E, Drosse I, Otto S, Stangelmayer A, Stengele M, Kallukalam BC, Mutschler W, Schieker M. Hypoxia in static and dynamic 3D culture systems for tissue engineering of bone. Tissue Eng. Part A. **2008**; 14(8): 1331-40.

Vuola J, Taurio R, Goransson H, Asko-Seljavaara S. Compressive strength of calcium carbonate and hydroxyapatite implants after bone-marrow-induced osteogenesis. Biomaterials **1998**; 19(1-3): 223-7.

Wall ME, Bernacki SH, Loboa EG. Effects of serial passaging on the adipogenic and osteogenic differentiation potential of adipose-derived human mesenchymal stem cells. Tissue Eng. **2007**; 13(6): 1291-8.

Walters MA, Leung YC, Blumenthal NC, LeGeros RZ, Konsker KA. A Raman and infrared spectroscopic investigation of biological hydroxyapatite. J Inorg Biochem. **1990**; 39(3): 193-200.

Wang C, Duan Y, Markovic B, Barbara J, Howlett RC, Zhang X, Zreiqat H. Proliferation and bone-related gene expression of osteoblast grown on hydroxyapatite ceramics sintered at different temperature. Biomaterials **2004**; 25(15): 2949-56.

Wang M. Developing bioactive composite materials for tissue replacement. Biomaterials **2003**; 24(13): 2133-51.

Warren SM, Nacamuli RK, Song HM, Longaker MT. Tissue-engineered bone using mesenchymal stem cells and a biodegradable scaffold. J Craniofac Surg. **2004**; 15(1): 34-7.

Washburn EW. Note on a Method of Determining the Distribution of Pore Sizes in a Porous Material. Proc Natl Acad Sci U S A. **1921**; 7(4):115-6.

Webb JCJ, Tricker J. A review of fracture healing. Current Orthopaedics **2000**; 14(6): 457-63.

Weibrich G, Hansen T, Kleis W, Buch R, Hitzler WE. Effect of platelet concentration in platelet-rich plasma on peri-implant bone regeneration. Bone **2004**; 34(4): 665-71.

Weibrich G, Kleis WK, Hafner G, Hitzler WE, Wagner W. Comparison of platelet, leukocyte, and growth factor levels in point-of-care platelet-enriched plasma, prepared using a modified Curasan kit, with preparations received from a local blood bank. Clin Oral Implants Res. **2003**; 14(3): 357-62.

Weinreb M, Shinar D, Rodan GA. Different pattern of alkaline phosphatase, osteopontin, and osteocalcin expression in developing rat bone visualized by in situ hybridization. J Bone Miner Res. **1990**; 5(8): 831-42.

Weiss RE, Reddi AH. Appearance of fibronectin during the differentiation of cartilage, bone, and bone marrow. J Cell Biol. **1981**; 88(3): 630-6.

Wiesmann HP, Joos U, Meyer U. Biological and biophysical principles in extracorporal bone tissue engineering. Part II. Int J Oral Maxillofac Surg. **2004**; 3(6): 23-30.

Winkler J, Hescheler J, Sachinidis A. Embryonic stem cells for basic research and potential clinical applications in cardiology. Biochim Biophys Acta. **2005** 30; 1740(2): 240-8.

Wippermann B, Donow C, Schratt HE, den Boer FC, Blokhuis T, Patka P. The influence of hydroxyapatite granules on the healing of a segmental defect filled with autologous bone marrow. Ann Chir Gynaecol. **1999**; 88(3): 194-7.

Wlodarski KH, Reddi AH. Alkaline phosphatase as a marker of osteoinductive cells. Calcif Tissue Int. **1986**; 39(6): 382-5.

Xiao Y, Qian H, Young WG, Bartold PM. Tissue engineering for bone regeneration using differentiated alveolar bone cells in collagen scaffolds. Tissue Eng. **2003**; 9(6):1167-77.

Xie H, Yang F, Deng L, Luo J, Qin T, Li X, Zhou GQ, Yang Z. The performance of a bone-derived scaffold material in the repair of critical bone defects in a rhesus monkey model. Biomaterials. **2007**; 28(22): 3314-24.

Xie J, Baumann MJ, McCabe LR. Osteoblasts respond to hydroxyapatite surfaces with immediate changes in gene expression. J Biomed Mater Res. A **2004**; 71(1): 108-17.

Xue W, Liu X, Zheng X, Ding C. Effect of hydroxyapatite coating crystallinity on dissolution and osseointegration in vivo. J Biomed Mater Res. A **2005**; 74(4): 553-61.

Xynos ID, Edgar AJ, Buttery LD, Hench LL, Polak JM. Gene-expression profiling of human osteoblasts following treatment with the ionic products of Bioglass 45S5 dissolution. J Biomed Mater Res. **2001**; 55(2): 151-7.

Yamada Y, Seong Boo J, Ozawa R, Nagasaka T, Okazaki Y, Hata K, Ueda M. Bone regeneration following injection of mesenchymal stem cells and fibrin glue with a biodegradable scaffold. J Craniomaxillofac Surg. **2003**; 31(1): 27-33.

Yamada Y, Ueda M, Naiki T, Takahashi M, Hata K, Nagasaka T. Autogenous injectable bone for regeneration with mesenchymal stem cells and platelet-rich plasma: tissue-engineered bone regeneration. Tissue Eng. **2004**; 10(5-6): 955-64.

Yamaguchi T, Chattopadhyay N, Kifor O, Butters RR Jr, Sugimoto T, Brown EM. Mouse osteoblastic cell line (MC3T3-E1) expresses extracellular calcium ($Ca^{2+}o$)-sensing receptor and its agonists stimulate chemotaxis and proliferation of MC3T3-E1 cells. J Bone Miner Res. **1998**; 13(10):1530-8.

Yamaguchi T, Chattopadhyay N, Kifor O, Sanders JL, Brown EM. Activation of p42/44 and p38 mitogen-activated protein kinases by extracellular calcium-sensing receptor agonists induces mitogenic responses in the mouse osteoblastic MC3T3-E1 cell line. Biochem Biophys Res Commun. **2000**; 279(2): 363-8.

Yoshikawa T, Ohgushi H, Okumura M, Tamai S, Dohi Y, Moriyama T. Biochemical and histological sequences of membranous ossification in ectopic site. Calcif Tissue Int. **1992**; 50(2): 184-8.

Younger EM, Chapman MW. Morbidity at bone graft donor sites. J. Orthop. Trauma **1989**; 3(3): 192-5.

Yuan H, van Blitterswijk CA, de Groot K, de Bruijn JD. Cross-species comparison of ectopic bone formation in biphasic calcium phosphate (BCP) and hydroxyapatite (HA) scaffolds. Tissue Eng. **2006**; 12(6): 1607-15.

Yuan J, Cui L, Zhang WJ, Liu W, Cao Y. Repair of canine mandibular bone defects with bone marrow stromal cells and porous beta-tricalcium phosphate. Biomaterials **2007**; 28(6): 1005-13.

Zagai U, Fredriksson K, Rennard SI, Lundahl J, Sköld CM. Platelets stimulate fibroblast-mediated contraction of collagen gels. Respir Res. **2003**; 4: 13.

Zangi L, Rivkin R, Kassis I, Levdansky L, Marx G, Gorodetsky R. High-yield isolation, expansion and differentiation of rat bone marrow-derived mesenchymal stem cells with fibrin microbeads. Tissue Eng. **2006**; 12(8): 2343- 54.

Zechner W, Tangl S, Tepper G, Fürst G, Bernhart T, Haas R, Mailath G, Watzek G. Influence of platelet-rich plasma on osseous healing of dental implants: a histologic and histomorphometric study in minipigs. Int J Oral Maxillofac Implants. **2003**; 18(1): 15-22.

Zhang C, Wang J, Feng H, Lu B, Song Z, Zhang X. Replacement of segmental bone defects using porous bioceramic cylinders: A biomechanical and X-ray diffraction

study. J Biomed Mater Res. **2001**; 54(3): 407-11.

Zhang CQ, Yuan T, Zeng BF. Experimental study of the effect of platelet-rich plasma on osteogenesis in rabbit. Chin Med J (Engl). **2004**; 117(12): 1853-5.

Zhang X, Xie C, Lin AS, Ito H, Awad H, Lieberman JR, Rubery PT, Schwarz EM, O'Keefe RJ, Guldberg RE. Periosteal progenitor cell fate in segmental cortical bone graft transplantations: implications for functional tissue engineering. J Bone Miner Res. **2005**; 20(12): 2124-37.

Zhu L, Liu W, Cui L, Cao Y. Tissue-engineered bone repair of goat-femur defects with osteogenically induced bone marrow stromal cells. Tissue Eng. **2006**; 12(3): 423-33.

Zhu X, Chen J, Scheideler L, Reichl R, Geis-Gerstorfer J. Effects of topography and composition of titanium surface oxides on osteoblast responses. Biomaterials **2004**; 25(18): 4087-103.

Zimmermann G, Henle P, Küsswetter M, Moghaddam A, Wentzensen A, Richter W, Weiss S. TGF-β1 as a marker of delayed fracture healing. Bone **2003**; 36(5): 779-85.

Zreiqat H, Standard OC, Gengenbach T, Steele J, Howlett CR. The role of surface characteristics in the initial adhesion of human bone-derived cells on ceramics. Cells and Materials **1996**; 6: 45–56.

zur Nieden NI, Kempka G, Ahr HJ. In vitro differentiation of embryonic stem cells into mineralized osteoblasts. Differentiation **2003**; 71(1): 18-27.

ANNEXURE - I

List of Buffers

1. Water for tissue culture

Tap water distilled three times, deionised by passing through Millipore water purifying system, autoclaved and used.

2. Phosphate buffered saline (pH 7.4)

NaCl	-	150 mM
KH_2PO_4	-	1.5 mM
Na_2HPO_4	-	10 mM
Distilled water	-	250 ml

3. Alkaline phosphatase buffer (pH 9.8)

Diethanol amine	-	0.1 M
Triton X-100	-	1%
$MgCl_2$	-	1 mM
Distilled water	-	100 ml

4. Alkaline phosphatase substrate

Mix 20 mg 4-paranitrophenyl phosphate (Sigma chemicals) with 20 mL ALP substrate buffer for ALP activity assays.

5. Tris-EDTA buffer (pH 7.5)

Tris(hydroxymethyl)methylamine	- 10 mM
Ethylenediaminetetraacetic acid disodium salt (EDTA)	- 1 mM

6. Sorensen phosphate buffer (pH 7.4)

NaH_2P0_4	-	0.2 M
Na_2HPO_4	-	0.2M
Distilled water	-	100 ml

ANNEXURE II

LIST OF PUBLICATIONS

1. **Nair MB**, Suresh Babu S, Varma HK, John A. A triphasic ceramic-coated porous hydroxyapatite for tissue engineering application. Acta Biomater. 2008; 4(1): 173-81 (**Selected as Featured article by Elsevier in the year 2008)**

2. John A, **Nair MB**, Varma HK, Bernhardt A, Gelinsky M. Biodegradation and cytocompatibility studies of a triphasic ceramic coated porous hydroxyapatite for bone substitute applications. Int. J. Appl. Ceram. Technol. 2008; 5: 11–19.

3. **Nair MB**, Bernhardt A, Lode A, Heinemann C, Thieme S, Hanke T, Varma H, Gelinsky M, John A. A bioactive triphasic ceramic-coated hydroxyapatite promotes proliferation and osteogenic differentiation of human bone marrow stromal cells. J Biomed Mater Res A. 2009; 90(2): 533-42.

4. **Nair MB**, Varma HK, John A. Triphasic ceramic coated hydroxyapatite as a niche for goat stem cell-derived osteoblasts for bone regeneration and repair. J Mater Sci Mater Med. 2008 Oct 14. [Epub ahead of print].

5. **Nair MB**, Varma HK, Menon KV, Shenoy SJ, John A. The regeneration and repair of goat segmental femur defect with bioactive triphasic ceramic coated hydroxyapatite scaffold. J Biomed Mater Res A. 2008 Dec 8. [Epub ahead of print]

6. **Nair MB**, Varma HK, John A. Platelet-rich plasma and fibrin glue coated bioactive ceramics enhances growth and differentiation of goat bone marrow-derived stem cells. Tissue Eng Part A. 2009; 15(7):1619-31.

7. **Nair MB**, Varma HK, Menon KV, Shenoy SJ, John A. The reconstruction of goat femur segmental defect using triphasic ceramic coated hydroxyapatite together with autologous cells and platelet-rich plasma. Acta Biomater. 2009; 5(5):1742-55.

8. **Nair MB**, Varma HK, Kumary TV, Babu S, John A. Cell Interaction Studies with Novel Bioglass Coated Hydroxyapatite Porous blocks. Trends Biomater. Artif. Organs. 2006; 19 (2): 108-14.

9. **Nair MB**, Varma HK, Shenoy SJ, John A. The treatment of goat femur segmental defects with silica coated hydroxyapatite – one year follow up. Tissue Eng Part A. (in press).

10. **Nair MB**, Varma HK, Mohanan PV, John A. Cell-engineered triphasic ceramic coated hydroxyapatite induces ectopic bone formation in rat model. Bulletin of Materials Science (communicated).

LIST OF PAPERS PRESENTED IN CONFERENCES

1. **Manitha B. Nair**, H. K. Varma, Annie John. The regeneration of segmental bone defects using tissue-engineered triphasic ceramic coated hydroxyapatite (poster) - NANOBIO 2009 The First International Conference on Tissue Engineering & Stem cells Research using Nanomaterials, Feb 17 – 19, 2009, Amrita Institute of Medical Sciences, Kochi, Kerala, India (**Best Poster presentation Award**).

2. **Manitha B. Nair**, H. K. Varma, Annie John. The relevance of tissue-engineered triphasic ceramic coated hydroxyapatite in the healing of bone segmental defect (oral) - International Conference on Medical Materials, Devices and Regenerative Medicine, College of Biomedical Engineering and Applied Sciences, Kathmandu, Nepal, November 23-24, 2008.

3. **Manitha B. Nair**, K. V. Menon, H. K. Varma, Annie John. Tissue-engineered construct in the healing of a long bone defect (poster) - TERMIS NA 2007, Westin Harbour Castle, Toronto, Canada, June 12 – 16, 2007.

4. **Manitha B. Nair**, H. K. Varma, Annie John. A novel interconnected porous bioactive ceramic as bone substitute for Orthopaedic applications (oral) - 19th Kerala Science Congress, Kannur, Kerala, Januvary 29 – 31, 2007 (**Young scientist award in Health Science category for this paper**).

5. **Manitha B. Nair**, Anne Bernhardt, Michael Gelinsky, P. R. Sanjay, Sachin J Shenoy, K. V. Menon, H. K. Varma, Annie John. Novel bioactive ceramic as bony scaffold for clinical skeletal reconstruction (poster) - Indo-Australian Conference BITE & RM, Sree Chitra Tirunal Institute for Medical Sciences & Technology, Trivandrum, Kerala, Januvary 10 – 12, 2007.

6. **Manitha B. Nair**, Anne Bernhardt, H. K. Varma, Michael Gelinsky, Annie John. Tissue-engineered bone construct for clinical Orthopaedic transplantation – an in vitro study (oral) - International Conference on Design of biomaterials (BIND – 06) & XVII Annual meeting of SBAOI, Indian Institute of Technology, Kanpur, December 8 -11, 2006.

7. **Manitha B. Nair**, Sachin Shenoy, P.R Sanjay, H.K.Varma, Annie John. Indigenous bioglass coated hydroxyapatite in the repair and regeneration of segmental defects in a goat model (poster) - Regenerate World Congress on Tissue Engineering and Regenerative Medicine, Westin Convention Center, Pittsburgh, USA, April 24-27, 2006.

8. **Manitha B. Nair**, Anne Bernhardt, H. K. Varma, Michael Gelinsky, Annie John. Bone constructs from a combination of cells and novel ceramics – Scanning Electron Microscopy Study (poster) - National Conference on Electron Microscopy and XXVIII Annual meeting of Electron Microscope Society of India (EMSI), Regional Research Laboratory, Trivandrum, Kerala, April 19-21, 2006 (**First Hitachi High Technologies Best Poster Award in Life Sciences for this paper**).